The Use of Genetic Code Expansion to Engineer Biological Tools for Studying the RNA Interference Pathway and Small Regulatory RNAs

Noreen Ahmed

Thesis submitted to the University of Ottawa
in partial fulfillment of the requirements for the
degree of doctorate in philosophy in Chemistry

Department of Chemistry and Biomolecular Sciences
Faculty of Science
University of Ottawa

Abstract

Over the past years, small RNAs (smRNAs) have been identified as important molecular regulators of gene expression and specifically eukaryotic messenger RNAs (mRNAs). Small RNAs including small-interfering RNAs (siRNAs) and microRNAs (miRNAs) take part in the RNA silencing pathway and regulate various pathways in the cell including transcription, genome integrity, chromatin structure, mRNA stability, and translation. siRNAs are usually from exogenously derived molecules, while miRNAs are expressed endogenously by the genome. The RNA silencing pathway is highly conserved between organisms and plays a critical part in maintaining homeostasis, host-pathogen interaction, and disease progression. Thus, a better understanding of the RNA silencing pathway and probing of the molecules involved in the process is instrumental in developing tools that can better regulate the expression of specific genes.

The viral suppressor of RNA silencing (VSRS) p19, is a 19 kDa protein that is expressed by tombusviruses and exhibits the highest reported affinity to small RNAs, including siRNA and miRNA. Further engineering of this protein acts as an interesting means to control the RNA silencing pathway and provides a platform to design novel tools to further modulate the activity of smRNAs in living systems.

The ability to incorporate new and useful chemical functionality into proteins within living organisms has been greatly enhanced by technologies that expand the genetic code. These usually involve bioorthogonal transfer RNA (tRNA) /aminoacyl-tRNA synthetase (aaRS) pairs that can selectively incorporate an unnatural amino acid (UAA) site specifically into ribosomally synthesized proteins. Site-specificity is coded for by using a rare codon such as the amber stop codon. In **Chapter 2**, we demonstrate the engineering of p19 for the development of a Förster resonance energy transfer (FRET) reporter system for the visualization of RNA delivery and release in cells using UAAs and bioorthogonal click chemistry, which was done by incorporating azidophenylalanine (AzF). In **Chapter 3**, by incorporating UAAs into p19's binding pocket, we were able to enhance its smRNA

suppressing activity by covalently trapping the bound substrates. We have demonstrated the engineering of a molecular switch that contains photo-crosslinking groups that covalently trap smRNAs. In **Chapter 4**, incorporating a metal-ion chelating UAA (2,2′-bipyridin-5-yl) alanine (BpyAla) into p19's binding pocket has successfully led to site-specific cleavage of small RNAs including siRNAs and endogenous miRNAs. The genetic introduction of BpyAla provides a unique method of introducing catalytic activity into proteins of interest. The developed unnatural enzyme provides a new tool for catalytic suppression of the RNA silencing pathway. These results demonstrate the power of adding new chemistries to proteins using UAAs to achieve possible, diverse applications in therapy and biotechnology.

Acknowledgments

To begin, I would like to express my gratitude to my supervisor Dr. John Paul Pezacki, who guided and supported me throughout my studies. John has had a great influence on my scientific and professional development. I appreciate his continuous support, encouragement, and guidance throughout the past five years. His mentorship has been instrumental to my success and growth as a scientist. John has provided a great environment in his lab to foster my independence and curiosity. I appreciate his insights and scientific discussions.

I am very grateful to all my colleagues in the lab with whom I have developed long-lasting friendships. Specials thanks to Roxana Filip, Rhea Alonzi, Geneviève Desrochers, Mariam Serhan, Dr. Shadi Masoud, Didier Bilodeau and Tyler Shaw. They have always been available for scientific discussions and helped answer any of my questions. I would also like to thank Dana Foss for her help and for getting me excited about protein engineering and p19. I would like to thank Dr. Mirka Strmiskova, Dr. David Prescott and Dr. Caroline Toudic for their help and scientific discussions.

I would like to thank my sister, Nadine, with whom I have been very lucky to share this journey. I acknowledge how lucky I am to have experienced grad school with my best friend.

To my parents, thank you so much for your unconditional support. You both inspire me to pursue my dreams. Thank you for all your unwavering encouragement and support.

This opportunity has been possible through generous funding from the Natural Sciences and Engineering Council (NSERC), the Government of Ontario, and the University of Ottawa. I would like to thank my thesis advisory committee for all their assistance and support.

Table of Contents

Abstract ii
Acknowledgments iv
List of Figures ix
List of Tables xi
List of Abbreviations xii
Chapter 1 1
1.1 Preface 1
1.2 The RNA Silencing Pathway 2
1.2.1 Roles of small RNAs in the RNA silencing Pathway 4
1.2.2 siRNA Interference 4
1.2.3 microRNA Biogenesis and the RNA Silencing Pathway 8
1.2.4 Role of Small RNAs and the RNA Silencing Pathway in Viral Infections 11
1.3 Viral Suppressors of RNA Silencing Pathway 14
1.3.1 The Viral Suppressor of RNA Silencing p19 15
1.3.2 p19 as a Tool to Study the RNA Silencing Pathway 19
1.3.3 p19 as Tool in Biotechnology 21
1.3.4 p19: A Tool for RNA Detection and Delivery 22
1.4 Protein Engineering and Genetic Code Expansion 27
1.4.1 Development of bioorthogonal aaRS/tRNA pair 27
1.4.2 Chemical Modifications 31
1.4.3 Improving Protein Functions 32
1.4.4 Azido-Phenylalanine Incorporation and Usage in Protein Engineering 32
1.4.5 Bipyridinylalanine and its Use in Protein Engineering 34
1.5 Rationale and Statement of Objectives 37
1.6 References 38
Chapter 2 1
2.1 Preface 54
2.2 Abstract 55
2.3 Introduction 56
2.4 Results and Discussion 59
2.4.1 Introduction of *p*-AzF in p19 mutants 59
2.4.2 Fluorescence labeling of p19-W19AzF and assessing RNA binding using FRET 62

2.4.3 Fluorescence labeling of p19-III mutants and assessing RNA binding using FRET 64
2.4.4 Determining Binding affinity of p19-III-W19AzF-Cy5 using FRET 69
2.4.5 Engineering a p19-based probe to detect small RNA delivery and release in cells 71
2.5 Conclusions 78
2.6 Materials and Methods 79
2.6.1 Cloning of CIRV-p19 79
2.6.2 Bacterial overexpression of CIRV p19 and mutants 80
2.6.3 Fluorescent Labeling 81
2.6.4 Immunoblotting 81
2.6.5 Circular Dichroism 82
2.6.6 Substrates 82
2.6.7 Electrophoretic Mobility Shift Assay 82
2.6.8 Fluorescence Resonance Energy Transfer Measurements 83
2.6.9 Cell Culture 84
2.6.10 Imaging of the Delivery of RNA using p19-W19AzF-III-TAT 84
2.6.11 Luciferase Assay 85
2.6.12 Cell Viability Assay 85
2.7 Acknowledgment 86
2.8 References 87
Chapter 3 90
3.1 Preface 90
3.2 Abstract 91
3.3 Introduction 92
3.4 Results 95
3.4.1 Incorporation of AzF into p19 97
3.4.2 Binding Affinity of AzF-containing p19 proteins 100
3.4.3 Crosslinking of p19 and small RNA substrates 103
3.5 Discussion 105
3.6 Conclusions 106
3.7 Materials and Experimental Details 107
3.7.1 Expression and purification wild type (WT) p19 and p19-K67AzF, -R115AzF and -T111AzF 107
3.7.2 Immunoblotting 108
3.7.3 Substrates 109

3.7.4 Electrophoretic Mobility Shift Assay (EMSA) 109
3.7.5 Crosslinking 110
3.7.6 Liquid Chromatography/ Mass Spectrometry 110
3.8 Acknowledgments 111
3.9 References 112
Chapter 4 115
4.1 Preface 115
4.2 Abstract 116
4.3 Introduction 117
4.4 Results 119
4.4.1 Site-specific introduction of (2,2′-bipyridin-5-yl)alanine into the p19 dimer 119
4.4.2 Small RNA cleavage using p19-T111BpyAla 125
4.4.3 Cleavage of siRNA by p19-T111BpyAla detected using fluorescence polarization 127
4.4.4 p19-T111BpyAla can cleave miRNAs isolated from hepatocellular carcinoma cell line 129
4.4.5 p19-T111BpyAla represses HCV replication 133
4.5 Discussion 136
4.6 Materials and Methods 139
4.6.1 Expression and purification of p19-WT, p19-K67BpyAla and p19-T111BpyAla 139
4.6.2 Immunoblotting 140
4.6.3 Substrates 140
4.6.4 Electrophoretic mobility shift assay (EMSA) 140
4.6.5 Fluorescence Polarization 141
4.6.6 Cell culture, RNA Isolation, miRNA profiling and RT-qPCR 141
4.6.7 E9 Subgenomic Replicon Luciferase Assay 143
4.6.8 JFH-1 Infections 143
4.6.9 Synthesis of (2,2′-bipyridin-5-yl)alanine 144
4.7 Acknowledgments 148
4.8 References 149
Chapter 5 154
5.1 Engineering p19-based probes for the detection of small RNAs 154
5.2 p19 as a tool for RNA delivery using unnatural amino acids 156
5.3 Engineering of p19-based photo-switches using UAA 159
5.4 Enhancing p19's activity in mammalian cells 161
5.5 Introduction of catalytic functionality into p19 163

5.6 General Conclusions 165
5.7 References 166
Chapter 6 Appendix 168
6.1 Supplemental information for chapter 2 168
6.2 Supplemental information for chapter 3 169
6.3 Supplemental information for chapter 4 170
6.3.1 NMR Spectra for compounds synthesized in Chapter 4 174

List of Figures

Figure 1.1. siRNA interference pathway.. 7
Figure 1.2. miRNA biogenesis and the RNA silencing pathway 10
Figure 1.3. p19 and its suppression of the RNA silencing pathway. 18
Figure 1.4. Incorporation of unnatural amino acids. 30
Figure 2.1 AzF incorporation in p19 and subsequent DBCO-Cy5 labeling in a site-specific manner using strain promoted alkyne-azide cycloaddition.. 58
Figure 2.2. Expression of Full length AzF mutants. 61
Figure 2.3. Fluorescence gel and FRET Spectra of Cy5 Labelled p19 Mutant. 63
Figure 2.4. Expression and Fluorescence spectra of Cy5 labelled triple Isoleucine mutants of p19. 65
Figure 2.5. Binding affinity determination using electrophoretic mobility shift assay. 67
Figure 2.6. Circular dichroism of p19-III and labeled mutants. Far UV spectra for p19-III-N46AzF-Cy5, p19-III-W19AzF-Cy5 and p19-III is recorded from 185-250 nm. 68
Figure 2.7. Binding affinity of p19-III-W19AzF-Cy5 as determined by FRET. 70
Figure 2.8. Fluorescence Labeling and Spectra of p19-2x-III-TAT. (A) p19-2x-III-wt-TAT and p19- 2x-III-W19AzF–TAT are labeled with DBCO-Cy5 and analyzed using in-gel fluorescence. 72
Figure 2.9. Delivery of siRNA to Huh7 cells. Fluorescence imaging of Cy5-2x-p19-III-W19AzF delivery of unlabeled siRNA in Huh7 cells. 73
Figure 2.10. Fluorescence imaging of Cy5-2x-p19-III-W19AzF delivery of BHQ-2-siRNA in Huh7 76
Figure 2.11 p19-2X-III-W19AzF-TAT delivers siRNA for gene knockdown in human cell culture. 77
Figure 3.1. Photocrosslinking of protein containing *p*-azido-L-phenylalanine (AzF) and a nucleic acid substrate. 96
Figure 3.2. AzF incorporation sites in p19 98
Figure 3.3. Mass spectrum to confirm incorporation of Azidophenylalanine site specifically. 99
Figure 3.4. Binding affinity measurements using electrophoretic mobility shift assay (EMSA) for mutants T111AzF, K67AzF and R115AzF. 102
Figure 3.5. Crosslinking of p19 and small RNAs. 104
Figure 4.1. Incorporation of BpyAla in 2 sites in the p19 dimer 122
Figure 4.2 The ICP-MS quantitative analysis of copper concentration bound to p19-WT and mutant p19-T111BpyAla 123
Figure 4.3 The UV-Vis absorption spectra of p19 WT and mutant p19-T111BpyAla. 124
Figure 4.4. siRNA cleavage by p19-T111BpyAla mutant. 126

Figure 4.5. siRNA cleavage by p19-T111BpyAla mutant.. 128
Figure 4.6. Cleavage of Huh7 miRNA samples using p19-T111BpyAla 132
Figure 4.7. p19-T111BpyAla effect of HCV replication.. 135
FigureS2.1. Purified p19-III and UAA mutants……..168
Figure S3.1. Crosslinking of p19 and small RNAs. 169
Figure S4.1. Expression and purification of p19-WT and p19-T111BpyAla purification……. 170
Figure S4.2 Determination of the Binding affinity of unnatural amino acid p19 mutants……....171
Figure S4.3 Determination of the Binding affinity of p19-T111BpyAla towards miR-122……..172

List of Tables

Table 2.1 Mutagenesis primers 80
Table 3.1. Dissociation constants representing the binding affinities of p19 mutants relative to the p19WT affinity to GL2 siRNA as measured using electrophoretic mobility shift assays..... 101
Table 3.2 Mutagenesis primers used in this study..... 107
Table S4.1 Summary of miRNAs downregulated upon treatment with p19-T111BpyAla relative to p19-WT..... 173

List of Abbreviations

aaRS	aminoacyl-tRNA synthetase
AGO	Argonaute
AzF	p-azido-L-phenylalanine
BHK-21	baby hamster kidney 21 cell line
BHQ	Black hole quencher
BpyAla	(2,2′-bipyridin-5-yl)alanine
CaMV	Cauliflower mosaic virus
CAP	catabolite activator proteins
Cas9	(CRISPR)-associated protein 9
CBD	chitin binding domain
CD	circular dichroism
CFP	cyan fluorescent protein
CIRV	Carnation Italian Rinspot Virus
CLIP	Crosslinking immunopercipetation
CRISPR	clustered regularly interspaced palindromic repeat
CuAAC	copper catalyzed azide-alkyne cycloaddition
CymRSV	cymbidium ringspot tombusvirus
DCL	Dicer- like enzymes
DCP2	decapping protein 2
DENV	Dengue virus
DPV	Differential Pulse Voltammetry
dsRNA	double stranded RNA
EBV	Epstein-Barr virus
ELP	elastin-like polypeptide
EMCV	encephalomyocarditis virus
EMSA	Electrophoretic mobility shift assays
FP	Fluorescence Polarization
FRET	Förster resonance energy transfer
HCV	Hepatitis C virus
HEV71	Human Enterovirus 71
hRdRp	Host encoded RNA-dependent RNA polymerase
huh7	Human hepatoma cells
IAV	Influenza A virus
ICP-MS	Inductively coupled plasma mass spectrometry
IFN	Interferon
IPTG	Isopropyl β-d-1-thiogalactopyranoside
LmrR	Lactoccocal multidrug resistance regulator
MBP	Maltose binding protein

mESCs	Mouse embryonic stem cells
miRISC	miRNA mediated RISC
miRNAs	MicroRNAs
Mj TyrRS	Methanococcus jannaschii tyrosyl-tRNA synthetase
MLFs	Murine lung fibroblasts
mRNA	messenger RNA
ncRNAs	non-coding RNA molecules
NoV	Nodamura virus
nt	nucleotide
ORFS	open reading frames
PAN2PAN3	polyadenylase complexes
PFV-1	Primate Foamy Virus type 1
piRNAs	Piwi-interacting RNA
PoLV	*Pothos latent virus*
ProFACE	Protein-facilitated affinity capillary electrophoresis
PTGS	Post-transcriptional gene silencing
RBPs	RNA binding proteins
RISC	RNA-induced silencing complex
RNAi	RNA interference
rRNA	Ribosomal RNA
RuV	Rubella virus
shRNAs	Short hairpin RNAs
siRNAs	Small interfering RNAs
smRNAs	Small RNAs
SPAAC	Strain-promoted azide-alkyne cycloaddition
sRNA-seq	Deep sequencing of small RNAs
TAT	HIV-1 transactivator of transcription
TCV	*Turnip crinkle virus*
TE	Transposable elements
TEV	Tobacco etch virus
TLR	Toll-like receptors
tRNA	Transfer RNA
UAAs	Unnatural amino acids
UV	Ultra-violet
VIGS	Virus-induced gene silencing
viRNAs	Virus-derived siRNAs
VSRS	Viral suppressors of RNA silencing
XRN1	Exoribonuclease 1
YSA	Ephrin mimetic peptide

Chapter 1

Introduction

1.1 Preface

The following chapter serves as a broad introduction to the RNA silencing pathway, RNA molecules involved in the pathway, the viral suppressor of RNA silencing p19, and its applications *in vitro* and in biotechnology. This introduction highlights the importance of the RNA silencing pathway and the RNA molecules involved in gene silencing and regulation. Additionally, this introduction emphasizes the potential of using protein engineering technologies such as unnatural amino acid incorporation and genetic code expansion techniques to enhance the functionalities of p19 and broaden its applications in living systems.

1.2 The RNA Silencing Pathway

The RNA silencing pathway is a general term encompassing phenomena involving small RNA molecules that trigger the suppression of homologous gene sequences[1,2]. This pathway is highly conserved within a variety of eukaryotic organisms[3]. It involves the utilization of short RNA molecules, typically between 21-28 nucleotides in length[4,5]. The RNA silencing pathway is evolutionarily conserved where the involved double-stranded RNA (dsRNA) molecules mediate potent and sequence-specific silencing of gene expression of target genes[4,6]. It is known that the structure and mechanisms in mammalian cells, plant cells, and invertebrates differ, however, the key components of the pathway are similar, where most of the components are shared. In plants, this process was described as a 'co-suppression' phenomenon or 'quelling' in *Neurospora*[7]. The process regulates gene expression in eukaryotes and it is as well known to be the primary immune defense mechanism against microbial pathogens such as viruses[8]. In plants, virus invasion leads to activation of the RNA silencing pathway, where several types of dsRNA molecules may act as RNA silencing pathway inducers[5]. dsRNA from RNA viruses, which are a result of virus replication in the host cells, in the case of RNA viruses, or from the bidirectional transcription of the viral genome in the case of DNA viruses, serve as RNA silencing pathway inducers[9].

The RNA silencing pathway, also known as the canonical RNA interference (RNAi) pathway has been characterized more extensively in *D. melanogaster*, where it has been determined that long dsRNA is cleaved and 'diced' into a pool of small 21-nucleotide small RNA duplexes by an ATP dependent, RNase III-like endoribonuclease, Dicer enzyme, specifically known by this nomenclature in invertebrates and mammals, while known as Dicer-like enzymes (DCL) in plants[10]. These small RNA duplexes are known as inducers of the RNA silencing pathway, which contain 3' 2 nucleotides (nt) overhangs, with 3' hydroxyl groups and 5' phosphate

groups[3,4,10–13]. These RNAs could be virus-derived RNAs or endogenous RNAs. The virus-derived RNAs share features with host endogenous RNAs known as small interfering RNAs (siRNAs), microRNAs (miRNAs), or piwi-interacting (piRNAs)[3,4,10,13–16]. The virus-derived RNAs are induced upon viral infection of eukaryotic hosts[12,15,17]. Both the viral and endogenous small RNAs activate and mediate the RNA silencing pathway. These pathways are also known to result in specific antiviral immunity, especially in plants[18–20]. The small RNAs are then assembled into the RNA-induced silencing complex (RISC) which involves the protein Argonaute (AGO), where these small RNA molecules select and destroy their mRNA targets by direct base-pairing with and guiding the endoribonuclease cleavage of the mRNA by AGO[12,14,21–23]. The loaded small RNA acts as a guide to dictate the target specificity of the AGO-mediated silencing in the RNA silencing pathway.

The AGO protein family is highly conserved and plays a central role in the regulation of gene expression networks. Historically, AGO proteins were discovered in a plant mutagenesis screen utilized to identify new genes involved in *Arabidopsis thaliana's* leaf development[23]. AGO proteins are conserved within the gene family suggesting their potential instrumental role in gene regulation[23]. Eukaryotic AGO proteins play an instrumental role in cellular processes and mediators of gene silencing[13], where they have been described for their cytoplasmic roles in small RNAs (smRNAs) biogenesis, being components of the RISC complex. In mammals, specifically, there are four AGO proteins (AGO 1-4), which comprise the RISC. AGO 1 has been implicated in heterochromatin silencing and has been linked to targeting pathways mediating the recognition of DNA. AGO 2 has been shown to exhibit similar functions but also was shown to be involved in miRNA-mediated repression as well as the siRNA silencing pathway [21]. AGO2 is the only mammalian AGO protein capable of mRNA cleavage[24].

Over the past two decades, the role of the RNA silencing pathway and the RNA molecules involved in these pathways have been uncovered, where they have been identified as major regulators of eukaryotic messenger RNA (mRNA) transcription. It has been highlighted that smRNAs play important roles in cellular processes such as cell differentiation and cellular proliferation and growth, cellular death and apoptosis, cellular antiviral defense, and cellular metabolism[14,25–29].

The main two classes smRNAs that will be the focus herein are siRNAs and miRNAs. They are similar in structure and function, however, possess different origins to be discussed later in this chapter.

1.2.1 Roles of Small RNAs in the RNA Silencing Pathway

SmRNAs have emerged as powerful regulators of gene expression and genome stability. Specifically, siRNAs and miRNAs have emerged as important regulatory molecules[10,11,14]. These two categories of small RNAs have become two of the most studied molecules when it comes to understanding the genetic regulatory landscape. miRNAs are viewed as regulators of endogenous genes, while siRNAs are understood to be defenders of genome integrity to foreign invasive nucleic acids, specifically those derived from viruses, transposons, and transgenes[30].

1.2.2 siRNA Interference

siRNAs are derived from exogenous dsRNA and were shown to be transcribed from transposable elements or other types of inverted repeats in eukaryotic cells[20]. There is an intrinsic antiviral nature associated with the RNAi pathway in fungi, plants, and invertebrates[2,6,9]. siRNAs are exogenous molecules, double-stranded, either derived from infecting pathogens or artificially introduced into the cells, and are processed by DCL enzymes[5]. It has been known that plant cells encode different DCLs. In Arabidopsis, the enzyme DCL4 is an important enzyme in the siRNA

pathway against positive-stranded RNA viruses[1]. On the other hand, DCL3 is known to have a role in long-distance silencing, while all known DCL enzymes (1-4) are known to possess an antiviral role against DNA viruses known to infect plants, for example, Cauliflower mosaic virus (CaMV)[31].

DCL4 has been implicated in cleaving viral dsRNA into small viral RNA molecules, which are also known as siRNA, which are between 21-23 nt in length with 2 nt overhangs on the 3' end. This processing event occurs in the cytoplasm[5,32]. The siRNA will then interact with the RISC and activates it, where the endonuclease AGO2 component of the RISC cleaves the passenger strand, which is the sense strand of the duplex, while the 'guide' *strand* (the antisense strand) remains associated with the RISC, and subsequently guides it to the target mRNA, where cleavage takes place by AGO2[16,33] (Figure 1.1). The selection of the RNA strand to act as a guide is usually governed by the thermodynamic profile of the RNA duplex termini[34,35]. The guide strand of the siRNA duplex is fully complementary to the target mRNA, and thus causes specific gene silencing[36]. The extensive pairing between the siRNA and mRNA target results in the cleavage of one phosphodiester bond in the target mRNA, this occurs usually between the 10th and the 11th nucleotide[35]. siRNAs are also expressed endogenously by plants and invertebrates[4]. A special feature of the silencing pathway involving siRNA in plants, fungi, and *C. elegans* is the ability to amplify the silencing signal, which leads to silencing along the target gene of interest[37]. The host-encoded RNA polymerase can produce dsRNA duplexes that can help amplify the siRNA silencing process, resulting in secondary siRNA molecules[38].

The siRNA interference pathway does play a role in mammalian cells, where the antiviral RNAi function is highly conserved. Mammalian host cells can produce abundant viral siRNAs, which are usually associated with viral infection, specifically positive and negative strand RNA

viruses. Studies published in 2013, were one of the first pieces of evidence for the production of viral-derived siRNAs during infection of mammalian cells by positive RNA viruses, Nodamura virus (NoV) and encephalomyocarditis virus (EMCV)[36,39]. The virus-derived siRNAs (vsiRNAs) targeting EMCV were detected in infected mouse embryonic stem cells (mESCs). Additionally, baby hamster kidney 21 cells (BHK-21), and newborn mice have been shown to produce viral-derived siRNAs in response to infection with NoV virus. Deep sequencing of small RNAs (sRNA-seq) from mammalian cells infected with NoV and EMCV revealed that small RNAs in the 21 nt to 23 nt range are the most abundant in response to NoV and EMCV infection. Small RNAs of 21 nt to 23 nt in size are typically in the range of Dicer products. These findings indicate that infection of mammalian cells by RNA viruses triggers Dicer processing of viral dsRNA[35,36].

In more recent reports, Dicer processing of vsiRNAs in mammalian cells, specifically human 293 cells has been reported[15,40]. Upon infection with either Influenza A virus (IAV) or Human Enterovirus 71 (HEV71), an increase in viral-derived siRNAs has been reported, specifically in cell lines not expressing viral suppressors of RNA silencing (VSRS)[15,40]. Additionally, accumulation of vsiRNAs has been reported in monkey Vero cells and human alveolar basal epithelial cells (A549) upon infection with VSRS deficient IAV. Similarly, upon infection with VSRS-deficient mutant HEV71, an increase in accumulated vsiRNA has been reported in primary murine lung fibroblasts (MLFs) and newborn mice[15]. Together these published data show the potential of RNA viruses to trigger the production of vsiRNAs in mammalian cells, suggesting Dicer dependent conserved mechanism responsible to produce siRNA in response to RNA viral infection[15].

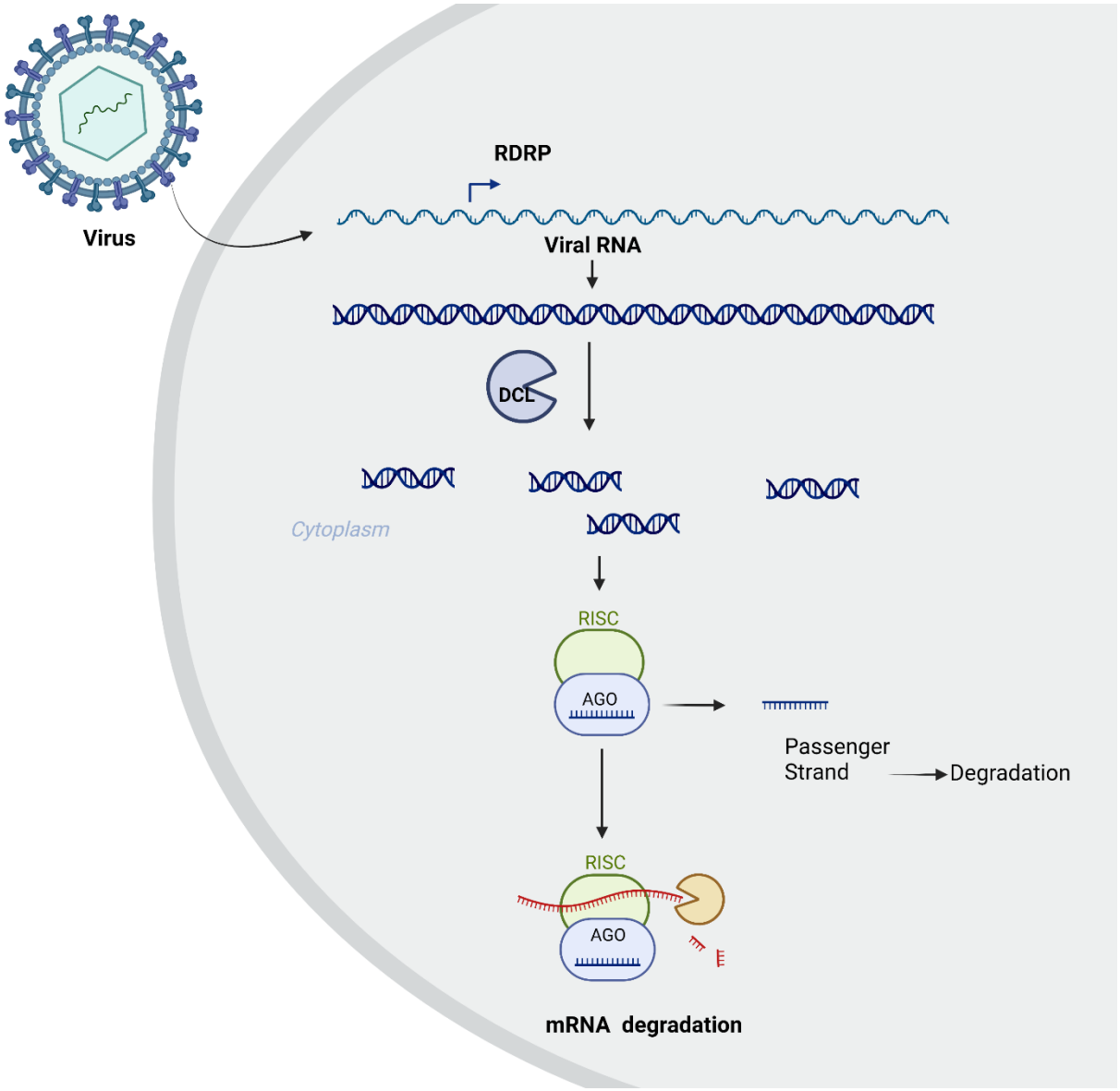

Figure 2.2. siRNA Interference pathway. RNA silencing is triggered by the accumulation of dsRNA, which can be due to an infection by a virus. Single-stranded viral RNA is replicated to form double-stranded RNA, which is cleaved further by dicer-like enzymes into small RNA duplexes (siRNAs) generally characterized by short length, 3' 2nt overhangs, and 5' phosphate groups. The small RNA duplexes are then loaded onto the RISC which unwinds the duplex and uses the guide stand to target complementary mRNA for degradation. Created with Biorender.com.

1.2.3 microRNA Biogenesis and the RNA Silencing Pathway

The first miRNA, which was discovered in 1993 by Ambros and Ruvkun group, *lin-4*, was found in *Caenorhabditis elegans*, and has revolutionized the field of molecular biology[41,42]. It was discovered then that *lin-4* is not a protein-coding RNA but a small non-coding RNA. New miRNAs are still being discovered and it is evident that they play an instrumental role in gene regulation. miRNAs are small non-coding RNAs, that are around 22 nt in length. Generally, miRNAs are transcribed from DNA sequences by RNA polymerase II as a large system loop RNA known as primary miRNAs (pri-miRNAs), then they are further processed in the nucleus by an RNase III-like enzyme, known as Drosha (in mammals and invertebrates) or DCL1 (plants), into precursor miRNAs (pre-miRNAs). Finally, the pre-miRNAs are further processed by Dicer or DCL enzymes into approximately 21 nt mature miRNAs. In contrast to siRNAs, miRNAs are endogenous RNAs, encoded by their distinct genes, within single or clustered transcriptional units[41].

Like siRNAs, miRNAs are assembled into the RISC, which consequently, guides them to the target mRNA for gene silencing[30] (Figure 1.2). Computational modeling and algorithms that combine comparative sequence analysis and thermodynamic modeling of RNA-RNA interactions are usually utilized to predict the miRNA target sites in the genome of eukaryotic organisms[13]. Most plant miRNAs target coding sequences by extensive sequence complementarity[14,38,43]. On the other hand, mammalian miRNAs are only partially complementary, where their mRNA targets can have mismatches and gaps. The binding specificity is mainly dictated by 7 nt of the 21 nt miRNA, usually nt number 2-8 in the 5' end, usually referred to as 'seed site' or 'seed sequence'. This region of complementarity allows a given miRNA to regulate an abundance of potential target mRNAs within the genome, thus being described as 'master regulators of gene expression'[29,44,45]. The majority of interactions between miRNA:mRNA in animal cells are not fully complementary,

and thus AGO2 can act as a mediator of RNA interference, rather than an endonuclease[11]. Therefore, miRNA-programmed RISC can induce not only RNA degradation, but also can promote translational inhibition, or accelerated deadenylation, which depends on the degree of base complementarity to the target mRNA[11]. The formation of miRNA-mediated RISC (miRISC) gets initiated with the recruitment of the GW182 family of proteins, which provides the scaffolding to recruit other effector proteins, such as polyadenylase complexes (PAN2-PAN3), which initiates deadenylation[46]. Subsequently, decapping enzymes get recruited, specifically decapping protein 2 (DCP2)[47] and associated proteins, followed by endonuclease activity by exoribonuclease 1 (XRN1), where degradation occurs from the 5'-3' end[48]. In general, the biogenesis of miRNAs is classified into two distinct categories: canonical biogenesis pathway and non-canonical biogenesis pathway. The canonical biogenesis pathway is the main, dominant pathway by which miRNAs are processed[3].

Given miRNA's role as posttranscriptional repressors of gene expression, their activities have been linked to normal development and physiology, disease, and evolution[10,14,19,27,28,46]. They participate in almost all cellular processes, thus dysregulation in their expression and function has been linked to plant, mammalian, and invertebrate pathologies, such as viral infections and diseases such as cancer[28,44,49–54]. Thus, it is instrumental to recognize they do possess therapeutic potential similar to siRNAs, where their regulation can present novel therapeutic methods to alter gene expression or modify the pathogenesis of either infectious diseases or endogenous, metabolic diseases.

Figure 2.3. miRNA biogenesis and the RNA silencing pathway. miRNAs arise through transcription in the nucleus to produce primary miRNAs. Pri-miRNAs are then converted to stem-loop pre-miRNAs by nuclear enzymes Drosha. Pre-miRNAs are exported to the cytoplasm by the nuclear receptor exportin-5 and converted to mature miRNAs by Dicer enzymes. The mature miRNAs can enter the RNA silencing pathway. Created with Biorender.com.

1.2.4 Role of Small RNAs and the RNA Silencing Pathway in Viral Infections

The RNA silencing pathway acts as the plant's first line of defense and innate immune system against invading viral pathogens. This basal antiviral response relies on the recognition of the ds viRNA (or viral-derived siRNAs). This discovery occurred accidentally during an attempt to engineer virus-resistant plants[55]. Studies of transgenic plants that were initially susceptible to infection by tobacco etch virus (TEV), subsequently became resistant to infection by homologous viruses. These were some of the first pieces of evidence of the protective role of the RNA silencing pathway in plant cells[55]. A decrease in the levels of the transgene mRNA and the establishment of an antiviral state was evidence that the infecting virus induced a post-transcriptional gene silencing, which led to viral RNA silencing. Additionally, it has been shown that transgenes encoding a replication-competent viral RNA genome are inducers of the RNA silencing [56]. This idea explains why non-virus-derived genes have been silenced following infection of plants by recombinant RNA or DNA virus carrying a corresponding gene[56–59]. This technique has helped demonstrate what is known as virus-induced gene silencing (VIGS), which has been developed into a high throughput platform for functional genomics studies in several different hosts[18].

It has been demonstrated that host plants that were compromised in RNA silencing possess enhanced susceptibility to viral infection. Vance *et al.* have shown that in *Arabidopsis thaliana,* AGO1 is essential for transgene-induced RNA silencing, and contributes to dsRNA production in this plant[18]. It has, additionally, been shown that mutants of *Arabidopsis thaliana* defective in these specified genes are more susceptible to viral infections[60,61]. This acts as evidence that functional RNA silencing is instrumental for plants' functional immune response against viruses. Perhaps the strongest support for a naturally occurring antiviral role of the RNA silencing pathway in plants is

the encoding of viral suppressors of RNA silencing by plant viruses, which will later be discussed in more detail in this chapter.

There has been evidence for the production of vsiRNAs during infection of mammalian cells as discussed earlier in this chapter[15,39,40]. It has been shown that EMCV, HEV71, NoV, and IAV trigger the production of abundant vsiRNAs in cultured mammalian cells or newborn mice, which suggests Dicer-dependent production of vsiRNA in response to RNA viral infection. Additionally, transgenic tobacco plant-derived siRNAs were shown to suppress the propagation of influenza A virus subtype H1N1 in mammalian cells[17].

It is, however, clearer that mammalian viruses have complex interactions with the endogenous miRNA pathway in mammalian cells. These virus-host interactions underscore the importance of the RNA silencing pathway in viral invasion and persistence in mammalian cells. It has been evident that host-encoded microRNAs can modulate the antiviral defense mechanism during viral infection. Some mammalian viruses have been shown to encode viral miRNAs (v-miRNAs), to evade the host immune response. The first v-miRNAs were identified in the Epstein-Barr virus (EBV)[62]. More than 250 v-miRNAs have been identified, which are mostly accounted for in DNA viruses such as *herpesvirus* [63]. On the other hand, there have not been many reports describing the detection of v-miRNAs in RNA viruses, and thus it has been more controversial. A few reports have, however, suggested the expression of non-canonical miRNA-like small RNAs during RNA virus infection, but they lack the canonical stem-loop structure found in RNAs[64,65].

Endogenous cellular miRNAs have been shown to interact with mammalian viruses, and thus contribute to either a pro-viral or antiviral state in the cell. Induction of some cellular miRNAs could help the virus evade the host immune responses by suppressing Interferon-α/β (IFN-α/β) signaling pathway while others could upregulate IFN-α/β production and inhibit the viral infection.

One of the earlier examples of the antiviral endogenous miRNA response is miR-32, which has been reported to effectively restrict primate foamy virus type I (PFV-1) replication by directly targeting the viral genome[66]. There has also been evidence that shows the ability of miRNAs to directly bind the viral genome, resulting in enhanced viral genome stability and translation, thus creating a pro-viral state. One of the most notable examples of such effects is miR-122, a liver-specific miRNA that contributes to the Hepatitis C virus (HCV) tropism[67]. miR-122 binds the HCV genome and forms an oligomeric complex that leads to the stabilization of the genome. It has also been reported that miR-122 binding protects the viral genome from nucleolytic degradation in liver cells[68]. Like plant viruses, there has been increasing evidence that mammalian viruses do express VSRS, further highlighting the role of the RNA silencing pathway in viral infections. For instance, the capsid protein of rubella virus (RuV) acts as VSRS by suppressing siRNA-induced RNAi in mammalian cells[69]. There are several validated suppressors of the RNA silencing pathway including B2 of Nodamura virus, NS1 of IAV, 3A encoded by enterovirus-A71, and NS2A of Dengue virus[70]. All the mentioned VSRS enforce their mechanism by sequestering the dsRNA. Other mammalian viruses have been found to encode their own VSRS, thus underscoring that suppressing the RNA silencing machinery is advantageous to the virus and emphasizing the role of small RNAs and the RNAi as an important regulator of viral infection and persistence in mammalian cells.

1.3 Viral Suppressors of RNA Silencing Pathway

Several VSRS have been identified in almost all plant virus genera, and mostly no obvious sequence similarity has been identified between these VSRS. These VSRS have been shown to inhibit the host antiviral response, which was achieved by interacting directly with proteins involved in the cellular silencing machinery[71]. All plant viruses and some mammalian viruses have been shown to express VSRS[36,72]. VSRS have been shown to employ different mechanisms that interfere with the host's silencing pathway. It has been demonstrated that some of the identified VSRS interfere directly with the silencing machinery of the host plants. Some of these VSRS are p38 expressed by *Turnip crinkle virus* (TCV), 2b expressed by *Tomato aspermy virus,* and p14 expressed by *Pothos latent virus* (PoLV)[73]. P38 mediates its function by interacting directly with AGO-1, through GW motifs[73,74]. On the other hand, 2b interacts directly with AGO-1 through its PAZ domain[75]. These VSRS were shown to also inhibit the formation of the RISC by interacting directly with AGO proteins[73–75].

Several other plant viruses VSRS have been identified to exert their activity by preventing RISC assembly. Such VSRS have been shown to target siRNAs or miRNAs. One of the most common strategies is dsRNA (specifically siRNA) sequestration[71,76–78]. One of the best-known and studied VSRS is the p19 protein of *tombusviruses.* p19 prevents the RNA silencing by sequestering ds siRNAs with high affinity, thus inactivating their functions[79,80].

VSRS, in addition to having an important function in plant viruses, are expressed by mammalian viruses as well, further emphasizing and underscoring the role of the RNA silencing pathway as an antiviral mechanism in mammalian cells. Cell culture assays have assisted in identifying one of the first VSRS in mammalian cells. B2 protein of NoV and NS1 of IAV were one of the first identified VSRS of mammalian viral origin. B2 is a potent suppressor of AGO-2-

dependent antiviral RNAi in *Drosophila* and mosquito cells[81–83]. Influenza NS1 was shown to potently suppress Dicer-mediated vsiRNA biogenesis during IAV infection[15]. Dengue virus (DENV) has also been shown to encode its own VSRS. DENV2 is a mosquito-transmissible enveloped virus of the genus *Flavivirus* in the *Flaviviridae* family[70,84]. By screening the seven structural proteins of the virus, it has been shown that the nonstructural protein NS2A exhibit VSRS activity. It has been identified as a dsRNA binding VSRS, even though it does not share sequence specificity with B2 of NoV or NS1 of IAV. It acts to suppress dicer processing by binding long dsRNA[85].

EV-A71 is a nonenveloped positive-strand RNA virus of the genus *Enterovirus* in the *Picornaviridae* family, which includes many important human and animal pathogens such as poliovirus. A set of experiments has demonstrated that one of the structural proteins of EV-A71 acts as a VSRS. Protein 3A has been confirmed to function as a VSRS and promotes infection both *in vitro* and *in vivo.* Similar to DENV2's NS2A, P3 is a dsRNA-binding protein that suppresses Dicer processing by directly sequestering long dsRNAs[40]. VSRS play an important role in the antiviral mechanism of both plant and mammalian cells. Therefore, their ability to bind RNA can be exploited to engineer tools to further study the RNA silencing pathway and probe potential protein-RNA interactions.

1.3.1 The Viral Suppressor of RNA Silencing p19

p19 is a VSRS that is expressed by tombusviruses. Tombusviruses are positive-sense single-stranded RNA viruses. They possess a linear monopartite genome containing five open reading frames (ORFs). ORF5 encodes p19, a 19-kDa protein. p19, when expressed at high levels, allows systemic invasion of plant cells. p19 was first identified as a tombusviral virulence factor, suggesting that it plays a role in overcoming host defense mechanisms [80,86,87]. Interestingly, p19

was shown to restore GFP expression in post-transcriptional gene silencing (PTGS)-inactivated transgenic plants, specifically in the newly emerging leaves[88]. In the absence of p19, cymbidium ringspot tombusvirus (CymRSV) infection results in a PTGS-associated recovery phenotype, further supporting the role of p19 in PTGS suppression[87]. A crystal structure of Carnation Italian ringspot and tomato bushy stunt virus bound to a siRNA complex helps explain its unique function of blocking the RNA silencing process[72,89]. p19 is known to exert its function by binding and sequestering small RNAs, where it prevents its incorporation into the RISC[89–92]. p19 competes with AGO proteins, however, it does not affect or bind small RNAs already loaded onto the RISC[93]. siRNA:p19 interactions were found to be reversible, and characterized with a dissociation rate constant of ($k_{off} = 0.062 \pm 0.002\ s^{-1}$)[94]. It was also observed that p19 efficiently competes with recombinant Dicer in mammalian cells, where inhibition of RISC is observed. Computational studies have confirmed that there is a formation of a ternary complex between human Dicer, siRNA, and p19[94].

Crystal structures and molecular dynamic stimulations show that p19 binds siRNAs as a homodimer, where it binds a single siRNA duplex in a positively charged surface cleft[95]. Pairs of tryptophan residues (W39 and W42) allow for π stacking interactions with the terminal base pairs of the bound siRNA molecule. The N-terminal helices of p19 clasp the edges of the duplex, with the tryptophan residues providing the stacking interactions[72,89] (Figure 1.3). Mutation of these two tryptophan residues was shown to greatly reduce RNAi suppression in *N. benthamiana* plants due to decreased binding of siRNA[89]. This binding characteristic allows for the dimer to establish a sequence-independent caliper-like size selection of the siRNA duplex, where the 8-stranded β-sheet forms a binding surface, where interactions with the small RNA backbone are achieved through electrostatic interactions [72,89]. The size selection involves siRNA duplexes of around 19

bp and 2-nucleotide-long 3' overhangs, and 5' phosphate groups[72,89]. Sequestration and binding of Dicer generated siRNA by p19 has been associated with reduction of viral RNA degradation, sustainability of viral phenotype post infection, and systemic symptom spread; further emphasizing the pro-viral role of p19[76,93,96].

Electrophoretic mobility shift assays (EMSAs) have helped determine the affinity of the dimeric p19 for siRNA duplexes. The apparent equilibrium dissociation constant of p19 was first determined by Vargason *et al.*to be K_D= 0.17±0.02 nmol/L[89], which is the highest reported affinity of a protein to siRNA duplexes to date. This affinity is reduced for siRNA duplexes that are longer or shorter than 19-22 nucleotides in length[94].

Interestingly, however, p19 has been shown to bind miRNAs, of approximately 21 nt in length, with high affinity[97–99]. p19 was shown to significantly reduce the levels of liver-specific miR-122 upon adenoviral delivery of p19 into Huh7 human hepatoma cell line[100]. Our laboratory has also been successful in further engineering p19 to exhibit a higher affinity towards miR-122, through mutational analysis of the p19 binding surface to create p19 mutants with an enhanced affinity towards miR-122[101]. Additionally, p19 was shown to induce the expression of some miRNAs that help reduce the levels of AGO1 in plants by targeting its mRNA for degradation and thus leading to an overall suppression of the RNA silencing pathway independent of the binding of siRNAs[102]. Expressing an inactive mutant of p19 (p19-3 M VSRS) can induce miR-168 levels, thus controlling the accumulation of AGO1, where it has been shown that this accumulation is related to enhanced accumulation of viral RNA, thus leading to antiviral activity. miR-168 was shown to target the mRNA of AGO1[102].

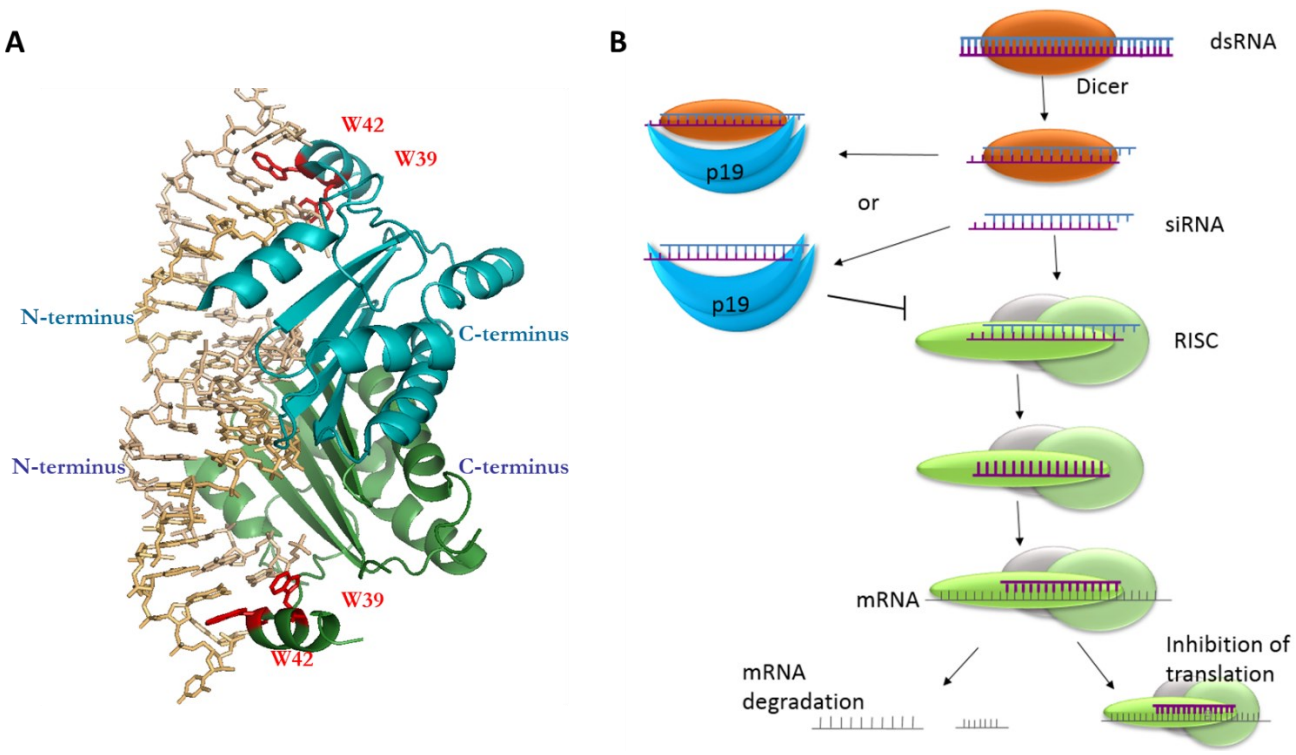

Figure 2.4. p19 and its suppression of the RNA silencing pathway. (A) Carnation Italian Ringspot Virus's (CIRV) p19 while in complex with a 21 nt siRNA. p19 binds siRNA in a sequence-independent manner. It functions as a dimer that clasps the ends of the RNAs using the end-capping interaction provided by the conserved tryptophan residues (W39 and W42 highlighted in red). (B) p19 sequesters viral-derived small RNAs and prevents them from getting loaded onto the RISC. **(PDB: 1RPU)**

1.3.2 p19 as a Tool to Study the RNA Silencing Pathway

Due to its unique binding characteristics to small RNA molecules, p19 has been used extensively to probe the RNA silencing pathway in different hosts and cell types. p19 has been used to study the RNA silencing pathways in Drosophila. In a study by Fagegaltier *et al.* p19 and its nuclear form (p19-NLS) expressed in Drosophila somatic cells were found to sequester transposable elements (TE) derived siRNAs, and thus suppressed the silencing of heterochromatin gene markers in adult flies[90]. Additionally, expressing p19 is linked to suppressing and altering histone H3-k9 methylation and chromosomal distribution of histone methyl transferases in larvae[90].

In plant cells, p19 has been used to interrogate the RNA silencing pathway. Nuclear expression of p19 in plants has provided the first evidence of nuclear processing of both siRNA and miRNAs. It has been demonstrated that expressing p19 prevents both siRNA and miRNA RISC loading onto AGO1, underscoring its role and ability to sequester both miRNAs and siRNA, which is unique to p19 in comparison to other VSRS[103]. More recently, In *Tombusvirus*-infected plants, p19 was shown to affect the levels miR-162, miR-168, and miR-403, which are known to regulate the expression of DCL1, AGO1, and AGO2 respectively[104]. The study suggests that differential binding of p19 to miRNAs is a widespread viral mechanism to modulate gene expression of endogenous genes in plant cells[104]. p19 was also found to prevent miRNA loading onto the RISC when systemic *in planta* analysis was conducted[105].

Transgenically expressing p19 was shown to inhibit miRNA methylation in *Arabidopsis* plants[106]. HUA ENHANCER1 (HEN1)- dependent methylation of the 3'-terminal nucleotide is a crucial step in plant miRNA biogenesis. p19 was demonstrated to bind and interfere with the methylation event. p19 could be used as a tool to study when and where the methylation process occurs[106]. On the other hand, interactions with some plant proteins can lead to the decrease of

p19's functions[107]. Depending on the host plant species, plant ALY proteins, a family of RNA binding proteins required for nucleo-cytosolic mRNA transport and modulate plant growth and development, could be expressed endogenously, leading to a decrease in p19's function as a VSRS. Canto *et al*., have demonstrated that p19's interactions with plant ALY proteins, led to its localization to the nucleus, and interfered with its ability to suppress the RNA silencing pathway[107].

p19 has been used to further study the role of RNA silencing as an anti-viral mechanism in mammalian cells. p19 has been shown to maintain its silencing activity in mammalian cells, where its RNA binding ability is directly related to the positively charged residues in the RNA binding interface[108]. p19 was demonstrated to maintain its activity in several mammalian cell types including HEK293T, HeLa, and mouse embryonic fibroblasts[108].

p19 was used to characterize short RNAs in mouse embryonic stem cells (ES)[109]. p19 was utilized to immunoprecipitate short RNAs from ES cells. The immunoprecipitated RNA have shown matches for ribosomal RNA (rRNA), which provides insight on the ability of p19 of binding other species of RNA, which aren't canonical as they are longer (32-35 nt). This study has demonstrated that mouse ES cells do not express abundant siRNA, and thus in the absence of canonical ligands, p19 can still bind other RNA species[109]. It is important to note that, even though they can bind these RNA species, it is associated with a decrease in binding affinity in comparison to its canonical substrates[109].

p19 was shown to function in hepatocellular carcinoma cell lines[110]. A study by Chen *et al.* has demonstrated that p19 from tomato bushy virus is fully functional upon transfection of HepG2 cells. When expressing p19 in mammalian HepG2 cells, the function of short hairpin RNAs (shRNAs) targeting GFP was suppressed[110]. Other hepatocellular carcinoma cell lines were also

successfully utilized to study the potential of using p19 as a suppressor of RNA silencing in mammalian cells. Upon combining the expression of p19 with small molecules that target the RNA silencing pathway in human hepatoma cells (Huh7), enhanced inhibition of the RNA silencing pathway was observed[91]. This further validates the potential of p19 to be used as a tool to study the RNA silencing pathway in other cellular models than plant cells.

Additionally, p19 has been expressed in Hek293T human cells to further study the pathogenesis of the PFV-1. It was demonstrated that upon ectopic expression of p19 in viral infected HEK293Ts, viral accumulation was observed, suggesting the importance of cellular miRNAs as an antiviral mechanism against PFV-1. p19 has aided in further emphasizing the role of specific cellular miRNAs in restricting the accumulation of PFV-1[66]. Conversely, when transiently expressing p19 in HIV-1 infected HEK293T cells, only a modest, but statistically significant accumulation of HIV-1 was observed[111]. Given the evidence of successful utilization of p19 to probe the RNA silencing pathway in mammalian cells, it is possible to further engineer p19 to explore its potential of being utilized as a tool to target small RNAs that may have a role in viral pathogenesis or metabolic diseases.

1.3.3 p19 as Tool in Biotechnology

Biotechnological tools have been applied in modern agriculture to control problems associated with plant virus diseases and resistance. The RNA silencing pathway is usually the main antiviral mechanism in plants that is usually enhanced to ensure viral resistance[112]. The RNA silencing pathway is also involved in response to ectopically expressed genes introduced in plants, which is usually introduced through viral vectors or agroinfiltration, allowing for higher yields in recombinant protein production in comparison to transient gene expression[113,114]. Plants have been used extensively for recombinant protein production including biologics such as antibodies and

vaccine[31,115–118]. In more recent years, deconstructed viral vectors have allowed the usage of plants as a platform for recombinant protein production, due to their speed, low cost, and easy scalability[31,115–118]. The RNA silencing pathway has however been shown to be problematic when attempting to express foreign genes in plants; thus, inhibition of the RNA silencing pathway has been an accepted strategy to enhance recombinant gene expression.

p19 was used to enhance the production of therapeutic antibodies in plant cells. A study by Garabagi *et al*. has demonstrated the successful enhancement in the levels of therapeutic antibodies produced in *Nicotiana tabacum* upon co-expression of p19[114]. Co-expression of p19 was used for antigen production for vaccine development. Expressing p19 along with anthrax receptor decoy protein (immunoadhesin), CMG2-Fc (which is used for vaccine production against anthrax) in *Nicotiana benthamiana* was shown to enhance its production[119]. Additionally, high expression of HIV-1 Nef protein was obtained upon co-expression of p19 in *Nicotiana benthamiana*[120]. Similarly, p19 was used to enhance the production of SARS-CoV Nucleocapsid protein in *Nicotiana benthamiana*, for plant-based vaccine production[121]. Inhibition of RNA silencing in plants using p19 has added to enhanced gene editing via clustered regularly interspaced palindromic repeat (CRISPR)-associated protein 9 system (Cas9) systems, in addition to enhanced viral vector delivery of both guide RNA and Cas9 CRISPR genes[122,123].

1.3.4 p19: A Tool for RNA Detection and Delivery

Due to p19's unique RNA binding potential, further utilization and engineering of the protein have been employed to use it as a tool for small RNA detection and diagnostics. miRNAs are abundant in mammalian cell types and as extracellular circulating RNA[3,29,124–126]. Like cellular miRNAs, circulating miRNAs can be indicative of disease[127–134]. Circulating miRNAs are usually released into body fluids such as blood and cerebrospinal fluid and can potentially act as diseased state

biomarkers[127–134]. Thus, detection methods to identify miRNAs are constantly being developed as potential diagnostic tools[135]. Since miRNAs are potent regulators of gene expression, even small changes and dysregulation in their expression have been linked to diseased phenotypes.

Recombinant p19 has been applied as a method to detect miRNAs. Since p19 possesses a high affinity towards miRNAs, it allows detection of miRNAs in samples; specifically, samples containing lower concentrations (example, extracellular biofluids). Since overexpression of p19 is possible in various cellular systems with high yields, it makes it an available tool to further engineer to bind small RNAs for detection purposes, specifically because the protein's ability to bind its ligands was unaffected upon introduction of a variety of gene fusions and modifications. A bifunctional p19 fusion probe has been previously designed with an N-terminal maltose binding protein (MBP), and a C-terminal chitin-binding domain (CBD) to bind p19 to chitin magnetic beads[136]. Even though both N-terminal and C-terminal modifications were introduced to p19, it did not affect its ability of detecting and binding miRNAs. p19 was engineered to detect radioactive miRNA probes in the sub-femtomole range, and the presence of a million fold-excess of total RNA[136]. Additionally, p19 has been further engineered as a magnetosensor for the detection of synthetic RNA targets and endogenous miR-21 from total RNA extracted from cancer cells and human breast-tumor specimens in the sub-femtomole range[137]. This opens the potential of utilizing p19 for the diagnosis of human cancers known to exhibit differential miRNA expression. Electrochemical biosensors based on p19 have also been developed to detect miR-21[136]. Changes in the oxidation signal of tryptophan residing in the binding cleft of p19 were used for the detection of miR-21 with high sensitivity in the picomolar range. This shows that Differential Pulse Voltammetry (DPV) can be utilized to detect the intrinsic change in p19 oxidation signals upon RNA ligand binding[136]. Other methods employing p19 for RNA detection have been developed.

miR-122 has been detected and quantified from small RNA isolates of hepatoma cells, where RNA probes were immobilized on gold surfaces, and miRNA-bound probes were further detected using p19 coupled with a rapid enzyme-linked immunoassay to increase the sensitivity of the assay[138]. Khan *et al.* has utilized p19 to develop a protein-facilitated affinity capillary electrophoresis (ProFACE) assay for rapid quantification of miRNA levels in blood serum using p19 as a separation enhancer[139]. The addition of p19 has allowed enhanced separation of single-stranded RNA probe and double-stranded p19-bound RNA probe, which consequently allowed sensitive detection in the femtomolar range[139].

Fluorescence-based RNA detection methods based on p19 have as well been developed in which Förster resonance energy transfer (FRET) was used to detect the binding of fluorescently-tagged siRNA. Koukiekolo *et al.* have demonstrated the ability to fuse p19 to a cyan fluorescent protein (CFP), to detect Cy3-tagged siRNA using FRET. This shows the tolerance of p19 to protein fusions and the ability to further engineer it to detect RNA using FRET[140].

p19 has as well been engineered as a delivery tool for small RNA molecules. One of the more challenging caveats of RNA therapeutics is cellular delivery. Therapeutic applications of siRNA for example have been limited due to rapid enzymatic degradation and poor cellular uptake. Nanoparticles hold promise for safe and effective delivery of RNAi-based molecules, however, physiological barriers and systemic toxicity remain a challenge associated with such molecules[141,142]. Various non-viral siRNA delivery have been developed including lipid-based systems and cationic peptides[143–145]. Some of these strategies include the utilization of p19 due to its unique RNA binding capabilities. For instance, Choi *et al.,* have synthesized a genetic RNA carrier based on p19, by fusing p19 to an ephrin mimetic peptide, YSA[146]. p19-YSA fusion protein was shown to deliver complexed siRNA specifically to tumor cells expressing EphA2 receptor,

leading to specific targeting, and emphasizing how p19 can be used for targeted delivery by fusion to a variety of cationic peptides[146]. Additionally, our lab has demonstrated that fusion of p19 to HIV-1 transactivator of transcription (TAT) peptide can act as an RNA delivery system for the efficient delivery of complexed siRNA in human hepatoma cells, with potent and sustained gene knockdown activity with no associated toxicity[147].

In addition to the development of p19 as a delivery tool, it has been engineered to possess enhanced and improved functionality. Recombinant p19 has been designed to possess higher thermal stability by linking the two monomers with a $(GGGGS)_2$ flexible linker, where there was an enhanced binding affinity of 3.5 fold observed in comparison to wt p19[148]. Systemic testing of the functional roles of cysteine residues on the surface of p19 through site-directed mutagenesis has highlighted that mutating C110, C134, and C160 to isoleucine has led to the increased thermostability of the dimer without compromising its RNA binding affinity and made p19 less sensitive to oxidizing environments[149]. Furthermore, additional mutagenesis studies can be conducted to improve p19's ability to bind specific miRNAs of interest. To develop new tools to study endogenous miRNAs, mutational analysis of p19's binding surface was performed to improve p19's binding affinity towards miR-122, without compromising its ability to bind siRNA[101]. Site-directed mutagenesis of a single residue in position T111 in the p19 dimer (which is near the miR-122 mismatch bulge) has improved the affinity of p19's binding towards miR-122 by 50 fold[101]. This shows that mutational analysis of p19's binding site can allow for enhanced binding towards a variety of miRNAs, based on the miRNA's base-pair mismatch locations.

Expanding on p19 functions and improving its RNA binding ability through protein engineering can help provide a unique tool for small RNA control and sequestration *in vivo* and *in*

vitro. Broader applications of p19 can be uncovered through further engineering efforts to improve its already existing functionality, including improving its ligand specificity.

A unique engineering tool that can be explored to improve p19's functions with minimal perturbations in its already existing RNA binding affinity, is genetic code expansion technology or the use of unnatural amino acids to fine-tune p19's functionality. Genetic code expansion tools will be further discussed in the following section.

1.4 Protein Engineering and Genetic Code Expansion

Unnatural amino acids (UAAs) offer the possibility to expand beyond the 20 naturally occurring amino acids in most species and install new and useful chemical functions[150]. UAAs have enabled site-specific incorporation of new and unique chemical functions into proteins of interest. UAAs allow the introduction of new and useful chemistries including fluorescence, ligand binding, crosslinking, and photo-caging with minimal to no perturbations to the protein's folding and structure[150–154]. Chatterjee and Shultz *et al.* have provided conceptual advances in the engineering of orthogonal aminoacyl-tRNA synthetase (aaRS)/ tRNA pairs that allow the site-specific incorporation of UAAs in living cells[155]. The evolution of bioorthogonal aaRS enzymes that can bind the UAAs and their unnatural tRNAs, while not interacting with naturally existing amino acids or tRNAs is unique[156]. The unnatural tRNA recognizes a unique stop (most commonly an amber stop codon), quadruplet base pair, or a frameshift codon[157]. In a typical amino acid incorporation experiment, the unnatural amino acid is added to the cell and the engineered, orthogonal aaRS recognize the UAA and is used to aminoacylate the orthogonal tRNA. An orthogonal tRNA is not a substrate for endogenous synthetases but is specifically aminoacylated by the orthogonal synthetase and directs amino acid incorporation in response to the unique codon, which was introduced to the gene of interest via site directed mutagenesis techniques (Figure 1.4).

1.4.1 Development of Bioorthogonal aaRS/tRNA Pair

There have been four orthogonal aaRS developed for incorporation of UAAs through directed evolution techniques: the *Methanococcus janaschii* tyrosyl-tRNA synthetase (MjTyrRS)/tRNACUA pair[158], the *E. coli* tyrosyl-tRNA synthetase (EcTyrRS)/tRNACUA pair, the *E. coli* leucyl-tRNA synthetase (EcLeuRS)/ tRNACUA pair[159–161] and pyrrolysyl tRNA synthetase (PylRS)/tRNACUA pairs from certain Methanosarcina[159]. The active site of the

engineered synthetase needs to specifically bind the unnatural amino acid while being unable to bind canonical ones. The transfer of the UAA must be done onto its cognate orthogonal tRNA. Since the development of the aaRS is based on naturally occurring enzymes, the evolution process requires the evolution of the active site to bind the UAA while destroying its ability to bind its naturally occurring counterpart[156].

Typically, the directed evolution processes to develop the aaRS occurs in *E. coli* or yeast cells. There are several rounds of selection, usually positive and negative selection, used to select an active variant that allows the incorporation of the UAA of interest. The positive selection process relies on the ability of the aaRS/tRNA pair to facilitate read-through of the amber suppression codon in an essential gene (for example, an antibiotic resistance gene). The positive selection processes provide aaRSs in surviving colonies that can incorporate the UAA or a natural amino acid. The evolved aaRSs are then subjected to a round of negative selection in the absence of the UAA with an amber codon encoding a toxic gene, thus, evolved aaRSs that can incorporate natural amino acids are depleted and the read through of the amber codon will lead to cell death in the absence of the UAA[150,157,158]. After several rounds of positive and negative selection processes, only the evolved aaRSs that can selectively incorporate the UAA will survive. This methodology has been used to engineer aaRSs for more than 100 UAAs, however some limitations still exist due to a decrease of protein yields in comparison to natural counter parts[157].

A wide range of UAAs with functions not found in canonical amino acids have been genetically encoded over the past couple of decades and have delivered insights into biological processes that are generally difficult to access using traditional molecular biology techniques. Since the system is bioorthogonal, minimal perturbation to the cellular processes or the designed protein is observed. UAAs have allowed the production of unique proteins with site-specific metal

binding capabilities, photo-crosslinking and site-specific chemical modifications[153]. Given the advantages of this system, we are interested in utilizing this technology to further improve p19's ability as a VSRS and expand on its already existing functionality.

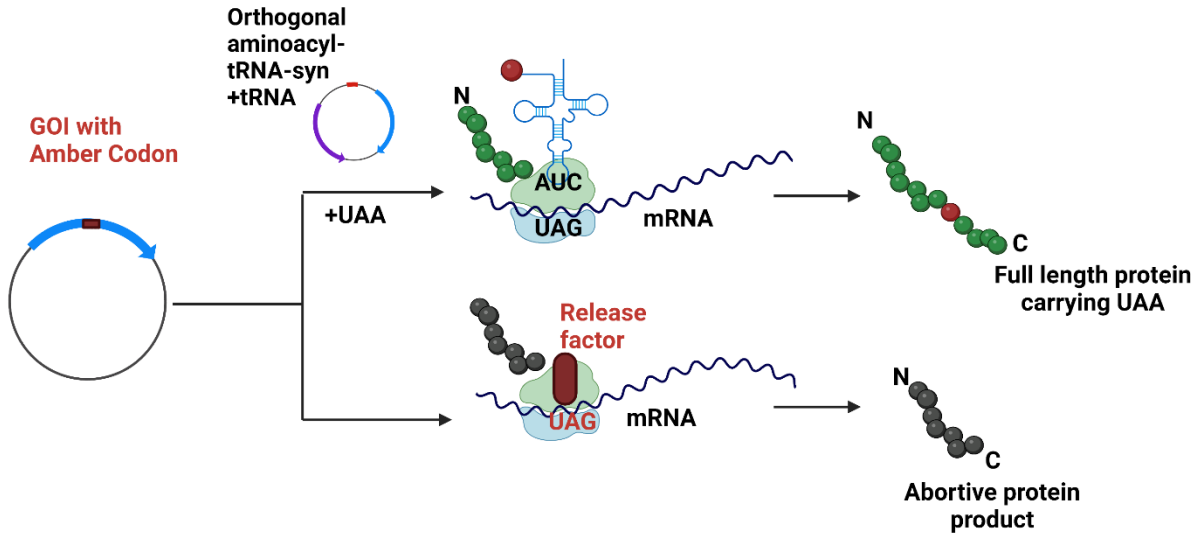

Figure 2.5. Incorporation of unnatural amino acids. Incorporation of UAAs occurs by the introduction of a rare codon in the gene of interest. Upon introduction of an orthogonal tRNA and aaRS which charges the tRNA with a specific UAA, the tRNA recognizes the reassigned codon (UAG here) and the UAA is added to the peptide. If the orthogonal tRNA and aaRS and the corresponding UAA are not introduced to the system, an abortive truncated produced is formed and the UAG will be recognized as a stop codon instead. Created with Biorender.com.

1.4.2 Chemical Modifications

Protein engineering through chemical modifications is an instrumental technique for protein labeling and selective addition of new chemical functionalities. Since canonical amino acids are limited in functionalities, concerning chemical reactivity, there is an intrinsic advantage to utilizing UAAs that permits the introduction of bioorthogonal reactivities, with great site selectivity and efficiency.

The use of UAAs has allowed the formation of covalent interactions/ linkages between proteins, and between proteins and small molecules. This has allowed for the creation of antibody-drug complexes[162]. Axup *et al.* have shown the potential value of UAAs in medicine compared to traditional methods, such as conjugation to cysteine or lysine residues. Site-specificity of UAA incorporation for chemical modifications allows for tight control that led to homogenous antibody-drug conjugates[162]. Additionally, UAAs have allowed for the site-specific incorporation of natural post-translational modifications into proteins of interest such as site-specific ubiquitination[163,164].

UAAs have also allowed for bioorthogonal reactions to occur in living cells site-specifically, where UAAs have been developed to include chemical handles such as tetrazine or azide moieties and thus eliminating bio-incompatible reagents[165–167]. The introduction of bioorthogonal chemical handles through UAAs has allowed for chemical conjugation with fluorescent tags onto proteins both *in vivo* and *in vitro*[165–167]. Several examples of these reactions have been demonstrated using UAAs. Some of the reactions include ketones/aldehydes with hydrazines /hydroxylamines, the classic copper-catalyzed azide-alkyne cycloadditions (CuAAC), the strain-promoted azide-alkyne cycloaddition (SPAAC), Staudinger ligation, some palladium-catalyzed cross-coupling reactions, photo-click reactions, and inverse-electron-demand Diels-Alder reactions. These chemoselective reactions exhibit rate constants in the order of 10^{-4}-10^{4} M^{-1} s^{-1} [152].

1.4.3 Improving Protein Functions

Improving the functionality or altering the specificity of pre-existing natural proteins has been the goal of protein engineering techniques. It took researchers many years to develop techniques that rely on random mutagenesis (i.e. directed evolution) which have led to desired functionalities in proteins.

Another method of improving proteins' functionalities is the incorporation of UAAs. The potential of UAAs in protein improvement has been established. The activity of nitroreductase towards non-native substrates was improved with a UAA, compared to any other canonical amino acid[168]. A 30-fold improvement of prodrug activator nitroreductase activity with a UAA was observed in comparison to that of the native active site and a more than 2.3-fold improvement over the best possible natural amino acid.

UAA incorporation has also been utilized to improve the functionality of bacterial phosphodiesterase by the introduction of (7-hydroxycoumarin-4-yl)ethylglycine[169]. This has improved its native catalytic function by 8-11fold. This study demonstrates that the introduction of designer amino acids can be used to enhance already existing functionalities in nature and can provide valuable information and functional space for the evolution of existing enzyme functions[169].

1.4.4 Azido-Phenylalanine Incorporation and Usage in Protein Engineering

An orthogonal aminoacyl tRNA synthetase/tRNA pair for *in vivo* incorporation of *p*-azido-L-phenylalanine (AzF) in *E. coli* has been reported by Chin et al. in 2002[170]. AzF contains a functional group not available in the 20 natural amino acids. The Aryl-azide group in AzF allows for site-specific incorporation of a photo-crosslinking functional group, which was first described as a photo-crosslinking agent in a biological context by Fleet et al. in 1969[171]. It has been

demonstrated that upon ultra-violet (UV) light irradiation at wavelengths below 310 nm, aryl-azides forms short-lived nitrenes that rearrange to form dehydroazepines, which react with amines to form covalent adducts [170,171]. Aryl-azides have been used as photo-crosslinking agents to probe protein-protein interactions, inactivate enzymes irreversibly and probe protein peptide interactions[171–174]. Therefore, site-specific incorporation of AzF into proteins opens an avenue to explore transient interactions and further probe protein interactions photo-chemically. Chin and coworkers have been able to develop and select an orthogonal aaRS/tRNA pair for the *in vivo* incorporation of AzF in response to an amber stop codon, TAG. The *Methanococcus jannaschii* tyrosyl-tRNA synthetase (Mj TyrRS) was utilized to engineer the orthogonal pair that specifically incorporate *p*-AzF, but not any of the 20 canonical amino acids, with high fidelity and efficiency. This study has opened the door to further use *p*-AzF in different living systems, including mammalian cells. *p*-AzF crosslinking has been used for a variety of applications in biotechnology. For instance, more recently, Li *et al.* have demonstrated that site-specific incorporation of *p*-AzF has enabled photo-crosslinking of vesicles composed of thermally responsive elastin-like polypeptide (ELP) fusion proteins for cargo/drug delivery to cells[175]. The cross-linked vesicles were shown to be more thermally stable, with a high potential for targeted drug delivery[175]. As mentioned previously, site-specific incorporation of AzF followed by photo-crosslinking has aided in identifying transient ligands and binding partners that might otherwise be more difficult to identify[176–179]. AzF photo-crosslinking has aided in the covalent capturing of low affinity or transient protein-protein interactions that would otherwise be lost when performing standard immunoprecipitation protocols. This UAA has also been used as a proximity sensor to reveal or map which positions in a protein are close to a binding partner in a complex [180–183].

In addition to the usage of AzF for photo-crosslinking applications, AzF had been extensively used for bioorthogonal chemistry applications due to the presence of the azide chemical handle. Click chemistry, a term introduced by K.B. Sharpless in 2001, describes a series of reactions that are high yielding, efficient, and bioorthogonal[184]. Azide functionalized molecules could react with phosphine-functionalized molecules, in a reaction described as Staudinger ligation[185]. Furthermore, azide functionalized molecules can react with terminal alkynes in a reaction known as CuAAC, and this reaction requires a Cu(I) catalyst as the name suggests. Additionally, a copper-free click reaction between an azide functionalized molecule and a strained alkyne (such a cyclooctynes) in a reaction known as SPAAC[186,187]. SPAAC is a non-toxic alternative to CuAAC as it does not require copper. SPAAC relies on the use of strained cyclooctynes that possess decreased activation energy in comparison to terminal alkynes and thus do not require an exogenous catalyst[188–190].

Due to click chemistry applications, AzF has allowed for site-specific fluorescent labeling of proteins for imaging, development of sensor proteins, bioconjugation of therapeutic molecules to proteins, and site-specific antibody conjugation of metal chelators for nuclear imaging and therapy, among other applications[191–194].

1.4.5 Bipyridinylalanine and its Use in Protein Engineering

Some of the interesting aspects of protein engineering are the ability to introduce catalytic functions into proteins. The introduction of catalytic or structural metal binding sites into proteins are of interest to provide and introduce new reactivity into peptides, recombinant proteins, and antibodies that can act as therapeutically relevant peptides[195]. Nature has created potent and diverse catalysts by using the natural canonical amino acids and cofactors as building blocks. Compared to natural amino acids, UAAs provide many more structural and chemical properties. By

incorporation of UAAs and non-native cofactors into a protein greatly enhance the ability to expand on the natural activity of an enzyme, and additionally design novel catalysts[196]. Some UAAs were developed to bind metal ions in a bidentate fashion making it possible to create cofactor binding sites[197]. UAAs with hydroxyquinoline, pyrazolylphenol, or bipyridine side chains were developed and have been incorporated into proteins. Their affinity to metal ions is much higher than native natural amino acids. Bipyridylalanine (BpyAla) is one of the first bidentate amino acids to be site-specifically incorporated into proteins[198]. The Schultz group has introduced BpyAla into *E. coli* catabolite activator proteins (CAP) which binds DNA in a sequence-specific manner. In the presence of copper, DNA cleavage was achieved[198]. In another example by Roelfes *et al.*, BpyAla was introduced in a site-specific manner in the interface of the dimer of the Lactoccocal multidrug resistance regulator (LmrR)[199]. Using LmrR as a scaffold where BpyAla was introduced, leading to copper chelation, the designed enzyme was able to catalyze Friedel-Crafts alkylation reaction with up to 94% substrate conversion[197].

BpyAla has as well been introduced in a site-specific manner to stabilize protein motifs. Luo *et al.* have used genetic incorporation of BpyAla into HIV gp41 to form a stable helical trimer that can chelate metals, leading to highly stable structures that can potentially serve as HIV vaccine candidates or inhibitors of viral entry[200]. This study shows the potential of utilizing BpyAla as a straightforward method to provide structural stability to motifs in recombinantly engineered proteins.

The introduction of BpyAla into enzymes has also provided dynamic control over their activity. Metal-responsive regulation of catalysis was achieved by the genetic introduction of BpyAla. Zubi *et al.* have successfully demonstrated that introduction of BpyAla into a serine protease and a firefly luciferase has affected their active conformations, leading to reversible

control of activity upon introduction of divalent ions[201]. Combining a computational analysis and molecular dynamic stimulations approaches to rationally pick residues for BpyAla incorporation has allowed the generation of enzymes with a 20-fold dynamic range in response to divalent ions. This shows the potential of combining UAA incorporation with computational, rational protein design approaches to design enzymes with controllable, enhanced activity[201]. Combining computational protein design with genetically encoded UAA was shown to be a powerful technique that can be used to drive the formation of precise metal-chelating protein assemblies for photophysical applications. Baker *et al.* have utilized Rosetta computational methodology to design homotrimeric protein complexes encoding BpyAla at interfaces of the monomers, suggesting that utilizing this method could generate novel photoactive proteins, where Bipyridine metal complexes can give rise to photochemical properties not present in natural amino acids[202]. Overall, BpyAla is a unique UAA that allows the introduction of unique functionalities to engineered protein. In chapter 4, we highlight the potential of utilizing BpyAla to introduce endonuclease activity to p19 for the targeting of its native substrates.

1.5 Rationale and Statement of Objectives

The *Tombusvirus* p19 is a unique tool to study the RNA silencing pathway. It can be further utilized to design methods to further control the activity of smRNAs in living organisms and *in vitro.* Understanding and further studying of the RNA silencing pathway is of interest to better understand the function of smRNAs in various diseased states, as well as to further develop tools in both therapy and biotechnology. VSRS are interesting proteins that were shown to potently inhibit the RNA silencing pathway, either by directly targeting small RNAs or other components of the pathway. Further engineering and fine-tuning the activity of the VSRS p19 can allow the design of protein-based tools to further control and manipulate the functions of the RNA silencing pathways.

The goal of this thesis is to engineer p19 to fine-tune its activity and enhance it using genetic code expansion technology to develop a new tool for RNA detection and RNA control. In **Chapter 2**, we attempt to engineer p19 as a FRET-based RNA detection tool, which further allows for the visualization of the delivery and release of siRNA into cells. This allows us to understand the potential of utilization of p19 as a siRNA delivery tool for subsequent gene knockdown. **Chapter 3** examines the potential of incorporation of UAA to allow for site-specific photo-crosslinking between p19 and its small RNA targets including siRNAs and miRNAs. This allows for the design of irreversible suppressors of the RNA silencing pathway. Finally, **Chapter 4** examines the potential of the introduction of metal-binding UAA in the binding pocket of p19, which allows for the introduction of a catalytic site into p19, leading to RNA endonuclease activity. The incorporation of BpyAla into p19 allowed for the site-specific cleavage of smRNA ligands and highlights the potential of utilizing UAAs for endonuclease design.

1.6 References

(1) Gonzalez-Gaitan, M.; Jessell, T.; Johnston, L.; Laufer, E.; McCabe, B.; Struhl, G.; Deleris, A.; Gallego-Bartolome, J.; Bao, J.; Kasschau, K. D.; Carrington, J. C.; Voinnet, O. Hierarchical Action and Inhibition of Plant Dicer-Like Proteins in Antiviral Defense. *Science (80-.).* **2004**, *305* (30), 1462–322. https://doi.org/10.1126/science.1128650.

(2) Samuel, G. H.; Adelman, Z. N.; Myles, K. M. Antiviral Immunity and Virus-Mediated Antagonism in Disease Vector Mosquitoes. *Trends Microbiol.* **2018**, *26* (5), 447–461. https://doi.org/10.1016/j.tim.2017.12.005.

(3) O'Brien, J.; Hayder, H.; Zayed, Y.; Peng, C. Overview of MicroRNA Biogenesis, Mechanisms of Actions, and Circulation. *Front. Endocrinol. (Lausanne).* **2018**, *9* (AUG), 1–12. https://doi.org/10.3389/fendo.2018.00402.

(4) Tijsterman, M.; Ketting, R. F.; Plasterk, R. H. A. The Genetics of RNA Silencing. *Annual Review of Genetics*. 2002, pp 489–519. https://doi.org/10.1146/annurev.genet.36.043002.091619.

(5) Agrawal, N.; Dasaradhi, P. V. N.; Mohmmed, A.; Malhotra, P.; Bhatnagar, R. K.; Mukherjee, S. K. RNA Interference: Biology, Mechanism, and Applications. *Microbiol. Mol. Biol. Rev.* **2003**, *67* (4), 657–685. https://doi.org/10.1128/mmbr.67.4.657-685.2003.

(6) Bronkhorst, A. W.; Van Rij, R. P. The Long and Short of Antiviral Defense: Small RNA-Based Immunity in Insects. *Curr. Opin. Virol.* **2014**, *7* (1), 19–28. https://doi.org/10.1016/j.coviro.2014.03.010.

(7) Cogoni, C.; Irelan, J. T.; Schumacher, M.; Schmidhauser, T. J.; Selker, E. U.; Macino, G. Transgene Silencing of the Al-1 Gene in Vegetative Cells of Neurospora Is Mediated by a Cytoplasmic Effector and Does Not Depend on DNA-DNA Interactions or DNA Methylation. *EMBO J.* **1996**, *15* (12), 3153–3163. https://doi.org/10.1002/j.1460-2075.1996.tb00678.x.

(8) Brodersen, P.; Voinnet, O. The Diversity of RNA Silencing Pathways in Plants. *Trends Genet.* **2006**, *22* (5), 268–280. https://doi.org/10.1016/j.tig.2006.03.003.

(9) Ding, S. W. RNA-Based Antiviral Immunity. *Nat. Rev. Immunol.* **2010**, *10* (9), 632–644. https://doi.org/10.1038/nri2824.

(10) Li, F.; Wang, A. RNA-Targeted Antiviral Immunity: More Than Just RNA Silencing. *Trends in Microbiology*. Elsevier Ltd September 1, 2019, pp 792–805. https://doi.org/10.1016/j.tim.2019.05.007.

(11) Tétreault, N.; De Guire, V. MiRNAs: Their Discovery, Biogenesis and Mechanism of Action. *Clin. Biochem.* **2013**, *46* (10–11), 842–845. https://doi.org/10.1016/j.clinbiochem.2013.02.009.

(12) Ding, S. W.; Han, Q.; Wang, J.; Li, W. X. Antiviral RNA Interference in Mammals. *Current Opinion in Immunology*. Elsevier Ltd October 1, 2018, pp 109–114. https://doi.org/10.1016/j.coi.2018.06.010.

(13) Bartel, D. P. Metazoan MicroRNAs. *Cell* **2018**, *173* (1), 20–51. https://doi.org/10.1016/j.cell.2018.03.006.

(14) Shivdasani, R. A. MicroRNAs: Regulators of Gene Expression and Cell Differentiation. *Blood* **2006**, *108* (12), 3646–3653. https://doi.org/10.1182/blood-2006-01-030015.

(15) Li, Y.; Basavappa, M.; Lu, J.; Dong, S.; Cronkite, D. A.; Prior, J. T.; Reinecker, H.-C.; Hertzog, P.; Han, Y.; Li, W.-X.; Cheloufi, S.; Karginov, F. V.; Ding, S.-W.; Jeffrey, K. L. Induction and Suppression of Antiviral RNA Interference by Influenza A Virus in Mammalian Cells. *Nat. Microbiol.* **2017**, *2* (3), 16250. https://doi.org/10.1038/nmicrobiol.2016.250.

(16) Almeida, R.; Allshire, R. C. RNA Silencing and Genome Regulation. *Trends Cell Biol.* **2005**, *15* (5), 251–258. https://doi.org/10.1016/j.tcb.2005.03.006.

(17) Zhou, Y.; Chan, J. H.; Chan, A. Y.; Chak, R. K. F.; Wong, E. Y. L.; Chye, M.-L.; Peiris, J. S. M.; Poon, L. L. M.; Lam, E. Transgenic Plant-Derived SiRNAs Can Suppress Propagation of Influenza Virus in Mammalian Cells. *FEBS Lett.* **2004**, *577* (3), 345–350. https://doi.org/10.1016/j.febslet.2004.10.027.

(18) Lu, R. Virus-Induced Gene Silencing in Plants. *Methods* **2003**, *30* (4), 296–303. https://doi.org/10.1016/S1046-2023(03)00037-9.

(19) Voinnet, O. Induction and Suppression of RNA Silencing: Insights from Viral Infections. *Nat. Rev. Genet.* **2005**, *6* (3), 206–220. https://doi.org/10.1038/nrg1555.

(20) Shabalina, S. A.; Koonin, E. V. Origins and Evolution of Eukaryotic RNA Interference. *Trends Ecol. Evol.* **2008**, *23* (10), 578–587. https://doi.org/10.1016/j.tree.2008.06.005.

(21) Janowski, B. A.; Huffman, K. E.; Schwartz, J. C.; Ram, R.; Nordsell, R.; Shames, D. S.; Minna, J. D.; Corey, D. R. Involvement of AGO1 and AGO2 in Mammalian Transcriptional Silencing. *Nat. Struct. Mol. Biol.* **2006**, *13* (9), 787–792. https://doi.org/10.1038/nsmb1140.

(22) Müller, M.; Fazi, F.; Ciaudo, C. Argonaute Proteins: From Structure to Function in Development and Pathological Cell Fate Determination. *Front. Cell Dev. Biol.* **2020**, *7* (January), 1–10. https://doi.org/10.3389/fcell.2019.00360.

(23) Bohmert, K.; Camus, I.; Bellini, C.; Bouchez, D.; Caboche, M.; Banning, C. AGO1 Defines a Novel Locus of Arabidopsis Controlling Leaf Development. *EMBO J.* **1998**, *17* (1), 170–180. https://doi.org/10.1093/emboj/17.1.170.

(24) Ruda, V. M.; Chandwani, R.; Sehgal, A.; Bogorad, R. L.; Akinc, A.; Charisse, K.; Tarakhovsky, A.; Novobrantseva, T. I.; Koteliansky, V. The Roles of Individual Mammalian Argonautes in RNA Interference in Vivo. *PLoS One* **2014**, *9* (7), 1–11. https://doi.org/10.1371/journal.pone.0101749.

(25) Jing, Q.; Huang, S.; Guth, S.; Zarubin, T.; Motoyama, A.; Chen, J.; Di Padova, F.; Lin, S.-C.; Gram, H.; Han, J. Involvement of MicroRNA in AU-Rich Element-Mediated MRNA Instability. *Cell* **2005**, *120* (5), 623–634. https://doi.org/10.1016/j.cell.2004.12.038.

(26) Shi, Y.; Jin, Y. X. MicroRNA in Cell Differentiation and Development. *Sci. China, Ser. C Life Sci.* **2009**, *52* (3), 205–211. https://doi.org/10.1007/s11427-009-0040-5.

(27) Baumjohann, D.; Ansel, K. M. MicroRNA-Mediated Regulation of T Helper Cell Differentiation and Plasticity. *Nat. Rev. Immunol.* **2013**, *13* (9), 666–678.

https://doi.org/10.1038/nri3494.

(28) Guo, Q.; Zhang, H.; Zhang, L.; He, Y.; Weng, S.; Dong, Z.; Wang, J.; Zhang, P. MicroRNA-21 Regulates Non-Small Cell Lung Cancer Cell Proliferation by Affecting Cell Apoptosis via COX-19. *Int. J. Clin. Exp. Med.* **2015**, *8* (6), 8835–8841.

(29) Agbu, P.; Carthew, R. W. MicroRNA-Mediated Regulation of Glucose and Lipid Metabolism. *Nat. Rev. Mol. Cell Biol.* **2021**, *22* (6), 425–438. https://doi.org/10.1038/s41580-021-00354-w.

(30) Carthew, R. W.; Sontheimer, E. J. Origins and Mechanisms of MiRNAs and SiRNAs. *Cell* **2009**, *136* (4), 642–655. https://doi.org/10.1016/j.cell.2009.01.035.

(31) Lindbo, J. A. High-Efficiency Protein Expression in Plants from Agroinfection-Compatible Tobacco Mosaic Virus Expression Vectors. *BMC Biotechnol.* **2007**, *7* (1), 52. https://doi.org/10.1186/1472-6750-7-52.

(32) Fire, A.; Xu, S.; Montgomery, M. K.; Kostas, S. A.; Driver, S. E.; Mello, C. C. Potent and Specific Genetic Interference by Double-Stranded RNA in Caenorhabditis Elegans. *Nature* **1998**, *391* (6669), 806–811. https://doi.org/10.1038/35888.

(33) Moazed, D. Small RNAs in Transcriptional Gene Silencing and Genome Defence. *Nature* **2009**, *457* (7228), 413–420. https://doi.org/10.1038/nature07756.

(34) Khvorova, A.; Reynolds, A.; Jayasena, S. D. Functional SiRNAs and MiRNAs Exhibit Strand Bias. *Cell* **2003**, *115* (2), 209–216. https://doi.org/10.1016/S0092-8674(03)00801-8.

(35) Leuschner, P. J. F.; Ameres, S. L.; Kueng, S.; Martinez, J. Cleavage of the SiRNA Passenger Strand during RISC Assembly in Human Cells. *EMBO Rep.* **2006**, *7* (3), 314–320. https://doi.org/10.1038/sj.embor.7400637.

(36) Maillard, P. V.; Ciaudo, C.; Marchais, A.; Li, Y.; Jay, F.; Ding, S. W.; Voinnet, O. Antiviral RNA Interference in Mammalian Cells. *Science (80-.).* **2013**, *342* (6155), 235–238. https://doi.org/10.1126/science.1241930.

(37) Baulcombe, D. RNA Silencing In. *Nature* **2004**, *17* (431), 356–363.

(38) Dugas, D. V.; Bartel, B. MicroRNA Regulation of Gene Expression in Plants. *Curr. Opin. Plant Biol.* **2004**, *7* (5), 512–520. https://doi.org/10.1016/j.pbi.2004.07.011.

(39) Li, Y.; Lu, J.; Han, Y.; Fan, X.; Ding, S. W. RNA Interference Functions as an Antiviral Immunity Mechanism in Mammals. *Science (80-.).* **2013**, *342* (6155), 231–234. https://doi.org/10.1126/science.1241911.

(40) Qiu, Y.; Xu, Y.; Zhang, Y.; Zhou, H.; Deng, Y. Q.; Li, X. F.; Miao, M.; Zhang, Q.; Zhong, B.; Hu, Y.; Zhang, F. C.; Wu, L.; Qin, C. F.; Zhou, X. Human Virus-Derived Small RNAs Can Confer Antiviral Immunity in Mammals. *Immunity* **2017**, *46* (6), 992-1004.e5. https://doi.org/10.1016/j.immuni.2017.05.006.

(41) Wightman, B.; Ha, I.; Ruvkun, G. Posttranscriptional Regulation of the Heterochronic Gene Lin-14 by Lin-4 Mediates Temporal Pattern Formation in C. Elegans. *Cell* **1993**, *75* (5), 855–862. https://doi.org/10.1016/0092-8674(93)90530-4.

(42) Feinbaum, R.; Ambros, V.; Lee, R. The C. Elegans Heterochronic Gene Lin-4 Encodes

Small RNAs with Antisense Complementarity to Lin-14. *Cell* **2004**, *116* (116), 843–854.

(43) Pandey, P.; Srivastava, P. K.; Pandey, S. P. Prediction of Plant MiRNA Targets. *Methods Mol. Biol.* **2019**, *1932*, 99–107. https://doi.org/10.1007/978-1-4939-9042-9_7.

(44) Roberts, A. P. E.; Lewis, A. P.; Jopling, C. L. The Role of MicroRNAs in Viral Infection. In *Cellular RNA Interference Mechanisms*; Elsevier Inc., 2011; Vol. 102, pp 101–139. https://doi.org/10.1016/B978-0-12-415795-8.00002-7.

(45) Lu, Y.; Leslie, C. S. Learning to Predict MiRNA-MRNA Interactions from AGO CLIP Sequencing and CLASH Data. *PLOS Comput. Biol.* **2016**, *12* (7), e1005026. https://doi.org/10.1371/journal.pcbi.1005026.

(46) Jonas, S.; Izaurralde, E. Towards a Molecular Understanding of MicroRNA-Mediated Gene Silencing. *Nat. Rev. Genet.* **2015**, *16* (7), 421–433. https://doi.org/10.1038/nrg3965.

(47) Behm-Ansmant, I.; Rehwinkel, J.; Doerks, T.; Stark, A.; Bork, P.; Izaurralde, E. MRNA Degradation by MiRNAs and GW182 Requires Both CCR4:NOT Deadenylase and DCP1:DCP2 Decapping Complexes. *Genes Dev.* **2006**, *20* (14), 1885–1898. https://doi.org/10.1101/gad.1424106.

(48) Braun, J. E.; Truffault, V.; Boland, A.; Huntzinger, E.; Chang, C. Te; Haas, G.; Weichenrieder, O.; Coles, M.; Izaurralde, E. A Direct Interaction between DCP1 and XRN1 Couples MRNA Decapping to 5′ Exonucleolytic Degradation. *Nat. Struct. Mol. Biol.* **2012**, *19* (12), 1324–1331. https://doi.org/10.1038/nsmb.2413.

(49) Bruscella, P.; Bottini, S.; Baudesson, C.; Pawlotsky, J.-M.; Feray, C.; Trabucchi, M. Viruses and MiRNAs: More Friends than Foes. *Front. Microbiol.* **2017**, *8*, 1–11. https://doi.org/10.3389/fmicb.2017.00824.

(50) Singaravelu, R.; O'Hara, S.; Jones, D. M.; Chen, R.; Taylor, N. G.; Srinivasan, P.; Quan, C.; Roy, D. G.; Steenbergen, R. H.; Kumar, A.; Lyn, R. K.; Özcelik, D.; Rouleau, Y.; Nguyen, M. A.; Rayner, K. J.; Hobman, T. C.; Tyrrell, D. L.; Russell, R. S.; Pezacki, J. P. MicroRNAs Regulate the Immunometabolic Response to Viral Infection in the Liver. *Nat. Chem. Biol.* **2015**, *11* (12), 988–993. https://doi.org/10.1038/nchembio.1940.

(51) Gupta, A.; Gartner, J. J.; Sethupathy, P.; Hatzigeorgiou, A. G.; Fraser, N. W. Anti-Apoptotic Function of a MicroRNA Encoded by the HSV-1 Latency-Associated Transcript. *Nature* **2006**, *442* (7098), 82–85. https://doi.org/10.1038/nature04836.

(52) Lam, J. K. W.; Chow, M. Y. T.; Zhang, Y.; Leung, S. W. S. SiRNA versus MiRNA as Therapeutics for Gene Silencing. *Mol. Ther. - Nucleic Acids* **2015**, *4* (9), e252. https://doi.org/10.1038/mtna.2015.23.

(53) Peng, Y.; Croce, C. M. The Role of MicroRNAs in Human Cancer. *Signal Transduct. Target. Ther.* **2016**, *1* (1), 15004. https://doi.org/10.1038/sigtrans.2015.4.

(54) Calin, G. a; Croce, C. M. MicroRNA Signatures in Human Cancers. *Nat. Rev. Cancer* **2006**, *6* (11), 857–866. https://doi.org/10.1038/nrc1997.

(55) Lindbo, J. A.; Silva-Rosales, L.; Proebsting, W. M.; Dougherty, W. G. Induction of a Highly Specific Antiviral State in Transgenic Plants: Implications for Regulation of Gene Expression and Virus Resistance. *Plant Cell* **1993**, *5* (12), 1749–1759.

https://doi.org/10.2307/3869691.

(56) Angell, S. M.; Baulcombe, D. C. Consistent Gene Silencing in Transgenic Plants Expressing a Replicating Potato Virus X RNA. *EMBO J.* **1997**, *16* (12), 3675–3684. https://doi.org/10.1093/emboj/16.12.3675.

(57) Ding, S. W.; Li, H.; Lu, R.; Li, F.; Li, W. X. RNA Silencing: A Conserved Antiviral Immunity of Plants and Animals. *Virus Res.* **2004**, *102* (1), 109–115. https://doi.org/10.1016/j.virusres.2004.01.021.

(58) Kjemtrup, S.; Sampson, K. S.; Peele, C. G.; Nguyen, L. V.; Conkling, M. A.; Thompson, W. F.; Robertson, D. Gene Silencing from Plant DNA Carried by a Geminivirus. *Plant J.* **1998**, *14* (1), 91–100. https://doi.org/10.1046/j.1365-313X.1998.00101.x.

(59) Teresa Ruiz, M.; Voinnet, O.; Baulcombe, D. C. Initiation and Maintenance of Virus-Induced Gene Silencing. *Plant Cell* **1998**, *10* (6), 937–946. https://doi.org/10.1105/tpc.10.6.937.

(60) Mourrain, P.; Béclin, C.; Elmayan, T.; Feuerbach, F.; Godon, C.; Morel, J. B.; Jouette, D.; Lacombe, A. M.; Nikic, S.; Picault, N.; Rémoué, K.; Sanial, M.; Vo, T. A.; Vaucheret, H. Arabidopsis SGS2 and SGS3 Genes Are Required for Posttranscriptional Gene Silencing and Natural Virus Resistance. *Cell* **2000**, *101* (5), 533–542. https://doi.org/10.1016/S0092-8674(00)80863-6.

(61) Boutet, S.; Vazquez, F.; Liu, J.; Béclin, C.; Fagard, M.; Gratias, A.; Morel, J.-B.; Crété, P.; Chen, X.; Vaucheret, H. Arabidopsis HEN1. *Curr. Biol.* **2003**, *13* (10), 843–848. https://doi.org/10.1016/S0960-9822(03)00293-8.

(62) Chien, M.; Russo, J. J.; Ju, J.; John, B.; Enright, A. J.; Marks, D.; Sander, C.; Tuschl, T.; Bar, T.; Bar, T. Identification of Virus-Encoded MicroRNAs Se. **2004**, *304* (April), 734–737.

(63) Kim, H.; Iizasa, H.; Kanehiro, Y.; Fekadu, S.; Yoshiyama, H. Herpesviral MicroRNAs in Cellular Metabolism and Immune Responses. *Front. Microbiol.* **2017**, *8* (JUL). https://doi.org/10.3389/fmicb.2017.01318.

(64) Varble, A.; tenOever, B. R. Implications of RNA Virus-Produced MiRNAs. *RNA Biol.* **2011**, *8* (2), 190–194. https://doi.org/10.4161/rna.8.2.13983.

(65) Aguado, L. C.; tenOever, B. RNA Virus Building Blocks—MiRNAs Not Included. *PLoS Pathog.* **2018**, *14* (5), 1–6. https://doi.org/10.1371/journal.ppat.1006963.

(66) Lecellier, C.-H.; Dunoyer, P.; Arar, K.; Lehmann-Che, J.; Eyquem, S.; Himber, C.; Saïb, A.; Voinnet, O. A Cellular MicroRNA Mediates Antiviral Defense in Human Cells. *Science (80-.).* **2005**, *308* (5721), 557–560. https://doi.org/10.1126/science.1108784.

(67) Jopling, C. L.; Yi, M. K.; Lancaster, A. M.; Lemon, S. M.; Sarnow, P. Molecular Biology: Modulation of Hepatitis C Virus RNA Abundance by a Liver-Specific MicroRNA. *Science (80-.).* **2005**, *309* (5740), 1577–1581. https://doi.org/10.1126/science.1113329.

(68) Henke, J. I.; Goergen, D.; Zheng, J.; Song, Y.; Schüttler, C. G.; Fehr, C.; Jünemann, C.; Niepmann, M. MicroRNA-122 Stimulates Translation of Hepatitis C Virus RNA. *EMBO J.* **2008**, *27* (24), 3300–3310. https://doi.org/10.1038/emboj.2008.244.

(69) Xu, J.; Kong, J.; Lyu, B.; Wang, X.; Qian, Q.; Zhou, X.; Qiu, Y. The Capsid Protein of Rubella Virus Antagonizes RNA Interference in Mammalian Cells. *Viruses* **2021**, *13* (2), 154. https://doi.org/10.3390/v13020154.

(70) Li, W.-X.; Ding, S.-W. Mammalian Viral Suppressors of RNA Interference. *Trends Biochem. Sci.* **2022**, 1–11. https://doi.org/10.1016/j.tibs.2022.05.001.

(71) Csorba, T.; Pantaleo, V.; Burgyán, J. RNA Silencing: An Antiviral Mechanism. *Adv. Virus Res.* **2009**, *75* (09), 35–71. https://doi.org/10.1016/s0065-3527(09)07502-2.

(72) Ye, K.; Malinina, L.; Patel, D. J. Recognition of Small Interfering RNA by a Viral Suppressor of RNA Silencing. *Nature* **2003**, *426* (6968), 874–878. https://doi.org/10.1038/nature02213.

(73) Iki, T.; Tschopp, M. A.; Voinnet, O. Biochemical and Genetic Functional Dissection of the P38 Viral Suppressor of RNA Silencing. *Rna* **2017**, *23* (5), 639–654. https://doi.org/10.1261/rna.060434.116.

(74) Mérai, Z.; Kerényi, Z.; Kertész, S.; Magna, M.; Lakatos, L.; Silhavy, D. Double-Stranded RNA Binding May Be a General Plant RNA Viral Strategy To Suppress RNA Silencing. *J. Virol.* **2006**, *80* (12), 5747–5756. https://doi.org/10.1128/jvi.01963-05.

(75) Chen, H. Y.; Yang, J.; Lin, C.; Yuan, Y. A. Structural Basis for RNA-Silencing Suppression by Tomato Aspermy Virus Protein 2b. *EMBO Rep.* **2008**, *9* (8), 754–760. https://doi.org/10.1038/embor.2008.118.

(76) Lakatos, L.; Csorba, T.; Pantaleo, V.; Chapman, E. J.; Carrington, J. C.; Liu, Y. P.; Dolja, V. V.; Calvino, L. F.; López-Moya, J. J.; Burgyán, J. Small RNA Binding Is a Common Strategy to Suppress RNA Silencing by Several Viral Suppressors. *EMBO J.* **2006**, *25* (12), 2768–2780. https://doi.org/10.1038/sj.emboj.7601164.

(77) Csorba, T.; Bovi, A.; Dalmay, T.; Burgyán, J. The P122 Subunit of Tobacco Mosaic Virus Replicase Is a Potent Silencing Suppressor and Compromises Both Small Interfering RNA- and MicroRNA-Mediated Pathways . *J. Virol.* **2007**, *81* (21), 11768–11780. https://doi.org/10.1128/jvi.01230-07.

(78) Mérai, Z.; Kerényi, Z.; Molnár, A.; Barta, E.; Válóczi, A.; Bisztray, G.; Havelda, Z.; Burgyán, J.; Silhavy, D. Aureusvirus P14 Is an Efficient RNA Silencing Suppressor That Binds Double-Stranded RNAs without Size Specificity. *J. Virol.* **2005**, *79* (11), 7217–7226. https://doi.org/10.1128/jvi.79.11.7217-7226.2005.

(79) Vargason, J. M.; Szittya, G.; Burgyán, J.; Hall, T. M. T. Size Selective Recognition of SiRNA by an RNA Silencing Suppressor. *Cell* **2003**, *115* (7), 799–811. https://doi.org/10.1016/S0092-8674(03)00984-X.

(80) Silhavy, D.; Molnár, A.; Lucioli, A.; Szittya, G.; Hornyik, C.; Tavazza, M.; Burgyán, J. A Viral Protein Suppresses RNA Silencing and Binds Silencing-Generated, 21- to 25-Nucleotide Double-Stranded RNAs. *EMBO J.* **2002**, *21* (12), 3070–3080. https://doi.org/10.1093/emboj/cdf312.

(81) Li, H.; Li, W. X.; Ding, S. W. Induction and Suppression of RNA Silencing by an Animal Virus. *Science (80-.).* **2002**, *296* (5571), 1319–1321. https://doi.org/10.1126/science.1070948.

(82) Aliyari, R.; Wu, Q.; Li, H. W.; Wang, X. H.; Li, F.; Green, L. D.; Han, C. S.; Li, W. X.; Ding, S. W. Mechanism of Induction and Suppression of Antiviral Immunity Directed by Virus-Derived Small RNAs in Drosophila. *Cell Host Microbe* **2008**, *4* (4), 387–397. https://doi.org/10.1016/j.chom.2008.09.001.

(83) Li, W. X.; Li, H.; Lu, R.; Li, F.; Dus, M.; Atkinson, P.; Brydon, E. W. A.; Johnson, K. L.; García-Sastre, A.; Ball, L. A.; Palese, P.; Ding, S. W. Interferon Antagonist Proteins of Influenza and Vaccinia Viruses Are Suppressors of RNA Silencing. *Proc. Natl. Acad. Sci. U. S. A.* **2004**, *101* (5), 1350–1355. https://doi.org/10.1073/pnas.0308308100.

(84) Barrows, N. J.; Campos, R. K.; Liao, K. C.; Prasanth, K. R.; Soto-Acosta, R.; Yeh, S. C.; Schott-Lerner, G.; Pompon, J.; Sessions, O. M.; Bradrick, S. S.; Garcia-Blanco, M. A. Biochemistry and Molecular Biology of Flaviviruses. *Chem. Rev.* **2018**, *118* (8), 4448–4482. https://doi.org/10.1021/acs.chemrev.7b00719.

(85) Qiu, Y.; Xu, Y. P.; Wang, M.; Miao, M.; Zhou, H.; Xu, J.; Kong, J.; Zheng, D.; Li, R. T.; Zhang, R. R.; Guo, Y.; Li, X. F.; Cui, J.; Qin, C. F.; Zhou, X. Flavivirus Induces and Antagonizes Antiviral RNA Interference in Both Mammals and Mosquitoes. *Sci. Adv.* **2020**, *6* (6), 1–15. https://doi.org/10.1126/sciadv.aax7989.

(86) Dalmay, T.; Rubino, L.; Burgyán, J.; Kollár, Á.; Russo, M. Functional Analysis of Cymbidium Ringspot Virus Genome. *Virology* **1993**, *194* (2), 697–704. https://doi.org/10.1006/viro.1993.1310.

(87) Scholthof, H. B.; Scholthof, K. B. G.; Jackson, A. O. Identification of Tomato Bushy Stunt Virus Host-Specific Symptom Determinants by Expression of Individual Genes from a Potato Virus X Vector. *Plant Cell* **1995**, *7* (8), 1157–1172. https://doi.org/10.2307/3870092.

(88) Voinnet, O.; Pinto, Y. M.; Baulcombe, D. C. Suppression of Gene Silencing: A General Strategy Used by Diverse DNA and RNA Viruses of Plants. *Proc. Natl. Acad. Sci. U. S. A.* **1999**, *96* (24), 14147–14152. https://doi.org/10.1073/pnas.96.24.14147.

(89) Vargason, J. M.; Szittya, G.; Burgyán, J.; Tanaka Hall, T. M. Size Selective Recognition of SiRNA by an RNA Silencing Suppressor. *Cell* **2003**, *115* (7), 799–811. https://doi.org/10.1016/S0092-8674(03)00984-X.

(90) Fagegaltier, D.; Bougé, A. L.; Berry, B.; Poisot, É.; Sismeiro, O.; Coppée, J. Y.; Théodore, L.; Voinnet, O.; Antoniewski, C. The Endogenous SiRNA Pathway Is Involved in Heterochromatin Formation in Drosophila. *Proc. Natl. Acad. Sci. U. S. A.* **2009**, *106* (50), 21258–21263. https://doi.org/10.1073/pnas.0809208105.

(91) Danielson, D. C.; Filip, R.; Powdrill, M. H.; O'Hara, S.; Pezacki, J. P. Suppressing RNA Silencing with Small Molecules and the Viral Suppressor of RNA Silencing Protein P19. *Biochem. Biophys. Res. Commun.* **2015**, *463* (4), 1135–1140. https://doi.org/10.1016/j.bbrc.2015.06.071.

(92) Kontra, L.; Csorba, T.; Tavazza, M.; Lucioli, A.; Tavazza, R.; Moxon, S.; Tisza, V.; Medzihradszky, A.; Turina, M.; Burgyán, J. Distinct Effects of P19 RNA Silencing Suppressor on Small RNA Mediated Pathways in Plants. *PLoS Pathog.* **2016**, *12* (10), 1–26. https://doi.org/10.1371/journal.ppat.1005935.

(93) Lakatos, L.; Szittya, G.; Silhavy, D.; Burgyán, J. Molecular Mechanism of RNA Silencing Suppression Mediated by P19 Protein of Tombusviruses. *EMBO J.* **2004**, *23* (4), 876–884. https://doi.org/10.1038/sj.emboj.7600096.

(94) Rawlings, R. A.; Krishnan, V.; Walter, N. G. Viral RNAi Suppressor Reversibly Binds SiRNA to Outcompete Dicer and RISC via Multiple Turnover. *J. Mol. Biol.* **2011**, *408* (2), 262–276. https://doi.org/10.1016/j.jmb.2011.02.038.

(95) Xia, Z.; Zhu, Z.; Zhu, J.; Zhou, R. Recognition Mechanism of SiRNA by Viral P19 Suppressor of RNA Silencing: A Molecular Dynamics Study. *Biophys. J.* **2009**, *96* (5), 1761–1769. https://doi.org/10.1016/j.bpj.2008.11.047.

(96) Havelda, Z.; Hornyik, C.; Válóczi, A.; Burgyán, J. Defective Interfering RNA Hinders the Activity of a Tombusvirus-Encoded Posttranscriptional Gene Silencing Suppressor. *J. Virol.* **2005**, *79* (1), 450–457. https://doi.org/10.1128/jvi.79.1.450-457.2005.

(97) Chapman, E. J.; Prokhnevsky, A. I.; Gopinath, K.; Dolja, V. V.; Carrington, J. C. Erratum: Viral RNA Silencing Suppressors Inhibit the MicroRNA Pathway at an Intermediate Step (Genes and Development (2004) 18 (1179-1186)). *Genes Dev.* **2004**, *18* (12), 1510. https://doi.org/10.1101/gad.1201204.cessing.

(98) Nasheri, N.; Singaravelu, R.; Goodmurphy, M.; Lyn, R. K.; Pezacki, J. P. Competing Roles of MicroRNA-122 Recognition Elements in Hepatitis C Virus RNA. *Virology* **2011**, *410* (2), 336–344. https://doi.org/10.1016/j.virol.2010.11.015.

(99) Berry, B.; Deddouche, S.; Kirschner, D.; Imler, J. L.; Antoniewski, C. Viral Suppressors of RNA Silencing Hinder Exogenous and Endogenous Small RNA Pathways in Drosophila. *PLoS One* **2009**, *4* (6). https://doi.org/10.1371/journal.pone.0005866.

(100) Rauschhuber, C.; Mueck-Haeusl, M.; Zhang, W.; Nettelbeck, D. M.; Ehrhardt, A. RNAi Suppressor P19 Can Be Broadly Exploited for Enhanced Adenovirus Replication and MicroRNA Knockdown Experiments. *Sci. Rep.* **2013**, *3* (1), 1363. https://doi.org/10.1038/srep01363.

(101) Cheng, J.; Danielson, D. C.; Nasheri, N.; Singaravelu, R.; Pezacki, J. P. Enhanced Specificity of the Viral Suppressor of RNA Silencing Protein P19 toward Sequestering of Human MicroRNA-122. *Biochemistry* **2011**, *50* (36), 7745–7755. https://doi.org/10.1021/bi2008273.

(102) Várallyay, É.; Oláh, E.; Havelda, Z. Independent Parallel Functions of P19 Plant Viral Suppressor of RNA Silencing Required for Effective Suppressor Activity. *Nucleic Acids Res.* **2014**, *42* (1), 599–608. https://doi.org/10.1093/nar/gkt846.

(103) Papp, I.; Mette, M. F.; Aufsatz, W.; Daxinger, L.; Schauer, S. E.; Ray, A.; Van Der Winden, J.; Matzke, M.; Matzke, A. J. M. Evidence for Nuclear Processing of Plant Micro RNA and Short Interfering RNA Precursors. *Plant Physiol.* **2003**, *132* (3), 1382–1390. https://doi.org/10.1104/pp.103.021980.

(104) Pertermann, R.; Tamilarasan, S.; Gursinsky, T.; Gambino, G.; Schuck, J.; Weinholdt, C.; Lilie, H.; Grosse, I.; Golbik, R. P.; Pantaleo, V.; Behrens, S.-E. A Viral Suppressor Modulates the Plant Immune Response Early in Infection by Regulating MicroRNA Activity. *MBio* **2018**, *9* (2). https://doi.org/10.1128/mBio.00419-18.

(105) Schott, G.; Mari-Ordonez, A.; Himber, C.; Alioua, A.; Voinnet, O.; Dunoyer, P. Differential Effects of Viral Silencing Suppressors on SiRNA and MiRNA Loading Support the Existence of Two Distinct Cellular Pools of ARGONAUTE1. *EMBO J.* **2012**, *31* (11), 2553–2565. https://doi.org/10.1038/emboj.2012.92.

(106) Yu, B.; Chapman, E. J.; Yang, Z.; Carrington, J. C.; Chen, X. Transgenically Expressed Viral RNA Silencing Suppressors Interfere with MicroRNA Methylation in Arabidopsis. *FEBS Lett.* **2006**, *580* (13), 3117–3120. https://doi.org/10.1016/j.febslet.2006.04.063.

(107) Canto, T.; Uhrig, J. F.; Swanson, M.; Wright, K. M.; MacFarlane, S. A. Translocation of Tomato Bushy Stunt Virus P19 Protein into the Nucleus by ALY Proteins Compromises Its Silencing Suppressor Activity . *J. Virol.* **2006**, *80* (18), 9064–9072. https://doi.org/10.1128/jvi.00953-06.

(108) Liu, X.; Houzet, L.; Jeang, K. Tombusvirus P19 RNA Silencing Suppressor (RSS) Activity in Mammalian Cells Correlates with Charged Amino Acids That Contribute to Direct. *Cell Biosci.* **2012**, *2* (1), 1. https://doi.org/10.1186/2045-3701-2-41.

(109) Calabrese, J. M.; Sharp, P. A. Characterization of the Short RNAs Bound by the P19 Suppressor of RNA Silencing in Mouse Embryonic Stem Cells. *Rna* **2006**, *12* (12), 2092–2102. https://doi.org/10.1261/rna.224606.

(110) Chen, W. X.; Chen, J.; Zhang, Z. Z.; Huang, A. L. P19 of Tomato Bushy Stunt Virus Suppresses RNA Silencing Induced by Short Hairpin RNA in Mammal Cells. *Virol. Sin.* **2007**, *22* (3), 199–206.

(111) de Vries, W.; Haasnoot, J.; van der Velden, J.; van Montfort, T.; Zorgdrager, F.; Paxton, W.; Cornelissen, M.; van Kuppeveld, F.; de Haan, P.; Berkhout, B. Increased Virus Replication in Mammalian Cells by Blocking Intracellular Innate Defense Responses. *Gene Ther.* **2008**, *15* (7), 545–552. https://doi.org/10.1038/gt.2008.12.

(112) Hefferon, K. Plant Virus Expression Vector Development: New Perspectives. *Biomed Res. Int.* **2014**, *2014*, 1–6. https://doi.org/10.1155/2014/785382.

(113) Chen, Q.; Lai, H. Gene Delivery into Plant Cells for Recombinant Protein Production. *Biomed Res. Int.* **2015**, *2015*, 1–10. https://doi.org/10.1155/2015/932161.

(114) Leuzinger, K.; Dent, M.; Hurtado, J.; Stahnke, J.; Lai, H.; Zhou, X.; Chen, Q. Efficient Agroinfiltration of Plants for High-Level Transient Expression of Recombinant Proteins. *J. Vis. Exp.* **2013**, No. 77, 1–9. https://doi.org/10.3791/50521.

(115) Fahad, S.; Khan, F. A.; Pandupuspitasari, N. S.; Ahmed, M. M.; Liao, Y. C.; Waheed, M. T.; Sameeullah, M.; Darkhshan; Hussain, S.; Saud, S.; Hassan, S.; Jan, A.; Jan, M. T.; Wu, C.; Chun, M. X.; Huang, J. Recent Developments in Therapeutic Protein Expression Technologies in Plants. *Biotechnol. Lett.* **2015**, *37* (2), 265–279. https://doi.org/10.1007/s10529-014-1699-7.

(116) Dubey, K. K.; Luke, G. A.; Knox, C.; Kumar, P.; Pletschke, B. I.; Singh, P. K.; Shukla, P. Vaccine and Antibody Production in Plants: Developments and Computational Tools. *Brief. Funct. Genomics* **2018**, *17* (5), 295–307. https://doi.org/10.1093/bfgp/ely020.

(117) Donini, M.; Marusic, C. Current State-of-the-Art in Plant-Based Antibody Production Systems. *Biotechnol. Lett.* **2019**, *41* (3), 335–346. https://doi.org/10.1007/s10529-019-

02651-z.

(118) Makatsa, M. S.; Tincho, M. B.; Wendoh, J. M.; Ismail, S. D.; Nesamari, R.; Pera, F.; de Beer, S.; David, A.; Jugwanth, S.; Gededzha, M. P.; Mampeule, N.; Sanne, I.; Stevens, W.; Scott, L.; Blackburn, J.; Mayne, E. S.; Keeton, R. S.; Burgers, W. A. SARS-CoV-2 Antigens Expressed in Plants Detect Antibody Responses in COVID-19 Patients. *Front. Plant Sci.* **2021**, *12* (March). https://doi.org/10.3389/fpls.2021.589940.

(119) Arzola, L.; Chen, J.; Rattanaporn, K.; Maclean, J. M.; McDonald, K. A. Transient Co-Expression of Post-Transcriptional Gene Silencing Suppressors for Increased in Planta Expression of a Recombinant Anthrax Receptor Fusion Protein. *Int. J. Mol. Sci.* **2011**, *12* (8), 4975–4990. https://doi.org/10.3390/ijms12084975.

(120) Lombardi, R.; Circelli, P.; Villani, M. E.; Buriani, G.; Nardi, L.; Coppola, V.; Bianco, L.; Benvenuto, E.; Donini, M.; Marusic, C. High-Level HIV-1 Nef Transient Expression in Nicotiana Benthamiana Using the P19 Gene Silencing Suppressor Protein of Artichoke Mottled Crinckle Virus. *BMC Biotechnol.* **2009**, *9*, 1–11. https://doi.org/10.1186/1472-6750-9-96.

(121) Zheng, N.; Xia, R.; Yang, C.; Yin, B.; Li, Y.; Duan, C.; Liang, L.; Guo, H.; Xie, Q. Boosted Expression of the SARS-CoV Nucleocapsid Protein in Tobacco and Its Immunogenicity in Mice. *Vaccine* **2009**, *27* (36), 5001–5007. https://doi.org/10.1016/j.vaccine.2009.05.073.

(122) Chiong, K. T.; Cody, W. B.; Scholthof, H. B. RNA Silencing Suppressor-Influenced Performance of a Virus Vector Delivering Both Guide RNA and Cas9 for CRISPR Gene Editing. *Sci. Rep.* **2021**, *11* (1), 1–13. https://doi.org/10.1038/s41598-021-85366-4.

(123) Mao, Y.; Yang, X.; Zhou, Y.; Zhang, Z.; Botella, J. R.; Zhu, J. K. Manipulating Plant RNA-Silencing Pathways to Improve the Gene Editing Efficiency of CRISPR/Cas9 Systems. *Genome Biol.* **2018**, *19* (1), 1–15. https://doi.org/10.1186/s13059-018-1529-7.

(124) Li, Y.; Kowdley, K. V. MicroRNAs in Common Human Diseases. *Genomics, Proteomics Bioinforma.* **2012**, *10* (5), 246–253. https://doi.org/10.1016/j.gpb.2012.07.005.

(125) Svoboda, P. A Toolbox for MiRNA Analysis. *FEBS Lett.* **2015**, *589* (14), 1694–1701. https://doi.org/10.1016/j.febslet.2015.04.054.

(126) Mendell, J. T.; Olson, E. N. MicroRNAs in Stress Signaling and Human Disease. *Cell* **2012**, *148* (6), 1172–1187. https://doi.org/10.1016/j.cell.2012.02.005.

(127) Gessner, I.; Fries, J. W. U.; Brune, V.; Mathur, S. Magnetic Nanoparticle-Based Amplification of MicroRNA Detection in Body Fluids for Early Disease Diagnosis. *J. Mater. Chem. B* **2021**, *9* (1), 9–22. https://doi.org/10.1039/d0tb02165b.

(128) Hoekstra, M.; van der Lans, C. A. C.; Halvorsen, B.; Gullestad, L.; Kuiper, J.; Aukrust, P.; van Berkel, T. J. C.; Biessen, E. A. L. The Peripheral Blood Mononuclear Cell MicroRNA Signature of Coronary Artery Disease. *Biochem. Biophys. Res. Commun.* **2010**, *394* (3), 792–797. https://doi.org/10.1016/j.bbrc.2010.03.075.

(129) Hunter, M. P.; Ismail, N.; Zhang, X.; Aguda, B. D.; Lee, E. J.; Yu, L.; Xiao, T.; Schafer, J.; Lee, M. L. T.; Schmittgen, T. D.; Nana-Sinkam, S. P.; Jarjoura, D.; Marsh, C. B. Detection of MicroRNA Expression in Human Peripheral Blood Microvesicles. *PLoS One*

2008, *3* (11). https://doi.org/10.1371/journal.pone.0003694.

(130) Schrauder, M. G.; Strick, R.; Schulz-Wendtland, R.; Strissel, P. L.; Kahmann, L.; Loehberg, C. R.; Lux, M. P.; Jud, S. M.; Hartmann, A.; Hein, A.; Bayer, C. M.; Bani, M. R.; Richter, S.; Adamietz, B. R.; Wenkel, E.; Rauh, C.; Beckmann, M. W.; Fasching, P. A. Circulating Micro-RNAs as Potential Blood-Based Markers for Early Stage Breast Cancer Detection. *PLoS One* **2012**, *7* (1). https://doi.org/10.1371/journal.pone.0029770.

(131) Foye, C.; Yan, I. K.; David, W.; Shukla, N.; Habboush, Y.; Chase, L.; Ryland, K.; Kesari, V.; Patel, T. Comparison of MiRNA Quantitation by Nanostring in Serum and Plasma Samples. *PLoS One* **2017**, *12* (12), 1–13. https://doi.org/10.1371/journal.pone.0189165.

(132) Gallego, J. A.; Gordon, M. L.; Claycomb, K.; Bhatt, M.; Lencz, T.; Malhotra, A. K. In Vivo MicroRNA Detection and Quantitation in Cerebrospinal Fluid. *J. Mol. Neurosci.* **2012**, *47* (2), 243–248. https://doi.org/10.1007/s12031-012-9731-7.

(133) Di Stefano, V.; Zaccagnini, G.; Capogrossi, M. C.; Martelli, F. MicroRNAs as Peripheral Blood Biomarkers of Cardiovascular Disease. *Vascul. Pharmacol.* **2011**, *55* (4), 111–118. https://doi.org/10.1016/j.vph.2011.08.001.

(134) Wang, J.; Chen, J.; Sen, S. MicroRNA as Biomarkers and Diagnostics. *J. Cell. Physiol.* **2016**, *231* (1), 25–30. https://doi.org/10.1002/jcp.25056.

(135) Dave, V. P.; Ngo, T. A.; Pernestig, A. K.; Tilevik, D.; Kant, K.; Nguyen, T.; Wolff, A.; Bang, D. D. MicroRNA Amplification and Detection Technologies: Opportunities and Challenges for Point of Care Diagnostics. *Lab. Investig.* **2019**, *99* (4), 452–469. https://doi.org/10.1038/s41374-018-0143-3.

(136) Jin, J.; Cid, M.; Poole, C. B.; McReynolds, L. A. Protein-Mediated MiRNA Detection and SiRNA Enrichment Using P19. *Biotechniques* **2010**, *48* (6), xvii–xxiii. https://doi.org/10.2144/000113364.

(137) Campuzano, S.; Torrente-Rodriguez, R. M.; Lopez-Hernandez, E.; Conzuelo, F.; Granados, R.; Sanchez-Puelles, J. M.; Pingarron, J. M. Magnetobiosensors Based on Viral Protein P19 for Microrna Determination in Cancer Cells and Tissues. *Angew. Chemie - Int. Ed.* **2014**, *53* (24), 6168–6171. https://doi.org/10.1002/anie.201403270.

(138) Nasheri, N.; Cheng, J.; Singaravelu, R.; Wu, P.; McDermott, M. T.; Pezacki, J. P. An Enzyme-Linked Assay for the Rapid Quantification of MicroRNAs Based on the Viral Suppressor of RNA Silencing Protein P19. *Anal. Biochem.* **2011**, *412* (2), 165–172. https://doi.org/10.1016/j.ab.2011.01.030.

(139) Khan, N.; Cheng, J.; Pezacki, J. P.; Berezovski, M. V. Quantitative Analysis of MicroRNA in Blood Serum with Protein-Facilitated Affinity Capillary Electrophoresis. *Anal. Chem.* **2011**, *83* (16), 6196–6201. https://doi.org/10.1021/ac2016213.

(140) Koukiekolo, R.; Jakubek, Z. J.; Cheng, J.; Sagan, S. M.; Pezacki, J. P. Studies of a Viral Suppressor of RNA Silencing P19-CFP Fusion Protein: A FRET-Based Probe for Sensing Double-Stranded Fluorophore Tagged Small RNAs. *Biophys. Chem.* **2009**, *143* (3), 166–169. https://doi.org/10.1016/j.bpc.2009.05.001.

(141) Pecot, C. V.; Calin, G. A.; Coleman, R. L.; Lopez-Berestein, G.; Sood, A. K. RNA Interference in the Clinic: Challenges and Future Directions. *Nat. Rev. Cancer* **2011**, *11*

(1), 59–67. https://doi.org/10.1038/nrc2966.

(142) Wu, Z.; Li, T. Nanoparticle-Mediated Cytoplasmic Delivery of Messenger RNA Vaccines: Challenges and Future Perspectives. *Pharm. Res.* **2021**, *38* (3), 473–478. https://doi.org/10.1007/s11095-021-03015-x.

(143) Shukla, R. S.; Qin, B.; Cheng, K. Peptides Used in the Delivery of Small Noncoding RNA. *Mol. Pharm.* **2014**, *11* (10), 3395–3408. https://doi.org/10.1021/mp500426r.

(144) Yokoo, H.; Oba, M.; Uchida, S. Cell-Penetrating Peptides: Emerging Tools for MRNA Delivery. *Pharmaceutics* **2022**, *14* (1), 1–13. https://doi.org/10.3390/pharmaceutics14010078.

(145) Yonezawa, S.; Koide, H.; Asai, T. Recent Advances in SiRNA Delivery Mediated by Lipid-Based Nanoparticles. *Adv. Drug Deliv. Rev.* **2020**, *154–155*, 64–78. https://doi.org/10.1016/j.addr.2020.07.022.

(146) Choi, K. M.; Park, G. L.; Hwang, K. Y.; Lee, J. W.; Ahn, H. J. Efficient SiRNA Delivery into Tumor Cells by P19-YSA Fusion Protein. *Mol. Pharm.* **2013**, *10* (2), 763–773. https://doi.org/10.1021/mp300344p.

(147) Danielson, D. C.; Sachrajda, N.; Wang, W.; Filip, R.; Pezacki, J. P. A Novel P19 Fusion Protein as a Delivery Agent for Short-Interfering RNAs. *Mol. Ther. - Nucleic Acids* **2016**, *5* (February), e303. https://doi.org/10.1038/mtna.2016.14.

(148) Cheng, J.; Sagan, S. M.; Assem, N.; Koukiekolo, R.; Goto, N. K.; Pezacki, J. P. Stabilized Recombinant Suppressors of RNA Silencing: Functional Effects of Linking Monomers of Carnation Italian Ringspot Virus P19. *Biochim. Biophys. Acta - Proteins Proteomics* **2007**, *1774* (12), 1528–1535. https://doi.org/10.1016/j.bbapap.2007.09.014.

(149) Cheng, J.; Koukiekolo, R.; Kieliszkiewicz, K.; Sagan, S. M.; Pezacki, J. P. Cysteine Residues of Carnation Italian Ringspot Virus P19 Suppressor of RNA Silencing Maintain Global Structural Integrity and Stability for SiRNA Binding. *Biochim. Biophys. Acta - Proteins Proteomics* **2009**, *1794* (8), 1197–1203. https://doi.org/10.1016/j.bbapap.2009.03.012.

(150) Wang, Q.; Parrish, A. R.; Wang, L. Expanding the Genetic Code for Biological Studies. *Chem. Biol.* **2009**, *16* (3), 323–336. https://doi.org/10.1016/j.chembiol.2009.03.001.

(151) Chin, J. W.; Martin, A. B.; King, D. S.; Wang, L.; Schultz, P. G. Addition of a Photocrosslinking Amino Acid to the Genetic Code of Escherichia Coli. *Proc. Natl. Acad. Sci.* **2002**, *99* (17), 11020–11024. https://doi.org/10.1073/pnas.172226299.

(152) Lang, K.; Chin, J. W. Cellular Incorporation of Unnatural Amino Acids and Bioorthogonal Labeling of Proteins. *Chem. Rev.* **2014**, *114* (9), 4764–4806. https://doi.org/10.1021/cr400355w.

(153) Nainar, S.; Kubota, M.; McNitt, C.; Tran, C.; Popik, V. V.; Spitale, R. C. Temporal Labeling of Nascent RNA Using Photoclick Chemistry in Live Cells. *J. Am. Chem. Soc.* **2017**, *139* (24), 8090–8093. https://doi.org/10.1021/jacs.7b03121.

(154) Li, F.; Dong, J.; Hu, X.; Gong, W.; Li, J.; Shen, J.; Tian, H.; Wang, J. A Covalent Approach for Site-Specific RNA Labeling in Mammalian Cells. *Angew. Chemie - Int. Ed.*

2015, *54* (15), 4597–4602. https://doi.org/10.1002/anie.201410433.

(155) Chatterjee, A.; Sun, S. B.; Furman, J. L.; Xiao, H.; Schultz, P. G. A Versatile Platform for Single- and Multiple-Unnatural Amino Acid Mutagenesis in Escherichia Coli. *Biochemistry* **2013**, *52* (10), 1828–1837. https://doi.org/10.1021/bi4000244.

(156) Shandell, M. A.; Tan, Z.; Cornish, V. W. Genetic Code Expansion: A Brief History and Perspective. *Biochemistry* **2021**, *60* (46), 3455–3469. https://doi.org/10.1021/acs.biochem.1c00286.

(157) Chin, J. W. Expanding and Reprogramming the Genetic Code of Cells and Animals. *Annu. Rev. Biochem.* **2014**, *83*, 379–408. https://doi.org/10.1146/annurev-biochem-060713-035737.

(158) Xie, J.; Schultz, P. G. An Expanding Genetic Code. *Methods* **2005**, *36* (3), 227–238. https://doi.org/10.1016/j.ymeth.2005.04.010.

(159) Xie, J.; Schultz, P. G. An Expanding Genetic Code. *Methods* **2005**, *36* (3), 227–238. https://doi.org/10.1016/j.ymeth.2005.04.010.

(160) Chin, J. W.; Cropp, T. A.; Chu, S.; Meggers, E.; Schultz, P. G. Progress Toward an Expanded Eukaryotic Genetic Code. *Chem. Biol.* **2003**, *10* (6), 511–519. https://doi.org/10.1016/S1074-5521(03)00123-6.

(161) Wu, N.; Deiters, A.; Cropp, T. A.; King, D.; Schultz, P. G. A Genetically Encoded Photocaged Amino Acid. *J. Am. Chem. Soc.* **2004**, *126* (44), 14306–14307. https://doi.org/10.1021/ja040175z.

(162) Axup, J. Y.; Bajjuri, K. M.; Ritland, M.; Hutchins, B. M.; Kim, C. H.; Kazane, S. A.; Halder, R.; Forsyth, J. S.; Santidrian, A. F.; Stafin, K.; Lu, Y.; Tran, H.; Seller, A. J.; Biroc, S. L.; Szydlik, A.; Pinkstaff, J. K.; Tian, F.; Sinha, S. C.; Felding-Habermann, B.; Smider, V. V.; Schultz, P. G. Synthesis of Site-Specific Antibody-Drug Conjugates Using Unnatural Amino Acids. *Proc. Natl. Acad. Sci. U. S. A.* **2012**, *109* (40), 16101–16106. https://doi.org/10.1073/pnas.1211023109.

(163) Virdee, S.; Kapadnis, P. B.; Elliott, T.; Lang, K.; Madrzak, J.; Nguyen, D. P.; Riechmann, L.; Chin, J. W. Traceless and Site-Specific Ubiquitination of Recombinant Proteins. *J. Am. Chem. Soc.* **2011**, *133* (28), 10708–10711. https://doi.org/10.1021/ja202799r.

(164) Castañeda, C.; Liu, J.; Chaturvedi, A.; Nowicka, U.; Cropp, T. A.; Fushman, D. Nonenzymatic Assembly of Natural Polyubiquitin Chains of Any Linkage Composition and Isotopic Labeling Scheme. *J. Am. Chem. Soc.* **2011**, *133* (44), 17855–17868. https://doi.org/10.1021/ja207220g.

(165) Lang, K.; Davis, L.; Torres-Kolbus, J.; Chou, C.; Deiters, A.; Chin, J. W. Genetically Encoded Norbornene Directs Site-Specific Cellular Protein Labelling via a Rapid Bioorthogonal Reaction. *Nat. Chem.* **2012**, *4* (4), 298–304. https://doi.org/10.1038/nchem.1250.

(166) Plass, T.; Milles, S.; Koehler, C.; Szymański, J.; Mueller, R.; Wießler, M.; Schultz, C.; Lemke, E. A. Amino Acids for Diels-Alder Reactions in Living Cells. *Angew. Chemie - Int. Ed.* **2012**, *51* (17), 4166–4170. https://doi.org/10.1002/anie.201108231.

(167) Plass, T.; Milles, S.; Koehler, C.; Schultz, C.; Lemke, E. A. Genetically Encoded Copper-Free Click Chemistry. *Angew. Chemie - Int. Ed.* **2011**, *50* (17), 3878–3881. https://doi.org/10.1002/anie.201008178.

(168) Jackson, J. C.; Duffy, S. P.; Hess, K. R.; Mehl, R. A. Improving Nature's Enzyme Active Site with Genetically Encoded Unnatural Amino Acids. *J. Am. Chem. Soc.* **2006**, *128* (34), 11124–11127. https://doi.org/10.1021/ja061099y.

(169) Ugwumba, I. N.; Ozawa, K.; Xu, Z. Q.; Ely, F.; Foo, J. L.; Herlt, A. J.; Coppin, C.; Brown, S.; Taylor, M. C.; Ollis, D. L.; Mander, L. N.; Schenk, G.; Dixon, N. E.; Otting, G.; Oakeshott, J. G.; Jackson, C. J. Improving a Natural Enzyme Activity through Incorporation of Unnatural Amino Acids. *J. Am. Chem. Soc.* **2011**, *133* (2), 326–333. https://doi.org/10.1021/ja106416g.

(170) Chin, J. W.; Santoro, S. W.; Martin, A. B.; King, D. S.; Wang, L.; Schultz, P. G. Addition of P-Azido-L-Phenylalanine to the Genetic Code of Escherichia Coli. *J. Am. Chem. Soc.* **2002**, *124* (31), 9026–9027. https://doi.org/10.1021/ja027007w.

(171) Fleet, G. W. J.; Porter, R. R.; Knowles, J. R. Affinity Labelling of Antibodies with Aryl Nitrene as Reactive Group. *Nature* **1969**, *224* (5218), 511–512. https://doi.org/10.1038/224511a0.

(172) Krieg, U. C.; Walter, P.; Johnson, A. E. Photocrosslinking of the Signal Sequence of Nascent Preprolactin to the 54-Kilodalton Polypeptide of the Signal Recognition Particle. *Proc. Natl. Acad. Sci. U. S. A.* **1986**, *83* (22), 8604–8608. https://doi.org/10.1073/pnas.83.22.8604.

(173) Nguyen, T. A.; Cigler, M.; Lang, K. Expanding the Genetic Code to Study Protein–Protein Interactions. *Angew. Chemie - Int. Ed.* **2018**, *57* (44), 14350–14361. https://doi.org/10.1002/anie.201805869.

(174) Baruah, H.; Puthenveetil, S.; Choi, Y.-A.; Shah, S.; Ting, A. Y. An Engineered Aryl Azide Ligase for Site-Specific Mapping of Protein-Protein Interactions through Photo-Cross-Linking. *Angew. Chemie* **2008**, *120* (37), 7126–7129. https://doi.org/10.1002/ange.200802088.

(175) Li, Y.; Champion, J. A. Photocrosslinked, Tunable Protein Vesicles for Drug Delivery Applications. *Adv. Healthc. Mater.* **2021**, *10* (15), 1–7. https://doi.org/10.1002/adhm.202001810.

(176) Coin, I. Application of Non-Canonical Crosslinking Amino Acids to Study Protein–Protein Interactions in Live Cells. *Curr. Opin. Chem. Biol.* **2018**, *46*, 156–163. https://doi.org/10.1016/j.cbpa.2018.07.019.

(177) Dehling, E.; Rüschenbaum, J.; Diecker, J.; Dörner, W.; Mootz, H. D. Photo-Crosslink Analysis in Nonribosomal Peptide Synthetases Reveals Aberrant Gel Migration of Branched Crosslink Isomers and Spatial Proximity between Non-Neighboring Domains. *Chem. Sci.* **2020**, *11* (33), 8945–8954. https://doi.org/10.1039/d0sc01969k.

(178) Li, J.; Guo, S.; Chai, F.; Sun, Q.; Li, P.; Gao, L.; Dai, L.; Ouyang, X.; Zhou, Z.; Zhou, L.; Cheng, W.; Qi, S.; Lu, K.; Ren, H. Genetically Incorporated Crosslinkers Reveal Nlee Attenuates Host Autophagy Dependent on Psmd10. *Elife* **2021**, *10*, 1–23.

https://doi.org/10.7554/eLife.69047.

(179) Choi, C. P.; Moon, A. S.; Back, P. S.; Jami-Alahmadi, Y.; Vashisht, A. A.; Wohlschlegel, J. A.; Bradley, P. J. A Photoactivatable Crosslinking System Reveals Protein Interactions in the Toxoplasma Gondii Inner Membrane Complex. *PLoS Biol.* **2019**, *17* (10), 1–25. https://doi.org/10.1371/journal.pbio.3000475.

(180) Seidel, L.; Zarzycka, B.; Zaidi, S. A.; Katritch, V.; Coin, I. Structural Insight into the Activation of a Class B G-Protein-Coupled Receptor by Peptide Hormones in Live Human Cells. *Elife* **2017**, *6*, 1–25. https://doi.org/10.7554/eLife.27711.

(181) Coin, I.; Katritch, V.; Sun, T.; Xiang, Z.; Siu, F. Y.; Beyermann, M.; Stevens, R. C.; Wang, L. XGenetically Encoded Chemical Probes in Cells Reveal the Binding Path of Urocortin-i to CRF Class B GPCR. *Cell* **2013**, *155* (6), 1258. https://doi.org/10.1016/j.cell.2013.11.008.

(182) Seidel, L.; Coin, I. Mapping of Protein Interfaces in Live Cells Using Genetically Encoded Crosslinkers. *Methods Mol. Biol.* **2018**, *1728*, 221–235. https://doi.org/10.1007/978-1-4939-7574-7_14.

(183) Kahl, G. Non-Canonical Amino Acid. In *The Dictionary of Genomics, Transcriptomics and Proteomics*; Wiley-VCH Verlag GmbH & Co. KGaA: Weinheim, Germany, 2015; pp 1–1. https://doi.org/10.1002/9783527678679.dg08406.

(184) Kolb, H. C.; Finn, M. G.; Sharpless, K. B. Click Chemistry: Diverse Chemical Function from a Few Good Reactions. *Angew. Chemie Int. Ed.* **2001**, *40* (11), 2004–2021. https://doi.org/10.1002/1521-3773(20010601)40:11<2004::AID-ANIE2004>3.0.CO;2-5.

(185) Kiick, K. L.; Saxon, E.; Tirrell, D. A.; Bertozzi, C. R. Incorporation of Azides into Recombinant Proteins for Chemoselective Modification by the Staudinger Ligation. *Proc. Natl. Acad. Sci.* **2002**, *99* (1), 19–24. https://doi.org/10.1073/pnas.012583299.

(186) Agard, N. J.; Prescher, J. A.; Bertozzi, C. R. A Strain-Promoted [3 + 2] Azide-Alkyne Cycloaddition for Covalent Modification of Biomolecules in Living Systems. *J. Am. Chem. Soc.* **2004**, *126* (46), 15046–15047. https://doi.org/10.1021/ja044996f.

(187) Nandivada, H.; Jiang, X.; Lahann, J. Click Chemistry: Versatility and Control in the Hands of Materials Scientists. *Adv. Mater.* **2007**, *19* (17), 2197–2208. https://doi.org/10.1002/adma.200602739.

(188) Kim, E.; Koo, H. Biomedical Applications of Copper-Free Click Chemistry:: In Vitro, in Vivo, and Ex Vivo. *Chem. Sci.* **2019**, *10* (34), 7835–7851. https://doi.org/10.1039/c9sc03368h.

(189) Smeenk, M. L. W. J.; Agramunt, J.; Bonger, K. M. Recent Developments in Bioorthogonal Chemistry and the Orthogonality Within. *Curr. Opin. Chem. Biol.* **2021**, *60*, 79–88. https://doi.org/10.1016/j.cbpa.2020.09.002.

(190) Dommerholt, J.; Van Rooijen, O.; Borrmann, A.; Guerra, C. F.; Bickelhaupt, F. M.; Van Delft, F. L. Highly Accelerated Inverse Electron-Demand Cycloaddition of Electron-Deficient Azides with Aliphatic Cyclooctynes. *Nat. Commun.* **2014**, *5*, 1–7. https://doi.org/10.1038/ncomms6378.

(191) Lee, T. C.; Kang, M.; Kim, C. H.; Schultz, P. G.; Chapman, E.; Deniz, A. A. Dual Unnatural Amino Acid Incorporation and Click-Chemistry Labeling to Enable Single-Molecule FRET Studies of P97 Folding. *ChemBioChem* **2016**, *17* (11), 981–984. https://doi.org/10.1002/cbic.201500695.

(192) Van Treel, N. D.; Mootz, H. D. SUMOylated RanGAP1 Prepared by Click Chemistry. *J. Pept. Sci.* **2014**, *20* (2), 121–127. https://doi.org/10.1002/psc.2591.

(193) Arts, R.; Ludwig, S. K. J.; Van Gerven, B. C. B.; Estirado, E. M.; Milroy, L. G.; Merkx, M. Semisynthetic Bioluminescent Sensor Proteins for Direct Detection of Antibodies and Small Molecules in Solution. *ACS Sensors* **2017**, *2* (11), 1730–1736. https://doi.org/10.1021/acssensors.7b00695.

(194) Moatsou, D.; Li, J.; Ranji, A.; Pitto-Barry, A.; Ntai, I.; Jewett, M. C.; O'Reilly, R. K. Self-Assembly of Temperature-Responsive Protein-Polymer Bioconjugates. *Bioconjug. Chem.* **2015**, *26* (9), 1890–1899. https://doi.org/10.1021/acs.bioconjchem.5b00264.

(195) Young, T. S.; Schultz, P. G. Beyond the Canonical 20 Amino Acids: Expanding the Genetic Lexicon. *J. Biol. Chem.* **2010**, *285* (15), 11039–11044. https://doi.org/10.1074/jbc.R109.091306.

(196) Yu, Y.; Hu, C.; Xia, L.; Wang, J. Artificial Metalloenzyme Design with Unnatural Amino Acids and Non-Native Cofactors. *ACS Catal.* **2018**, *8* (3), 1851–1863. https://doi.org/10.1021/acscatal.7b03754.

(197) Drienovská, I.; Rioz-Martínez, A.; Draksharapu, A.; Roelfes, G. Novel Artificial Metalloenzymes by in Vivo Incorporation of Metal-Binding Unnatural Amino Acids. *Chem. Sci.* **2015**, *6* (1), 770–776. https://doi.org/10.1039/c4sc01525h.

(198) Hyun, S. L.; Schultz, P. G. Biosynthesis of a Site-Specific DNA Cleaving Protein. *J. Am. Chem. Soc.* **2008**, *130* (40), 13194–13195. https://doi.org/10.1021/ja804653f.

(199) Drienovská, I.; Alonso-Cotchico, L.; Vidossich, P.; Lledós, A.; Maréchal, J. D.; Roelfes, G. Design of an Enantioselective Artificial Metallo-Hydratase Enzyme Containing an Unnatural Metal-Binding Amino Acid. *Chem. Sci.* **2017**, *8* (10), 7228–7235. https://doi.org/10.1039/c7sc03477f.

(200) Luo, X.; Wang, T. S. A.; Zhang, Y.; Wang, F.; Schultz, P. G. Stabilizing Protein Motifs with a Genetically Encoded Metal-Ion Chelator. *Cell Chem. Biol.* **2016**, *23* (9), 1098–1102. https://doi.org/10.1016/j.chembiol.2016.08.007.

(201) Zubi, Y. S.; Seki, K.; Li, Y.; Hunt, A. C.; Liu, B.; Roux, B.; Jewett, M. C.; Lewis, J. C. Metal-Responsive Regulation of Enzyme Catalysis Using Genetically Encoded Chemical Switches. *Nat. Commun.* **2022**, *13* (1), 1–10. https://doi.org/10.1038/s41467-022-29239-y.

(202) Mills, J. H.; Sheffler, W.; Ener, M. E.; Almhjell, P. J.; Oberdorfer, G.; Pereira, J. H.; Parmeggiani, F.; Sankaran, B.; Zwart, P. H.; Baker, D. Computational Design of a Homotrimeric Metalloprotein with a Trisbipyridyl Core. *Proc. Natl. Acad. Sci. U. S. A.* **2016**, *113* (52), 15012–15017. https://doi.org/10.1073/pnas.1600188113.

Chapter 2

Visualization of the delivery and release of small RNAs using genetic code expansion and unnatural RNA-binding proteins

2.1 Preface

This Chapter consists of data previously published in Bioconjugate Chem. 2018, 29, 12, 3982–3986. Copyright 2018, American Chemical Society. It is adapted here with the permission of the publisher. The main text and supplemental information are combined.

This article is authored by Noreen Ahmed, Joanna Fréderique De Graaf, Nadine Ahmed, Dana V. Foss, Julie Delcorde, Peter G. Schultz, and John Paul Pezacki.

As the first author of this publication, I made significant experimental and intellectual contributions to this article. I performed most of the experiments and sample preparations, including FRET assays and *in vitro* characterizations of the proteins. F. De Graaf performed some of the site-directed mutagenesis experiments and initial optimization experiments. Nadine Ahmed aided with the fluorescence imaging experiments. D.V. Foss, J. Delcorde, and J.P. Pezacki provided intellectual contributions. I wrote the first draft of the manuscript and editing was performed by all authors.

2.2 Abstract

Endogenously expressed non-coding RNAs (ncRNAs) are regulators of mRNA translation and affect diverse biological pathways spanning embryogenesis to cholesterol and fatty acid metabolism. Recently, microRNAs and siRNAs have become important therapeutic molecules with strategies that employ oligonucleotides as both mimics and inhibitors. However, delivery of these exogenous effectors remains a major challenge. Here, we present a method for evaluating ncRNA delivery using the viral suppressor of RNA silencing (VSRS) protein p19, optimized for cellular delivery of small RNAs. Using genetic code expansion technology, *p*-azidophenylalanine (*p*-AzF) was incorporated into a recombinant p19 protein and used to develop a fluorescence resonance energy transfer (FRET) sensor. AzF was used to attach FRET acceptor moieties using bioorthogonal chemistry. We show that this strategy not only gives rise to FRET signals that report on small RNA binding but also allows for fluorescence quenching as well, convenient for measuring RNA release. We demonstrate the successful use of a modified version of the probe to track the delivery and release of small RNAs into mammalian cells. The results provide a basis for further development of vehicles for small RNA delivery and release for intervening in non-coding RNA biology.

2.3 Introduction

MicroRNAs (miRNAs) are small non-coding RNAs that are involved in post-transcriptional gene regulation, where silencing of the target genes takes place[1–3]. miRNAs have been implicated in several diseases[4] and as a result, have been utilized as targets for therapeutic purposes[4]. However, there are some limitations associated with the delivery of miRNAs such as poor miRNA penetration[5–7]. Additionally, miRNA antagonists and miRNA mimics are quickly degraded and cleared from the blood circulation[5–7]. Immunotoxicity associated with miRNA treatments and delivery, mainly through the engagement of toll-like receptors (TLRs), can also arise[5]. Efficient delivery of miRNAs and small interfering RNAs (siRNAs) is of great interest due to the potential of these molecules in therapy and biotechnology. Lipid-based delivery systems are used to encapsulate biologically active miRNAs and siRNAs[7]. Even though liposomes and lipid nanoparticles are commonly used for the delivery of small RNA cargo[8,9], such methods are intrinsically disadvantaged owing to cytotoxicity, which remains a major hurdle[8,9]. Thus, protein-based methods for delivering miRNAs and siRNAs have emerged. Direct delivery of RNA binding proteins (RBPs) across the cell membrane can be achieved through chemical conjugation or genetic fusion of moieties that allow cell penetration[10–14]. These protein-mediated RNA delivery approaches have been shown to exhibit lower toxicity than lipid carriers, viral vector-mediated expression, and other nanotechnology delivery platforms[10–14].

Recombinant p19, a *Tombusvirus* viral suppressor of RNA silencing, has been employed for siRNA delivery in human cells[12,14–16]. A recombinant linked p19 dimer fused to Human Immunodeficiency Virus-1's (HIV) Trans-Activator of Transcription (TAT) peptide was highly efficient in RNA delivery to human cells[11]. Another approach employed p19 linked to capsid proteins of hepatitis B virus[17]. Additionally, fusions of p19 to ephrin mimetic peptide (YSA) were

efficiently used to target tumor cells for siRNA therapy[10]. As a delivery tool, engineered p19 proteins are effective because they exhibit high affinity towards their RNA ligands, typically being K_D = 0.2 nmol/L, the highest affinity protein carrier of small RNAs used for this purpose. Thus, we have used it here to develop general methods for monitoring the delivery and release of RNA. Fluorescence-based probes for imaging delivery and oligonucleotide release can help uncover molecular details since the intracellular release of small RNAs is ultimately required to facilitate their biological effects. To address this challenge, we present a method for evaluating small RNA delivery using the viral suppressor of RNA silencing (VSRS) protein p19, optimized for cellular delivery of small RNAs, with the use of genetic code expansion technology through the introduction of unnatural amino acids (UAAs), specifically *p*-AzF, to design a p19 sensor protein to detect small RNA binding and release.

There are several reported methods for small RNA imaging upon delivery, none of which confirm the time interval of RNA release[18,19]. Most methods depend on indirect confirmation of successful RNA delivery without explicit release being monitored. The indirect confirmation mainly depends on the downstream effects of the released RNA cargo[18,19]. In this study, we utilize genetic code expansion technology to improve the functionality of p19 as a tool for small RNA sensing and directly visualize the release of RNA. The incorporation of UAAs allows the introduction of unique functional characteristics not naturally present in the 20 canonical amino acids[20,21]. In our work, we are incorporating *p*-AzF (Fig. 1A) in a site-specific manner in response to an amber suppression codon[20,21]. UAAs were genetically incorporated using an orthogonal aminoacyl-tRNA (aa-tRNA)/aminoacyl-tRNA synthetase (aaRS) pair[20–22]. The incorporated azide group was used to label the protein through strain-promoted alkyne-azide cycloaddition (SPAAC) for Förster resonance energy transfer (FRET) studies of binding and release of small RNA cargo[23].

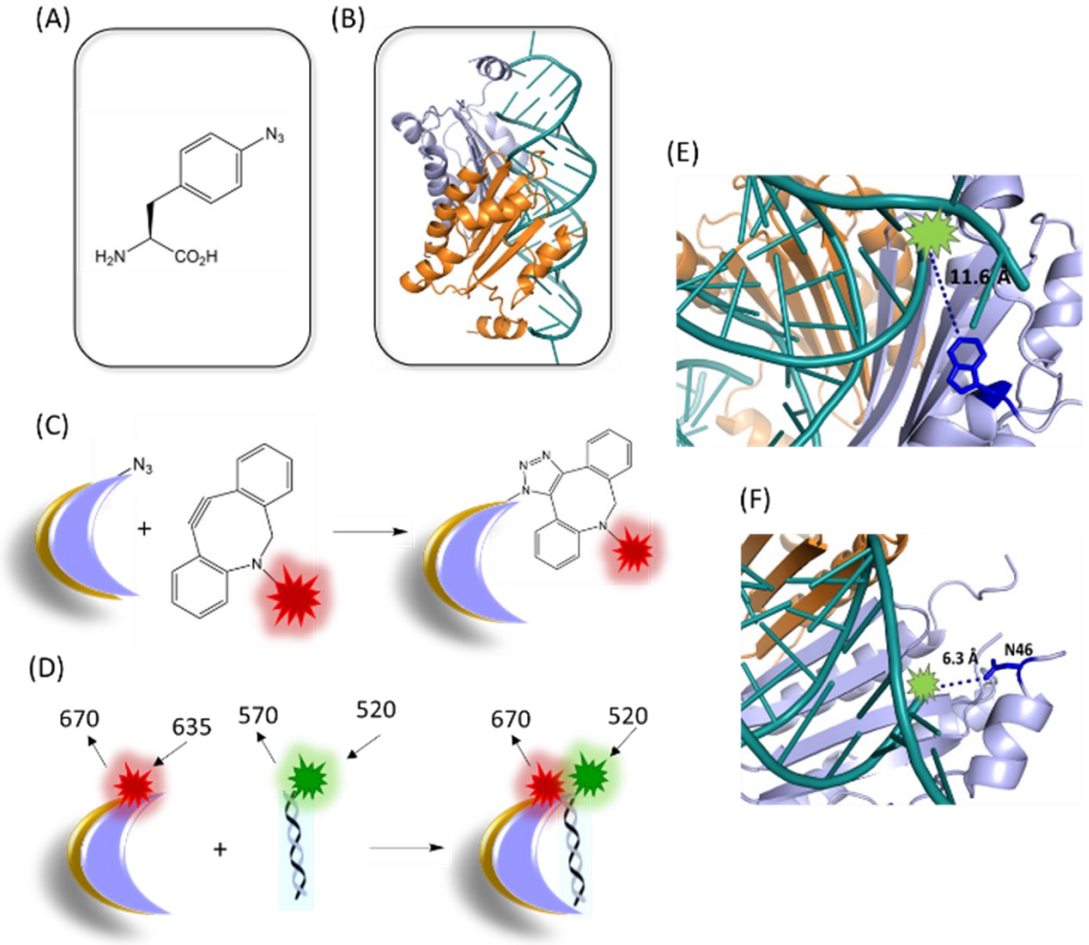

Figure 2.1 AzF incorporation in p19 and subsequent DBCO-Cy5 labeling in a site-specific manner using strain promoted alkyne-azide cycloaddition. (A) The chemical structure of para-azidophenylalanine (AzF). (B) Crystal structure of Carnation Italian Ringspot Virus (CIRV) p19 complex with a 21- nt siRNA (PDB: 1RPU). (C) A schematic representation of p19 mutant labeling using DBCO-Cy5 through strain-promoted alkyne-azide cycloaddition (SPAAC). (D) Schematic representation of the designed sensor protein where the UAA is incorporated in a site-specific manner in response to an amber mutation. Upon the binding of small RNA molecules, binding is detected via FRET. (E and F) A close-up of surface residues in p19, W19 and N46 positions chosen for AzF incorporation, and their relative position from a fluorophore labeled RNA.

2.4 Results and Discussion

2.4.1 Introduction of *p*-AzF in p19 mutants

First, we sought to identify potential residues that are optimal candidates for UAA incorporation. Examination of the x-ray crystal structures of p19 enabled the identification of two residues in p19 that are within FRET distance (0-100 Å) from the 5' end of the bound dsRNA, the location where FRET donor fluorophore was conjugated (Figure 2.1B)[24,25]. Among the options, residues W19 and N46 were chosen due to their relative proximity to the location of the tagging site on the RNA substrate and the likelihood that residue substitution would affect ligand binding since they are located outside of the ligand binding pocket. The distance of these residues from the 5' substrate RNA according to the x-ray structures is 11.6 Å and 6.3 Å respectively (Fig. 2.1E, F)[24]. Additionally, sites of UAA incorporation were chosen based on their accessibility to the subsequent click chemistry reactions. Mutating conserved residues was avoided, where conserved residues were determined by an alignment of p19 proteins of *Tombusviridae* family members[24,25]. Amber suppressor codons were introduced into residues W19 and N46 of p19 DNA constructs containing an 8x Histidine tag at the C-terminus for ease of purification. These plasmids were expressed in *E. coli* co-transformed with a plasmid expressing the corresponding aa-tRNA and aaRS as well as co-treated with *p*-AzF. Full-length protein expression was confirmed by western blot analysis, where expected bands were observed upon the introduction of the AzF (Fig. 2.2A). Some background expression was observed in the controls, where AzF wasn't supplemented in the culture media (Fig. 2.2A). Polyspecific *Methanococcus janannaschi* (MJ) tyrosyl synthetase is used in this study, and therefore misincorporation of Tyrosine residues is observed in response to an amber mutation in the absence of the supplemented UAA. Next, we sought to assess the purity and yields of protein by fast protein liquid chromatography (FPLC) (Fig. 2.2B). Yields for mutants

N46AzF and W19AzF were reasonable at 2.5 mg/L and 3.68 mg/L, respectively. These yields compare well with the yields of p19-wt, which was 7.5 mg/L. The slightly lower yields may be attributed to lower translation efficiencies associated with the evolved bioorthogonal aa-tRNA /aaRS and relative protein stability during the purification process. Since p19 binds RNA as a dimer, each of the monomer will contain the mutation leading to the incorporation of AzF.

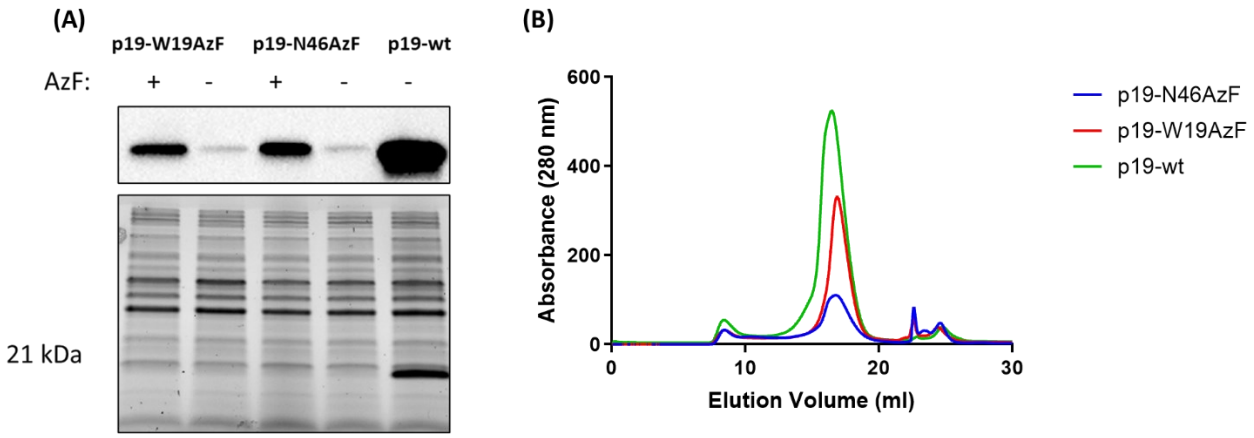

Figure 2.2. Expression of Full length AzF mutants. (A) A western blot depicting the expression of mutants (p19-W19AzF and p19-N46AzF) in the presence and absence of 1mmol/L *p*-AzF from bacterial (*E.coli*) lysates. Bottom panel represents stain-free loading control. (B) Size exclusion chromatography profile for p19-wt, p19-W19AzF and p19-N46AzF run in 1x PBS, pH 7.5 on a Superdex 200 column (GE).

2.4.2 Fluorescence labeling of p19-W19AzF and assessing RNA binding using FRET

Upon purification of the wild-type protein and mutants, we then performed strain-promoted azide-alkyne cycloadditions (SPAAC), according to Fig. 2.1 C, D. The products of these reactions were then analyzed for labeling using in-gel fluorescence experiments. From Fig. 2.3A, it is evident that the mutant, p19-W19AzF, is more efficiently labeled in comparison to the p19-wt. However, some background labeling was still observed in the p19-wt. To assess the FRET interactions, we performed binding studies with a model siRNA substrate GL2 targeting Firefly luciferase and containing Cy3 at the 5' end of the guide strand. We have performed the FRET binding experiments with Cy5 labeled protein (p19-wt and p19-W19AzF) and Cy3-siRNA and we were able to observe the FRET signal between p19-W19AzF-Cy5 and Cy3-siRNA (Fig. 2.3 B, C), However, background FRET signal was still observed with p19-wt.

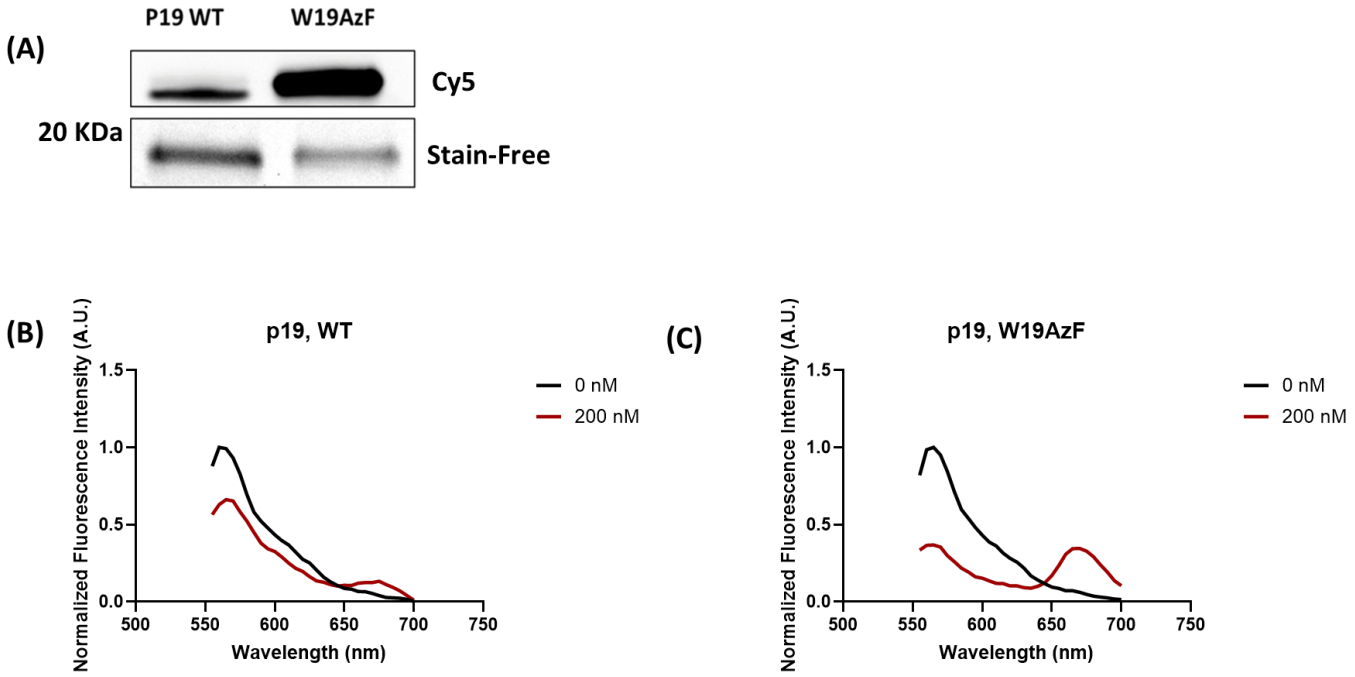

Figure 2.3. Fluorescence gel and FRET Spectra of Cy5 Labeled p19 Mutant. (A) Purified p19-wt and p19-W19AzF are labeled using DBCO-Cy5 and analyzed using SDS-PAGE in-gel fluorescence (Cy5). 'Stain-Free' refers to TGX stain-free gel. (B, C) 200 nmol/L of p19-wt -Cy5 and p19-W19AzF-Cy5 are incubated with 10 nmol/L Cy3-Gl2 siRNA duplex for 1 hour at room temperature. The spectra are recorded for p19-wt-Cy5 and p19-W19Azf-Cy5 with excitation at 520 nm with emission recorded from 555 to 700 nm. Spectra represents the mean of three trials.

2.4.3 Fluorescence labeling of p19-III mutants and assessing RNA binding using FRET

Background labeling in p19-wt is attributed to the presence of three cysteine residues in p19, C110, C134, C160[25–27]. Cysteine residues will react slowly with the strained alkyne, leading to the background labeling[26]. To overcome this issue, we mutated the three cysteine residues present in p19 into isoleucine (p19-III) as previously described[28]. Cysteine replacement does not affect RNA binding to p19-wt and was shown to be more stabilizing, specifically for residue C110 since it is located in the binding pocket of p19. The transition from a polar cysteine to a hydrophobic isoleucine side chain may strengthen the Van der Waals interactions of the p19 protein hydrophobic interior leading to enhanced binding [28].

Successful incorporation of AzF in the mutated p19-III at positions W19 and N46 was observed and confirmed via western blot (Fig. 2.4A). Further purification and confirmation of full-length proteins were conducted using FPLC (Fig. 2.4B, S2.1). Cy5-DBCO labeling of p19-III-W19AzF and p19-III-N46AzF using SPAAC was performed, with no labeling observed for p19-III-wt (Fig. 2.4C).

Similarly, binding interactions using FRET for p19-III-W19AzF-Cy5 and p19-III-N46AzF-Cy5 have been successfully observed post-labeling (Fig. 2.4D, E). These results provide evidence that it is possible to measure the interactions of p19 with its RNA ligands through intermolecular FRET with a minimal perturbation on the structure and size of the proteins.

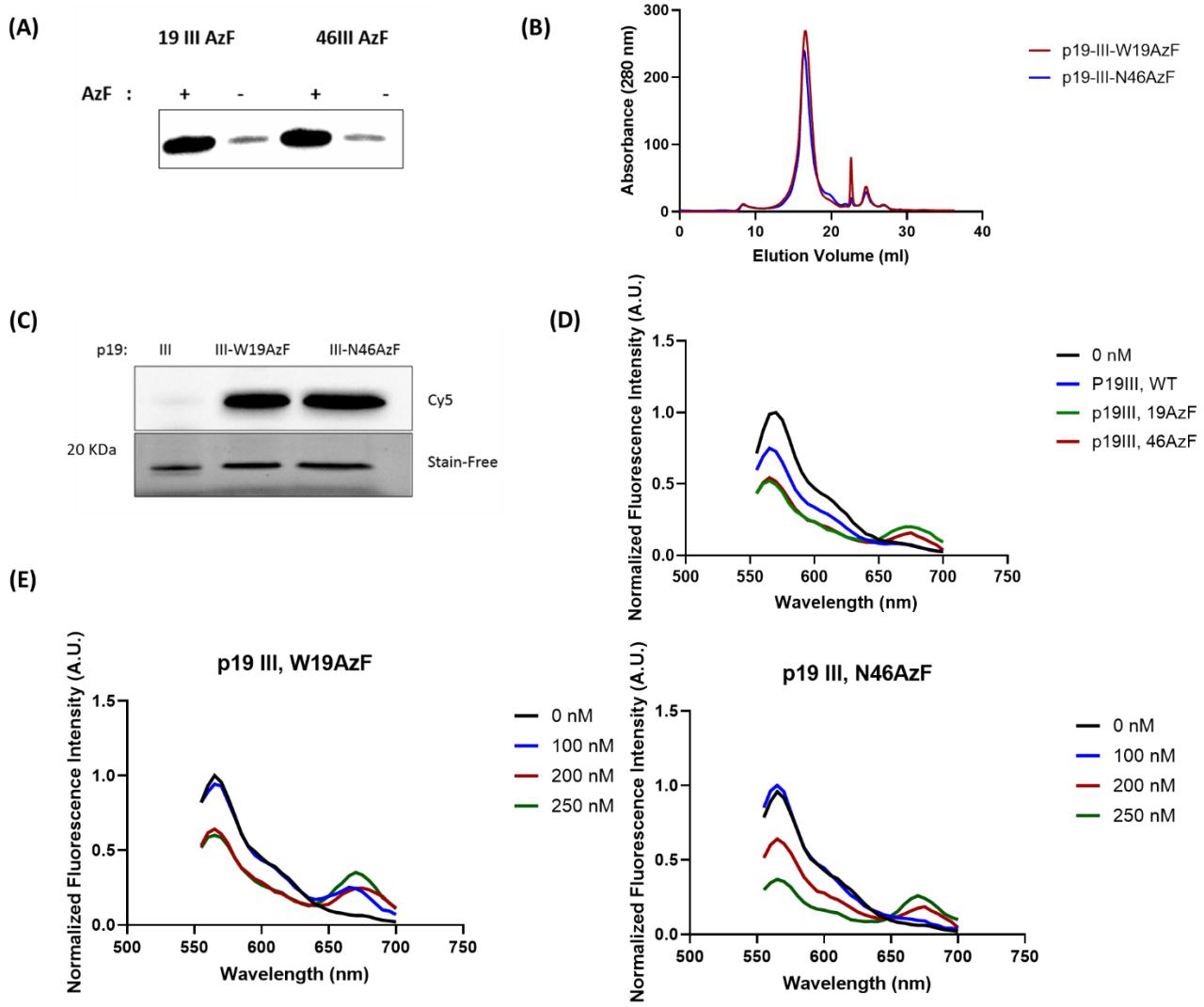

Figure 2.4. Expression and Fluorescence spectra of Cy5 labeled triple Isoleucine mutants of p19. (A)Western blot of mutants (p19-III-W19AzF and p19-III-N46AzF) expressed in the presence and absence of 1mmol/L AzF. Western blot was used to show the full-length expression of p19 mutants using anti-histag antibody (B) Size exclusion chromatography profile for p19-III-W19AzF and p19-III-N46AzF in 1x PBS, pH 7.5 on a Superdex 200 column (GE). (C) p19-III and mutants (p19-III-W19AzF and p19-III-N46AzF) are labeled with DBCO-Cy5 and analyzed using in-gel fluorescence. Stain-Free represents TGX-Stain-free gel as a loading control. (D) p19-III-Cy5 and mutants (p19-III-W19AzF-Cy5 and p19-III-N46AzF-Cy5) were incubated with 10 nmol/L Cy3-Gl2 siRNA duplex for 1 hour at room temperature. The spectra are recorded for p19 III, p19 III-W19Azf, and p19 III- N46AzF at 200 nmol/L, with excitation at 520 nm with emission recorded from 555 to 700 nm. (E)Fluorescence spectra of various concentrations of p19-III-W19AzF-Cy5 and p19-III-N46AzF-Cy5 upon incubation with 10 nmol/L Cy3-Gl2 siRNA for 1 hour. Spectra represents the mean of three trials

Electrophoretic mobility shift assays were used to determine the binding affinity of the labeled mutants. The dissociation constants (K_D) were determined for the DBCO-Cy5 labeled mutants, to determine the effects of labeling on the binding affinity. The K_D values were determined to be 1.6 ± 0.44 nmol/L and 0.44± 0.12 nmol/L for p19-III N46AzF-Cy5 and p19-III W19AzF-Cy5 respectively upon binding a fluorescein-labeled (FAM) GL2 siRNA (Fig. 2.5). Additionally, circular dichroism (CD) analysis was conducted on the labeled mutants in comparison to the p19-III. The CD analysis has identified that the incorporation of AzF and dye labeling has minimal effects on the secondary structure of the proteins in comparison to p19-III (Fig. 2.6).

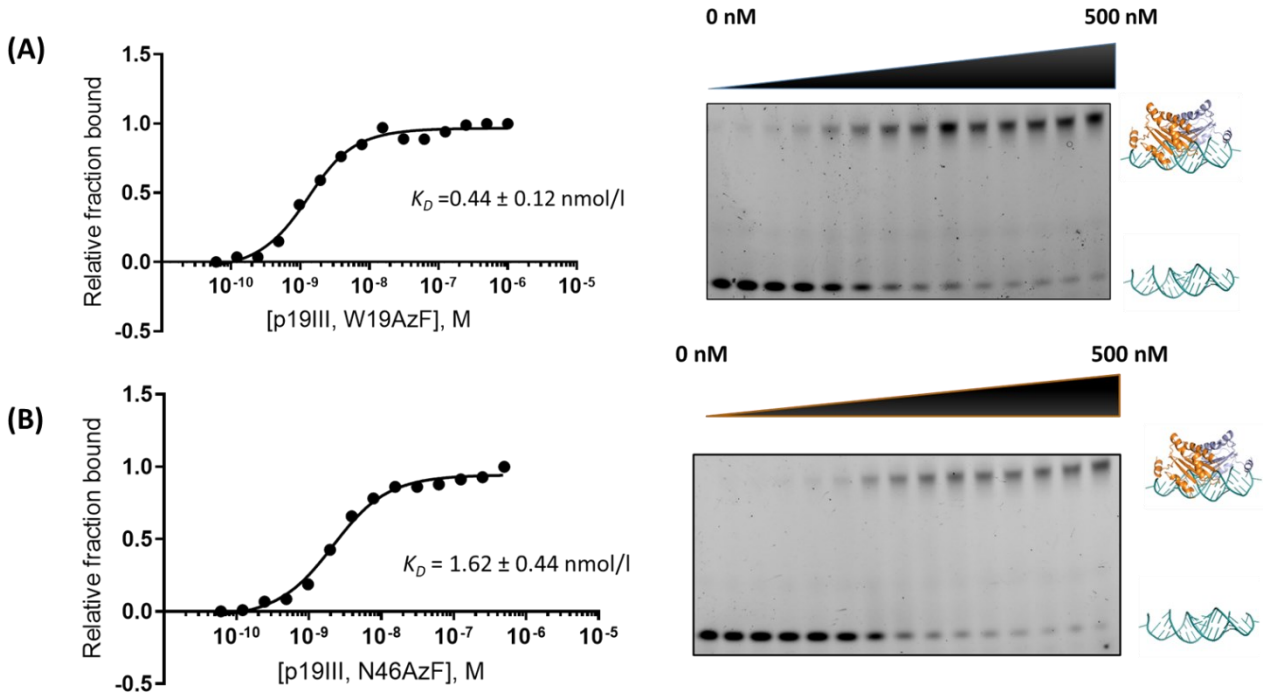

Figure 2.5. Binding affinity determination using electrophoretic mobility shift assay. Binding affinity of (A) p19-III-W19AzF-Cy5 and (B) p19-III-N46AzF-Cy5 as measured by EMSA using 1 nmol/L 5' FAM labeled Gl2 siRNA (21 mer). Varying concentrations of protein (0 nmol/L-500 nmol/L) were incubated with fixed concentrations of siRNA at room temperature in EMSA buffer for 1 hour.

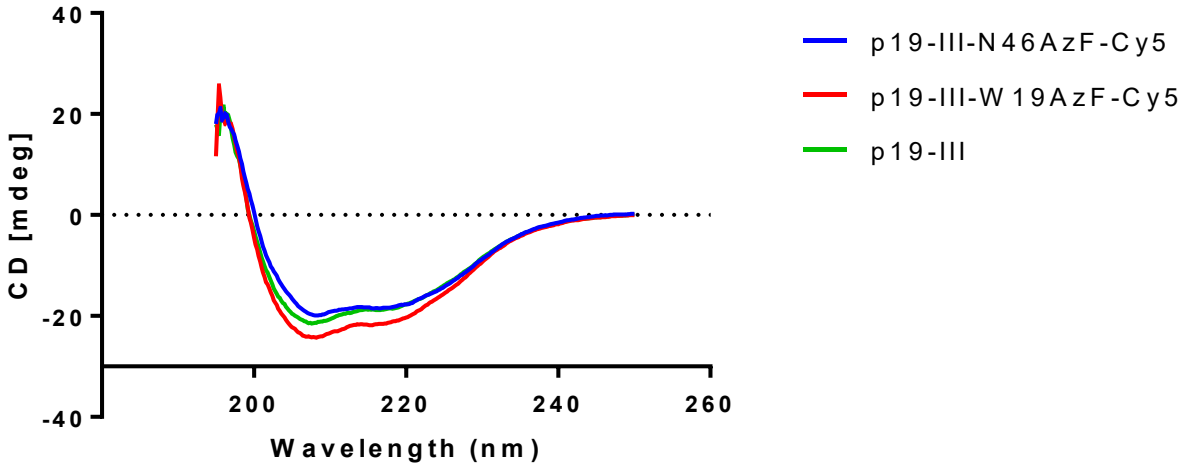

Figure 2.6. **Circular dichroism of p19-III and labeled mutants.** Far UV spectra for p19-III-N46AzF-Cy5, p19-III-W19AzF-Cy5 and p19-III is recorded from 185-250 nm.

2.4.4 Determining Binding affinity of p19-III-W19AzF-Cy5 using FRET

FRET signal was efficiently detected allowing for measurements of binding interactions and determining affinity measurements. The resultant concentration-dependent increase in Cy5 fluorescence signal induced via FRET was used to calculate the binding affinity of the mutant, p19-III-W19AzF-Cy5, towards Cy3-labeled GL2 siRNA. In these experiments, a concentration of 10 nmol/L Cy3-siRNA was used, and the concentration of the protein varied from 0 to 0.5 µmol/L. The measured dissociation constant is K_D= 55.07 nmol/L which agrees with values previously determined using other fluorescence-based methods such as fluorescence polarization [27] (Fig. 2.7). Given that the calculated K_D is higher than that determined using EMSAs, we speculate that it could be related to experimental conditions of both presented methods.

Moving forward, we will optimize the experimental conditions to ensure that the percentage of labeled protein is high. Some reports have identified that complete protein labeling via SPAAC required 6-10 hours depending on the nature of the protein and accessibility of the labeling site[29]. Slower reaction rates when labeling solvent-exposed residues of a protein using hydrophobic DBCO and DIBO is usually observed compared to the apparent rates observed in a homogenous system[30].

Additionally, there may be a population of p19-III-W19AzF that remains unlabeled, but able to still bind siRNA. During purification *in vitro* reduction of *p*-AzF to para-azidomethyl-l-phenylalanine (*p*-AmF) by the reducing agents being used, leading to an unlabeled population of protein[30]. Nonetheless, through careful preparation of p19 mutants with AzF incorporation and subsequent SPAAC labeling procedures, we were able to visualize p19 binding to its ligands via FRET and thus, the engineered p19 can be used as a reporter system for assessing the binding and release of small RNA cargo.

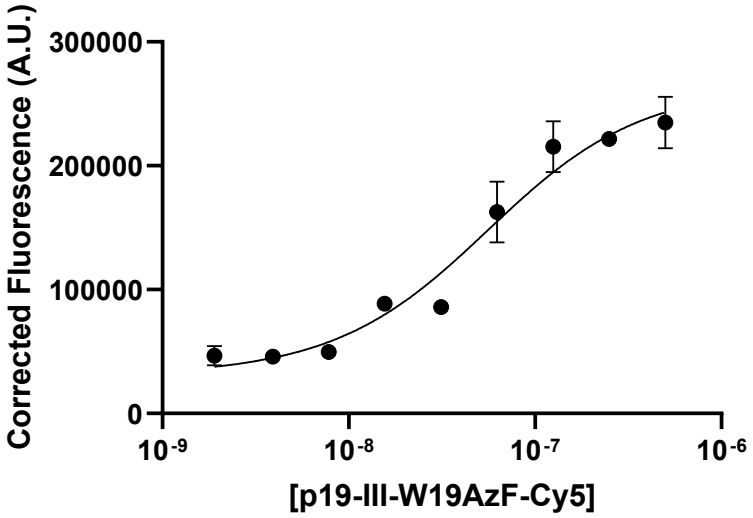

Figure 2.7. Binding affinity of p19-III-W19AzF-Cy5 as determined by FRET. Binding affinity of p19-III-W19AzF-Cy5 as measured by FRET using 10 nmol/L 5' Cy3-Gl2 siRNA (21 mer). Varying concentrations of protein were incubated with fixed concentrations of siRNA at room temperature for 1 hour. n=2, error bars represent ±standard deviation (SD). Recorded fluorescence excitation: 520 nm and emission:670 nm. Background fluorescence was subtracted upon incubation with unlabeled GL2 siRNA.

2.4.5 Engineering a p19-based probe to detect small RNA delivery and release in cells

To further utilize the designed probe as a mean to track RNA release *in situ*, we prepared an engineered p19 protein based on a previously designed fusion protein by our group[11]. Cloning of p19-2x-III-W19AzF–TAT was performed as previously described[11]. We built upon a previously constructed plasmid where the two p19-III monomers were linked via a flexible (GGGGSGGGGS) linker[25]. The linked recombinant CIRV p19-III dimer represents a stabilized version of the viral suppressor of RNA silencing. The linking of the dimer resulted in a protein that possesses improved stability and binding properties, which are generally beneficial characteristics for p19's development as a biotechnological tool[25]. The linked p19-III dimer, containing the W19AzF amber mutation, was then fused, at the C-terminus, to the TAT peptide derived from amino acids 49–57 of the HIV-1 TAT protein (RKKRRQRRR), similar to what has been described previously[11]. The p19-2x-III-W19AzF-TAT was subsequently labeled using SPAAC with DBCO-Cy5 (Cy5-p19-2x-III-W19AzF-TAT) (Fig. 2.8A). Successful delivery of the engineered Cy5-p19-2x-III-W19AzF-TAT to human hepatoma cell line (Huh7) was confirmed, where delivery of labeled protein: unlabeled siRNA complexes were also demonstrated by visualizing the fluorescence of Cy5-labeled p19-2x-III-W19AzF-TAT over 24 hours (Fig. 2.8C, 2.9).

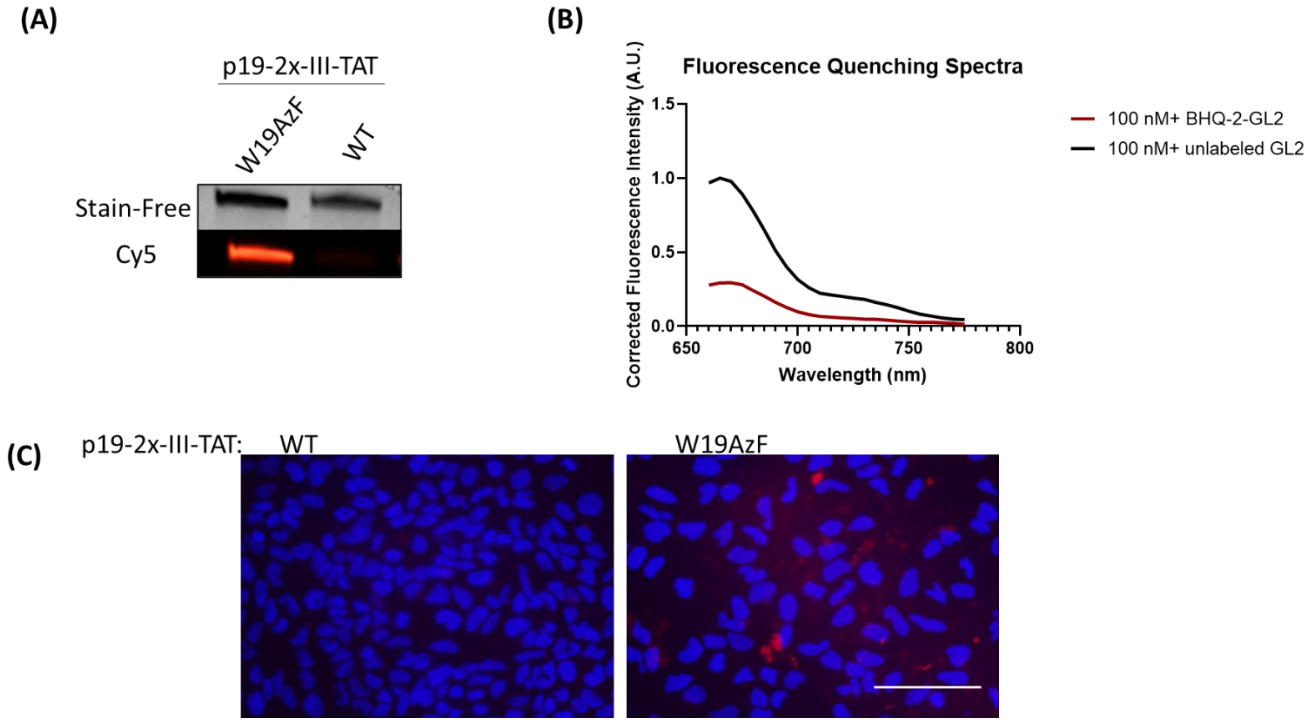

Figure 2.8. Fluorescence Labeling and Spectra of p19-2x-III-TAT. (A) p19-2x-III-wt-TAT and p19- 2x-III-W19AzF–TAT are labeled with DBCO-Cy5 and analyzed using in-gel fluorescence. Stain-Free represents TGX-Stain-free gel as a loading control. (B) Fluorescence quenching spectra of 100 nmol/L Cy5-labeled p19-2x-III-W19AzF-TAT upon incubation with either 100 nmol/L BHQ-2 tagged RNA or unlabeled RNA. Spectra represents the mean of three trials. (C) Fluorescence images of Huh7 cells treated with Cy5-2x-p19-III-W19AzF or Cy5-2x-p19III-WT and unlabeled GL2 siRNA for 24 hours. Images are taken at 40x magnification. Scale bar= 100 µm. Nuclei were stained with DAPI (blue).

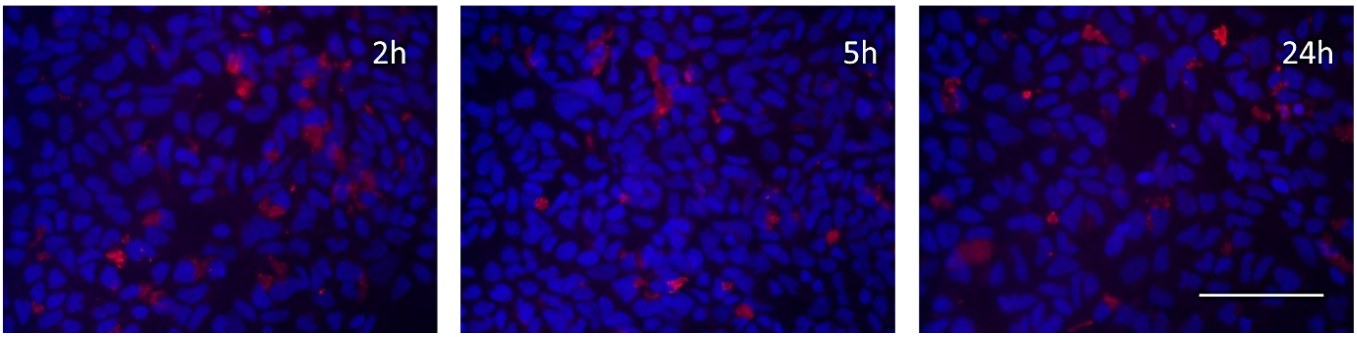

Figure 2.9. Delivery of siRNA to Huh7 cells. Fluorescence imaging of Cy5-2x-p19-III-W19AzF delivery of unlabeled siRNA in Huh7 cells. Cells were treated with Cy5-2x-p19-III-W19AzF for 2hours, 5 hours and 24 hours. Images were taken at 20x magnification. Scale bar= 100 μm. Nuclei were stained with DAPI (blue).

For visualization of RNA release into the cells, we used a slightly different strategy employing a quencher-labeled siRNA (BHQ-2 GL2 siRNA), and then applied it to cells for RNA delivery and release (Fig. 2.10A). The ability of BHQ-2 GL2 to quench the fluorescence signal of Cy5-labeled p19-2x-III-W19AzF-TAT was evaluated and confirmed *in vitro* (Fig. 2.8B).

Using a 'turn on' fluorescence approach we were able to measure small RNA release directly in cells. Cy5-p19-2x-III-W19AzF-TAT was complexed with a black-hole quencher (BHQ-2) labeled Gl2-RNA. Huh7 cells were treated with the protein: RNA complexes for 2 hours, 5 hours, and 24 hours. Here we were able to confirm the successful delivery of Cy5-p19-2x-III-W19AzF-TAT (Fig. 2.9, 2.10B). Due to the quenching effect of the BHQ-2 GL2 siRNA, we were able to visualize a gradual increase in red fluorescence over time, giving a direct visualization of RNA release (Fig. 2.10B). In Huh7 human hepatoma cells, we see that the p19-2x-III-W19AzF–TAT releases its RNA cargo slowly over 24 hours, with initial release observed after 2 hours of treatment. No gradual increase in fluorescence signal was observed upon delivery of unlabeled GL2 siRNA (Fig. 2.9).

We have confirmed that treatment with p19-2x-III-W19AzF-TAT is not cytotoxic to the cells being used in the assay when compared to other RNAiMAX, which is a lipid-based ncRNAs delivery reagent. We used 3-(4,5-dimethylthiazol-2-yl)-2,5-diphenyl-2H-tetrazolium bromide (MTT) assay to report on cell viability over 48 hours (Figure 2.11A). To validate that the delivered RNA is functional, a luciferase assay was performed, where the knockdown activity of the delivered RNA was tested for its ability to target firefly luciferase mRNA in 48 hours. Huh7 cells were transfected with dual luciferase reporter (psiCHECK-2) and treated with p19-2x-III-W19AzF-TAT delivering siRNA targeting firefly luciferase. From the presented data (Fig. 2.11B),

it is evident that the knockdown of the luciferase signal is observable at 48 hours, confirming that the delivered siRNA is intact and functional.

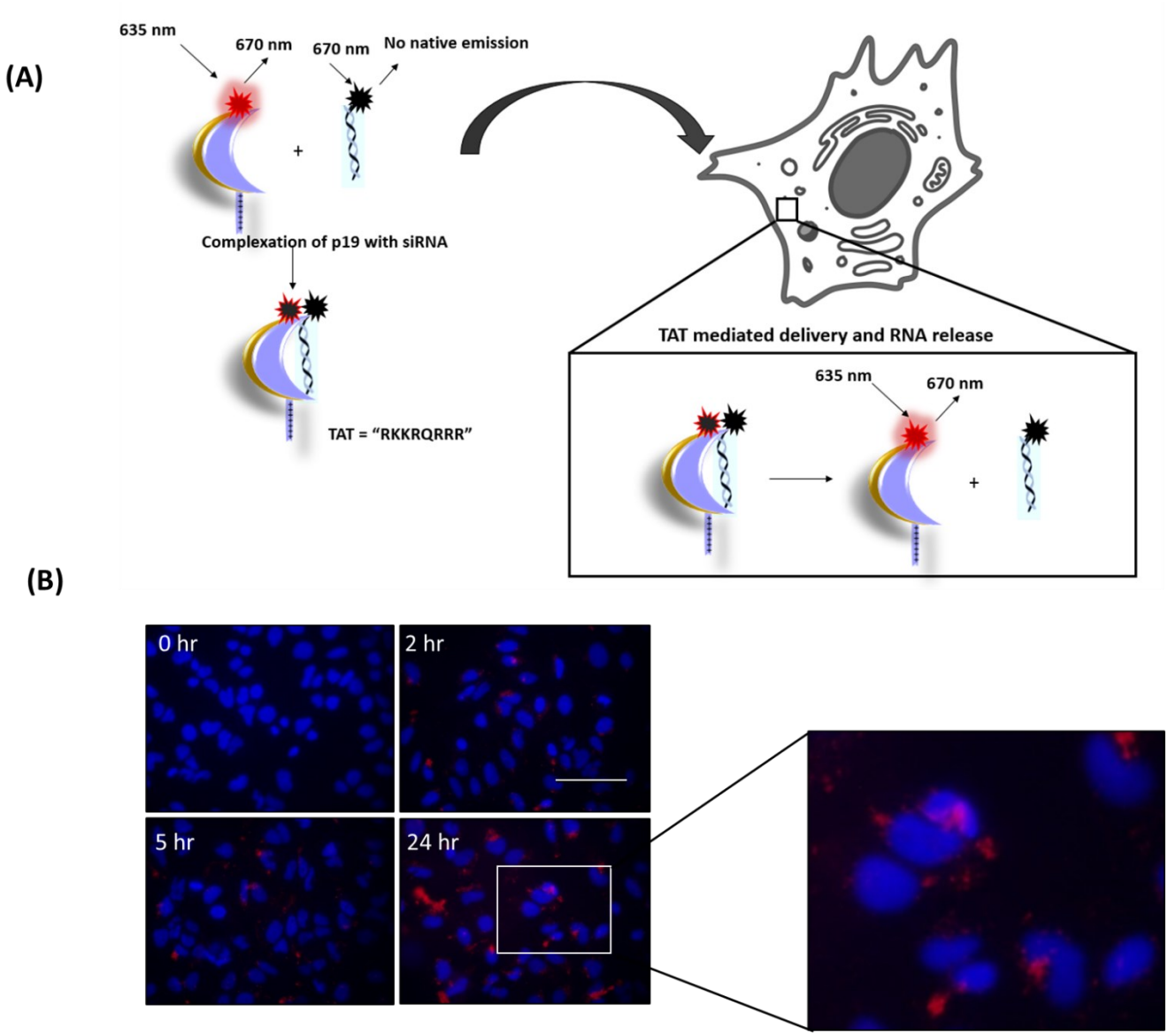

Figure 2.10. Fluorescence imaging of Cy5-2x-p19-III-W19AzF delivery of BHQ-2-siRNA in Huh7 cells. (A) A schematic representation depicting RNA delivery and release via the designed p19 fusion protein. The designed p19 fusion protein dimer is linked via flexible linker that allows C-terminus fusion to a TAT peptide. The p19 dimer has AzF incorporated in a site-specific manner to allow Cy5 red fluorescence detection and subsequent "fluorescence turn-on" based RNA release tracking upon cellular uptake. (B) Cells were treated with Cy5-2x-p19-III-W19AzF for 2hours, 5 hours and 24 hours. Scale bar= 100 µm. DAPI nuclear stain was used (blue) to identify the nuclei. Images were taken at 40x magnification.

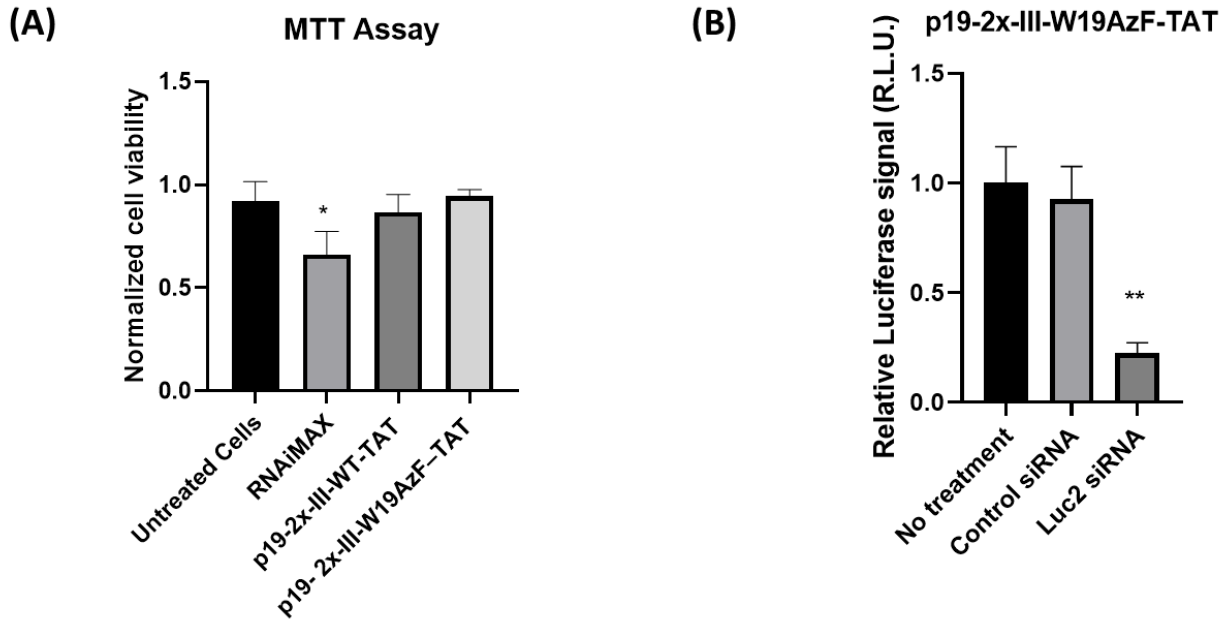

Figure 2.11 p19-2X-III-W19AzF-TAT delivers siRNA for gene knockdown in human cell culture. (A) MTT assays reporting on cell viability following p19-2x-III-WT-TAT, p19-2x-III-W19AzF-TAT, or RNAiMAX-mediated siRNA delivery for 48 hours. The 2x-p19-TAT:siRNA. Error bars represent SD, where n=3 and*P<0.05 (B) Gene knockdown reporter assay using dual luciferase reporter vector (psiCHECK-2) allows for observing luciferase gene knockdown after 48-hour treatments with p19-2X-III-W19AzF-TAT: Luc2 complex. Error bars represent SD, **P<0.01and n=3.

2.5 Conclusions

Overall, we have engineered a p19 protein incorporating AzF in a site-specific manner, where the incorporated azide handle can be used for copper-free click chemistry. The azide group is reacted with a strained alkyne to introduce a fluorophore that acts as a FRET acceptor upon the binding of the fluorophore-labeled RNA ligand. Here we show that the use of expanded genetic codes and bioorthogonal chemistry allows for simple and efficient generation of FRET reporter systems to evaluate RNA transport, delivery, and release at a target cell using a fluorescence turn-on strategy. The engineered p19 protein retains its ability to act as a molecular caliper by binding duplexed siRNAs in a size-selective manner. We have demonstrated a novel strategy for the detection of p19 for its ligands. This strategy can be used as a tool for sensing small RNA duplexes including miRNAs[31,32]. This represents a strategy that can be applied in designing high throughput methods for reporting on the levels of small RNA molecules. We expect that these methods should be transferable to other protein-based delivery systems. Furthermore, the approaches presented offer the opportunity to dissect and optimize the different steps of RNA transfer from the delivery agent through other interactions ultimately binding to Argonaute (Ago) proteins, where the ultimate function will take place.

2.6 Materials and Methods

2.6.1 Cloning of CIRV-p19

The codon optimized CIRV p19 was designed and cloned into pTriEx-Neo-4 vector, as described before[28,33]. Amber codon (TAG) has been incorporated using site-directed mutagenesis resulting in the following constructs pTriEx-p19-W19AzF and pTriEX-p19-N46AzF using QuickChange Site-Directed Mutagenesis (Agilent) according to the manufacturer's instructions using primers in table 2.1. The obtained constructs were validated by DNA sequencing to confirm the mutated nucleotides. Sequencing to confirm mutations was performed at Génome Québec (Montreal, Canada). pTriEX-p19-2x-III-W19AzF-TAT cloning was achieved as described previously[11], however with p19 containing the specified mutations C110I, C134I, C160I[28], and W19AzF. Briefly, the 2x-p19-TAT fusion protein was created by PCR amplification of the p19 monomer with an N-terminal linker and C-terminal TAT sequence by generating PCR primers to contain the TAT sequence at the C-terminus of the linker-p19 monomer, with a terminal 8-histidine tag flanked by Xho1 restriction sites. The forward primer used was: 5'TTAG CTC GAG GGC GGC GGC GGC TCC GGC GGC GGC GGC TCT ATG GAA CGC GCT ATC CAA G3' and the reverse primer used was: 5'TTAG CTC GAG GCG GCG GCG CTG GCG GCG TTT CTT GCG CTC GCT TTC TTT CTT GAA G3'. The PCR product was then digested with the Xho1 restriction enzyme and inserted into pTriEx vector containing the p19 monomer.

CIRV p19 containing three different cysteine residues (C110, C134, and C160) mutated to Isoleucine using QuikChange Site-Directed Mutagenesis kit (Agilent). Amber codons (TAG) have been introduced resulting in the following constructs pTriEx-p19III-W19AzF and pTriEX-p19III-N46AzF using primers presented in table 2.1.

Table 2.1 Mutagenesis primers

PRIMER	SEQUENCE
W19TAG FWD	ctaacggtgaagctaggatggcggctcc
W19TAG REV	ggagccgccatcctagcgttcaccgttag
N46TAG FWD	ctgagtggcgcctgtattaggatgagaccaattcc
N46TAG REV	ggaattggtctcatcctaatacaggcgccactcag

2.6.2 Bacterial overexpression of CIRV p19 and mutants

E.coli strain BL21 (DE3) (Thermofisher Scientific) transformed with the constructs were grown at 37ºC in the presence of 100 ug/ mL ampicillin in LB media until the optical density at 600 nm reached 0.5. Constructs containing the amber mutation (pTriEx-p19-W19AzF and pTriEX-p19-N46AzF, pTriEx-p19III-W19AzF and pTriEX-p19III-N46AzF, pTriEx-p19III-W19AzF and pTriEX-p19III-N46AzF) were transformed in *E.coli* Bl21 (DE3) pre-transformed with pULTRA-CNF[34], a vector bearing a polyspecific MJ tyrosyl synthetase and tRNA pair. The plasmid encoding the *p*-cyanophenylalanine specific aminoacyl-tRNA synthetase/suppressor tRNA pair was a kind gift from Dr. Peter Schultz (The Scripps Research Institute).

Expression of p19-TAG mutants was induced by IPTG at a final concentration of 1mmol/L. Additionally, a final concentration of 1mmol/L p-Azidophenylalanine (Bachem) has been added to the media upon induction. Post induction, the cultures were grown for 4 hours at 25 ^{o}C. Cells were harvested at 5000xg for 5 minutes. The pellets were suspended in lysis buffer (50 mmol/L Tris, 300 mmol/L NaCl, 1mmol/L DTT, 10 mmol/L Imidazole, pH 8.0) and subsequently lysed by sonication for 2 minutes with one-second pulse on/ off at 50% amplitude. Cells were then centrifuged at 20,000xg for 20 minutes at 4ºC to obtain the soluble fraction. Recombinant p19-wt

and mutants were purified using the Ni^{2+}NTA column (HisTrap FF, GE Health). Proteins were washed using washing buffer (50 mmol/L TRIS, 600 mmol/L NaCl, 1mmol/L DTT, 60 mmol/L Imidazole, pH 8.0). Proteins were then eluted using elution buffer (50 mmol/L TRIS, 300 mmol/L NaCl, 250 mmol/L Imidazole, 10 mmol/L β-mercaptoethanol). The eluted fraction was then concentrated using centrifugation tubes (10 kDa MWCO, Amicon). Pure dimerized p19-wt or mutants were further fractionated using size exclusion chromatography using S200 column (FPLC ÄKTA pure). Samples were then concentrated using centrifugation tubes (10 kDa MWCO, Amicon) and the concentration was determined using Bradford assay (Bio-Rad).

2.6.3 Fluorescent Labeling

p19-wt and p19-TAG mutants, as well as p19-III and corresponding III mutants, were purified as described above. Fluorescent labeling was performed for all mutants using DBCO-Cy5 (Sigma Aldrich) in 1:2 protein: dye ratio in 1x PBS buffer pH 7.4 where the SPAAC reaction took place. 40 µmol/L of p19-wt or mutants were incubated with the dye at room temperature for 3 hours. To remove excess dye, the labeled proteins were loaded on p30 gel microspin columns (Bio-Rad). Subsequently, samples were concentrated and labeled protein was analyzed via SDS-PAGE and in-gel fluorescence to visualize the labeling.

2.6.4 Immunoblotting

p19 expression and UAA incorporation were analyzed using SDS-PAGE and western blotting. 20µl of the soluble fraction per sample were analyzed using 12% stain-free polyacrylamide gel electrophoresis (TGX Stain-Free Fastcast Acrylamide kit, Bio-Rad) and western blotting. A control culture, without *p*-AzF addition, was grown under the same conditions. Proteins were transferred to a PVDF membrane using the Trans-blot Turbo RTA Transfer Kit (Bio-Rad). Blots were blocked in tris-buffered saline with 0.05% Tween-20 (TBS-T) containing 5% W/V milk and

washed then in TBS-T. Proteins were probed by α-histag HRP antibody (1:1000, life technologies). The antibody was detected via clarity western ECL substrate (Bio-Rad) and visualized on a ChemiDoc MP imaging system (Bio-Rad).

2.6.5 Circular Dichroism

CD measurements were performed for p19III, p19III-W19AzF, and p19III-N46AzF using JASCO J-815 (JASCO) with a quartz cell path length of 0.01 cm at 25°C. Proteins were prepared in phosphate-buffered saline (PBS buffer pH 7.5) at 10 μmol/L protein concentration. Spectra reflect an average of 8 scans recorded from 185-250 nm with a 0.2 nm step resolution, speed of 20 nm/ minute, and a bandwidth of 1 nm.

2.6.6 Substrates

GL2 siRNA cyanine 3 or labeled guide strand (5'-Cy3-CGU ACG CGG AAU ACU UCG AUU-3') and passenger strand (5'-UCG AAG UAU UCC GCG UAC GUU-3'; Sigma-Aldrich); GL2 siRNA FAM 3 labeled guide strand (5'-FAM-CGU ACG CGG AAU ACU UCG AUU-3') and passenger strand (5'-UCG AAG UAU UCC GCG UAC GUU-3'; Sigma-Aldrich); GL2 siRNA BHQ-2 labeled guide strand (5'-BHQ-2-CGU ACG CGG AAU ACU UCG AUU-3') and passenger strand (5'-UCG AAG UAU UCC GCG UAC GUU-3'; Dharmacon) were annealed at a 1:1.2 molar ratio of unlabeled/labeled RNA in a buffer containing 100 mmol/L potassium acetate, 30 mmol/L HEPES pH 7.5, and 2 mmol/L magnesium acetate by heating to 95°C for 2 min and cooling to 25°C at a rate of 1°C/min.

2.6.7 Electrophoretic Mobility Shift Assay

Samples were prepared by incubating 1 nmol/L FAM-labeled GL2 siRNA with 0–500 μmol/L of purified p19III or mutants in 20 mmol/L Tris, 100 mmol/L NaCl, 1 mmol/L EDTA, 0.02% v/v

TritonX-100, 2 mmol/L dithiothreitol, pH 7 for 1 hour at room temperature. The samples were analyzed by electrophoresis, where 5× Tris/Borate/EDTA (TBE) sample buffer (90 mmol/L Tris, 90 mmol/L boric acid, 2 mmol/L EDTA, 15% Ficoll type 400, 0.02% xylene cyanol) was diluted to 1× in the binding reaction and then 10 µl applied to a 6% TBE gel (Thermofisher Scientific). The gel was run at 100 V for 45 minutes in 0.5x TBE. The gels were imaged using ChemiDoc MP System (Bio-Rad) and the densitometry was performed with ImageJ software (NIH). The fraction of RNA bound by p19 was determined by dividing the band intensity of p19-bound RNA by the sum of the band intensities from the bound and unbound RNA. The data were analyzed by plotting the fraction bound values against p19 concentration and fitted using GraphPad Prism 7 according to the following equation (1):

$$\Delta P = \Delta P_{max}\left(\frac{K_D+np+x}{2np} - \sqrt{\left(\frac{K_D+np+x}{2np}\right)^2 - \frac{x}{np}}\right) (1)$$

where $^{\triangle}P$ denotes the change in fluorescence intensity, $^{\triangle}P_{max}$ is the maximal change in fluorescence intensity, K_D is the dissociation constant, n is the number of equivalent sites on the p19 dimer, p is the concentration of labeled small RNA, and x is the concentration of the p19 dimer.

2.6.8 Fluorescence Resonance Energy Transfer Measurements

Measurements were carried out using SpectraMax i3 (Molecular devices). All measurements were carried out in a 96-well plate. A sample solution containing variable concentrations of p19-wt and mutants (p19-W19AzF) or p19III and corresponding mutants (p19III-W19AzF and p19III-N46AzF) diluted in phosphate-buffered saline (50 mmol/L potassium phosphate, pH 7.5; 150

mmol/L NaCl). 10 nmol/L Cy3-siRNA or unlabeled siRNA were incubated with the proteins. Samples containing labeled proteins and unlabeled siRNA were used to normalize the collected emission spectra. After 1-hour equilibration, the fluorescence emission spectra were recorded. Samples were excited at 520 with 5 nm excitation bandwidth and fluorescence spectra were recorded from 555 to 700 nm. Equation (1) was used to determine the K_D using FRET, where ΔP_{max} represented the increase in Cy5 fluorescence upon excitation at 520 nm and emission at 670 nm. Cy5 fluorescence was corrected upon incubation with unlabeled GL2 siRNA. For fluorescence quenching experiments, 100 nmol/L Cy5-2x-p19-III-W19AzF was incubated with either 100 nmol/L BHQ-2-GL2 siRNA or unlabeled siRNA for 1 hour. Fluorescence emission spectra were recorded. Samples were excited at 650 nm with 5 nm excitation bandwidth and emission fluorescence spectra were recorded from 660 nm to 775 nm.

2.6.9 Cell Culture

Huh7 cells were cultured at 37ºC with 5% CO_2 in DMEM (Gibco-Invitrogen) with 10% fetal bovine serum and 100 nmol/L nonessential amino acids.

2.6.10 Imaging of the Delivery of RNA using p19-W19AzF-III-TAT

Purified 2x-p19-W19AzF-III-TAT or 2xp19-III-TAT was concentrated using Amicon Ultra 10-kDa MWCO centrifugal filter device to 100 µmol/l as determined by DC assay (Bio-Rad). DBCO-Cy5 in 1:2 protein: dye ratio in 1x PBS buffer pH 7.4. Proteins were then incubated at room temperature and protected from light. To remove excess dye-DBCO-Cy5, the labeled proteins were loaded on p30 gel microspin columns (Bio-Rad). Proteins were then complexed with BHQ-2 GL2 RNA (Dharmacon) for 45 minutes at room temperature, protected from light, and applied to cells in optimem media (Gibco) at a final concentration of 500 nmol/L. Huh7 cells were seeded at 60% confluency in 8-well chamber slides (Thermofisher). After 24 hours, protein treatments

were applied as described above at 3 different time points 2 hours, 5 hours, or 24 hours. The cells were then washed with phosphate-buffered saline and fixed using 4% formaldehyde and 4% sucrose solution in PBS. The cells were then mounted using ProLong™ Gold Antifade Mountant with DAPI (Thermofisher). The fluorescence imaging was performed using 20X or 40X objective on a Zeiss Axiophot Fluorescence Microscope (Zeiss). The images were captured at (Blue: Ex 365, Em 420) and Cy5 fluorescence (Red: 546, LP 590). The images were false-colored with imageJ and the same brightness and contrast were applied to images within the same time point.

2.6.11 Luciferase Assay

Huh7 cells were seeded into a 24-well plate at 40,000 cells/well, after 24 hours (at 70% confluency), cells were transfected with a dual luciferase reporter vector, psiCHECK-2 (Promega) using Lipofectamine2000 (Invitrogen) as per manufacturer's instructions. After 24 hours, the psiCHECK-2 expressing Huh7 cells were treated with 2x-p19-W19AzF-III-TAT: Luc2 complexes as discussed above. Cells were lysed after 48 hours and analyzed using a Lmax luminometer microplate reader (Molecular Devices). Relative knockdown was obtained through calculating Luciferase firefly/ Renilla signal and normalizing to siRNA control samples.

2.6.12 Cell Viability Assay

Huh7 cells were seeded at 15,000 cells per well in a 96-well plate, and after 24 hours (at approximately 70% confluency), cells were treated with 500 nmol/L protein (2x-p19-W19AzF-III-TAT or 2x-p19-wt-III-TAT) or treated with RNAiMAX (Invitrogen) as per manufacturer’s protocol. Cells were treated for 48 hours, then the media was removed and 50µL of a solution containing 2.5 mg/ml MTT reagent in phosphate-buffered saline was added to each well. Cells were then incubated for 3 hours; the liquid was removed, and the formazan crystals were dissolved in 150 µL of dimethyl sulfoxide (DMSO). Absorbance at 570 nm was then measured using a

SpectraMax i3 (Molecular devices). Data were recorded in triplicates and normalized against untreated control samples to reflect percent cell viability.

2.7 Acknowledgment

We thank the Natural Sciences and Engineering Council of Canada (NSERC) and the Canadian Foundation for Innovation for supporting this research. N.A. and D.V.F. thank the Ontario Graduate Scholarships program for funding. N.A. and J.D. thank NSERC for support in the form of graduate scholarships.

2.8 References

(1) Ghildiyal, M.; Zamore, P. D. Small Silencing RNAs: An Expanding Universe. *Nat. Rev. Genet.* **2009**, *10* (2), 94–108. https://doi.org/10.1038/nrg2504.

(2) Dunoyer, P.; Himber, C.; Voinnet, O. DICER-LIKE 4 Is Required for RNA Interference and Produces the 21-Nucleotide Small Interfering RNA Component of the Plant Cell-to-Cell Silencing Signal. *Nat. Genet.* **2005**, *37* (12), 1356–1360. https://doi.org/10.1038/ng1675.

(3) Turchinovich, A.; Tonevitsky, A. G.; Cho, W. C.; Burwinkel, B. Check and Mate to Exosomal Extracellular MiRNA: New Lesson from a New Approach. *Front. Mol. Biosci.* **2015**, *2* (April), 11. https://doi.org/10.3389/fmolb.2015.00011.

(4) Calin, G. a; Croce, C. M. MicroRNA Signatures in Human Cancers. *Nat. Rev. Cancer* **2006**, *6* (11), 857–866. https://doi.org/10.1038/nrc1997.

(5) Pecot, C.; Calin, G.; Coleman, R.; Lopez-Berestein, G. RNAi in the Clinic: Challenges and Future Directions. *Nat Rev Cancer* **2011**, *11* (1), 59–67. https://doi.org/10.1038/nrc2966.RNA.

(6) Stylianopoulos, T.; Jain, R. K. Combining Two Strategies to Improve Perfusion and Drug Delivery in Solid Tumors. *Proc. Natl. Acad. Sci.* **2013**, *110* (46), 18632–18637. https://doi.org/10.1073/pnas.1318415110.

(7) Pereira, D. M.; Rodrigues, P. M.; Borralho, P. M.; Rodrigues, C. M. P. Delivering the Promise of MiRNA Cancer Therapeutics. *Drug Discov. Today* **2013**, *18* (5–6), 282–289. https://doi.org/10.1016/j.drudis.2012.10.002.

(8) Lorenzer, C.; Dirin, M.; Winkler, A. M.; Baumann, V.; Winkler, J. Going beyond the Liver: Progress and Challenges of Targeted Delivery of SiRNA Therapeutics. *J. Control. Release* **2015**, *203*, 1–15. https://doi.org/10.1016/j.jconrel.2015.02.003.

(9) Schmidt, M. M.; Wittrup, K. D. A Modeling Analysis of the Effects of Molecular Size and Binding Affinity on Tumor Targeting. *Mol. Cancer Ther.* **2009**, *8* (10), 2861–2871. https://doi.org/10.1158/1535-7163.MCT-09-0195.

(10) Choi, K. M.; Park, G. L.; Hwang, K. Y.; Lee, J. W.; Ahn, H. J. Efficient SiRNA Delivery into Tumor Cells by p19-YSA Fusion Protein. *Mol. Pharm.* **2013**, *10* (2), 763–773. https://doi.org/10.1021/mp300344p.

(11) Danielson, D. C.; Sachrajda, N.; Wang, W.; Filip, R.; Pezacki, J. P. A Novel p19 Fusion Protein as a Delivery Agent for Short-Interfering RNAs. *Mol. Ther. - Nucleic Acids* **2016**, *5* (February), e303. https://doi.org/10.1038/mtna.2016.14.

(12) Choi, K. M.; Choi, S. H.; Jeon, H.; Kim, I. S.; Ahn, H. J. Chimeric Capsid Protein as a Nanocarrier for SiRNA Delivery: Stability and Cellular Uptake of Encapsulated SiRNA. *ACS Nano* **2011**, *5* (11), 8690–8699. https://doi.org/10.1021/nn202597c.

(13) Chen, B.; Xu, W.; Pan, R.; Chen, P. Design and Characterization of a New Peptide Vector for Short Interfering RNA Delivery. *J. Nanobiotechnology* **2015**, *13* (1), 39. https://doi.org/10.1186/s12951-015-0098-0.

(14) Zhang, Y.; Røise, J. J.; Lee, K.; Li, J.; Murthy, N. Recent Developments in Intracellular Protein Delivery. *Curr. Opin. Biotechnol.* **2018**, *52*, 25–31. https://doi.org/10.1016/j.copbio.2018.02.009.

(15) Suh, J. S.; Lee, J. Y.; Choi, Y. S.; Chong, P. C.; Park, Y. J. Peptide-Mediated Intracellular Delivery of MiRNA-29b for Osteogenic Stem Cell Differentiation. *Biomaterials* **2013**, *34* (17), 4347–4359. https://doi.org/10.1016/j.biomaterials.2013.02.039.

(16) Medarova, Z.; Pham, W.; Farrar, C.; Petkova, V.; Moore, A. In Vivo Imaging of SiRNA Delivery and Silencing in Tumors. *Nat. Med.* **2007**, *13* (3), 372–377. https://doi.org/10.1038/nm1486.
(17) Choi, K. M.; Kim, K.; Kwon, I. C.; Kim, I. S.; Ahn, H. J. Systemic Delivery of SiRNA by Chimeric Capsid Protein: Tumor Targeting and RNAi Activity in Vivo. *Mol. Pharm.* **2013**, *10* (1), 18–25. https://doi.org/10.1021/mp300211a.
(18) Zrazhevskiy, P.; Sena, M.; Gao, X. Designing Multifunctional Quantum Dots for Bioimaging, Detection, and Drug Delivery. *Chem. Soc. Rev.* **2010**, *39* (11), 4326–4354. https://doi.org/10.1039/b915139g.
(19) Liu, C. C.; Schultz, P. G. Adding New Chemistries to the Genetic Code. *Annu. Rev. Biochem.* **2010**, *79* (1), 413–444. https://doi.org/10.1146/annurev.biochem.052308.105824.
(20) Chin, J. W.; Santoro, S. W.; Martin, A. B.; King, D. S.; Wang, L.; Schultz, P. G. Addition of P-Azido-L-Phenylalanine to the Genetic Code of Escherichia Coli. *J. Am. Chem. Soc.* **2002**, *124* (31), 9026–9027. https://doi.org/10.1021/ja027007w.
(21) Lang, K.; Chin, J. W. Cellular Incorporation of Unnatural Amino Acids and Bioorthogonal Labeling of Proteins. *Chem. Rev.* **2014**, *114* (9), 4764–4806. https://doi.org/10.1021/cr400355w.
(22) Ko, W.; Kim, S.; Lee, S.; Jo, K.; Lee, H. S.; Vinkenborg, J. L.; Koay, M. S.; Merkx, M.; Looger, L. L.; Lalonde, S.; Frommer, W. B.; Carter, K. P.; Young, A. M.; Palmer, A. E.; Lindenburg, L.; Merkx, M.; Miyawaki, A.; Llopis, J.; Heim, R.; McCaffery, J. M.; Adams, J. A.; Ikura, M.; Tsien, R. Y.; Nagai, T.; Yamada, S.; Tominaga, T.; Ichikawa, M.; Miyawaki, A.; Ponsioen, B.; Zhao, J.; Riedl, J.; Zwartkruis, F.; Krogt, G. van der; Zaccolo, M.; Moolenaar, W. H.; Bos, J. L.; Jalink, K.; Nagai, Y.; Miyazaki, M.; Aoki, R.; Zama, T.; Inouye, S.; Hirose, K.; Iino, M.; Hagiwara, M.; Vanderklish, P. W.; Krushel, L. A.; Holst, B. H.; Gally, J. A.; Crossin, K. L.; Edelman, G. M.; Mitra, R. D.; Silva, C. M.; Youvan, D. C.; Piston, D. W.; Kremers, G. J.; Wang, J.; Xie, J.; Schultz, P. G.; Speight, L. C.; Muthusamy, A. K.; Goldberg, J. M.; Warner, J. B.; Wissner, R. F.; Willi, T. S.; Woodman, B. F.; Mehl, R. A.; Petersson, E. J.; Summerer, D.; Chen, S.; Wu, N.; Deiters, A.; Chin, J. W.; Schultz, P. G.; Lee, H. S.; Guo, J.; Lemke, E. A.; Dimla, R. D.; Schultz, P. G.; Chatterjee, A.; Guo, J.; Lee, H. S.; Schultz, P. G.; Luo, J.; Uprety, R.; Naro, Y.; Chou, C.; Nguyen, D. P.; Chin, J. W.; Deiters, A.; Chin, J. W.; Liu, C. C.; Schultz, P. G.; Wang, L.; Schultz, P. G.; Park, H.; Kang, H.; Ko, W.; Lee, W.; Jo, K.; Lee, H. S.; Wada, A.; Mie, M.; Aizawa, M.; Lahoud, P.; Cass, A. E.; Kobatake, E.; Sun, Y. J.; Rose, J.; Wang, B. C.; Hsiao, C. D.; Hsiao, C. D.; Sun, Y. J.; Rose, J.; Cottam, P. F.; Ho, C.; Wang, B. C.; Kim, S. G.; Hoffman, G. R.; Poulogiannis, G.; Buel, G. R.; Jang, Y. J.; Lee, K. W.; Kim, B.-Y.; Erikson, R. L.; Cantley, L. C.; Choo, A. Y.; Blenis, J.; Jewell, J. L.; Kim, Y. C.; Russell, R. C.; Yu, F.-X.; Park, H. W.; Plouffe, S. W.; Tagliabracci, V. S.; Guan, K.-L.; Young, T. S.; Ahmad, I.; Yin, J. A.; Schultz, P. G.; Lajoie, M. J.; Rovner, A. J.; Goodman, D. B.; Aerni, H. R.; Haimovich, A. D.; Kuznetsov, G.; Mercer, J. A.; Wang, H. H.; Carr, P. A.; Mosberg, J. A.; Rohland, N.; Schultz, P. G.; Jacobson, J. M.; Rinehart, J.; Church, G. M.; Isaacs, F. J.; Ko, W.; Kim, S.; Jo, K.; Lee, H. S.; Amaro, M.; Brezovský, J.; Kováčová, S.; Sýkora, J.; Bednář, D.; Nêmec, V.; Lišková, V.; Kurumbang, N. P.; Beerens, K.; Chaloupková, R.; Paruch, K.; Hof, M.; Damborský, J.; Ormo, M.; Cubitt, A. B.; Kallio, K.; Gross, L. A.; Tsien, R. Y.; Remington, S. J.; Fink, D. W.; Koehler, W. R.; Weiner, J. H.; Heppel, L. A.; Brosnan, J. T.; Nakazato, M.; Hashimoto, K.; Schmidt, U.;

Tchanturia, K.; Campbell, I. C.; Collier, D. A.; Iyo, M.; Treasure, J. Genetically Encoded FRET Sensors Using a Fluorescent Unnatural Amino Acid as a FRET Donor. *RSC Adv.* **2016**, *6* (82), 78661–78668. https://doi.org/10.1039/C6RA17375F.

(23) Agard, N. J.; Prescher, J. A.; Bertozzi, C. R. A Strain-Promoted [3 + 2] Azide-Alkyne Cycloaddition for Covalent Modification of Biomolecules in Living Systems. *J. Am. Chem. Soc.* **2004**, *126* (46), 15046–15047. https://doi.org/10.1021/ja044996f.

(24) Vargason, J. M.; Szittya, G.; Burgyán, J.; Hall, T. M. T. Size Selective Recognition of SiRNA by an RNA Silencing Suppressor. *Cell* **2003**, *115* (7), 799–811. https://doi.org/10.1016/S0092-8674(03)00984-X.

(25) Cheng, J.; Sagan, S. M.; Assem, N.; Koukiekolo, R.; Goto, N. K.; Pezacki, J. P. Stabilized Recombinant Suppressors of RNA Silencing: Functional Effects of Linking Monomers of Carnation Italian Ringspot Virus p19. *Biochim. Biophys. Acta - Proteins Proteomics* **2007**, *1774* (12), 1528–1535. https://doi.org/10.1016/j.bbapap.2007.09.014.

(26) Hoogenboom, R. Thiol-Yne Chemistry: A Powerful Tool for Creating Highly Functional Materials. *Angew. Chemie - Int. Ed.* **2010**, *49* (20), 3415–3417. https://doi.org/10.1002/anie.201000401.

(27) Cheng, J.; Sagan, S. M.; Jakubek, Z. J.; Pezacki, J. P. Studies of the Interaction of the Viral Suppressor of RNA Silencing Protein p19 with Small RNAs Using Fluorescence Polarization. *Biochemistry* **2008**, *47* (31), 8130–8138. https://doi.org/10.1021/bi800401y.

(28) Cheng, J.; Koukiekolo, R.; Kieliszkiewicz, K.; Sagan, S. M.; Pezacki, J. P. Cysteine Residues of Carnation Italian Ringspot Virus p19 Suppressor of RNA Silencing Maintain Global Structural Integrity and Stability for SiRNA Binding. *Biochim. Biophys. Acta - Proteins Proteomics* **2009**, *1794* (8), 1197–1203. https://doi.org/10.1016/j.bbapap.2009.03.012.

(29) Kim, S.; Ko, W.; Park, H.; Lee, H. S. Efficient and Site-Specific Antibody Labeling by Strain-Promoted Azide-Alkyne Cycloaddition. *J. Vis. Exp.* **2016**, *2016* (118), 1–6. https://doi.org/10.3791/54922.

(30) Tian, H.; Sakmar, T. P.; Huber, T. A Simple Method for Enhancing the Bioorthogonality of Cyclooctyne Reagent. *Chem. Commun.* **2016**, *52* (31), 5451–5454. https://doi.org/10.1039/C6CC01321J.

(31) Sibley, C. R.; Seow, Y.; Curtis, H.; Weinberg, M. S.; Wood, M. J. A. Silencing of Parkinson's Disease-Associated Genes with Artificial Mirtron Mimics of MiR-1224. *Nucleic Acids Res.* **2012**, *40* (19), 9863–9875. https://doi.org/10.1093/nar/gks712.

(32) Alvarez-Erviti, L.; Seow, Y.; Yin, H.; Betts, C.; Lakhal, S.; Wood, M. J. A. Delivery of SiRNA to the Mouse Brain by Systemic Injection of Targeted Exosomes. *Nat. Biotechnol.* **2011**, *29* (4), 341–345. https://doi.org/10.1038/nbt.1807.

(33) Sagan, S. M.; Koukiekolo, R.; Rodgers, E.; Goto, N. K.; Pezacki, J. P. Inhibition of SiRNA Binding to a p19 Viral Suppressor of RNA Silencing by Cysteine Alkylation. *Angew. Chemie - Int. Ed.* **2007**, *46* (12), 2005–2009. https://doi.org/10.1002/anie.200603284.

(34) Young, D. D.; Young, T. S.; Jahnz, M.; Ahmad, I.; Spraggon, G.; Schultz, P. G. An Evolved Aminoacyl-TRNA Synthetase with Atypical Polysubstrate Specificity. *Biochemistry* **2011**, *50* (11), 1894–1900. https://doi.org/10.1021/bi101929e.

Chapter 3

Site-specific crosslinking of a p19 viral suppressor of RNA silencing protein and its RNA targets using an expanded genetic code

3.1 Preface

This Chapter consists of data previously published in Biochemistry 2019, 58, 33, 3520–3526.

This article is authored by Noreen Ahmed, Dana V. Foss, Megan H. Powdrill, and John Paul Pezacki. As the first author of this publication, I made significant experimental and intellectual contributions to this article. I performed most of the experiments and sample preparations, including purification and *in vitro* characterizations of the proteins. D.V. Foss and M.H. Powdrill contributed to experiments and sample preparations. D.V. Foss and M.H. Powdrill provided intellectual contributions and aided with experimental design. I wrote the first draft of the manuscript. Editing and assistance with the writing were performed by all authors.

3.2 Abstract

The p19 viral suppressor of RNA silencing protein has useful applications in biotechnology due to its high affinity for binding to small RNAs such as small interfering RNAs (siRNAs). Also, its applications for the study and modulation of microRNAs are actively growing. Here we demonstrate the successful incorporation of a photoactivatable unnatural amino acid (UAA), *p*-azido-L-phenylalanine (AzF), for crosslinking to RNA substrates site-specifically into the p19 sequence. Incorporation of AzF was performed at three positions in the protein near the RNA binding site: K67, R115, and T111. Incorporation of AzF at position T111 of p19 did not affect the binding affinity of p19 for siRNAs and showed nanomolar affinity towards the human microRNA miR-122. The affinity was less favorable with AzF incorporation at two other positions suggesting sensitivity of placement of the UAA. Exposure of the T111AzF in a complex with either siRNA or miRNA to UV light resulted in crosslinking of the protein with the RNA, but no crosslinking was detectable with the wild-type protein. Our results demonstrate that p19-T111AzF can be used for the detection of small RNAs including the human miR-122 with high sensitivity and to irreversibly sequester these RNAs through covalent photo-crosslinking.

3.3 Introduction

A significant percentage of the mammalian genome is transcribed to RNAs, however, only a small subset is used to serve as a template for protein translation[1,2]. Non-coding RNAs (ncRNAs) are shown to serve diverse roles in cell regulation, signaling pathways, and gene expression. The most well-understood non-coding RNAs are small non-coding RNAs including microRNAs (miRNA) and small interfering RNAs (siRNA). microRNAs are potent regulators of gene expression that can destabilize or inhibit the translation of messenger RNAs (mRNAs)[1,2] giving rise to repression of protein synthesis post-transcriptionally. In eukaryotes, it is estimated that approximately 97% of the genome is transcribed into ncRNAs[1,2]. It has been reported that the misregulation of these molecules is associated with disease progression. High sensitivity detection methods of microRNAs are thus required to understand their mechanism in human disease[3].

The p19 protein, a 19 kDa protein expressed by plant *Tombusviruses* that acts as a viral suppressor of RNA silencing, has been used extensively to study the RNA silencing pathways[4–6]. As a homodimer, the protein binds small double-stranded RNAs with nanomolar affinity[7]. In plants, the viral protein helps subvert host immune defenses by binding and sequestering siRNAs, preventing their incorporation into the RNA-induced silencing complex and effectively disrupting the RNA silencing pathway[8]. Interactions between p19 and siRNA are size-dependent (21-25 nucleotides), with stacking interactions between two tryptophan residues in the N-terminal subdomain and bases 1 and 19 of the siRNA duplex accounting for the size specificity[7]. As the protein interacts only with the phosphate backbone of the RNA substrate, interactions are sequence-independent[4]. The p19 dimer can also bind miRNAs, but the affinity is lower than with siRNAs due to structural differences in the RNAs, which vary depending on the miRNA sequence[9,10], although we have shown that rational mutation can be used to develop mutant p19s

capable of binding human miRNAs of therapeutic interest, such as miR-122[10,11]. The p19 protein has several reported applications in biotechnology, including the highly sensitive detection of small RNAs[12,13], delivery of siRNAs[14,15], and in the study of the RNA silencing pathway[6].

Methods for identifying protein-RNA interactions have been critical for the discovery and understanding of ncRNA function. Some methods take advantage of crosslinking between proteins and their bound RNA using UV light to identify the targets of RNA binding proteins, using techniques such as crosslinking immunoprecipitation (CLIP), photoactivatable ribonucleoside-enhanced crosslinking, and immunoprecipitation (PAR-CLIP), and CLIP-RNA sequencing (CLIP-Seq)[16,17] and these techniques have been used to map and validate mRNA targets of miRNAs (e.g. Argonaute-CLIP)[18–20]. One drawback to this approach is a lack of specificity or control over where the crosslinking is occurring. Ideally, site-specific photo-crosslinking would allow precise mapping of the exact RNA binding sites in RNA binding proteins. UV-crosslinking between proteins and RNA have been hindered by low efficiency (~1-5%), and thus improvements are necessary to fully characterize RNA binding proteins and their targets[17]. One relatively unexplored approach for site-specific photo-crosslinking of protein-RNA complexes involves the incorporation of unnatural amino acids (UAAs) with photo-crosslinkable side chains into an RNA binding protein of interest using expanded genetic code technologies. Herein, we describe a method of utilizing genetic code expansion technology to engineer an RNA binding protein, p19, that is able to crosslink its RNA ligands in a site-specific manner using AzF. This approach offers an alternative to currently available methodologies for crosslinking RNA binding proteins (RBPs) and their bound RNAs, such as nucleotide analogs (5-thoiuridine) and chemical crosslinkers (methylene blue)[21] with the advantage of site-specific crosslinking. We show the successful incorporation of AzF, a photo-crosslinkable UAA, site-specifically into that p19 protein that when

irradiated in the presence of different RNA ligands leads to an irreversible crosslink between the two species. This gives rise to higher sensitivity of detection and irreversible sequestration of small RNAs.

3.4 Results

In creating an unnatural p19 protein containing a photo-crosslinkable UAA site-specifically, we decided to use the UAA *p*-azido-L-phenylalanine (AzF) because it is relatively small and tolerable in the sites of interest for incorporation. AzF contains an aryl azide that is photoactivated upon exposure to UV light and can crosslink with proximal nucleobases (Figure 3.1A, B). The incorporation of UAAs into proteins can be accomplished with an orthogonal aminoacyl tRNA synthetase/tRNA pair that has been evolved to incorporate specific UAAs. Work by Young et al. generated an aminoacyl tRNA synthetase/tRNA, evolved from *Methanococcus jannaschii* tyrosyl tRNA synthetase/tRNA pair that we have used here to incorporate the UAA AzF into proteins[22]. Since p19 binds small RNAs as a dimer, each of the monomers will contain the mutation leading to the incorporation of AzF, thus crosslinking with the RNA will occur at 2 sites (one with each monomer).

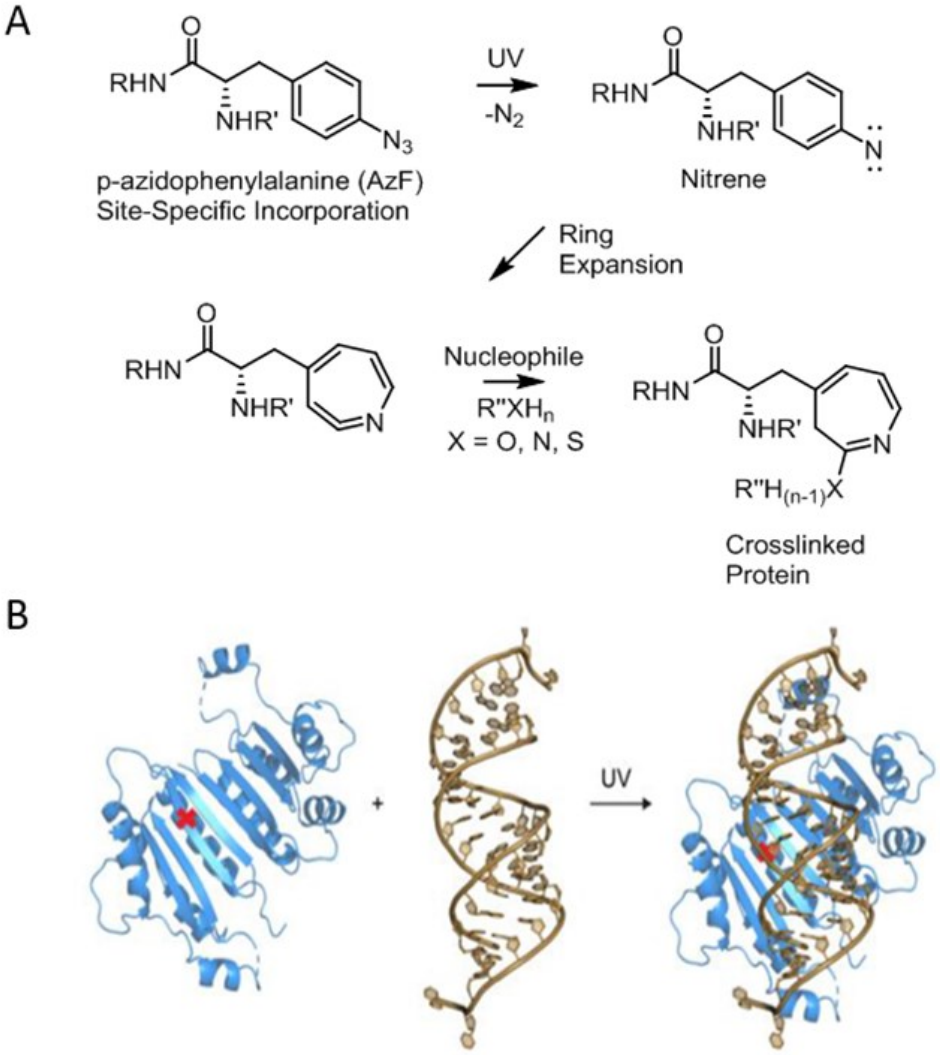

Figure 3.1. Photocrosslinking of protein containing *p*-azido-L-phenylalanine (AzF) and a nucleic acid substrate. A) Photo-induced reactivity of AzF. Exposure of the aryl azide to UV light results in the formation of a reactive nitrene that undergoes ring expansion to form a dehydroazapine that reacts with nucleophilic amines. B) AzF is site-specifically incorporated into the protein. UV exposure results in activation of the UAA and covalent bond formation between the UAA and a proximal nucleobase. PDB: 1RPU

3.4.1 Incorporation of AzF into p19

We generated three constructs of the CIRV p19 protein with the TAG amber suppressor codon at the K67, T111, or R115 positions. Based on available crystal structures of p19 in complex with siRNA[4,11], these residues are situated along the β-sheet binding surface of p19 and either interact directly with the phosphate backbone of the siRNA molecule (K67, R115) or are in close proximity (Figure 3.2A). We have previously shown that mutation of the T111 residue has a negligible effect on the binding affinity for siRNA[10]. Other studies have shown that the mutations K67G and R115G decrease binding affinity, although RNA silencing is not affected[23]. We first examined the expression of the His-tagged AzF-containing p19 proteins by western blot. Each of the proteins showed expression in the presence of AzF following induction with IPTG, while no expression was observed when the UAA wasn't added to the culture media (Figure 3.2B). To confirm that AzF was successfully incorporated, we performed liquid chromatography-mass spectrometry analysis of WT p19 and p19-T111AzF (Figure 3.3), as has been done with other proteins where AzF was successfully incorporated[24–27]. The mass spectrum of WT p19 shows a peak at 20673.9 Da, while p19-T111AzF shows a major peak at 20759.7 Da corresponding to the incorporation of azido-phenylalanine and a second peak corresponding to the reduction of an azide to an amine, which is expected since purification and preparation of the protein for mass spectrometry required the use of reducing agents to prevent protein aggregation.

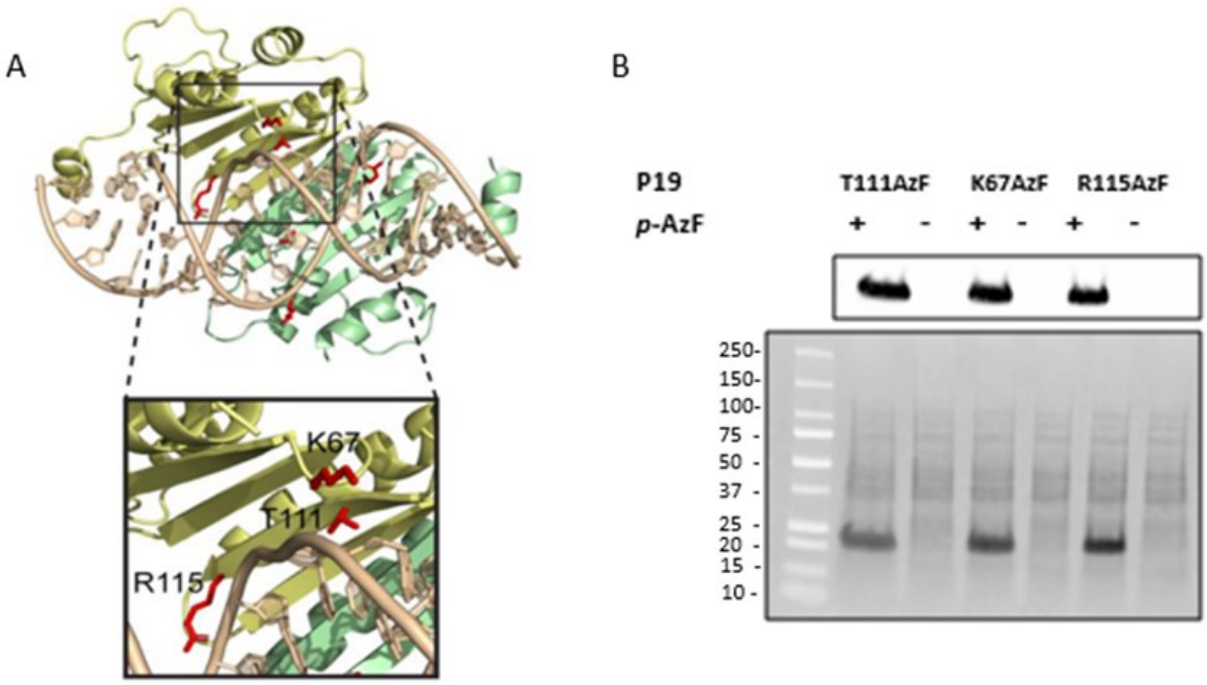

Figure 3.2. AzF incorporation sites in p19. A) The three sites chosen to test AzF incorporation are shown in the context of the p19 dimer. The black box provides a closer view of the three residues and their proximity to the bound RNA. PDB: 1RPU B) Western blot of the expression of WT p19 and AzF-containing mutants. Expression of the mutants was carried out with the addition of IPTG in the presence of AzF. Expression was allowed for 16 hours post-induction and AzF supplementation. Top panel represents a western blot depicting full length expression of p19 using an anti-histag antibody. Bottom panel is a TGX stain-free gel representing total protein loaded on the gel.

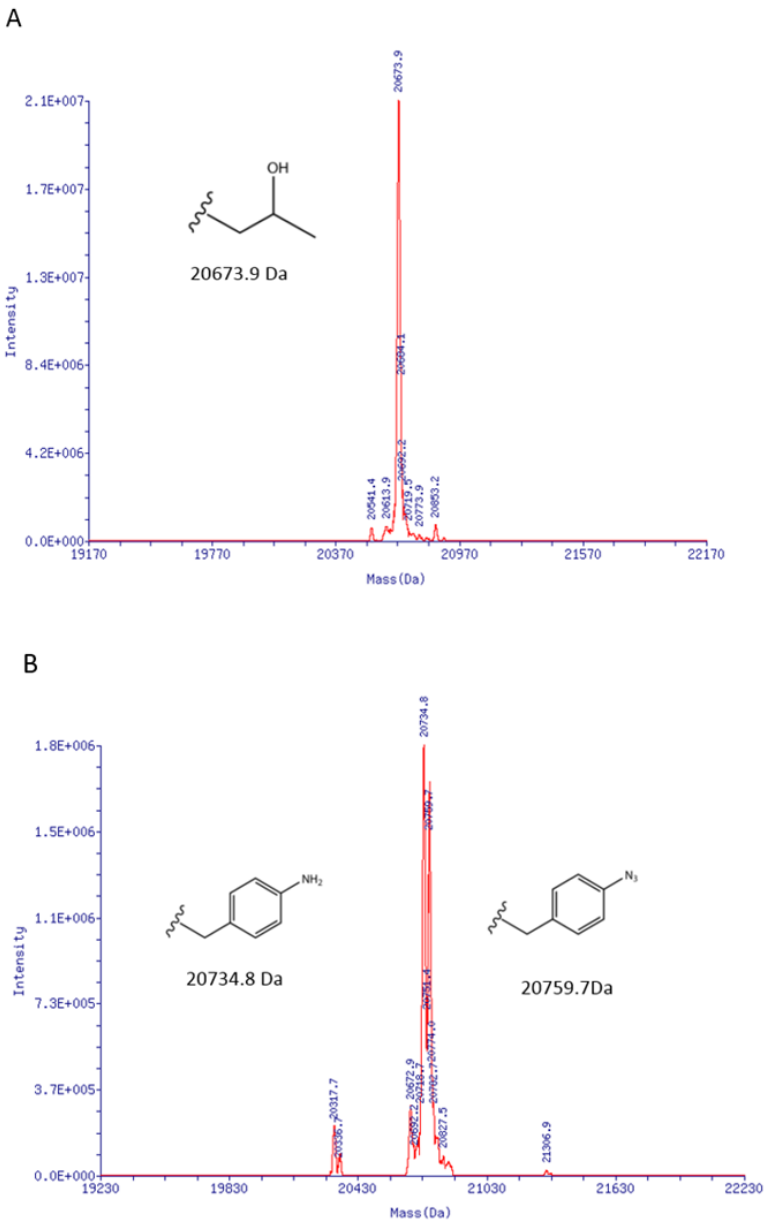

Figure 3.3. Mass spectrum to confirm incorporation of Azidophenylalanine site specifically. A) mass spectra showing major peak at 20673.9 Da representing p19 WT. B) Mass spectra for the mutant T111AzF representing the incorporation of AzF in a site-specific manner, showing two species due to reduction of azide during the purification and preparation of protein for the MS experiment.

3.4.2 Binding Affinity of AzF-containing p19 proteins

The UAA and RNA substrate require a specific geometric arrangement to ensure the crosslinking reaction occurs. Mutations that disrupt RNA binding could prevent the reaction. We examined the effects of AzF incorporation in p19 on the binding affinity of the protein for siRNAs by measuring the dissociation constants by electrophoretic mobility shift assay (EMSA). As shown in Table 3.1 and figure 3.4, p19-T111AzF binds the siRNA substrate with a similar affinity to the WT protein. In contrast, the K67 and R115 mutants show decreased affinity. Likely, the loss of the electrostatic interactions between the positively charged amino acids and the RNA backbone accounts for the change in binding affinity. Overall, the binding affinity for the T111AzF mutant is still maintained at a high affinity (K_D=0.34±0.083 nmol/L, see Table 3.1). Our lab has recently shown that mutations in this specific residue (T111) do not lead to major changes in p19 architecture[10,11]. Thus, we decided to conduct the RNA photo-crosslinking experiments with the p19-T111AzF mutant.

Table 3.1. Dissociation constants representing the binding affinities of p19 mutants relative to the p19WT affinity to GL2 siRNA as measured using electrophoretic mobility shift assays

Mutant	***K_D***	***Relative K_D***
P19 Wt	0.20 nmol/l[4,10]	-
T111AzF	0.34±0.083 nmol/l	1.7
K67AzF	3.8±0.55 nmol/l	19
R115AzF	33±4.6 nmol/l	165

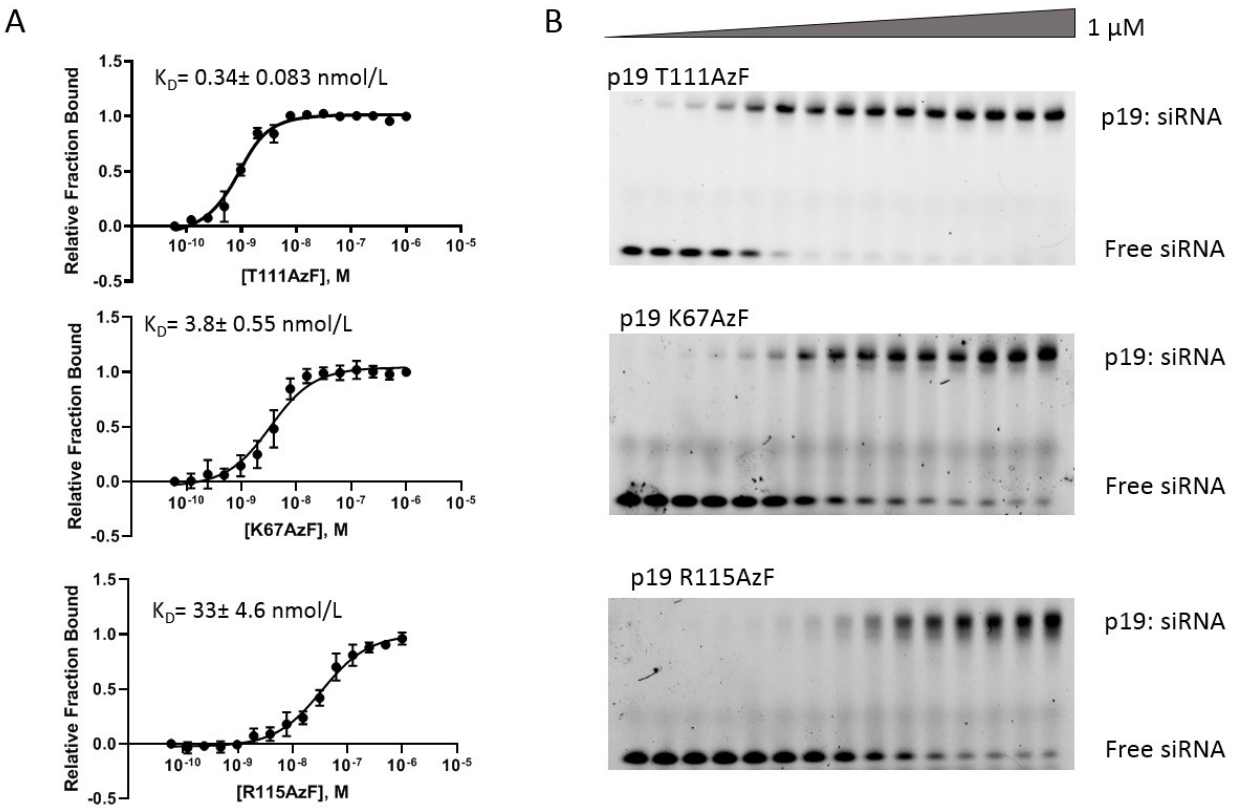

Figure 3.4. Binding affinity measurements using electrophoretic mobility shift assay (EMSA) for mutants T111AzF, K67AzF and R115AzF. A) Binding plots were constructed using varying concentration (0-1 µmol/L) of protein and 2 nmol/L Cy3 labeled GL2 siRNA. B) EMSA gels used to determine the binding affinity of the mutants. EMSA gels were run in duplicates. EMSA gels shown are representative trials.

3.4.3 Crosslinking of p19 and small RNA substrates

To establish whether the incorporated AzF was oriented in a manner that allowed it to react with a nucleobase, we performed photo-crosslinking studies with small RNAs. We first examined the effects of crosslinking on band shifts using denaturing SDS-PAGE gels. As shown in figures 3.5A, B, and S3.1A, a shift in the mass of the Cy3-labeled GL2 siRNA, indicating binding to the p19 protein, was observed. This band shift is only detected with the p19-T111AzF protein after UV exposure, consistent with a photo-crosslinked product. Two bands are visible at masses that likely correspond to single or double-stranded RNA crosslinked to a monomeric unit of p19. The WT protein does not show crosslinking with UV light exposure, confirming that the crosslinking reaction is site-specific, occurring only at the T111AzF residue.

Next, we conducted photo-crosslinking and EMSA analysis with the p19 T111AzF mutant and a Cy3-labeled miR-122, a miRNA highly expressed by hepatic cells and reported to be involved in facilitating HCV replication and propagation[10]. Figure 3.5D and figure S3.1B show successful site-specific crosslinking of p19 with miR-122 at residue T111AzF. This is interesting as our group was able to engineer a p19 variant (T111H) that can bind miR-122 with a similar affinity to that of p19 to its canonical siRNA ligands[10,11]. We have as well confirmed the ability of the mutant of binding miR-122 with high affinity using EMSA that has displayed an apparent K_D = 10.2±0.76 nmol/L and thus establishing a new tool for the investigation of miR-122.

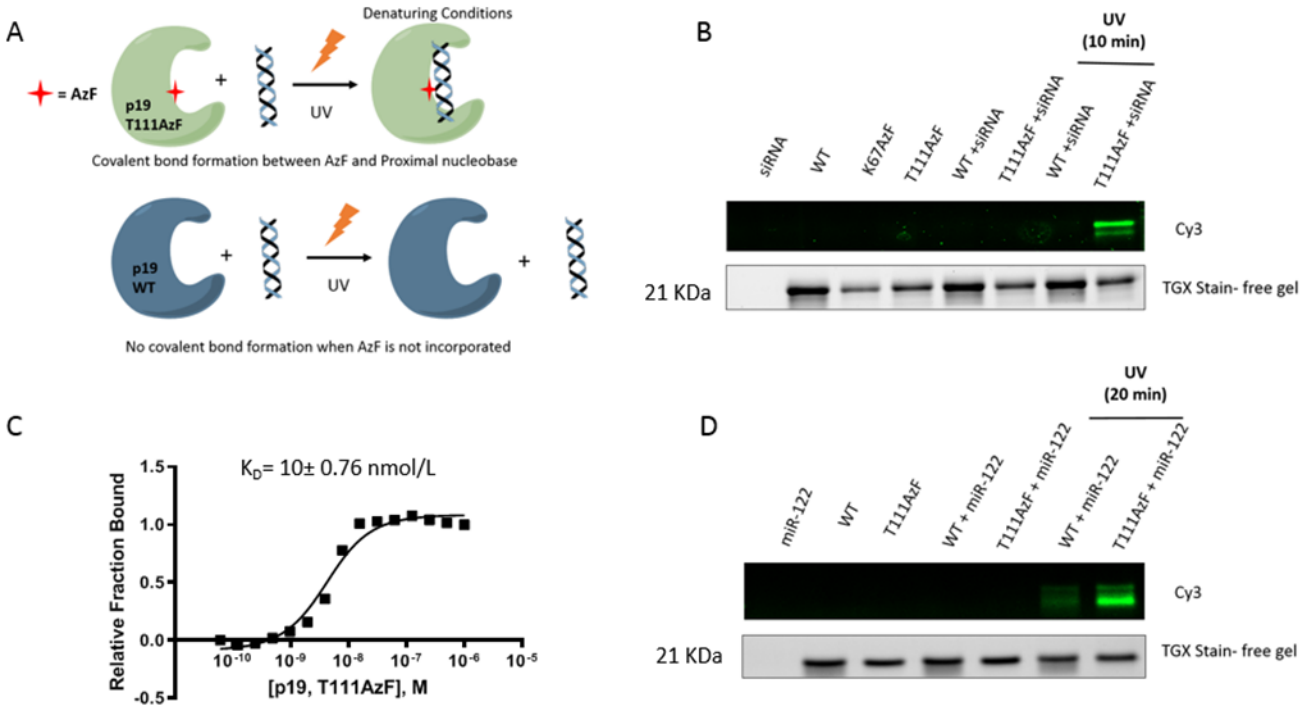

Figure 3.5. Crosslinking of p19 and small RNAs. A) A schematic representation of UV crosslinking between p19 T111AzF and small regulatory RNAs (GL2 siRNA and miR-122). B) Cy3 scan showing crosslinking of p19-T111AzF to cy3 labeled RNA. In the absence of UV light (320 nm), no shift is observed in the RNA mass. C) Binding plot of T111AzF mutant and Cy3-miR-122 as determined using EMSA. D) Crosslinking of p19 and miR-122. Cy3 scan showing binding of p19-T111AzF to labeled RNA. In the absence of UV light, no shift is observed in the RNA mass. Bottom TGX stain free gels (B, D) represent loading control, confirming equal loading at 21 kDa.

3.5 Discussion

Protein-RNA interactions are essential for many key pathways in living systems, particularly in facilitating and regulating transcription and translation. Small noncoding RNAs can also regulate mRNA translation using RNA silencing pathways. Many of the existing crosslinking methodologies for capturing RNA-Protein interactions can capture transient and even weak binding interactions[28]. However, the usage of expanded genetic code permits the incorporation of UAAs with photoactivatable functional groups to allow crosslinking at longer wavelengths that are less likely to induce cellular damage[29,30]. We have shown that it is possible to mutate and incorporate photo-crosslinkable UAA in p19, as a representative RBP.

In studying the properties of p19 proteins with AzF incorporated at different positions site-specifically, we were able to assess the tolerance and efficiency of crosslinking. We successfully demonstrated the photo-crosslinking of siRNA and miRNA to p19 in a site-specific manner using the T111AzF mutant. Residue 111 was shown to be a good site for UAA incorporation, with the T111AzF mutant showing high affinity for both siRNA and miRNA substrates in the nano- to picomolar range of K_D. Taken together these data demonstrate the unique opportunities for protein engineering and the study of protein-RNA interactions through genetic code expansion and incorporation of photo-crosslinkable UAAs such as AzF. Furthermore, this approach shows that it should be possible to engineer proteins like p19 for applications in biological settings to improve small RNA detection or control of regulatory RNAs involved in disease progression through covalent sequestration.

3.6 Conclusions

We have generated mutant p19 proteins that contain the AzF UAA incorporated site-specifically for the purpose of irreversible ligand binding. We established which sites are amenable to incorporation of the UAA and studied the effects of these mutations on the binding affinity. Finally, we identified a single site of incorporation that permits photo-crosslinking of p19 to its RNA substrates including miR-122. The enhanced irreversible RNA binding capacity of p19-T111AzF could be applied to the studies of RNA silencing or for the detection of low-abundance small RNAs, as well as improving currently available methods of RNA-protein interaction studies. Additionally, this research demonstrates the opportunity to apply genetic code expansion technology in already available techniques that involve the binding and crosslinking of RNA binding proteins to their ligands (such as HITS-CLIP and PAR-CLIP). Furthermore, with irreversible modification of p19's target RNAs, new therapeutic applications for these engineered proteins are revealed. Our group is currently examining these possibilities.

3.7 Materials and Experimental Details

3.7.1 Expression and purification wild type (WT) p19 and p19-K67AzF, -R115AzF and -T111AzF

The coding sequence of C-terminal histidine-tagged Carnation Italian ringspot virus (CIRV; GenBank accession number NC_003500) p19 was subjected to site-directed mutagenesis using the QuikChange Lightning Site-Directed Mutagenesis kit (Agilent) according to the manufacturer's instructions. An amber TAG codon was introduced in the sites corresponding to amino acid positions 67, 111, or 115 of the protein using the primers listed in Table 3.2. Sequencing to confirm the mutations was performed at Génome Québec (Montreal, Canada).

Table 3.2. Mutagenesis primers used in this study

RESIDUE	FORWARD PRIMER (5'-3')	REVERSE PRIMER (5'-3')
K67	aggaaagctgggtttcgggtaggttgtctttaagcgctatc	gatagcgcttaaagacaacctacccgaaacccagctttcct
T111	agcgagatgctgcatactaaacggaatcgccggtc	gaccggcgattccgtttagtatgcagcatctcgct
T115	ctaacgccgcgaaactaaatgctataggacagccgacctggt	accaggtcggctgtcctatagcatttagtttcgcggcgttag

The plasmid encoding the *p*-cyanophenylalanine polyspecific aminoacyl-tRNA synthetase/suppressor tRNA pair[16] was a kind gift from Dr. Peter Schultz (The Scripps Research Institute). The plasmid was transformed into One Shot BL21 (DE3) chemically competent *Escherichia coli* cells (ThermoFisher) which were selected with spectinomycin (50 μg/mL), remade competent, and then transformed with p19 expression vectors containing the TAG mutation at designated sites. Cells were plated in the presence of spectinomycin (50 μg/mL) and ampicillin (100 μg/mL) and colonies were selected for expression.

Cells transformed with the p19-TAG mutants and the synthetase vectors were grown at 37°C in lysogeny broth in the presence of ampicillin (100 μg/mL) and spectinomycin (50 μg/mL) until an optical density of 0.6 was reached. Protein expression was induced with the addition of 1 mmol/L IPTG in the presence of 1 mmol/L AzF (Bachem) for 4 h at 25°C. Cells were pelleted and frozen at -80°C. Protein purification was performed in a two-step process involving affinity and size-exclusion chromatography. Briefly, cells were lysed by sonication, and clarified lysates were loaded onto a HisTrap FF column (GE Healthcare Life Sciences) and gradient eluted in a buffer containing 50 mmol/L Tris pH 8, 300 mmol/L NaCl, 1 mmol/L DTT, and 250 mmol/L imidazole. Fractions containing p19 were pooled and purified by size exclusion chromatography on an S75 column (GE Healthcare Life Sciences) in a buffer containing 20 mmol/L Tris pH 8, 150 mmol/L NaCl and 1 mmol/L DTT. Protein concentration was determined by measurement of absorbance at 280 nm on a Nanodrop (Thermo Fisher Scientific).

3.7.2 Immunoblotting

Cell lysates were resolved by 12% sodium dodecyl sulfate polyacrylamide gel electrophoresis (TGX Stain-Free Fastcast Acrylamide kit, Bio-Rad) and transferred onto Hybond-P

polyvinylidene membranes using the Trans-blot Turbo RTA Transfer Kit (Bio-Rad). Membranes were blocked in 5% milk in tris-buffered saline with 0.05% Tween-20 (TBS-T) then incubated with a 6× His Tag horse-radish peroxidase-conjugated antibody (1:5000 dilution; Thermo Fisher) for 1 h at room temperature. Membranes were washed 1 × 15 min and 3 × 5 min in TBS-T then incubated with Clarity western ECL substrate (Bio-Rad) and visualized on a ChemiDoc MP imaging system (Bio-Rad).

3.7.3 Substrates

GL2 siRNA cyanine 3 labeled guide strand (5'-Cy3-CGU ACG CGG AAU ACU UCG AUU-3') and passenger strand (5'-UCG AAG UAU UCC GCG UAC GUU-3'; Sigma-Aldrich) and miRNA-122 guide strand (5′-UGG AGU GUG ACA AUG GUG UUU GU-3′) and passenger strand (5′-Cy3-AAA CGC CAU UAU CAC ACU AAA UA-3′) were annealed at a 1:1.2 molar ratio of unlabeled/labeled RNA in a buffer containing 100 mmol/L potassium acetate, 30 mmol/L HEPES pH 7.5, and 2 mmol/L magnesium acetate by heating to 95°C for 2 min and cooling to 25°C at a rate of 1°C/min. The presence of duplexed siRNA was confirmed on 6% non-denaturing acrylamide gels (Thermo Fisher Scientific).

3.7.4 Electrophoretic Mobility Shift Assay (EMSA)

Varying concentrations of p19 up to 1 μmol/L were incubated for 1 h with 2 nmol/L GL2 siRNA duplexed substrate in 20 mmol/L Tris pH 7, 100 mmol/L NaCl, 1 mmol/L EDTA, 0.02% v/v Tween-20 and 2 mmol/L DTT. Following incubation, samples were resolved on a 6% non-denaturing acrylamide gel. Visualization of products was performed using a ChemiDoc MP imaging system. Quantification of bound RNA was performed using Quantity One software (Bio-Rad). Data were analyzed using GraphPad Prism and fit the equation:

$$Y = b + A_{max}\left(\frac{K_D + ns + x}{2ns} - \sqrt{\left(\frac{K_D + ns + x}{2ns}\right)^2 - \frac{x}{ns}}\right)$$

Where K_D is the dissociation constant, n is the number of equivalent sites on the p19 dimer, s is the concentration of labeled small RNA, and x is the concentration of the p19 dimer.

3.7.5 Crosslinking

The p19 protein (WT or T111AzF) at a concentration of 4 μmol/L, was incubated with 250 nmol/L duplexed RNA substrate in a buffer containing 20 mmol/L HEPES pH 7, 100 mmol/L NaCl, 1 mmol/L EDTA, and 0.02% Tween-20 for 1 h. Following the incubation, designated samples were subjected to 10 or 20 min UV exposure at 320 nm. Samples were diluted in SDS loading buffer, boiled for 10 minutes, and resolved on a 12% denaturing gel. Visualization of samples was undertaken on a ChemiDoc MP imaging system (Bio-Rad).

3.7.6 Liquid Chromatography/ Mass Spectrometry

2 mg/mL p19 WT and T111AzF were prepared in 10 mmol/L Tris pH 7.0, 20 mmol/L NaCl, and run through an HPLC (Agilent HP1100 POROS R2 2.1x30 mm) and followed by a mass spectrometer (LTQ-Orbitrap-XL).

3.8 Acknowledgments

JPP thanks the Natural Sciences and Engineering Council of Canada (NSERC) for funding this work. N.A. and D.V.F. thank the Ontario Graduate Scholarships program for funding. We thank Julie Delcorde for help with protein expression and Levi Tamming for help with running EMSAs. We would like to thank Yanouchka Rouleau, Luc Tessier, and Dr. Susan Twine for their help with the mass spectrometry experiments.

The authors declare no competing financial interest.

UniprotKB accession IDs

UniProtKB - Q66104 (p19_CIRV)

3.9 References

(1) Peng, Y.; Croce, C. M. The Role of MicroRNAs in Human Cancer. *Signal Transduct. Target. Ther.* **2016**, *1* (1), 15004. https://doi.org/10.1038/sigtrans.2015.4.

(2) Roberts, A. P. E.; Lewis, A. P.; Jopling, C. L. The Role of MicroRNAs in Viral Infection. In *Cellular RNA Interference Mechanisms*; Elsevier Inc., 2011; Vol. 102, pp 101–139. https://doi.org/10.1016/B978-0-12-415795-8.00002-7.

(3) Dave, V. P.; Ngo, T. A.; Pernestig, A.-K.; Tilevik, D.; Kant, K.; Nguyen, T.; Wolff, A.; Bang, D. D. MicroRNA Amplification and Detection Technologies: Opportunities and Challenges for Point of Care Diagnostics. *Lab. Investig.* **2019**, *99* (4), 452–469. https://doi.org/10.1038/s41374-018-0143-3.

(4) Vargason, J. M.; Szittya, G.; Burgyán, J.; Hall, T. M. T. Size Selective Recognition of SiRNA by an RNA Silencing Suppressor. *Cell* **2003**, *115* (7), 799–811. https://doi.org/10.1016/S0092-8674(03)00984-X.

(5) Calabrese, J. M.; Sharp, P. A. Characterization of the Short RNAs Bound by the p19 Suppressor of RNA Silencing in Mouse Embryonic Stem Cells. *Rna* **2006**, *12* (12), 2092–2102. https://doi.org/10.1261/rna.224606.

(6) Danielson, D. C.; Pezacki, J. P. Studying the RNA Silencing Pathway with the p19 Protein. *FEBS Lett.* **2013**, *587* (8), 1198–1205. https://doi.org/10.1016/j.febslet.2013.01.036.

(7) Silhavy, D.; Molnár, A.; Lucioli, A.; Szittya, G.; Hornyik, C.; Tavazza, M.; Burgyán, J. A Viral Protein Suppresses RNA Silencing and Binds Silencing-Generated, 21- to 25-Nucleotide Double-Stranded RNAs. *EMBO J.* **2002**, *21* (12), 3070–3080. https://doi.org/10.1093/emboj/cdf312.

(8) Lakatos, L.; Szittya, G.; Silhavy, D.; Burgyán, J. Molecular Mechanism of RNA Silencing Suppression Mediated by p19 Protein of Tombusviruses. *EMBO J.* **2004**, *23* (4), 876–884. https://doi.org/10.1038/sj.emboj.7600096.

(9) Pertermann, R.; Tamilarasan, S.; Gursinsky, T.; Gambino, G.; Schuck, J.; Weinholdt, C.; Lilie, H.; Grosse, I.; Golbik, R. P.; Pantaleo, V.; Behrens, S. E. A Viral Suppressor Modulates the Plant Immune Response Early in Infection by Regulating MicroRNA Activity. *MBio* **2018**, *9* (2), 1–19. https://doi.org/10.1128/mBio.00419-18.

(10) Cheng, J.; Danielson, D. C.; Nasheri, N.; Singaravelu, R.; Pezacki, J. P. Enhanced Specificity of the Viral Suppressor of RNA Silencing Protein p19 toward Sequestering of Human MicroRNA-122. *Biochemistry* **2011**, *50* (36), 7745–7755. https://doi.org/10.1021/bi2008273.

(11) Foss, D. V; Schirle, N. T.; MacRae, I. J.; Pezacki, J. P. Structural Insights into Interactions between Viral Suppressor of RNA Silencing Protein p19 Mutants and Small RNAs. *FEBS Open Bio* **2019**, *9* (6), 1042–1051. https://doi.org/10.1002/2211-5463.12644.

(12) Jin, J.; Cid, M.; Poole, C. B.; McReynolds, L. A. Protein-Mediated MiRNA Detection and SiRNA Enrichment Using p19. *Biotechniques* **2010**, *48* (6), xvii–xxiii. https://doi.org/10.2144/000113364.

(13) Khan, N.; Cheng, J.; Pezacki, J. P.; Berezovski, M. V. Quantitative Analysis of MicroRNA in Blood Serum with Protein-Facilitated Affinity Capillary Electrophoresis. *Anal. Chem.* **2011**, *83* (16), 6196–6201. https://doi.org/10.1021/ac2016213.

(14) Choi, K. M.; Park, G. L.; Hwang, K. Y.; Lee, J. W.; Ahn, H. J. Efficient SiRNA Delivery into Tumor Cells by p19-YSA Fusion Protein. *Mol. Pharm.* **2013**, *10* (2), 763–773. https://doi.org/10.1021/mp300344p.

(15) Danielson, D. C.; Sachrajda, N.; Wang, W.; Filip, R.; Pezacki, J. P. A Novel p19 Fusion Protein as a Delivery Agent for Short-Interfering RNAs. *Mol. Ther. - Nucleic Acids* **2016**, *5* (February), e303. https://doi.org/10.1038/mtna.2016.14.

(16) Haque, N.; Hogg, J. R. Technology Preview Easier , Better , Faster , Stronger : Improved Methods for RNA-Protein Interaction Studies. *Mol. Cell* **2016**, *62* (5), 650–651. https://doi.org/10.1016/j.molcel.2016.05.019.

(17) Darnell, R. B. HITS-CLIP : Panoramic Views of Protein-RNA Regulation in Living Cells. **2010**, *1* (2), 266–286.

(18) Luna, J. M.; Barajas, J. M.; Teng, K.; Rice, C. M.; Darnell, R. B.; Ghoshal, K.; Luna, J. M.; Barajas, J. M.; Teng, K.; Sun, H.; Moore, M. J.; Rice, C. M. Argonaute CLIP Defines a Deregulated MiR-122- Bound Transcriptome That Correlates with Patient Survival in Human Liver Cancer Article Argonaute CLIP Defines a Deregulated MiR-122-Bound Transcriptome That Correlates with Patient Survival in Human Liver Can. **2017**, 400–410. https://doi.org/10.1016/j.molcel.2017.06.025.

(19) Lu, Y.; Leslie, C. S. Learning to Predict MiRNA-MRNA Interactions from AGO CLIP Sequencing and CLASH Data. *PLOS Comput. Biol.* **2016**, *12* (7), e1005026. https://doi.org/10.1371/journal.pcbi.1005026.

(20) Chi, S. W.; Zang, J. B.; Mele, A.; Darnell, R. B. Ago HITS-CLIP Decodes MiRNA-MRNA Interaction Maps. **2010**, *460* (7254), 479–486. https://doi.org/10.1038/nature08170.Ago.

(21) Li, X. Genome-Wide Mapping of Cellular Protein – RNA Interactions Enabled by Chemical Crosslinking. **2014**, *12*, 72–78. https://doi.org/10.1016/j.gpb.2014.03.001.

(22) Young, D. D.; Young, T. S.; Jahnz, M.; Ahmad, I.; Spraggon, G.; Schultz, P. G. An Evolved Aminoacyl-TRNA Synthetase with Atypical Polysubstrate Specificity. *Biochemistry* **2011**, *50* (11), 1894–1900. https://doi.org/10.1021/bi101929e.

(23) Liu, X.; Houzet, L.; Jeang, K. Tombusvirus p19 RNA Silencing Suppressor (RSS) Activity in Mammalian Cells Correlates with Charged Amino Acids That Contribute to Direct. *Cell Biosci.* **2012**, *2* (1), 1. https://doi.org/10.1186/2045-3701-2-41.

(24) Kirshenbaum, K.; Carrico, I. S.; Tirrell, D. A. Biosynthesis of Proteins Incorporating a Versatile Set of Phenylalanine Analogues. **2002**, No. 02, 235–237.

(25) Deiters, A.; Cropp, T. A.; Summerer, D.; Mukherji, M.; Schultz, P. G. Site-Specific PEGylation of Proteins Containing Unnatural Amino Acids. **2004**, *14*, 5743–5745. https://doi.org/10.1016/j.bmcl.2004.09.059.

(26) Chin, J. W.; Santoro, S. W.; Martin, A. B.; King, D. S.; Wang, L.; Schultz, P. G. Addition

of P-Azido-L-Phenylalanine to the Genetic Code of Escherichia Coli. *J. Am. Chem. Soc.* **2002**, *124* (31), 9026–9027. https://doi.org/10.1021/ja027007w.

(27) Ahmed, N.; De Graaf, J. F.; Ahmed, N.; Foss, D. V; Delcorde, J.; Schultz, P. G.; Pezacki, J. P. Visualization of the Delivery and Release of Small RNAs Using Genetic Code Expansion and Unnatural RNA-Binding Proteins. *Bioconjug. Chem.* **2018**, *29* (12), 3982–3986. https://doi.org/10.1021/acs.bioconjchem.8b00649.

(28) Shetlar, M. D.; Christensen, J.; Hom, K. Photochemical Addition of Amino Acids and Peptides to DNA. *Photochem. Photobiol.* **1984**, *39* (2), 125–133. https://doi.org/10.1111/j.1751-1097.1984.tb03417.x.

(29) Chin, J. W.; Schultz, P. G. In Vivo Photocrosslinking with Unnatural Amino Acid Mutagenesis. *ChemBioChem* **2002**, *3* (11), 1135–1137. https://doi.org/10.1002/1439-7633(20021104)3:11<1135::AID-CBIC1135>3.0.CO;2-M.

(30) Hafner, M.; Landthaler, M.; Burger, L.; Khorshid, M.; Hausser, J.; Berninger, P.; Rothballer, A.; Ascano, M.; Jungkamp, A.; Munschauer, M.; Ulrich, A.; Wardle, G. S.; Dewell, S.; Zavolan, M.; Tuschl, T. Resource Transcriptome-Wide Identification of RNA-Binding Protein and MicroRNA Target Sites by PAR-CLIP. *Cell* **2010**, *141* (1), 129–141. https://doi.org/10.1016/j.cell.2010.03.009.

Chapter 4

An Unnatural Enzyme with Endonuclease Activity Towards Small Non-coding RNAs

4.1 Preface

As the first author of this chapter, I made significant intellectual and experimental contributions to the work presented here. J.P. Pezacki and I conceived the research ideas and the experimental plans. I performed most of the experimental procedures and sample preparations. Nadine Ahmed assisted in mammalian cell optimization work and JFH-1 infections. D. A. Bilodeau synthesized (2,2′-bipyridin-5-yl)alanine used in this study.

This chapter's first draft was written by myself and edited by all authors.

4.2 Abstract

Endonucleases are enzymes that cleave internal phosphodiester bonds within double-stranded DNA or RNA and are essential for biological functions including DNA replication, repair, RNA splicing, and RNA silencing. Engineered endonucleases used in cloning and gene editing are also important tools. Herein, we used genetic code expansion to create an unnatural endonuclease that cleaves small non-coding RNAs including short interfering RNA (siRNA) and microRNAs (miRNAs), a function that does not exist in nature. We introduced a metal-chelating unnatural amino acid, (2,2′-bipyridin-5-yl)alanine (BpyAla) to impart endonuclease activity to the viral suppressor of RNA silencing protein p19. Upon binding of copper, the mutant p19-T111BpyAla displayed catalytic site-specific cleavage of siRNA and human miRNAs. Catalysis was confirmed using two independent assays. Global profiling of miRNAs revealed that the engineered enzyme cleaves miRNAs in human hepatoma cells. The therapeutic potential was demonstrated by targeting miR-122's a critical host factor for the hepatitis C virus (HCV). Unnatural endonuclease function depleted miR-122 levels significantly with similar effects to an antagomir that reduced HCV levels therapeutically.

4.3 Introduction

Endonucleases catalyze the cleavage of internal phosphodiester bonds in RNA and DNA leading to the scissile rupture of genetic material or their transcription products. Endonuclease function in many organisms is involved in DNA damage repair mechanisms, restricting gene expression and antiviral responses to infection in bacteria[1]. Endonucleases that target RNA substrates are involved in mRNA splicing, RNA silencing pathways, maturation of tRNAs, and other non-coding RNAs (ncRNAs)[2–5]. Adapting and engineering these natural enzyme catalysts has led to cornerstone biotechnologies from recombinant DNAs to gene editing technologies[6–8].

Short non-coding RNA molecules such as microRNAs (miRNAs) have important regulatory roles[9,10]. miRNAs have been identified to play critical roles in gene expression regulation during transcriptional processes[11], as well as different biological and biochemical processes ranging from cellular metabolism to immunity[10,12,13]. As products of the RNA silencing pathway, miRNAs are usually 21-25 nucleotides in length[9,14,15]. They exert their function by targeting specific messenger RNAs (mRNA) for degradation or translational repression[10,13,16]. Also, miRNA-based regulation has been linked to disease progression, which makes them interesting targets for protein-based therapeutics[10,17]. While there do exist natural suppressors of RNA silencing[18–21], these typically bind and sequester RNA intermediates.

Designing endonuclease enzymes, and indeed any enzyme, based on substrate binding scaffolds (e.g. proteins, aptamers, catalytic antibodies) has had limited success because the product closely resembles the bound transition state, causing product inhibition that prevents enzymatic turnover[22–26]. Thus, the product needs to be significantly different from the substrate and the transition state structures for the designed endonuclease enzyme to be successful. The binding protein needs to retain enough selectivity to its substrate, that once the preferential binding

characteristics are lost, the product is released, and product inhibition is avoided[26]. Here we utilized p19, an RNA binding protein with high selectivity to double-stranded small RNAs of 19-25 nucleotides in length[18], but displays a very low affinity for single-stranded (ssRNA) and shorter double-stranded RNA (dsRNA). We hypothesize that p19 is an ideal protein candidate for endonuclease design, as once the RNA substrate is cleaved, p19 can no longer bind the cleaved product due to the loss of preferential binding characteristics.

4.4 Results

4.4.1 Site-specific introduction of (2,2′-bipyridin-5-yl)alanine into the p19 dimer

To engineer a new endonuclease capable of specifically targeting miRNAs, we started with the *Tombusvirus* p19 viral suppressor of RNA silencing (VSRS), which naturally binds and sequesters small RNA duplexes with picomolar affinity, thereby preventing the activation of the RNA silencing pathway[19,27–32] (Fig. 4.1 A, C). p19 binds RNA sequences with size selectivity [28,29]. Rational design and protein engineering of the p19 VSRS has allowed the development of biotechnological tools with diverse applications[27,29,30,33–39]. p19 has proved to be a potent inhibitor of small RNA function, which opens the door to further engineering the protein to exhibit "super suppressor" activity with added endonuclease functionality [18,35–38]. Previously, it has been shown that using the pioneering technologies of genetic code expansion in combination with unnatural amino acids (UAAs), organisms can code for more than the 20 canonical amino acids allowing for the incorporation of unique chemical side chains into the desired location in a protein of interest[40–42]. It has been shown that the attachment of metal chelating molecules such as EDTA and phenanthroline derivatives to nucleic acid binding agents have led to oxidative and hydrolytic cleavage[43]. We sought to explore the potential of introducing metals site-specifically into p19. The introduction of (2,2′-bipyridin-5-yl)alanine (BpyAla) chelates metal divalent ions, leading to site-specific RNA cleavage. This strategy can provide a new therapeutic tool targeting miRNAs involved in disease progression, as well as showing the potential of introducing catalytic activity into proteins of interest with affinities towards nucleic acids.

We introduced BpyAla[44,45] within the RNA binding pocket of p19 to insert a catalytic site (Fig. 4.1B). The UAA bearing a bipyridyl moiety provides an unnatural side chain capable of

binding transition metal ions such as copper and iron that can catalyze the cleavage of the phosphodiester backbone of nucleic acids[44,46].

We previously established the successful incorporation of Azidophenylalanine (AzF) into p19 at positions K67 and T111, in which full-length expression of the mutants and successful irreversible photo-crosslinking to their canonical substrates was achieved to produce crosslinked products with intermediates of the RNA silencing pathway,[39] with potential applications to CLIP assays. These two sites are found in the binding pocket of the p19 dimer, near the phosphate backbone of the RNA (Fig. 4.1B). To incorporate BpyAla, amber codons (TAG) were introduced in place of K67 and T111, to determine which position would allow for optimal cleavage of the bound RNA product. We expressed p19 mutants in the presence of the evolved tRNA/aaRS pair, and the presence of 1 mmol/L BpyAla. (Fig. S4.1). Bacterial cells (BL2l (DE3)) expressing the tRNA/BpyRS pair and the mutant p19 genes were grown in Lysogency Broth (LB). The full-length expression was detected using western blot analysis under the induction of Isopropyl β-d-1-thiogalactopyranoside (IPTG) (Fig. S4.1)[44]. Since p19 binds small RNAs as a dimer, each of the monomers will contain the mutation leading to the incorporation of BpyAla, thus cleavage of the RNA will occur at 2 sites.

We have confirmed the formation of the p19-T111BpyAla enzyme-copper (II) complex using inductively coupled plasma mass spectrometry (ICP-MS). ICP-MS data shows that the associated copper (II) concentrations with p19-T111BpyAla are higher than that associated with the control p19-WT samples, thus confirming copper ion chelation to T111BpyAla (Fig. 4.2). Additionally, the UV-Vis absorption spectra of p19-T111BpyAla showed two new absorption bands at 319 nm and 304 nm upon the addition of $CuSO_4$, and a decrease in absorption at 283 nm (Fig. 4.3). Spectral changes are consistent with the red-shift of $\pi - \pi^*$ transition of the incorporated

bipyridyl moiety upon chelation of Cu^{2+} ion, further confirming the formation of the artificial metal-bound enzyme. These data taken together confirm the specific binding of copper to the BpyAla residue within p19-T111BpyAla.

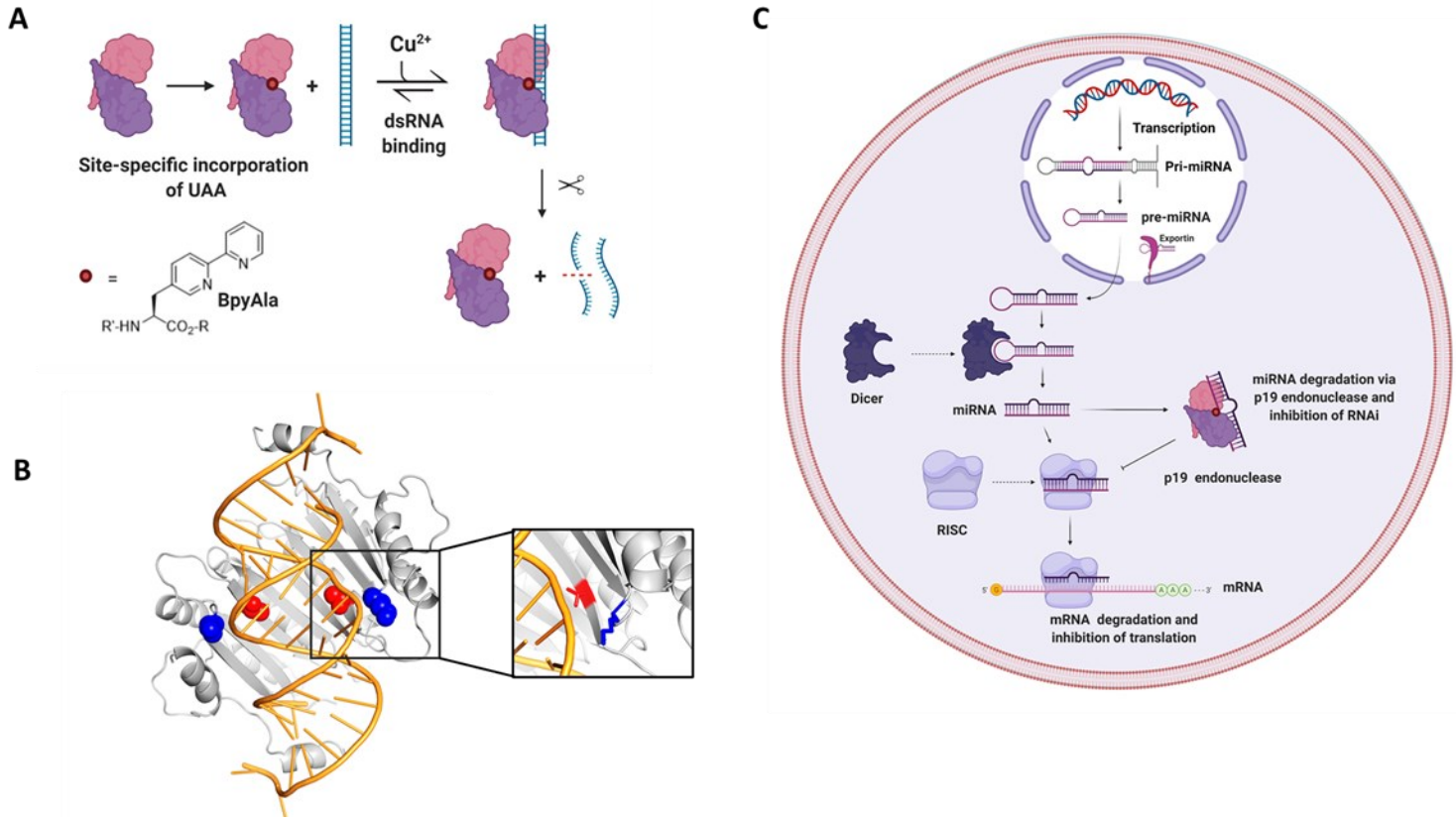

Figure 4.1. Incorporation of BpyAla in 2 sites in the p19 dimer. (A) Incorporation of BpyAla site-specifically into the VSRS protein p19 dimer introduces a metal binding site. Here we used copper to bind to BpyAla. If the metal can cleave the phosphodiester linkage within the RNA substrate, then it should induce site-specific strand cleavage of the bound siRNA or miRNA. Cleavage can occur on either strand. (B) Crystal structure of the p19 dimer with K67 (Blue) and T111 (red) highlighted PDB: 1RPU. (C) Overall Schematic representation of the potential disruption of the RNA silencing pathway upon treatment with the engineered p19 endonuclease.

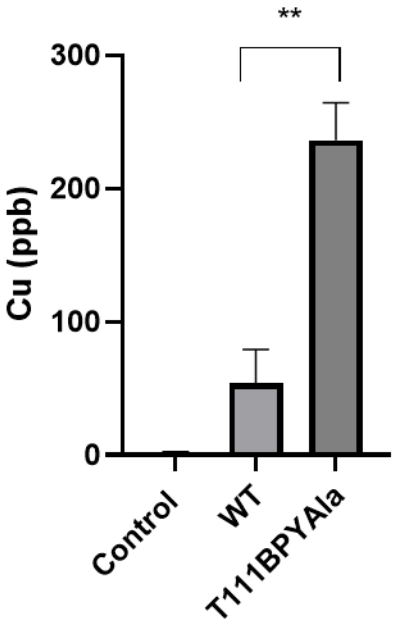

Figure 4.2 The ICP-MS quantitative analysis of copper concentration bound to p19-WT and mutant p19-T111BpyAla. Copper concentrations were determined using ICP-MS for samples of p19-WT and p19-T111BpyAla in parts per billion (ppb), for each condition n=3, error bars represent ±SD, **P<0.01. Data confirm specific binding and the formation of Cu^{2+} artificial enzyme.

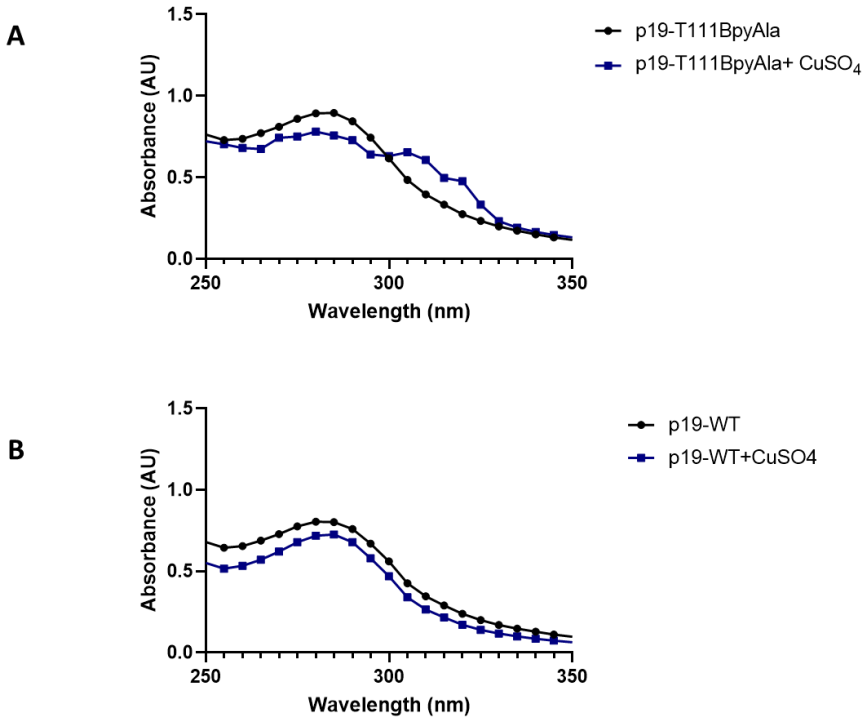

Figure 4.3 The UV-Vis absorption spectra of p19 WT and mutant p19-T111BpyAla. The UV-Vis absorption spectra of 20 µmol/L p19-T111BpyAla mutant upon addition of CuSO4 40 µmol/L in 25 mmol/L Tris, 30 mmol/L NaCl (pH = 7.4) showed two new absorption bands at 319 nm and 304 nm, and a decrease in absorption at 283 nm. Spectral changes are consistent with the red-shift of $\pi - \pi^*$ transition of the incorporated bipyridyl moiety upon chelation of Cu^{2+} ion.

4.4.2 Small RNA cleavage using p19-T111BpyAla

Next, we sought to assess the binding affinity of the mutants to a 21-nt GL2 siRNA targeting Firefly luciferase and containing Cy3 at the 5′ end of the guide strand (Fig. 4.4 A, S4.2). We determined the binding affinities of the purified recombinant mutants using an electrophoretic mobility shift assay (EMSA). The binding affinity of p19-T111BpyAla was determined to be 2.38±0.63 nmol/L, while p19 K67BpyAla is 8.41±0.49 nmol/L (Fig. 4.4 A, S4.2). Overall, both mutants were shown to bind siRNA with high affinity.

To further assess the success of introducing the catalytic functionality into the selected sites in the p19 dimer, both mutants were tested for their ability to cleave the Cy3 labeled GL2 siRNA. The site-specific cleavage of RNA was investigated using a gel-retardation assay (Fig. 4.4 B, C). The Cy3-tagged siRNA duplexes were incubated with p19-T111BpyAla, p19-K67BpyAla, or p19-WT, in the presence of Cu (II). The cleavage reactions were analyzed using denaturing UREA-PAGE (Fig. 4.4 B, C). The gel has revealed that only p19-T111BpyAla was able to catalyze the cleavage of the siRNA tagged ligand leading to a lower size band appearing on the gel. On the other hand, p19-K67BpyAla did not catalyze the cleavage of the substrate. No cleavage occurred with p19-WT under the same conditions (Fig. 4.4 C).

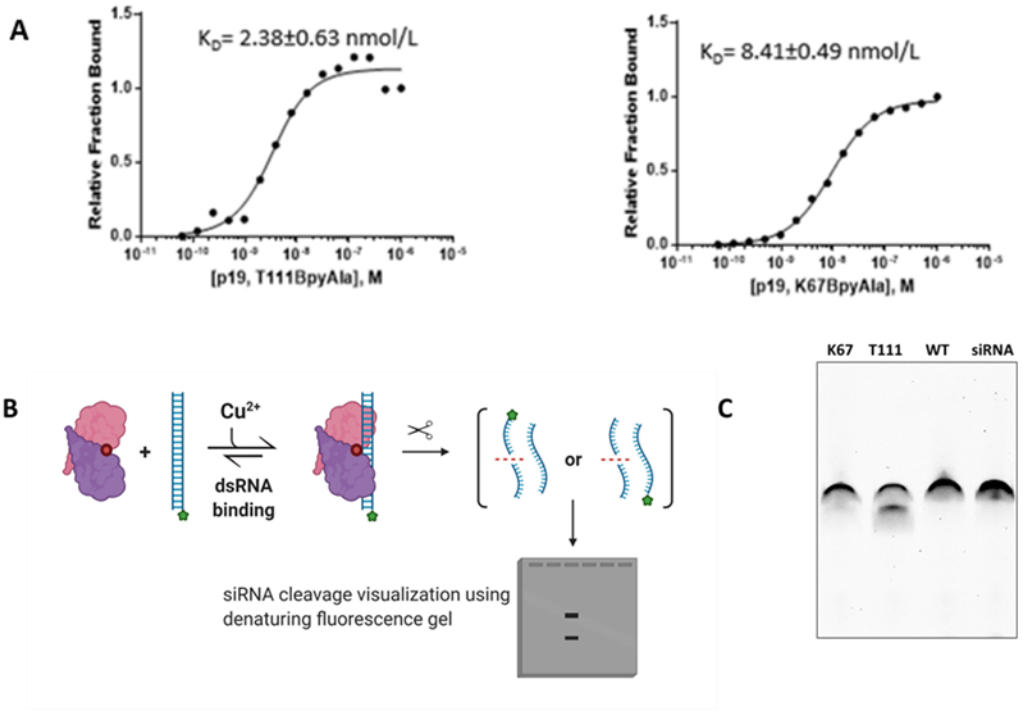

Figure 4.4. siRNA cleavage by p19-T111BpyAla mutant. (A) Binding plots for p19-T111BpyAla and p19-K67BpyAla using electrophoretic mobility shift assays. Binding plots were constructed by varying the concentrations of the protein (0-1 µmol/L) while maintaining the concentration of Cy3-labeled GL2 at 2 nmol/L. (B) An overall schematic representation of the experimental strategy, in which Cy3-GL2 siRNA cleavage was assessed using a denaturing UREA-PAGE gel (C) 20% urea-PAGE gel was used to visualize the degradation product of Cy3-Gl2 siRNA by the engineered p19-T111BpyAla mutant in the presence of $CuSO_4$.

4.4.3 Cleavage of siRNA by p19-T111BpyAla detected using fluorescence polarization

Next, we sought to validate the catalytic function using fluorescence polarization assays, in which p19-T111BpyAla was incubated with a fluorescently tagged siRNA. A decrease in polarization has been observed over time, which is expected upon cleavage and release. Upon cleavage by p19-T111BpyAla, the fluorescently tagged RNA is released from the enzyme, leading to faster rotation and consequently, a lower polarization signal (Fig. 4.5). The fluorescence polarization assay measured the degree of polarization of the fluorophore-tagged RNA and the change in fluorescence polarization as measured by the ratio of parallel and perpendicular light[47,48]. We used a Cy3-tagged double-stranded siRNA, which when unbound exhibits a low signal, however, upon being bound to the target protein, the fluorophore exhibits a higher polarization signal due to the increase in molecular mass and resultant slower rotation of the fluorophore bound to the complex[47]. When p19-T111BpyAla is combined with Cy3-siRNA, a time-dependent decrease in fluorescence polarization signal is observed (Fig. 4.5 B, C). The decrease in fluorescence polarization signal is attributed to the cleavage of the bound siRNA molecules, leading to the release of the Cy3-siRNA from the protein complex. The release of the fragmented RNA exhibits a faster rotation[47,48]. These results are consistent with the hydrolytic cleavage of small RNAs due to the site-specific introduction of BpyAla into p19.

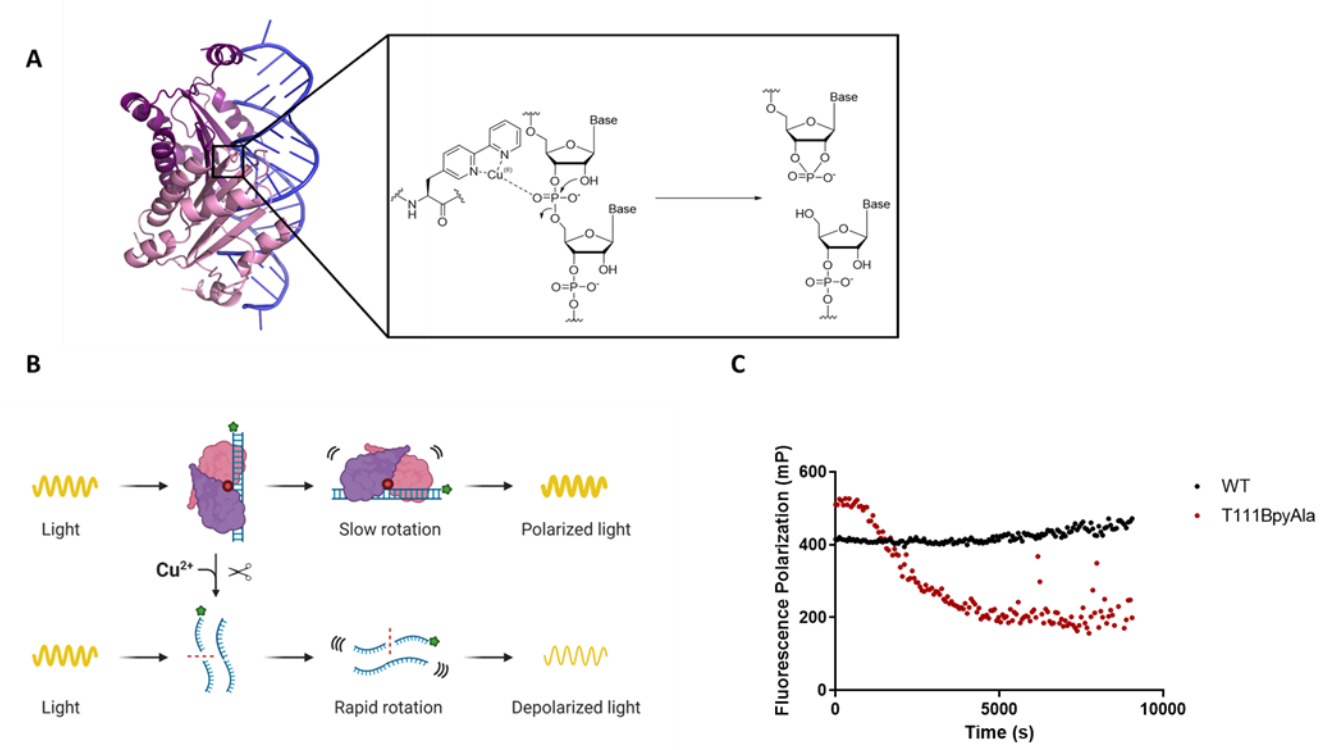

Figure 4.5. siRNA cleavage by p19-T111BpyAla mutant and visualization using fluorescence polarization. (A) The overall hydrolytic RNA cleavage mechanism due to the incorporation of BpyAla into p19 (B) An overall schematic representation of the experimental strategy, in which Cy3-Gl2 siRNA cleavage was assessed using fluorescence polarization. (C) A fluorescence polarization assay was used to visualize the cleaving potential of p19-T111BpyAla. The assay was conducted using 5 µmol/L p19-T111BpyAla or p19-WT and 200 nmol/L RNA, n=3, in which n values represent 3 biological replicates.

4.4.4 p19-T111BpyAla can cleave miRNAs isolated from hepatocellular carcinoma cell line

To further demonstrate the utility of p19-T111BpyAla as an artificial endonuclease for degrading small double-stranded RNA intermediates, we examined its ability to enzymatically cleave the small RNA fractions from Huh7 human hepatoma cells. The small RNA fractions from Huh7 cells were treated with either p19-WT treatment, or p19-T111BpyAla in the presence of $CuSO_4$ for 4 hours at 37°C. The treated RNA was then further purified and concentrated to ensure the removal of the proteins from the samples (Fig. 4.6 A). To uncover the identities of the substrates for the engineered endonuclease, we conducted a miRNA profiling experiment using NanoString technology (Fig. 4.6 B). We isolated the small RNA fractions from Huh7 cell line and treated with either p19-WT or p19-T111BpyAla. When comparing the profile of p19-T111BpyAla to that of the WT protein, we identified a list of statistically significant miRNAs that are differentially downregulated compared to the p19-WT ($P \leq 0.05$) (Fig. 4.6 B). These data suggest that the engineered protein degrades select miRNAs and gives rise to an amplified effect on the small RNA milieu as compared to that of the WT p19 which can only sequester miRNAs but not degrade them (Table S4.1). Interestingly, the miR-122-5p was observed to be downregulated by 2.0-fold when treated with p19-T111BpyAla in comparison to treatment with WT. miR-122 is one of the miRNAs of the highest abundance in the liver, and it is known to bind p19 with high affinity. Other miRNAs are identified in this screen, however, p19's affinity to these identified miRNAs has not been previously examined. It is possible, however, that p19-T111BpyAla could potentially exhibit preferential binding to these miRNAs based on the positioning of the mismatched bulges in their secondary structure, which could give rise to enhanced binding, and thus preferential cleavage[29]. However, further, structure-function studies need to be performed to validate the preferential cleavage pattern obtained from the Nanostring screen. p19 is known to exhibit a high degree of

size selectivity, and some degree of sequence dependence when it comes to the binding of miRNAs[29].

Next, we validated the Nanostring results by measuring the levels of miR-122, upon treatment with the mutant in the isolated samples using RT-qPCR. From Fig. 4.6 C, it is evident that there is an observed decrease in the levels of miR-122 in p19-T111BpyAla treated samples, relative to treatment with p19-WT in the presence of copper, which aligns with the results from the NanoString profiling (Fig. 4.6 B, C). To further validate the effect of p19-T111BpyAla on degrading miR-122, we decided to examine its the effects on the expression levels of a miR-122 direct target, STAT3. We were able to observe derepression of STAT3 expression upon treatment with p19-T111BpyAla (Fig. 4.6 E). The effects of p19-T111BpyAla on STAT3 expression is similar to that upon transfection of miR-122 antagomir (Fig. 4.6 F).

We attribute these observed effects to the degradation of miR-122 by the mutant enzyme, as an enhanced degradation/ decrease in miR-122 levels is only observed upon the introduction of copper ions (Fig.4.6 D). These results together aid in demonstrating biocatalysis in a complex sample. There is no enhanced binding observed towards miR-122 by p19-T111BpyAla by EMSA when compared to the previously reported affinity of WT p19 towards miR-122 [48](Fig. S4.3).
For this study, we chose to next focus on miR-122 as it is a highly expressed miRNA in hepatic cells. miR-122 represents more than 70% of the miRNA pool in hepatoma cells and is known to play a major role as a proviral host factor in the propagation of HCV, a positive-sense single-stranded RNA virus of the family Flaviviridae[40-42].

HCV is known to be the causative agent of hepatitis C and hepatocellular carcinoma and lymphomas in humans. It is well established that HCV uniquely requires the liver-specific miR-122 for its replication. It exerts a positive effect on HCV RNA levels by binding directly to a site

in the 5’-UTR of the viral RNA and contributes to the stability, translation, and replication of the viral RNA [49–51].

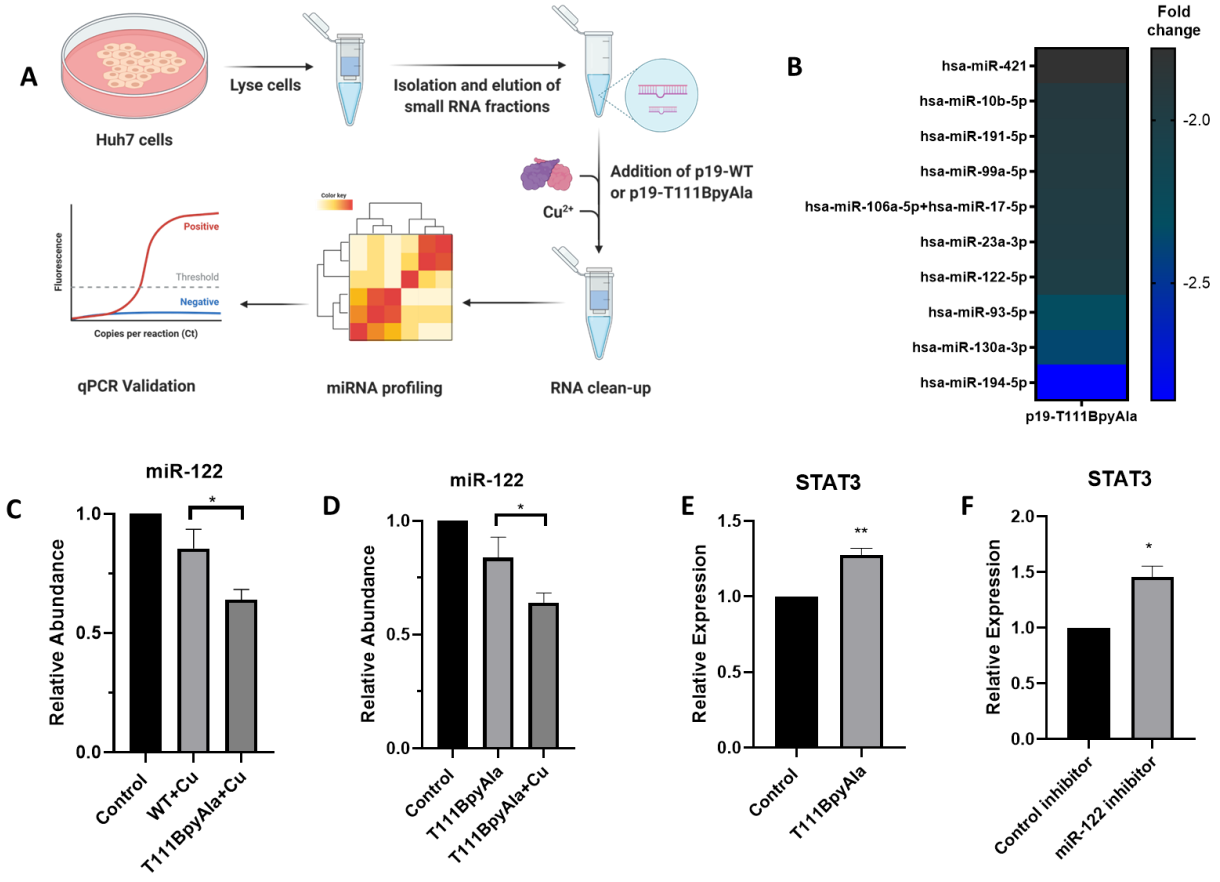

Figure 4.6. Cleavage of Huh7 miRNA samples using p19-T111BpyAla (A) Schematic representation of the workflow for small RNA isolation for NanoString profiling and RT-qPCR analysis. RNA used was isolated from Huh7 hepatocellular carcinoma cell line and treated in the presence of $CuSO_4$. (B) A heat map depicting the significant downregulated fold changes in miRNAs upon treatment with p19-T111BpyAla relative to p19-WT treated miRNAs n=2, n represents 2 biological trials, where RNA is isolated from 2 independent cell passages. Changes presented are more than 1.5-fold change ($p<0.05$). (C) qRT-PCR analysis of the relative miR-122 expression in p19-T111BpyAla treated samples in comparison to that treated with p19-WT in the presence of copper ions. Error bars represent ±SD n=3, n values represent the treatment of RNA isolated from 3 different passages (D) qRT-PCR analysis of the relative miR-122 expression in p19-T111BpyAla treated samples in the presence and absence of copper ions. (E) Derepression of miR-122's downstream direct target STAT3 upon treatment with p19-T111BpyAla (F) or miR-122 inhibitor, Error bars represent ±SD n=3, * $P<0.05$. n values represent the transfection of cells from 3 different passages.

4.4.5 p19-T111BpyAla represses HCV replication

To investigate the effects of p19-T111BpyAla on the levels of miR-122, we sought to utilize a hepatocellular carcinoma cell line harboring the HCV subgenomic replicon pFK-I389neo/luc/NS3-3′/5.1 (Fig. 4.7 A). This replicon system (our version is referred to as the E9 cell line) has been widely used to investigate the replication of HCV in cell culture[52]. Replication of HCV is significantly diminished in miR-122 knockout cell line[53]. Thus, we wanted to validate the antiviral role that p19-T111BpyAla can potentially play. We have treated cells with p19-T111BpyAla by directly transfecting the enzyme-Cu^{2+} complex into cells or transfecting miR-122 antagomir inhibitor as a control, to validate the effects of the mutant protein on HCV replication. The levels of miR-122 are directly correlated with HCV replication, which is linked to the relative luciferase signal in E9 cells. The effects of both miR-122 antagomir, and p19-T111BpyAla are investigated and correlated to the successful HCV subgenomic replication. Importantly, we were able to show that the designed protein led to almost the same level of HCV inhibition of replication as the levels achieved by the antagomir (Fig. 4.7 B, C).

The basis for the antiviral effects of the antagomir arises from the fact that it binds to the guide strand of miR-122 more tightly than the competing genomic viral RNA. Thus, it prevents binding to and sequestering of miR-122 by HCV. The p19-T111BpyAla enzyme can sequester miR-122 away from HCV and reduce the overall amount of miRNA through biocatalysis. Thus, with the engineered enzyme, there is the advantage of cleaving the target miRNA reducing its overall levels in the infected cell, which was confirmed by quantification of miRNA-122 using Taqman qPCR (Fig. 4.6 C).

In addition to validating the effects of p19-T111BpyAla on HCV subgenomic replication, we wanted to see the effects on Huh7.5 cells infected with the $JFH1_T$ strain of HCV. Upon HCV

infection and then direct protein transfection with p19-T111BpyAla-Cu^{2+}, an inhibition of HCV replication of approximately 50% was achieved (Fig. 4.7 D). Taken together these data support the conclusion that p19-T111BpyAla possesses unique anti-HCV properties by acting as an unnatural endonuclease targeting the pro-viral miRNA miR-122 (Fig.4.7).

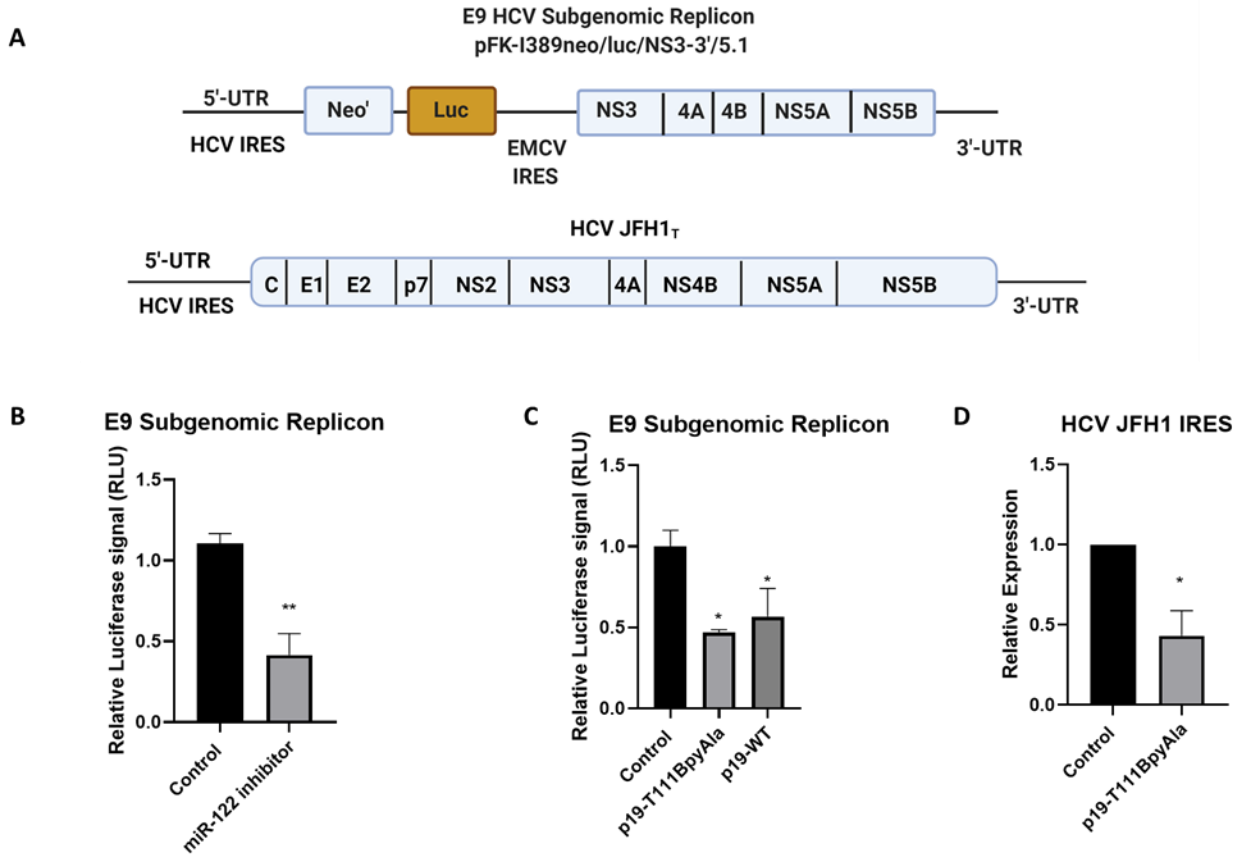

Figure 4.7. p19-T111BpyAla effect of HCV replication. (A) Schematic representation of the subgenomic HCV replicon (pFK-I389neo/luc/NS3-3′/5.1) used in this study[52] and HCV $JFH1_T$ strain. (B) Relative luciferase signal upon treatment of E9 cells with either miR-122 antagomir,(C) p19-T111BpyAla, or p19-WT. The levels of miR-122 are directly correlated with HCV replication, which is linked to the relative luciferase signal in E9 cells. The effects of both miR-122 antagomir, and p19-T111BpyAla were investigated, with both treatments leading to a similar reduction in HCV subgenomic replication. n=3, error bars represent ±SEM where, * P<0.05, **P<0.01. (D) Relative expression of HCV JFH1 IRES in Huh7.5 cells upon treatment with p19-T111BpyAla, n=3, error bars represent ±SD, where * P<0.05. n values represent the transfection of different cell passages.

4.5 Discussion

Herein, we show the possibility of engineering endonucleases targeting small RNAs using expanded genetic code techniques to introduce the unnatural amino acid BpyAla site-specifically into p19 protein. We show that upon the addition of copper ions, the engineered p19 VSRS takes on artificial endonuclease activity not found in the wild-type protein[54]. Engineered endonucleases have been previously designed through protein fusions, which in nature can be bulky and could interfere with the functionality and proper folding of the designed enzyme[55]. Thus far, the engineering of RNA endonucleases has been achieved by combining different functional modules of proteins[54]. Similar designs have been applied to DNA binding proteins by introducing a zinc finger DNA binding domain along with an established DNA cleavage domain, with strict selectivity toward a specific DNA sequence[54,55]. However, for the first time, we showed that this approach can be successfully applied specifically to design RNA binding proteins into ribonucleases by a single UAA.

An endonuclease based on the viral protein p19 is a good candidate for an RNA endonuclease design that specifically targets miRNAs due to the intrinsic size specificity associated with the protein[28]. We have confirmed that position T111 in the p19 dimer accommodates the introduction of the UAAs as well as copper binding without drastically affecting substrate binding. Position T111 in the p19 dimer has been shown to accommodate different amino acids[33,39].

As a new artificial enzyme, p19-T111BpyAla should have wide applications in catalytic suppression of the RNA silencing pathway. We demonstrated an application showing that p19-T111BpyAla reduced the levels of the human miR-122 which resulted in the downregulation of HCV replication in a cell culture model. RNA therapy and usage of antagomirs, while effective,

do have some disadvantages, mainly in costs associated with scale-up and challenges in terms of delivery. In contrast, protein therapeutics have been used and engineered to retain tissue specificity through the employment of protein fusions with tissue-specific peptides, thus holding an advantage over RNA therapeutics[56–58].

For HCV, it is well established that the virus has evolved a dependence on human miR-122 and those oligonucleotide antagonists (antagomirs) for miR-122 can restrict and eliminate HCV, even in clinical trials[59,60]. We demonstrated that p19-T111BpyAla was as effective as the corresponding antagomir at reducing miR-122 pools and limiting HCV replication while doing so catalytically and through enzyme-like function. This illustrates the potential for engineered enzymes like p19-T111BpyAla as antiviral strategies in the case where either the virus encodes its viral miRNA or interacts directly with the host's miRNA as well as in other diseases where miRNAs are disease causing[10,61–64]. Recently, the usage of catalytic enzymes to inhibit viral infections has been investigated, however, it is still a relatively new concept[65,66].

The p19-T111BpyAla endonuclease shows some selectivity and reasonable potency in different model systems. One challenge is the lack of sequence specificity[18], which is overcome in the case of HCV replication by the high abundance of the target miRNA. In future iterations, this limitation can be mitigated by utilizing directed evolution techniques to identify other mutants with preferential binding to individual miRNAs of interest, while maintaining the characteristics of p19-T111BpyAla. The current system however can be expressed in specific cells with high expression of a miRNA of interest, in which the engineered endonuclease can preferentially cleave. In this study, miR-122 is the most highly expressed miRNA in liver cells, and thus preferentially targeted.

From the Nanostring profiling experiment, it is evident that other miRNAs exhibit a higher degree of cleavage, which can potentially be attributed to the enhanced binding of p19 mutant to these miRNAs. The differences in affinity could be attributed to the mismatches in the miRNA sequences, which create bulges in the secondary structure of the miRNA, thus affecting the potential binding affinity to p19, depending on the location of the bulge[29,37,48].

Designing new enzymes based on adding catalytic residues/centers to high affinity binding motifs, has proved challenging mainly due to issues pertaining to product inhibition. Catalytic RNAs, antibodies, and other strategies have a common challenge of lack of substrate turnover due to product inhibition[22–25]. Designing endonucleases based on substrate binding scaffolds face the same challenges[26]. However, a key element of our system is the fact that recombinant p19 proteins retain their strong selectivity towards dsRNA of 19-25 nt in length[18], and high selectivity towards the products of the dicer complex. p19-T111BpyAla at the same time displays little or no affinity towards the ssRNA or 10-11 nt dsRNA products of copper-mediated miRNA cleavage. This may allow the potential for multiple turnovers and efficient catalysis to occur. The low affinity for cleaved products, allowing for the release of the cleaved product from the enzyme, is a unique aspect of our design. It is important to note that further experiments need to be conducted to determine the kinetic parameters of the engineered enzyme and compare it with naturally existing enzymes.

In conclusion, we have created the artificial enzyme, p19-T111BpyAla, capable of cleaving and eliminating the products of dicer. This enzyme should have wide applications in catalytic suppression of the RNA silencing pathway. The enzyme also has the potential to be deployed as a therapeutic. It is interesting to think about catalytic systems for targeting human viruses. Our work lays the groundwork for new versions with enhanced targeting.

4.6 Materials and Methods

4.6.1 Expression and purification of p19-WT, p19-K67BpyAla and p19-T111BpyAla

The coding sequence of p19 retrieved from Carnation Italian Ringspot was cloned in pTriEX-Neo plasmid and subjected to site directed mutagenesis to incorporate amber mutations (TAG) in the positions of interest K67 and T111. Mutagenesis was performed using the Quick-change lightning Site-Directed Mutagenesis kit (Agilent) according to the manufacturer's protocol. Cloning of the gene was conducted as previously described[67]. Sanger sequencing to confirm the appropriate mutations was performed at Génome Québec (Montreal, Canada).

The plasmid encoding BpyAlaRS/tRNA (pEVOL-BpyAla) was a kind gift from Dr. Peter Schultz (The Scripps Research Institute). Transformation of the plasmid encoding BpyAlaRS/tRNA (pEvol-BpyAla) was transformed in OneShot BL21 (DE3) Chemically competent cells (ThermoFisher) and then selected under Chloramphenicol (25µg/ml). Cells were then re-made competent and transformed with p19 plasmids bearing the appropriate amber mutations, where cells were then plated under the selection of Chloramphenicol and ampicillin (100µg/ml). Colonies were then selected for protein expression. Cells were then grown in Lysogeny Broth in the presence of the appropriate antibiotics at 37ºC until the optical density of 0.6 was reached. Protein expression was induced using 1 mmol/L IPTG in the presence of 1 mmol/L BpyAla (synthesized as previously described[44,68]) for 4 hours at 25ºC. Cells were then harvested and purified using a two-step nickel affinity chromatography and size exclusion chromatography as previously described[69].

4.6.2 Immunoblotting

Cell pellets were harvested from 1 mL aliquots via centrifugation and lysed in 1x SDS Laemmli sample buffer. Cell lysates were resolved using 12% SDS gel electrophoresis (SDS-PAGE) and then transferred onto a TGX stain-free PVDF membrane (Bio-Rad). Membranes were blocked in 3% BSA in Tris-buffered saline with 0.05% tween (TBS-T). Blot was then incubated with 6xhistag HRP-conjugated antibody (1:5000 dilution; ThermoFisher). Membranes were then washed and incubated for 5 minutes with the ECL Plus Western Blotting System (Bio-Rad). The blot was visualized using ChemiDoc MP imaging system (Bio-Rad).

4.6.3 Substrates

GL2 siRNA cyanine 3 labeled guide strand (5'-Cy3-CGU ACG CGG AAU ACU UCG AUU-3') and passenger strand (5'-UCG AAG UAU UCC GCG UAC GUU-3'; Sigma-Aldrich). Strands were annealed at 1:1.2 molar ratio in buffer containing 100 mmol/L potassium acetate, 30 mmol/L HEPES pH 7.5 and 2 mmol/L magnesium acetate by heating to 95°C for 2 min and cooling to 25°C at a rate of 1°C/min. The presence of duplexed siRNA was confirmed on a 6% non-denaturing agarose gels (ThermoFisher Scientific).

4.6.4 Electrophoretic mobility shift assay (EMSA)

Varying concentrations of p19 up to 1 μmol/L (with GL2 substrate) or 2 μmol/L (with miR-122) were incubated for 1 h with 2 nmol/L GL2 siRNA or miR-122 duplexed substrate in 20 mmol/L Tris pH 7, 100 mmol/L NaCl, 1 mmol/L EDTA, 0.02% v/v Tween-20 and 2 mmol/L DTT. Following incubation, samples were resolved on a 6% non-denaturing agarose gels. Visualization of products was performed using a ChemiDoc MP imaging system. Quantification of bound RNA was performed using ImageJ. Data were analyzed using GraphPad Prism and fit to the equation (1):

(1)

$$Y = b + A_{max}\left(\frac{K_D + ns + x}{2ns} - \sqrt{\left(\frac{K_D + ns + x}{2ns}\right)^2 - \frac{x}{ns}}\right)$$

Where K_D is the dissociation constant, n is the number of equivalent sites on the p19 dimer, s is the concentration of labeled small RNA, and x is the concentration of the p19 dimer.

4.6.5 Fluorescence Polarization

The assay was performed in a black 96-well plate to measure FP. Experiments measuring fluorescence polarization were carried out using excess enzyme [E]= 5000 nmol/L, and Cy3-GL2 siRNA concentration of 200 nmol/L. Reactions were performed in phosphate-buffered saline (PBS) with 10 mmol/L DTT, 10μmol/L $CuSO_4$, and 2.5 mmol/L β-mercaptopropionic acid.

Fluorescence polarization measurements were carried out using SpectraMax i3 (Molecular Devices). Polarization was monitored at 560 nm with excitation at 546 nm. Polarization is expressed as (2) where I_V and I_H are the vertically and horizontally polarized emission intensities, respectively.

(2)

$$P = \frac{I_V - GI_H}{I_V + GI_H}$$

4.6.6 Cell culture, RNA Isolation, miRNA profiling and RT-qPCR

Huh7 cells were seeded in a 6-well plate at 500,000 cells/ well. Forty-eight hours post seeding, the cells were lysed using ML lysis buffer. Small RNA fractions were isolated using NucleoSpin miRNA (Macherey-Nagel). 900 ng RNA was then treated with 5 μmol/L protein (p19 WT or T111BpyAla), 10 μmol/L $CuSO_4$, 2.5 mmol/L β-mercaptopropionic acid and allowed to incubate

for 4 hours at 37ºC. 100 attomoles of Cel-miR248 were used as a spike-in oligo control (IDT technologies), serving as an internal monitor to account for any changes caused during RNA purification. RNA was then further purified and concentrated using an RNA concentrator kit to remove any protein complexes, according to the manufacturer's protocol (Zymo Research). Following treatment, relative miRNA levels were quantified using the TaqMan miRNA Assay (Applied Biosystems), with 10 ng of total RNA used for reverse transcription using the TaqMan MicroRNA Reverse Transcription Kit (Applied Biosystems). For miR-122 quantification, the $2^{-\Delta\Delta Ct}$ method was used to calculate fold changes in expression relative to mock or control-treated samples, with RNU6β levels being used for normalization.

To analyze miRNA expression on the Nanostring ncounter platform, the RNA treated with either p19-WT or p19-T111BpyAla was prepared as per the manufacturer's protocol for the ncounter human v3 miRNA expression kit. Briefly, 50 ng of RNA was hybridized to the Reporter and Capture probes for 16 hours at 65 ºC. The prepared samples were loaded onto the nCounter Prep Station to wash the unbound probes and immobilize the samples on the cartridge for analysis and data collection. The target probes were counted using the nCounter Digital Analyzer. The collected data were processed and analyzed using the nSolver analysis software version 3.0. The ratio of expression of miRNAs for p19-T111BpyAla treated samples against p19-WT treated samples were calculated, n=2. Cel-miR248 was used as a spike-in oligo control (IDT technologies), serving as an internal monitor to account for any changes caused during RNA purification. Cel-miR248 levels were used to normalize the quantified RNA levels.

For quantification of STAT3 mRNA levels upon treatments with p19-T111BpyAla, cells were seeded at 100,000 cells in a 12-well plate. After 24 hours, 1 µmol/L p19-T111BpyAla-$Cu^{2+}$was combined with transfection reagent ProteoJuice (Novagen) in optimum media as per

manufacturer's protocol, then supplemented with full media. After another 24 hours, cells were lysed for analysis and RNA isolation. RNA isolation from Huh7 cells was done using RNeasy kits (Qiagen) according to the manufacturer's protocol. Primers targeting STAT3 (forward primer 5'-CAGCAGCTTGACACACACGGTA-3'; reverse primer 5'-AAACACCAAAGTGGCATGTGA -3')

4.6.7 E9 Subgenomic Replicon Luciferase Assay

1 μmol/L p19-T111BpyAla pre-complexed with $CuSO_4$ in which the protein was pre-incubated with $CuSO_4$ for 30 minutes on ice, and excess $CuSO_4$ was removed by buffer exchange in PBS using 10KDa Amicon Ultra centrifugal filters (Millipore). HCV subgenomic replicon pFK-I389neo/luc/NS3-3′/5.1 (E9) cells were seeded at 4×10^4 cells/well in 24-well plates, then either treated with 1 μmol/L p19-T111BpyAla combined with ProteoJuice transfection reagent, or 50 nmol/L hsa-miR-122-5p mirVana miRNA inhibitor (Ambion) transfected using RNAiMax (Life Technologies). Transfections were performed according to the manufacturer's protocol. Cells were lysed after 24 hours post-transfection in 1× passive lysis buffer (Promega), and the Luciferase assay was carried out using a SpectraMax L luminometer (Molecular Devices).

4.6.8 JFH-1 Infections

Huh7.5 Cells were seeded one day before infection in full media (DMEM, 10% FBS, NEAAs) at 20000 cells/well in 24 well plates. After 24 hours, the cells were incubated with the virus at MOI 0.1 in serum-free DMEM for 5 hours. 1μmol/L of p19-T111BpyAla complexed with $CuSO_4$ in which the protein was pre-incubated with $CuSO_4$ for 30 minutes on ice and excess $CuSO_4$ was removed by buffer exchange in PBS using 10KDa Amicon Ultra centrifugal filters (Millipore). p19-T111BpyAla was then combined with transfection reagent ProteoJuice (Novagen) in optimum media as per manufacturers protocol, then supplemented with full media and added to the cells.

The cells were incubated for 48 hours after which they were lysed in RL buffer and RNA was isolated using the Norgen Single Cell RNA purification kit (Norgen Biotek) as per the manufacturer's protocol. Reverse transcription and RT-qPCR were performed as described above with primers targeting the HCV JFH1 IRES (forward primer 5'-GTCTGCGGAACCGGTGAGTA-3'; reverse primer 5'-GCCCAAATGGCCGGGATA-3')

4.6.9 Synthesis of (2,2′-bipyridin-5-yl)alanine

(2-pyridacyl)pyridium Iodide

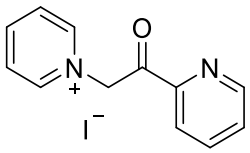

(2-pyridacyl)pyridium Iodide was synthesized according to previously reported synthetic methods.[68] Iodine (2.0 g, 16 mmol, 0.6 eq.) was dissolved in warm pyridine (7.0 mL, 80 ^{o}C) under an argon atmosphere. 2-acetyl pyridine (3.0 mL, 26.7 mmol, 1.0 eq.) was slowly added and the mixture was stirred for 4 hours. After cooling, the precipitated solid was collected by filtration and washed with cold pyridine (23 mL). The black solid was then added to boiling ethanol (100 mL) to which 2 spatulas of activated carbon were added. After 1 hour, the mixture was filtered via hot filtration. The filtrate was cooled down in an ice bath and the precipitate was collected to yield the desired product as yellow crystals (5.0 g, 15.3 mmol, 57% yield). ^{1}H-NMR data matched previously reported data.[68] **^{1}H-NMR** (300 MHz, DMSO-d_6) δ, 9.00-9.01 (m, 2H), 8.87-8.89 (m, 1H), 8.70-8.76 (m, 1H), 8.25-8.32 (m, 2H), 8.12-8.17 (m, 1H), 8.06-8.09 (m, 1H), 7.81-7.86 (m, 1H), 6.50 (s, 2H).

5-methyl-2,2'-bipyridine

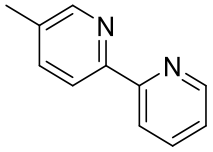

5-methyl-2,2'-bipyridine was synthesized according to previously reported synthetic methods.[68] In a dry round-bottomed flask, (2-pyridacyl)pyridium iodide (5.0 g, 15.3 mmol, 1.0 eq.) was added with ammonium acetate (2.4 g, 30.6 mmol, 2 eq.). The solid mixture was dissolved in formamide (15 mL) and methacrolein (1.8 mL, 21.4 mmol, 1.4 eq.) was slowly added. The mixture was heated to 75 ºC and stirred for 12 hours. Once cooled to room temperature, the reaction mixture was poured into saturated $NaHCO_3$ and extracted 6 times with 20 mL of EtOAc. The combined organic layers were washed with brine (100 mL), dried with Na_2SO_4, and concentrated under reduced pressure. The crude oil was passed through a short silica pad, eluting with 19:1 (DCM: MeOH). The desired product was obtained as a pale yellow oil (1.57g, 9.2 mmol, 60% yield). ^{1}H-NMR data matched previously reported data.[68] **^{1}H-NMR** (300 MHz, $CDCl_3$) δ 8.66 (ddd, *J* = 4.8, 1.8, 0.9 Hz, 1H), 8.50 (dt, *J* = 2.3, 0.8 Hz, 1H), 8.35 (dt, *J* = 8.0, 1.1 Hz, 1H), 8.28 (dd, *J* = 8.1, 0.8 Hz, 1H), 7.79 (td, *J* = 7.8, 1.8 Hz, 1H), 7.67 – 7.56 (m, 1H), 7.32 – 7.21 (m, 1H), 2.38 (s, 3H).

5-bromomethyl-2,2′-bipyridine

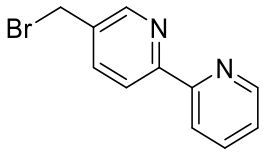

5-bromomethyl-2,2′-bipyridine was synthesized according to modified previously reported synthetic methods.[68] 5-Methyl-2,2'-bipyridine (2.9g, 17.3 mmol, 1.0 eq.) was dissolved in CCl_4 (100 mL) and the solution was degassed via bubbling argon. N-bromosuccinimide (4.0 g, 22.5 mmol, 1.3 eq.) and AIBN (284 mg, 1.73 mmol, 0.1 eq.) were then added to the mixture. A reflux condenser was attached and the mixture was refluxed under an inert atmosphere for 3 hours. The solvent was then removed under reduced pressure and the crude product was dissolved in 100 mL of CH_2Cl_2. 100 mL saturated $NaHCO_3$ was poured onto the mixture and it was extracted 3 times with 30 mL of CH_2Cl_2. The organic layers were combined, washed with 50 mL of saturated $NaHCO_3$, dried with Na_2SO_4, and concentrated under reduced pressure. The obtained mixture of mono and bis-brominated products was then dissolved in THF (20 mL) under an argon atmosphere. Diethyl phosphite (0.8 mL, 6.2 mmol, 0.36 eq.) and N,N-diisopropylethylamine (1.1 mL, 6.2 mmol, 0.36 eq.) were added to the mixture and it was stirred for 18 hours at room temperature. After full consumption of the dibromide (verified via ^{1}H-NMR), the THF was evaporated under reduced pressure and 25 mL of saturated $NaHCO_3$ was added to the residue. The mixture was extracted 3 times with 30 mL of EtOAc. The combined organic layers were dried over Na_2SO_4 and concentrated under a vacuum. The crude product was loaded onto a silica gel column and eluted initially with 200 mL of CH_2Cl_2, followed by approx. 500 mL of 200:1 (CH_2Cl_2:MeOH). The mono-bromide was obtained as a white solid (2.25g, 9.0 mmol, 52% yield). ^{1}H-NMR data matched previously reported data.[68] **^{1}H-NMR** (300 MHz, $CDCl_3$) δ 8.73 – 8.63 (m, 2H), 8.40 (dt, *J* = 8.0, 1.1 Hz, 2H), 7.91 – 7.74 (m, 2H), 7.32 (ddd, *J* = 7.5, 4.8, 1.2 Hz, 1H), 4.54 (s, 2H).

3-(2,2'-bipyridin-5-yl)-L-Alanine

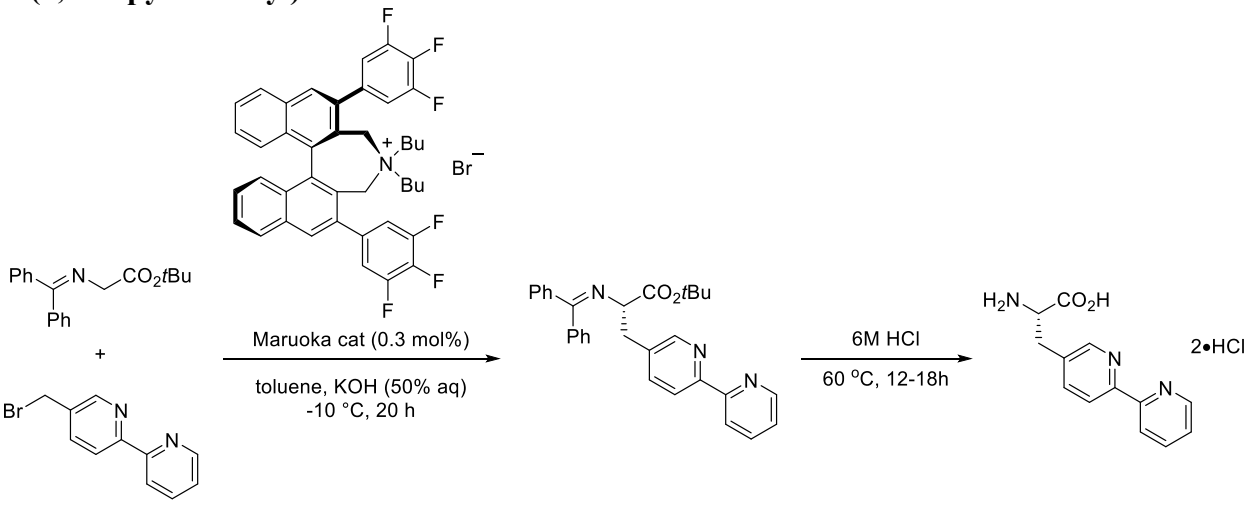

Under an inert atmosphere, 5-(bromomethyl)-2,2'-bipyridine (2.3 g, 9.0 mmol, 1.0 eq.), glycine t-butyl ester benzophenone imine (2.80 g, 9.5 mmol, 1.05 eq.) and Maruoka's catalyst ((11bR)-(–)-4,4-Dibutyl-4,5-dihydro-2,6-bis(3,4,5-trifluorophenyl)-3H-dinaphth[2,1-c:1′,2′-e]azepinium bromide) (20.3 mg, 0.027 mmol, 0.03 eq.) were added to toluene (23 mL) and a 50% aqueous solution of KOH (4.5 mL) was subsequently added. The mixture was stirred for 40 hours at -10 °C. The mixture was then diluted with brine (20 mL) and extracted 5 times with diethyl ether (20 mL); the organic layers were combined, dried with Na_2SO_4 and concentrated under reduced pressure. The residue was purified by column chromatography on silica gel, eluting with 50:1 (CH_2Cl_2:MeOH) to yield the target compound as a yellow oil (3.70 g, 8.0 mmol, 88% yield). **^{1}H NMR** (300 MHz, $CDCl_3$) δ 8.71 – 8.61 (m, 1H), 8.42 (d, *J* = 2.2 Hz, 1H), 8.36 (d, *J* = 8.0 Hz, 1H), 8.24 (d, *J* = 8.1 Hz, 1H), 7.81 (d, *J* = 1.8 Hz, 1H), 7.65 – 7.51 (m, 3H), 7.42 – 7.27 (m, 7H), 6.75 (d, *J* = 7.1 Hz, 2H), 4.17 (d, *J* = 7.4 Hz, 1H), 3.27 (d, *J* = 5.3 Hz, 2H), 1.45 (s, 9H).

The intermediate product was then dissolved in 6M HCl (8 mL) and stirred at 60 °C for 12 hours. After heating, the solution was cooled down to room temperature and washed 3 times with diethyl ether to remove benzophenone. The aqueous phase was then concentrated and dried under reduced pressure to give the product as a pale white solid (Bpy-Ala•3 HCl) (2.81 g, 8.0 mmol, quant.).

Spectral data matched previously reported data.[44] **^{1}H NMR** (300 MHz, MeOD-d_4) δ 8.84 – 8.80 (m, 2H), 8.67 (dt, J = 8.2, 1.1 Hz, 1H), 8.55 (ddd, J = 8.2, 7.7, 1.6 Hz, 1H), 8.47 (dd, J = 8.3, 0.8 Hz, 1H), 8.21 (dd, J = 8.3, 2.2 Hz, 1H), 7.96 (ddd, J = 7.6, 5.6, 1.2 Hz, 1H), 4.40 (t, J = 6.8 Hz, 1H), 3.41 (qd, J = 14.6, 6.8 Hz, 2H).

4.7 Acknowledgments

JPP thanks the Natural Sciences and Engineering Council of Canada (NSERC) for funding this work. N.A. and N.A. thank NSERC for funding in the form of post-graduate scholarships. Illustrations were generated using Biorender. J.P.P. and N.A. conceptualized the study. N.A., N.A., and D.A.B. performed experiments. N.A. and J.P.P. wrote the manuscript. All authors edited the manuscript. We thank Dr. Peter G. Schultz for providing the plasmid encoding BpyAlaRS/tRNA (pEVOL-BpyAla). The $JFH1_T$ strain of the hepatitis C virus was a kind gift from the laboratory of Dr. Rodney Russel (Memorial University, Newfoundland, Canada).

4.8 References

(1) Jinek, M.; Chylinski, K.; Fonfara, I.; Hauer, M.; Doudna, J. A.; Charpentier, E. A Programmable Dual-RNA–Guided DNA Endonuclease in Adaptive Bacterial Immunity. *Science* **2012**, *337* (6096), 816–821. https://doi.org/10.1126/science.1225829.

(2) Paroo, Z.; Liu, Q.; Wang, X. Biochemical Mechanisms of the RNA-Induced Silencing Complex. *Cell Res* **2007**, *17* (3), 187–194. https://doi.org/10.1038/sj.cr.7310148.

(3) Song, M. S.; Rossi, J. J. Molecular Mechanisms of Dicer: Endonuclease and Enzymatic Activity. *Biochemical Journal* **2017**, *474* (10), 1603–1618. https://doi.org/10.1042/BCJ20160759.

(4) Kisiala, M.; Kowalska, M.; Pastor, M.; Korza, H. J.; Czapinska, H.; Bochtler, M. Restriction Endonucleases That Cleave RNA/DNA Heteroduplexes Bind DsDNA in A-like Conformation. *Nucleic Acids Res* **2020**, *48* (12), 6954–6969. https://doi.org/10.1093/nar/gkaa403.

(5) Bentley, D. L. Coupling mRNA Processing with Transcription in Time and Space. *Nat Rev Genet* **2014**, *15* (3), 163–175. https://doi.org/10.1038/nrg3662.

(6) Bondeson, D. P.; Mares, A.; Smith, I. E.; Ko, E.; Campos, S.; Miah, A. H.; Mulholland, K. E.; Routly, N.; Buckley, D. L.; Gustafson, J. L.; Zinn, N.; Grandi, P.; Shimamura, S.; Bergamini, G.; Faelth-Savitski, M.; Bantscheff, M.; Cox, C.; Gordon, D. A.; Willard, R. R.; Flanagan, J. J.; Casillas, L. N.; Votta, B. J.; den Besten, W.; Famm, K.; Kruidenier, L.; Carter, P. S.; Harling, J. D.; Churcher, I.; Crews, C. M. Catalytic in Vivo Protein Knockdown by Small-Molecule PROTACs. *Nat Chem Biol* **2015**, *11* (8), 611–617. https://doi.org/10.1038/nchembio.1858.

(7) Doudna, J. A.; Charpentier, E. The New Frontier of Genome Engineering with CRISPR-Cas9. *Science* **2014**, *346* (6213), 1258096–1258096. https://doi.org/10.1126/science.1258096.

(8) Nelles, D. A.; Fang, M. Y.; O'Connell, M. R.; Xu, J. L.; Markmiller, S. J.; Doudna, J. A.; Yeo, G. W. Programmable RNA Tracking in Live Cells with CRISPR/Cas9. *Cell* **2016**, *165* (2), 488–496. https://doi.org/10.1016/j.cell.2016.02.054.

(9) Li, Y.; Kowdley, K. v. MicroRNAs in Common Human Diseases. *Genomics Proteomics Bioinformatics* **2012**, *10* (5), 246–253. https://doi.org/10.1016/j.gpb.2012.07.005.

(10) Peng, Y.; Croce, C. M. The Role of MicroRNAs in Human Cancer. *Signal Transduct Target Ther* **2016**, *1* (1), 15004. https://doi.org/10.1038/sigtrans.2015.4.

(11) Wahid, F.; Shehzad, A.; Khan, T.; Young, Y. Biochimica et Biophysica Acta MicroRNAs : Synthesis , Mechanism , Function , and Recent Clinical Trials. *BBA - Molecular Cell Research* **2010**, *1803* (11), 1231–1243. https://doi.org/10.1016/j.bbamcr.2010.06.013.

(12) Roberts, A. P. E.; Lewis, A. P.; Jopling, C. L. The Role of MicroRNAs in Viral Infection. In *Cellular RNA Interference Mechanisms*; Elsevier Inc., 2011; Vol. 102, pp 101–139. https://doi.org/10.1016/B978-0-12-415795-8.00002-7.

(13) Mendell, J. T.; Olson, E. N. Review MicroRNAs in Stress Signaling and Human Disease. *Cell* **2012**, *148* (6), 1172–1187. https://doi.org/10.1016/j.cell.2012.02.005.

(14) Wahid, F.; Shehzad, A.; Khan, T.; Kim, Y. Y. MicroRNAs: Synthesis, Mechanism, Function, and Recent Clinical Trials. *Biochim Biophys Acta Mol Cell Res* **2010**, *1803* (11), 1231–1243. https://doi.org/10.1016/j.bbamcr.2010.06.013.

(15) Peng, Y.; Croce, C. M. The Role of MicroRNAs in Human Cancer. *Signal Transduct Target Ther* **2016**, *1* (1), 15004. https://doi.org/10.1038/sigtrans.2015.4.
(16) Calin, G. a; Croce, C. M. MicroRNA Signatures in Human Cancers. *Nat Rev Cancer* **2006**, *6* (11), 857–866. https://doi.org/10.1038/nrc1997.
(17) Kuno, G.; Chang, G. J.; Tsuchiya, K. R.; Karabatsos, N.; Cropp, C. B. Phylogeny of the Genus Flavivirus. *J Virol* **1998**, *72* (1), 73–83. https://doi.org/10.1006/mpev.2000.0874.
(18) Vargason, J. M.; Szittya, G.; Burgyán, J.; Hall, T. M. T. Size Selective Recognition of SiRNA by an RNA Silencing Suppressor. *Cell* **2003**, *115* (7), 799–811. https://doi.org/10.1016/S0092-8674(03)00984-X.
(19) Silhavy, D.; Molnár, A.; Lucioli, A.; Szittya, G.; Hornyik, C.; Tavazza, M.; Burgyán, J. A Viral Protein Suppresses RNA Silencing and Binds Silencing-Generated, 21- to 25-Nucleotide Double-Stranded RNAs. *EMBO Journal* **2002**, *21* (12), 3070–3080. https://doi.org/10.1093/emboj/cdf312.
(20) Calabrese, J. M.; Sharp, P. A. Characterization of the Short RNAs Bound by the p19 Suppressor of RNA Silencing in Mouse Embryonic Stem Cells. *Rna* **2006**, *12* (12), 2092–2102. https://doi.org/10.1261/rna.224606.
(21) Kontra, L.; Csorba, T.; Tavazza, M.; Lucioli, A.; Tavazza, R.; Moxon, S.; Tisza, V.; Medzihradszky, A.; Turina, M.; Burgyán, J. Distinct Effects of p19 RNA Silencing Suppressor on Small RNA Mediated Pathways in Plants. *PLoS Pathog* **2016**, *12* (10), 1–26. https://doi.org/10.1371/journal.ppat.1005935.
(22) Stewart, J. D.; Benkovic, S. J. Catalytic Antibodies: Mechanistic and Practical Considerations. *Chem Soc Rev* **1993**, *22* (4), 213–219.
(23) Palermo, G.; Cavalli, A.; Klein, M. L.; Alfonso-Prieto, M.; Dal Peraro, M.; de Vivo, M. Catalytic Metal Ions and Enzymatic Processing of DNA and RNA. *Acc Chem Res* **2015**, *48* (2), 220–228. https://doi.org/10.1021/ar500314j.
(24) Miyashita, H.; Karaki, Y.; Kikuchi, M.; Fujii, I. Prodrug Activation via Catalytic Antibodies. *Proceedings of the National Academy of Sciences* **1993**, *90* (11), 5337–5340. https://doi.org/10.1073/pnas.90.11.5337.
(25) Hu, L.; Arifuzzaman, M. D.; Zhao, Y. Controlling Product Inhibition through Substrate-Specific Active Sites in Nanoparticle-Based Phosphodiesterase and Esterase. *ACS Catal* **2019**, *9* (6), 5019–5024. https://doi.org/10.1021/acscatal.9b00630.
(26) Robinson, P. K. Enzymes: Principles and Biotechnological Applications. *Essays Biochem* **2015**, *59*, 1–41. https://doi.org/10.1042/BSE0590001.
(27) Vargason, J. M.; Szittya, G.; Burgyán, J.; Tanaka Hall, T. M. Size Selective Recognition of SiRNA by an RNA Silencing Suppressor. *Cell* **2003**, *115* (7), 799–811. https://doi.org/10.1016/S0092-8674(03)00984-X.
(28) Danielson, D. C.; Pezacki, J. P. Studying the RNA Silencing Pathway with the p19 Protein. *FEBS Lett* **2013**, *587* (8), 1198–1205. https://doi.org/10.1016/j.febslet.2013.01.036.
(29) Cheng, J.; Danielson, D. C.; Nasheri, N.; Singaravelu, R.; Pezacki, J. P. Enhanced Specificity of the Viral Suppressor of RNA Silencing Protein p19 toward Sequestering of Human MicroRNA-122. *Biochemistry* **2011**, *50* (36), 7745–7755. https://doi.org/10.1021/bi2008273.
(30) Ream, J. A.; Lewis, L. K.; Lewis, K. A. Rapid Agarose Gel Electrophoretic Mobility Shift Assay for Quantitating Protein: RNA Interactions. *Anal Biochem* **2016**, *511*, 36–41. https://doi.org/10.1016/j.ab.2016.07.027.

(31) Campuzano, S.; Torrente-Rodriguez, R. M.; Lopez-Hernandez, E.; Conzuelo, F.; Granados, R.; Sanchez-Puelles, J. M.; Pingarron, J. M. Magnetobiosensors Based on Viral Protein p19 for Microrna Determination in Cancer Cells and Tissues. *Angewandte Chemie - International Edition* **2014**, *53* (24), 6168–6171. https://doi.org/10.1002/anie.201403270.
(32) Khan, N.; Cheng, J.; Pezacki, J. P.; Berezovski, M. v. Quantitative Analysis of MicroRNA in Blood Serum with Protein-Facilitated Affinity Capillary Electrophoresis. *Anal Chem* **2011**, *83* (16), 6196–6201. https://doi.org/10.1021/ac2016213.
(33) Foss, D. V; Schirle, N. T.; MacRae, I. J.; Pezacki, J. P. Structural Insights into Interactions between Viral Suppressor of RNA Silencing Protein p19 Mutants and Small RNAs. *FEBS Open Bio* **2019**, *9* (6), 1042–1051. https://doi.org/10.1002/2211-5463.12644.
(34) Danielson, D. C.; Sachrajda, N.; Wang, W.; Filip, R.; Pezacki, J. P. A Novel p19 Fusion Protein as a Delivery Agent for Short-Interfering RNAs. *Mol Ther Nucleic Acids* **2016**, *5* (October 2015), e303. https://doi.org/10.1038/mtna.2016.14.
(35) Rawlings, R. A.; Krishnan, V.; Walter, N. G. Viral RNAi Suppressor Reversibly Binds SiRNA to Outcompete Dicer and RISC via Multiple Turnover. *J Mol Biol* **2011**, *408* (2), 262–276. https://doi.org/10.1016/j.jmb.2011.02.038.
(36) Fagegaltier, D.; Bougé, A. L.; Berry, B.; Poisot, É.; Sismeiro, O.; Coppée, J. Y.; Théodore, L.; Voinnet, O.; Antoniewski, C. The Endogenous SiRNA Pathway Is Involved in Heterochromatin Formation in Drosophila. *Proc Natl Acad Sci U S A* **2009**, *106* (50), 21258–21263. https://doi.org/10.1073/pnas.0809208105.
(37) Lecellier, C.-H.; Dunoyer, P.; Arar, K.; Lehmann-Che, J.; Eyquem, S.; Himber, C.; Saïb, A.; Voinnet, O. A Cellular MicroRNA Mediates Antiviral Defense in Human Cells. *Science* **2005**, *308* (5721), 557–560. https://doi.org/10.1126/science.1108784.
(38) Nasheri, N.; Cheng, J.; Singaravelu, R.; Wu, P.; McDermott, M. T.; Pezacki, J. P. An Enzyme-Linked Assay for the Rapid Quantification of MicroRNAs Based on the Viral Suppressor of RNA Silencing Protein p19. *Anal Biochem* **2011**, *412* (2), 165–172. https://doi.org/10.1016/j.ab.2011.01.030.
(39) Ahmed, N.; Foss, D. V.; Powdrill, M. H.; Pezacki, J. P. Site-Specific Crosslinking of a p19 Viral Suppressor of RNA Silencing Protein and Its RNA Targets Using an Expanded Genetic Code. *Biochemistry* **2019**, *58* (33), 3520–3526. https://doi.org/10.1021/acs.biochem.9b00428.
(40) Lang, K.; Chin, J. W. Cellular Incorporation of Unnatural Amino Acids and Bioorthogonal Labeling of Proteins. *Chem Rev* **2014**, *114* (9), 4764–4806. https://doi.org/10.1021/cr400355w.
(41) Liu, C. C.; Schultz, P. G. Adding New Chemistries to the Genetic Code. *Annu Rev Biochem* **2010**, *79* (1), 413–444. https://doi.org/10.1146/annurev.biochem.052308.105824.
(42) Wang, Q.; Parrish, A. R.; Wang, L. Review Expanding the Genetic Code for Biological Studies. *Chem Biol* **2009**, *16* (3), 323–336. https://doi.org/10.1016/j.chembiol.2009.03.001.
(43) Schultz, P. G.; Dervan, P. B. Sequence-Specific Double-Strand Cleavage of DNA by Penta-N-Methylpyrrolecarboxamide-EDTA X Fe(II). *Proceedings of the National Academy of Sciences* **1983**, *80* (22), 6834–6837. https://doi.org/10.1073/pnas.80.22.6834.
(44) Hyun, S. L.; Schultz, P. G. Biosynthesis of a Site-Specific DNA Cleaving Protein. *J Am Chem Soc* **2008**, *130* (40), 13194–13195. https://doi.org/10.1021/ja804653f.

(45) Drienovská, I.; Rioz-Martínez, A.; Draksharapu, A.; Roelfes, G. Novel Artificial Metalloenzymes by in Vivo Incorporation of Metal-Binding Unnatural Amino Acids. *Chem Sci* **2015**, *6* (1), 770–776. https://doi.org/10.1039/c4sc01525h.
(46) Lee, H. S.; Spraggon, G.; Schultz, P. G.; Wang, F. Genetic Incorporation of a Metal-Ion Chelating Amino Acid into Proteins as a Biophysical Probe. *J Am Chem Soc* **2009**, *131* (7), 2481–2483. https://doi.org/10.1021/ja808340b.
(47) He, Y.-C.; Yin, B.-C.; Jiang, L.; Ye, B.-C. The Rapid Detection of MicroRNA Based on p19-Enhanced Fluorescence Polarization. *Chemical Communications* **2014**, *50* (47), 6236–6239. https://doi.org/10.1039/c4cc00705k.
(48) Cheng, J.; Sagan, S. M.; Jakubek, Z. J.; Pezacki, J. P. Studies of the Interaction of the Viral Suppressor of RNA Silencing Protein p19 with Small RNAs Using Fluorescence Polarization. *Biochemistry* **2008**, *47* (31), 8130–8138. https://doi.org/10.1021/bi800401y.
(49) Luna, J. M.; Barajas, J. M.; Teng, K.; Rice, C. M.; Darnell, R. B.; Ghoshal, K.; Luna, J. M.; Barajas, J. M.; Teng, K.; Sun, H.; Moore, M. J.; Rice, C. M. Argonaute CLIP Defines a Deregulated MiR-122- Bound Transcriptome That Correlates with Patient Survival in Human Liver Cancer Article Argonaute CLIP Defines a Deregulated MiR-122-Bound Transcriptome That Correlates with Patient Survival in Human Liver Can. **2017**, 400–410. https://doi.org/10.1016/j.molcel.2017.06.025.
(50) Luna, J. M.; Scheel, T. K. H.; Danino, T.; Shaw, K. S.; Mele, A.; Fak, J. J.; Nishiuchi, E.; Takacs, C. N.; Catanese, M. T.; De Jong, Y. P.; Jacobson, I. M.; Rice, C. M.; Darnell, R. B. Hepatitis C Virus RNA Functionally Sequesters MiR-122. *Cell* **2015**, *160* (6), 1099–1110. https://doi.org/10.1016/j.cell.2015.02.025.
(51) Schult, P.; Roth, H.; Adams, R. L.; Mas, C.; Imbert, L.; Orlik, C.; Ruggieri, A.; Pyle, A. M.; Lohmann, V. MicroRNA-122 Amplifies Hepatitis C Virus Translation by Shaping the Structure of the Internal Ribosomal Entry Site. *Nat Commun* **2018**, *9* (1). https://doi.org/10.1038/s41467-018-05053-3.
(52) Lohmann, V.; Körner, F.; Koch, J. O.; Herian, U.; Theilmann, L.; Bartenschlager, R. Replication of Subgenomic Hepatitis C Virus RNAs in a Hepatoma Cell Line. *Science* **1999**, *285* (5424), 110–113. https://doi.org/10.1126/science.285.5424.110.
(53) Ono, C.; Fukuhara, T.; Motooka, D.; Nakamura, S.; Okuzaki, D.; Yamamoto, S.; Tamura, T.; Mori, H.; Sato, A.; Uemura, K.; Fauzyah, Y.; Kurihara, T.; Suda, T.; Nishio, A.; Hmwe, S. S.; Okamoto, T.; Tatsumi, T.; Takehara, T.; Chayama, K.; Wakita, T.; Koike, K.; Matsuura, Y. Characterization of MiR-122-Independent Propagation of HCV. *PLoS Pathog* **2017**, *13* (5), e1006374. https://doi.org/10.1371/journal.ppat.1006374.
(54) Shotwell, C. R.; Cleary, J. D.; Berglund, J. A. The Potential of Engineered Eukaryotic RNA-Binding Proteins as Molecular Tools and Therapeutics. *Wiley Interdiscip Rev RNA* **2020**, *11* (1), 1–21. https://doi.org/10.1002/wrna.1573.
(55) Choudhury, R.; Tsai, Y. S.; Dominguez, D.; Wang, Y.; Wang, Z. Engineering RNA Endonucleases with Customized Sequence Specificities. *Nat Commun* **2012**, *3* (1), 1147. https://doi.org/10.1038/ncomms2154.
(56) Jung, E.; Lee, N. K.; Kang, S. K.; Choi, S. H.; Kim, D.; Park, K.; Choi, K.; Choi, Y. J.; Jung, D. H. Identification of Tissue-Specific Targeting Peptide. *J Comput Aided Mol Des* **2012**, *26* (11), 1267–1275. https://doi.org/10.1007/s10822-012-9614-6.
(57) Zahid, M.; Robbins, P. D. Cell-Type Specific Penetrating Peptides: Therapeutic Promises and Challenges. *Molecules* **2015**, *20* (7), 13055–13070. https://doi.org/10.3390/molecules200713055.

(58) Svensen, N.; Walton, J. G. A.; Bradley, M. Peptides for Cell-Selective Drug Delivery. *Trends Pharmacol Sci* **2012**, *33* (4), 186–192. https://doi.org/10.1016/j.tips.2012.02.002.
(59) van der Ree, M. H.; van der Meer, A. J.; van Nuenen, A. C.; de Bruijne, J.; Ottosen, S.; Janssen, H. L.; Kootstra, N. A.; Reesink, H. W. Miravirsen Dosing in Chronic Hepatitis C Patients Results in Decreased MicroRNA-122 Levels without Affecting Other MicroRNAs in Plasma. *Aliment Pharmacol Ther* **2016**, *43* (1), 102–113. https://doi.org/10.1111/apt.13432.
(60) van der Ree, M. H.; de Vree, J. M.; Stelma, F.; Willemse, S.; van der Valk, M.; Rietdijk, S.; Molenkamp, R.; Schinkel, J.; van Nuenen, A. C.; Beuers, U.; Hadi, S.; Harbers, M.; van der Veer, E.; Liu, K.; Grundy, J.; Patick, A. K.; Pavlicek, A.; Blem, J.; Huang, M.; Grint, P.; Neben, S.; Gibson, N. W.; Kootstra, N. A.; Reesink, H. W. Safety, Tolerability, and Antiviral Effect of RG-101 in Patients with Chronic Hepatitis C: A Phase 1B, Double-Blind, Randomised Controlled Trial. *The Lancet* **2017**, *389* (10070), 709–717. https://doi.org/10.1016/S0140-6736(16)31715-9.
(61) Sullivan, C. S.; Grundhoff, A. T.; Tevethia, S.; Pipas, J. M.; Ganem, D. SV40-Encoded MicroRNAs Regulate Viral Gene Expression and Reduce Susceptibility to Cytotoxic T Cells. *Nature* **2005**, *435* (7042), 682–686. https://doi.org/10.1038/nature03576.
(62) Gupta, A.; Gartner, J. J.; Sethupathy, P.; Hatzigeorgiou, A. G.; Fraser, N. W. Anti-Apoptotic Function of a MicroRNA Encoded by the HSV-1 Latency-Associated Transcript. *Nature* **2006**, *442* (7098), 82–85. https://doi.org/10.1038/nature04836.
(63) Bruscella, P.; Bottini, S.; Baudesson, C.; Pawlotsky, J.-M.; Feray, C.; Trabucchi, M. Viruses and MiRNAs: More Friends than Foes. *Front Microbiol* **2017**, *8* (MAY), 1–11. https://doi.org/10.3389/fmicb.2017.00824.
(64) Jopling, C. L.; Yi, M. K.; Lancaster, A. M.; Lemon, S. M.; Sarnow, P. Molecular Biology: Modulation of Hepatitis C Virus RNA Abundance by a Liver-Specific MicroRNA. *Science* **2005**, *309* (5740), 1577–1581. https://doi.org/10.1126/science.1113329.
(65) Lopez-Tejedor, D.; Claveria-Gimeno, R.; Velazquez-Campoy, A.; Abian, O.; Palomo, J. M. In Vitro Antiviral Activity of Tyrosinase from Mushroom Agaricus Bisporus against Hepatitis C Virus. *Pharmaceuticals* **2021**, *14* (8). https://doi.org/10.3390/ph14080759.
(66) Li, J.; Zhao, J.; Xu, S.; Zhang, S.; Zhang, J.; Xiao, J.; Gao, R.; Tian, M.; Zeng, Y.; Lee, K.; Tarakanova, V.; Lan, K.; Feng, H.; Feng, P. Antiviral Activity of a Purine Synthesis Enzyme Reveals a Key Role of Deamidation in Regulating Protein Nuclear Import. *Sci Adv* **2019**, *5* (10).
(67) Cheng, J.; Danielson, D. C.; Nasheri, N.; Singaravelu, R.; Pezacki, J. P. Enhanced Specificity of the Viral Suppressor of RNA Silencing Protein p19 toward Sequestering of Human MicroRNA-122. *Biochemistry* **2011**, *50* (36), 7745–7755. https://doi.org/10.1021/bi2008273.
(68) Ballardini, R.; Balzani, V.; Clemente-León, M.; Credi, A.; Teresa Gandolfi, M.; Ishow, E.; Perkins, J.; Fraser Stoddart, J.; Tseng, H. R.; Wenger, S. Photoinduced Electron Transfer in a Triad That Can Be Assembled/Disassembled by Two Different External Inputs. Toward Molecular-Level Electrical Extension Cables. *J Am Chem Soc* **2002**, *124* (43), 12786–12795. https://doi.org/10.1021/ja025813x.
(69) Ahmed, N.; De Graaf, J. F.; Ahmed, N.; Foss, D. V.; Delcorde, J.; Schultz, P. G.; Pezacki, J. P. Visualization of the Delivery and Release of Small RNAs Using Genetic Code Expansion and Unnatural RNA-Binding Proteins. *Bioconjug Chem* **2018**, *29* (12). https://doi.org/10.1021/acs.bioconjchem.8b00649.

Chapter 5

General Discussion and Future Directions

5.1 Engineering p19-based Probes for the Detection of Small RNAs

In Chapter 2 we focused on the utilization of genetic code expansion to help engineer p19-based probes for the detection of siRNA binding. This was done by utilizing the UAA, AzF. We aimed to design a FRET-based probe by incorporating AzF, site-specifically, in the p19 dimer, in a position that is within FRET distance (1-100 Å) from the labeled 3'end of a siRNA substrate. By introducing the UAA, we were able to label p19 with a fluorophore using copper-free strain promoted alkyne-azide cycloaddition (SPAAC). This work has allowed for the detection of labeled siRNA *in vitro* using a FRET-based assay. To further apply this system in cells, we developed and incorporated the probe in a previously designed p19 system that is fused to a cell-penetrating peptide (CPP), HIV's transactivator of transcription peptide (TAT), By doing so, we were able to deliver the target siRNA into cells successfully. The FRET probe was successful at aiding in the visualization of the delivery and release of the RNA into cells. This was done by monitoring the fluorescence "turn-on" over 24 hours. By delivering and releasing a quencher-tagged siRNA into cells, we were able to successfully visualize the fluorescently tagged protein as the siRNA is being released over time. Future work for this study should include activity analysis of the designed probe in a range of different cell types, including primary cells.

Future work should include the design of FRET-based probes for the detection of unlabeled RNAs. We were successfully able to detect fluorescently tagged RNAs, however, the design of the presented probe would not be successful in detecting unlabeled RNA in cells, to address this, we can utilize the structural information available for p19. p19 binds RNA as a dimer, thus

designing a FRET-based probe would be possible by identifying residues on either monomer that would change position upon binding of RNA ligands. Labeling one of the identified positions with a FRET acceptor fluorophore, while the other with a donor fluorophore would allow for the detection of the binding event. This can be successful by linking the monomers using a flexible linker to form a stable, linked dimer as previously described. This strategy, however, presents some challenges. We do not have structural information about p19 in the apo state. The available structural information presents p19 in the holo state with an RNA ligand bound.

To successfully label a position with a FRET donor, and another with a FRET acceptor, one will need to utilize different bioorthogonal chemistry for each position. Thus, we cannot depend on the utilization of just AzF for the labeling process, we will need to utilize another UAA that gets incorporated using a different codon, other than an Amber codon. For instance, an evolved pyrrolysyl–tRNA synthetase (PylRS)/tRNA pair from a Methanosarcina species can be utilized to incorporate a tetrazine containing amino acid in response to a quadruplet codon for one of the chosen sites, while the other site can incorporate AzF in response to the amber mutation[1]. By doing so, we ensure that each position would be labeled with a donor FRET fluorophore or an acceptor FRET fluorophore exclusively, thus aiding in the success of the methodology adopted.

This methodology will offer novel applications in the detection of RNA *in vitro* and can be useful as a biotechnological tool for the detection of small RNAs involved in diseased states. An increased repertoire of tools to detect and modulate the activity of miRNAs is of interest and provides a new mechanism for utilizing RNA-binding proteins. We are currently working on such described strategy, and we will report on it in due course. The described strategy can be applied to other proteins and allows for an opportunity for optimized orthogonal translation to enable spontaneous protein double-labeling and FRET.

5.2 p19 as a Tool for RNA Delivery Using Unnatural Amino Acids

In Chapter 2, we describe the usage of UAAs to help visualize the delivery and release of small RNA cargo into mammalian cells upon delivery using p19. p19 was used as a delivery agent for siRNA by using the p19 dimer to a cell-penetrating peptide to generate a FRET-based probe that can detect the release of RNA into cells upon delivery across the membrane and endosomal release. Using p19-2x-III-W19AzF–TAT, we were able to observe the release of RNA over 24 hours post-treatment. The release was observed as early as 2 hours post-treatment with the protein. pH could potentially play a role in the release of the RNA from the p19 complex. Delivery via TAT peptide occurs through the endosomal route, and thus release from the endosome occurs via acidification. Thus, the acidification of the p19:RNA complex could potentially affect its release. Additionally, p19 is marked with a reversible RNA binding, thus in the presence of other cellular miRNAs in the cytoplasm, release and displacement can be achieved[2]. Delivery via TAT cationic peptides is known to be very rapid, with total cellular uptake as fast as 1 hour[3]. Endosomal trapping of p19 proteins upon delivery of RNA can potentially occur, thus this issue should be addressed to ensure efficient delivery of RNA. In our paper, we showed that delivery and release were achieved, and functional RNA was successfully delivered. However, to ensure optimal activity, we can fuse p19 to endosomolytic peptides to enhance the endosomal escape, and thus functional RNA can be released into the cytoplasm almost instantaneously. This can be achieved through conventional molecular fusions to either the C or N terminus of the p19 dimer or can be done through the usage of UAA. As mentioned in chapter 2, AzF allows for covalent conjugation through SPAAC, thus an engineered endosomolytic peptide with a strained alkyne can be synthesized to tag the p19 dimer, and thus allows for efficient endosomal escape upon delivery.

AzF allows for the conjugation of any molecule with a strained alkyne, thus future work could build on this technology to generate clickable cell-type specific cell-penetrating peptides. This will allow the direct conjugation of p19-III-W19AzF to an array of different peptides for cell-specific cargo delivery instead of utilizing general cell entry peptides. This can help explore the potential of utilizing p19 to address tissue-specific delivery of siRNA.

p19's high affinity to small RNAs remains advantageous[4]. Its unique structure, high affinity towards siRNA, and the stability of the complex are of benefit when designing proteins with the potential to use as *in vivo* RNA delivery agents. p19's high affinity and capping of RNA would limit RNA dissociation pre-cellular delivery and would protect the bound RNA from potential degradation via nucleases. Further studies need to be conducted to determine the extent of its high affinity on its ability to release RNA cargo in cells. From our study, we were able to visualize the release of RNA into cells, as well as confirm that the RNA is functional upon delivery, which aligns with what has been previously reported. Previous reports have confirmed that p19's affinity did not negatively impact the release of siRNA cargo *in situ*[4]. Further studies need to be conducted to compare this specific method of RNA delivery to already available methods such as cationic lipids and other RNA binding proteins -based siRNA delivery agents, to ensure that the exhibited high affinity of p19 does not pose a disadvantage[4]. Our engineered p19 protein has been shown to exhibit low toxicity in comparison to lipid-based systems which is an intrinsic advantage to protein-based delivery of RNA[5]. To apply such system *in vivo* for siRNA delivery, it will be critical to assess the immunogenicity of p19 fusion proteins. Ensuring that the administration of the p19:siRNA complex does not lead to an increased production of inflammatory cytokines and interferons is instrumental to ensuring the success of such system. The immunogenicity profile of p19 proteins will need to be assessed should the system be applied for *in vivo* delivery.

We have shown here that the incorporation of UAAs to serve as bioorthogonal handles allowed for protein labeling and conjugation, which provided a novel opportunity for tracking p19's RNA delivery and release inside a cellular model. This as well can act as a future opportunity to track p19's localization inside the cell and help uncover some insights into its potential use as a delivery agent. UAAs incorporation provides an opportunity to engineer p19 to have site-selectivity by easily conjugating different types of cell-penetrating peptides through bioorthogonal chemistry[6,7].

5.3 Engineering of p19-based Photo-switches using UAA

In chapter 3, we focused on identifying sites in the p19 RNA binding pocket that are in close contact with the phosphate backbone of the bound RNA ligand. We used the crystal structure of p19 bound to its canonical siRNA substrate to approximate residues in close contact with the RNA's backbone residues T111, K67, and R115. These residues are situated along the β-sheet binding surface and are shown to interact directly with the RNA based on the crystal structure information available[8]. This study highlighted the potential of utilizing UAAs bearing photo-crosslinking groups to help identify protein-RNA interactions. Protein-RNA interactions have been critical for the discovery and understanding of the non-coding RNA functions. Previous studies have taken advantage of utilizing cross-linkable groups to study the interactions between proteins and their bound RNA targets, however, these methods lack specificity and control over the crosslinking location, and thus can exhibit high background noise. Site-specific crosslinking allows for precise mapping of the exact RNA binding site of interest and allows for identifying the precise targets of the protein. In chapter 3, we successfully show the utilization of UAAs as a tool to site-specifically crosslink p19's targets *in vitro.* This approach can be used for high sensitivity detection of bound p19 substrates while also providing irreversible sequestrations of small RNAs in cells.

This method provides the ability to design a molecular switch for spatial-temporal sequestration of endogenous miRNAs. Future studies should focus on applying this system in mammalian cells, in which UV-irradiation would allow for control of covalent miRNA sequestration *in situ*. Modulation of miRNA activity in living systems is of interest, due to their linked function to disease progression and infectious states[9–11].

Specifically, this method could be applied in mammalian cells to identify canonical miRNA ligands of p19 in different tissue types. UV-crosslinking provides a mechanism to identify transient targets of p19 and would help identify p19's differential binding activity. This can help uncover the understanding of p19's differential binding to the mammalian miRNA repertoire. CLIP assays will help underscore whether differences in the small RNA population of different cell types are impacting p19's endogenous activity.

It is possible to utilize a different UAA to design a photo-switch to control the activity of p19 and provide spatial-temporal control in cells. Future studies will focus on utilizing UAAs bearing photo-caged groups for optical control of p19's activity in cells similar to what has been previously done with Cas9 proteins[12]. Such a design will add another level of control to p19's binding potential to small RNAs. To successfully do that, we will need to identify, through mutational scanning, residues that are sensitive to the introduction of the photocaged groups. Thus, upon incorporation, binding potential should be perturbed, while optical uncaging should help regain p19's binding and RNA suppression ability. It would therefore be essential to identify which residues in the p19's binding pocket are sensitive to this incorporation of a bulkier photocaged group for the design to be successful. Some examples of photocaged unnatural amino acids are photocaged lysine, tyrosine, and cysteine residues among others[13–15]. Expanding the scope of recombinant p19, using UAAs, provides an opportunity to engineer proteins with new functionalities and highlights the novel applications of p19 as a tool in biotechnology.

5.4 Enhancing p19's Activity in Mammalian Cells

Our laboratory has previously presented an approach to enhance the activity of p19 in mammalian cells using a chemical biology approach to further inhibit the RNA silencing pathway. This was performed by applying p19 in conjugation with a small molecule, suramin to potently inhibit the RNA silencing pathway in human hepatoma cell lines[16].

In chapters 3 and 4, we have shown the potential of utilizing p19 as a tool to suppress the RNA silencing pathway in mammalian cells, however, it was shown that modest inhibition of the RNA silencing pathway is achieved upon applying p19 in mammalian cells in comparison to its activity in plant cells[16,17]. Thus, to optimally utilize the potential of p19, we need to characterize factors that influence its activity and level of expression in different types of cells that may help identify differences and provide insights into p19's activity in plant and mammalian cell lines. Future work should focus on identifying endogenous factors that influence p19's activity in human cell lines. Identifying protein-interacting partners in mammalian cells can help shed light on ways to enhance the endogenous activity of p19. Site-specific incorporation of UAA-bearing photo-crosslinkable groups into p19 followed by immunoprecipitation can help identify transient protein interacting partners that potentially influence p19's activity[18]. Protein interactions will be examined through site-specific incorporation of AzF, which upon UV irradiation, will allow the formation of covalent adducts with interacting protein partners that may either enhance or inhibit its activity *in vivo*[18,19]. Immunoprecipitation studies should be performed, where p19 will be expressed in a range of human cell lines, and subsequent mass spectrometry and western blotting techniques will be utilized to identify the cell-type specific interactions, followed by studies to link these proteins to p19's activity. These experiments will allow the identification of potential proteins that can be co-expressed along with p19 to enhance its activity *in vivo*. Additionally, loss

and gain-of-function studies will be conducted where CRISPRi (inhibition) or CRISPRa (activation) experiments will be utilized to create cell lines that either lack or overexpress the identified proteins that may play a part in modulating p19's activity[20]. These experiments will help validate and delineate the interacting partners' role in either enhancing or inhibiting p19's activity.

5.5 Introduction of Catalytic Functionality into p19

Chapter 4 focused on the introduction of catalytic functionality to p19. This was done by incorporation of a metal ion chelating UAA, BpyAla. Site-specific incorporation of BpyAla has been utilized previously to engineer a site-specific DNA cleaving protein[21]. This method may be useful in mapping molecular details of protein-nucleic acid interactions. In chapter 3, we chose 2 different sites in p19 to achieve cleavage of the bound RNA. Since the introduction of BpyAla only requires simple mutagenesis as previously described, it should be possible to rapidly generate and test a series of BpyAla mutants to define optimal sites for incorporation, even in the absence of protein structural information. The presented approach in chapter 4 highlights the possibility of BpyAla utilization to map protein-RNA interactions or even protein-protein interfaces. It has been previously shown that Cu^{2+}- phenanthroline results in selective protein backbone cleavage[22]. Thus, the incorporation of BpyAla provides a new avenue for the introduction of catalytic activity in proteins.

Future work will focus on characterizing p19-T111BpyAla biochemically, in which the catalytic efficiency of the enzyme will be determined. This will be performed using a real-time fluorescence "turn on" assay, where a fluorophore-tagged RNA signal is quenched via a black hole quencher on the 3'end of the RNA, and when cleavage and release of the RNA occur via p19-T111Bpyla, a turn on/ increase in the fluorophore signal will be achieved. Steady-state kinetic parameters under multiple turn-over conditions (excess substrate) will be determined for the artificial enzyme and compared to other RNA cleaving enzymes, such as Dicer. These experiments will provide information on the potential future applications for the engineered enzyme.

Additionally, future work will focus on characterizing the catalytic efficiency of the engineered enzyme toward other miRNAs. The Nanostring profiling experiments have provided information

about p19-T111BpyAla preferential cleavage of miRNAs when a complex pool of miRNA is presented. Even though miR-122 is highly expressed in the liver, and represents around 70% of the miRNA population, it was not the most highly downregulated. Thus, the structure of miRNA should be further examined to elucidate the potential preferential activity of p19. miRNAs are known to contain nucleotide mismatches, that result in "bulges" in their secondary structures. The presented "bulges" can affect the binding affinity of p19 towards a specific RNA[23]. Further mutagenesis studies can be conducted, including directed evolution approaches, to further enhance the binding affinity of p19 towards a specific miRNA of interest.

5.6 General Conclusions

Overall, the work presented here describes the utilization of genetic code expansion technology to further enhance the activity of recombinant p19 proteins in the detection and sequestering of small RNAs. p19's binding properties have allowed it to be utilized extensively in biotechnology as a tool for miRNA detection, delivery, and enhancement of protein expression. The work presented here provides an avenue for the utilization of a plethora of already existing UAA to further enhance the activity of p19 in cells and living systems. UAAs provide an easy method to introduce new functionality to proteins with very minimal perturbations to their existing structures and functions. p19 is very accommodating to modifications that makes it an easy tool for future modifications. In this thesis, we utilized an azide-modified UAA that allowed site-specific labeling of p19 for the detection of modified RNA. AzF has also allowed for the development of a photo-switch that site specifically allows covalent sequestration of both siRNA and miRNA targets of p19. Finally, the incorporation of BpyAla has allowed for the site-specific cleavage of p19's targets allowing for the potential of enhanced suppression activity for p19. This work contributes to the larger field of RNA binding protein engineering. These technologies can be applied to other RBPs and allow for a large range of biotechnological applications.

5.7 References

(1) Wang, K.; Sachdeva, A.; Cox, D. J.; Wilf, N. W.; Lang, K.; Wallace, S.; Mehl, R. A.; Chin, J. W. Optimized Orthogonal Translation of Unnatural Amino Acids Enables Spontaneous Protein Double-Labelling and FRET. *Nat. Chem.* **2014**, *6* (5), 393–403. https://doi.org/10.1038/nchem.1919.

(2) Xia, Z.; Zhu, Z.; Zhu, J.; Zhou, R. Recognition Mechanism of SiRNA by Viral p19 Suppressor of RNA Silencing: A Molecular Dynamics Study. *Biophys. J.* **2009**, *96* (5), 1761–1769. https://doi.org/10.1016/j.bpj.2008.11.047.

(3) Hällbrink, M.; Florén, A.; Elmquist, A.; Pooga, M.; Bartfai, T.; Langel, Ü. Cargo Delivery Kinetics of Cell-Penetrating Peptides. *Biochim. Biophys. Acta - Biomembr.* **2001**, *1515* (2), 101–109. https://doi.org/10.1016/S0005-2736(01)00398-4.

(4) Yang, N. J.; Kauke, M. J.; Sun, F.; Yang, L. F.; Maass, K. F.; Traxlmayr, M. W.; Yu, Y.; Xu, Y.; Langer, R. S.; Anderson, D. G.; Wittrup, K. D. Cytosolic Delivery of SiRNA by Ultra-High Affinity DsRNA Binding Proteins. *Nucleic Acids Res.* **2017**, *45* (13), 7602–7614. https://doi.org/10.1093/nar/gkx546.

(5) Yonezawa, S.; Koide, H.; Asai, T. Recent Advances in SiRNA Delivery Mediated by Lipid-Based Nanoparticles. *Adv. Drug Deliv. Rev.* **2020**, *154–155*, 64–78. https://doi.org/10.1016/j.addr.2020.07.022.

(6) Svensen, N.; Walton, J. G. A.; Bradley, M. Peptides for Cell-Selective Drug Delivery. *Trends Pharmacol. Sci.* **2012**, *33* (4), 186–192. https://doi.org/10.1016/j.tips.2012.02.002.

(7) Zahid, M.; Robbins, P. D. Cell-Type Specific Penetrating Peptides: Therapeutic Promises and Challenges. *Molecules* **2015**, *20* (7), 13055–13070. https://doi.org/10.3390/molecules200713055.

(8) Vargason, J. M.; Szittya, G.; Burgyán, J.; Tanaka Hall, T. M. Size Selective Recognition of SiRNA by an RNA Silencing Suppressor. *Cell* **2003**, *115* (7), 799–811. https://doi.org/10.1016/S0092-8674(03)00984-X.

(9) Calin, G. a; Croce, C. M. MicroRNA Signatures in Human Cancers. *Nat. Rev. Cancer* **2006**, *6* (11), 857–866. https://doi.org/10.1038/nrc1997.

(10) Wang, J.; Chen, J.; Sen, S. MicroRNA as Biomarkers and Diagnostics. *J. Cell. Physiol.* **2016**, *231* (1), 25–30. https://doi.org/10.1002/jcp.25056.

(11) Roberts, A. P. E.; Lewis, P.; Catherine, L. *The Role of MicroRNAs in Viral Infection I . Introduction*, 1st ed.; Elsevier Inc., 2011; Vol. 102. https://doi.org/10.1016/B978-0-12-415795-8.00002-7.

(12) Zhou, X. X.; Zou, X.; Chung, H. K.; Gao, Y.; Liu, Y.; Qi, L. S.; Lin, M. Z. A Single-Chain Photoswitchable CRISPR-Cas9 Architecture for Light-Inducible Gene Editing and Transcription. *ACS Chem. Biol.* **2018**, *13* (2), 443–448. https://doi.org/10.1021/acschembio.7b00603.

(13) Wu, N.; Deiters, A.; Cropp, T. A.; King, D.; Schultz, P. G. A Genetically Encoded Photocaged Amino Acid. *J. Am. Chem. Soc.* **2004**, *126* (44), 14306–14307. https://doi.org/10.1021/ja040175z.

(14) Chen, P. R.; Groff, D.; Guo, J.; Ou, W.; Cellitti, S.; Geierstanger, B. H.; Schultz, P. G. A Facile System for Encoding Unnatural Amino Acids in Mammalian Cells. *Angew. Chemie - Int. Ed.* **2009**, *48* (22), 4052–4055. https://doi.org/10.1002/anie.200900683.

(15) Luo, J.; Torres-Kolbus, J.; Liu, J.; Deiters, A. Genetic Encoding of Photocaged Tyrosines with Improved Light-Activation Properties for the Optical Control of Protease Function. *ChemBioChem* **2017**, *18* (14), 1442–1447. https://doi.org/10.1002/cbic.201700147.

(16) Danielson, D. C.; Filip, R.; Powdrill, M. H.; O'Hara, S.; Pezacki, J. P. *Suppressing RNA Silencing with Small Molecules and the Viral Suppressor of RNA Silencing Protein p19*; 2015; Vol. 463. https://doi.org/10.1016/j.bbrc.2015.06.071.

(17) Pertermann, R.; Tamilarasan, S.; Gursinsky, T.; Gambino, G.; Schuck, J.; Weinholdt, C.; Lilie, H.; Grosse, I.; Golbik, R. P.; Pantaleo, V.; Behrens, S. E. A Viral Suppressor Modulates the Plant Immune Response Early in Infection by Regulating MicroRNA Activity. *MBio* **2018**, *9* (2), 1–19. https://doi.org/10.1128/mBio.00419-18.

(18) Nguyen, T. A.; Cigler, M.; Lang, K. Expanding the Genetic Code to Study Protein–Protein Interactions. *Angew. Chemie - Int. Ed.* **2018**, *57* (44), 14350–14361. https://doi.org/10.1002/anie.201805869.

(19) Chin, J. W.; Schultz, P. G. In Vivo Photocrosslinking with Unnatural Amino Acid Mutagenesis. *ChemBioChem* **2002**, *3* (11), 1135–1137. https://doi.org/10.1002/1439-7633(20021104)3:11<1135::AID-CBIC1135>3.0.CO;2-M.

(20) Anzalone, A. V; Koblan, L. W.; Liu, D. R. Genome Editing with CRISPR-Cas Nucleases, Base Editors, Transposases and Prime Editors. *Nat. Biotechnol.* **2020**. https://doi.org/10.1038/s41587-020-0561-9.

(21) Hyun, S. L.; Schultz, P. G. Biosynthesis of a Site-Specific DNA Cleaving Protein. *J. Am. Chem. Soc.* **2008**, *130* (40), 13194–13195. https://doi.org/10.1021/ja804653f.

(22) Hoyer, D.; Cho, H.; Schultz, P. G. New Strategy for Selective Protein Cleavage. *J. Am. Chem. Soc.* **1990**, *112* (8), 3249–3250. https://doi.org/10.1021/ja00164a076.

(23) Cheng, J.; Danielson, D. C.; Nasheri, N.; Singaravelu, R.; Pezacki, J. P. Enhanced Specificity of the Viral Suppressor of RNA Silencing Protein p19 toward Sequestering of Human MicroRNA-122. *Biochemistry* **2011**, *50* (36), 7745–7755. https://doi.org/10.1021/bi2008273.

Chapter 6

Appendix

6.1 Supplemental information for chapter 2

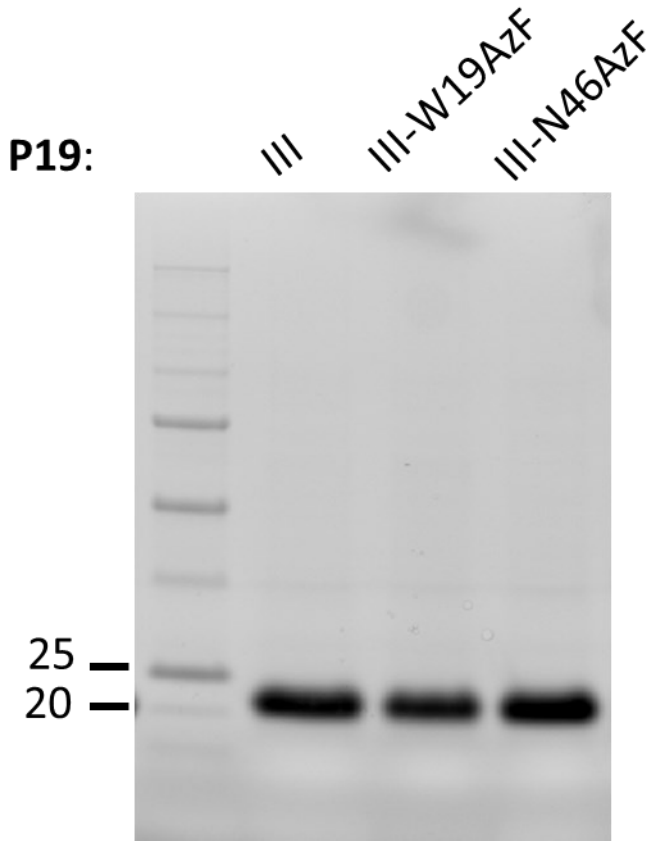

FigureS2.1. Purified p19-III and UAA mutants. Expression gel of purified p19-III, p19-III-W19AzF and p19-III-N46AzF post his-tag purification and size exclusion chromatography.

6.2 Supplemental information for chapter 3

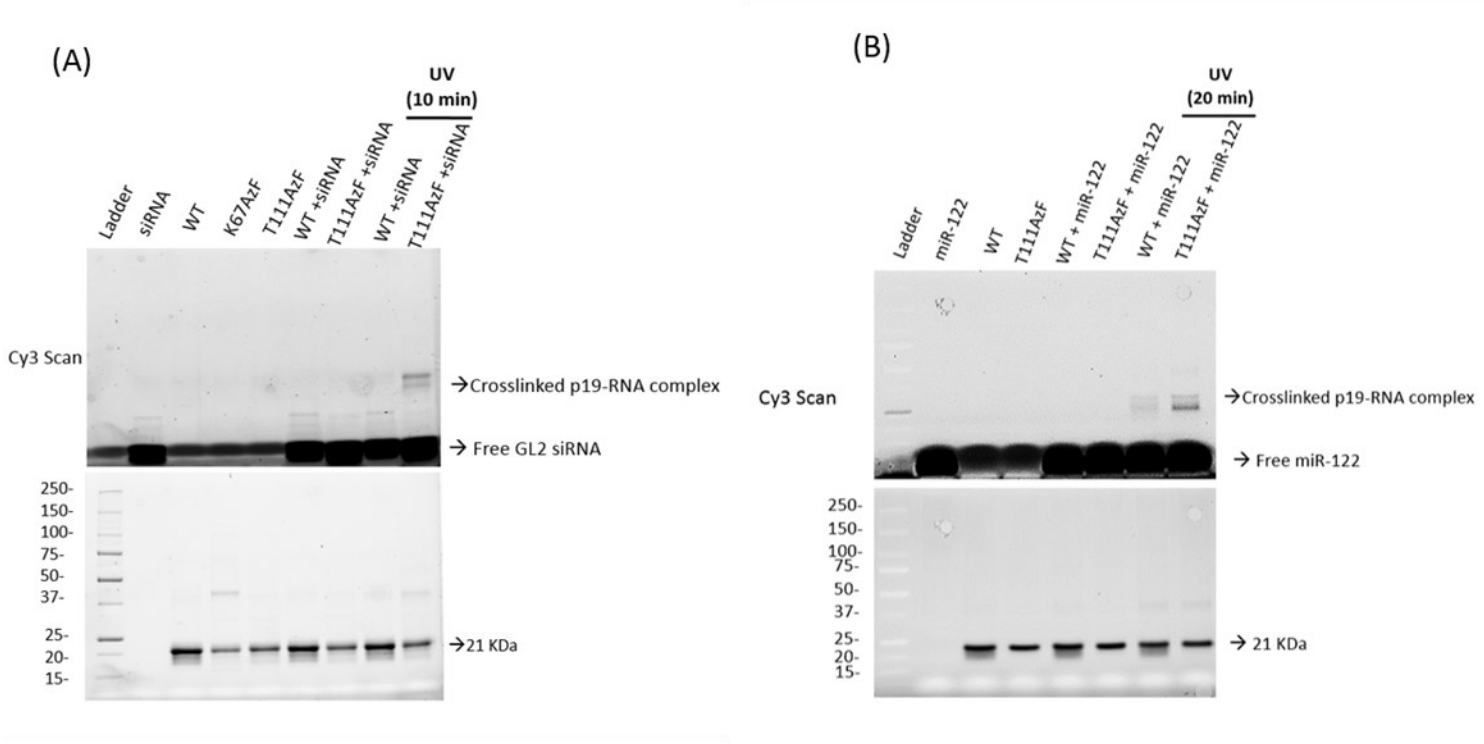

Figure S3.1 Crosslinking of p19 and small RNAs. A) Gel of p19 WT and T111AzF after UV exposure for 10 minutes at 320 nm. Top gel is the Cy3 Scan, confirming crosslinking of GL2 siRNA to T111AzF, while unbound Cy3 labelled GL2 siRNA appears at the bottom of the gel. Bottom gel is the loading control to confirm equal loading (TGX-Stain Free). B) Gel of p19 T111AzF after UV exposure for 20 minutes at 320 nm. Top gel is the Cy3 Scan, confirming photo-crosslinking of miR-122 to T111AzF, while unbound Cy3 labelled miR-122 appears at the bottom of the gel. Bottom gel is the loading control to confirm equal loading (TGX-Stain Free).

6.3 Supplemental information for chapter 4

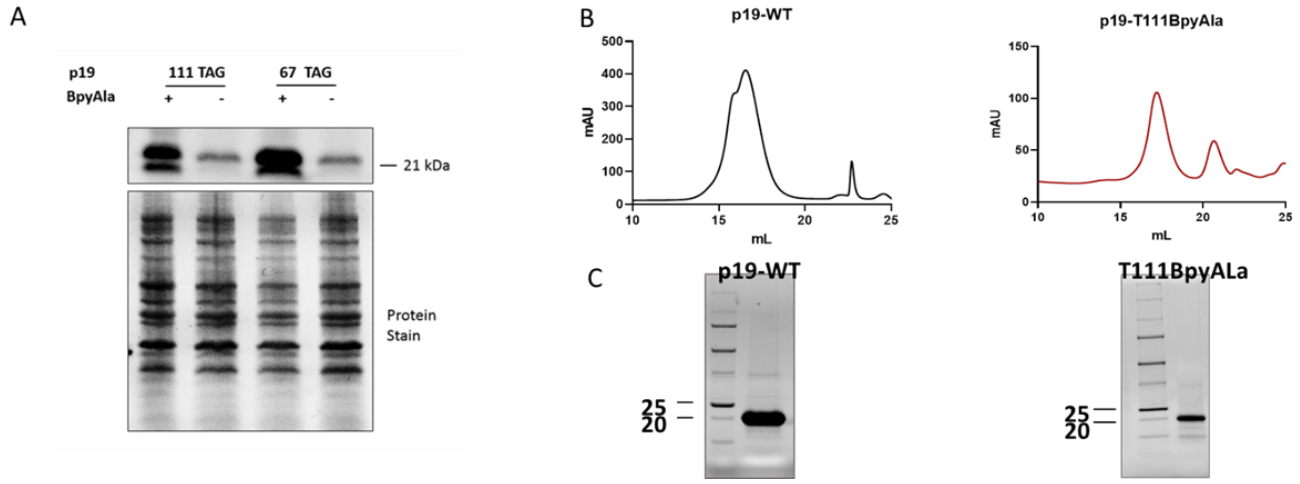

Figure S4.1. Expression and purification of p19-WT and p19-T111BpyAla purification. (A) western blot depicting the expression of p19-T111BpyAla and p19-K67BpyAla in *E. coli* cell lysates (B) size exclusion chromatography (SEC) chromatograms for p19-WT and p19-T111BpyAla on a Superdex 200 column (GE). (C) 5 µL of the concentrated fractions from the SEC were ran on an SDS-PAGE gel to confirm the purification of p19-WT and p19-T111BpyAla.

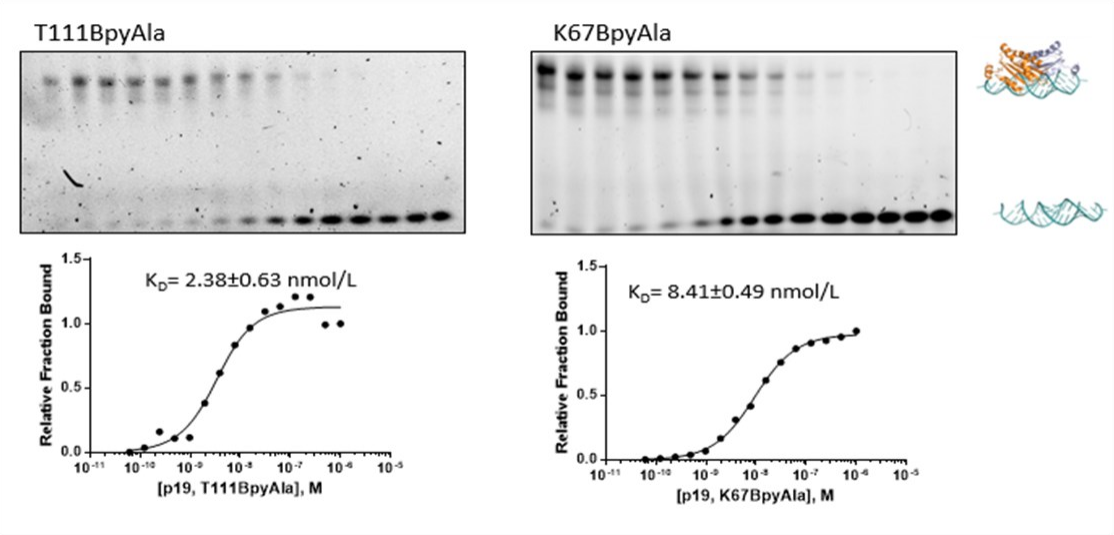

Figure S4.2 Determination of the Binding affinity of unnatural amino acid p19 mutants. Binding plot for p19-T111BpyAla and for p19-K67BpyAla using electrophoretic mobility shift assay. Binding plots were constructed by varying the concentrations of the protein (0-1 μmol/L), while maintaining the concentration of Cy3-labeled GL2 at 2 nmol/L.

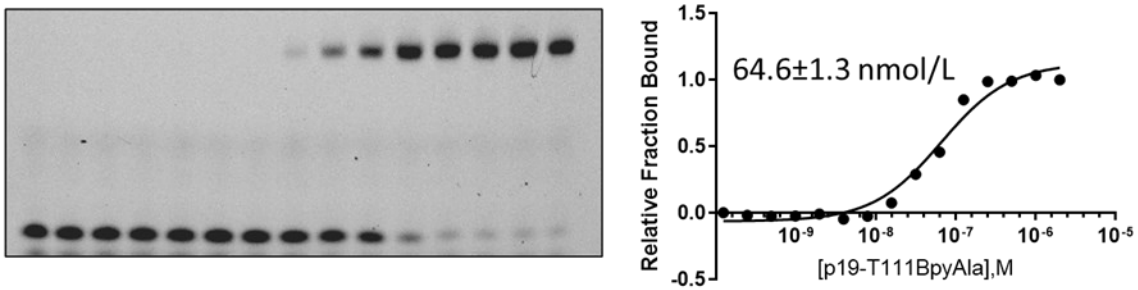

Figure S4.3 Determination of the Binding affinity of p19-T111BpyAla towards miR-122. EMSA gels for p19-T111BpyAla using 2nmol/L Cy3-labeled miR-122. Binding plots were constructed by varying the concentrations of the protein (0-2 μmol/L), while maintaining the concentration of Cy3-labeled miR-122 at 2 nmol/L.

Table S4.1 Summary of miRNAs downregulated upon treatment with p19-T111BpyAla relative to p19-WT.

miRNA	Fold Change	*P*-Value
hsa-miR-421	-1.78	0.035541
hsa-miR-10b-5p	-1.93	0.031897
hsa-miR-191-5p	-1.95	0.043329
hsa-miR-99a-5p	-1.96	0.039619
hsa-miR-106a-5p+hsa-miR-17-5p	-1.98	0.028491
hsa-miR-23a-3p	-1.99	0.036581
hsa-miR-122-5p	-2.02	0.034148
hsa-miR-93-5p	-2.31	0.021533
hsa-miR-130a-3p	-2.37	0.012802
has-miR-194-5p	-2.86	0.044898

Table includes miRNAs which were modulated by at least 1.2-fold during p19-T111BpyAla treatment of small RNA fractions isolated from Huh7 cell line relative to p19-WT treatments.

6.3.1 NMR Spectra for compounds synthesized in Chapter 4

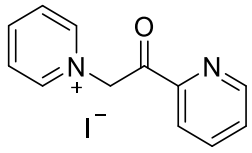

(2-pyridacyl)pyridium Iodide

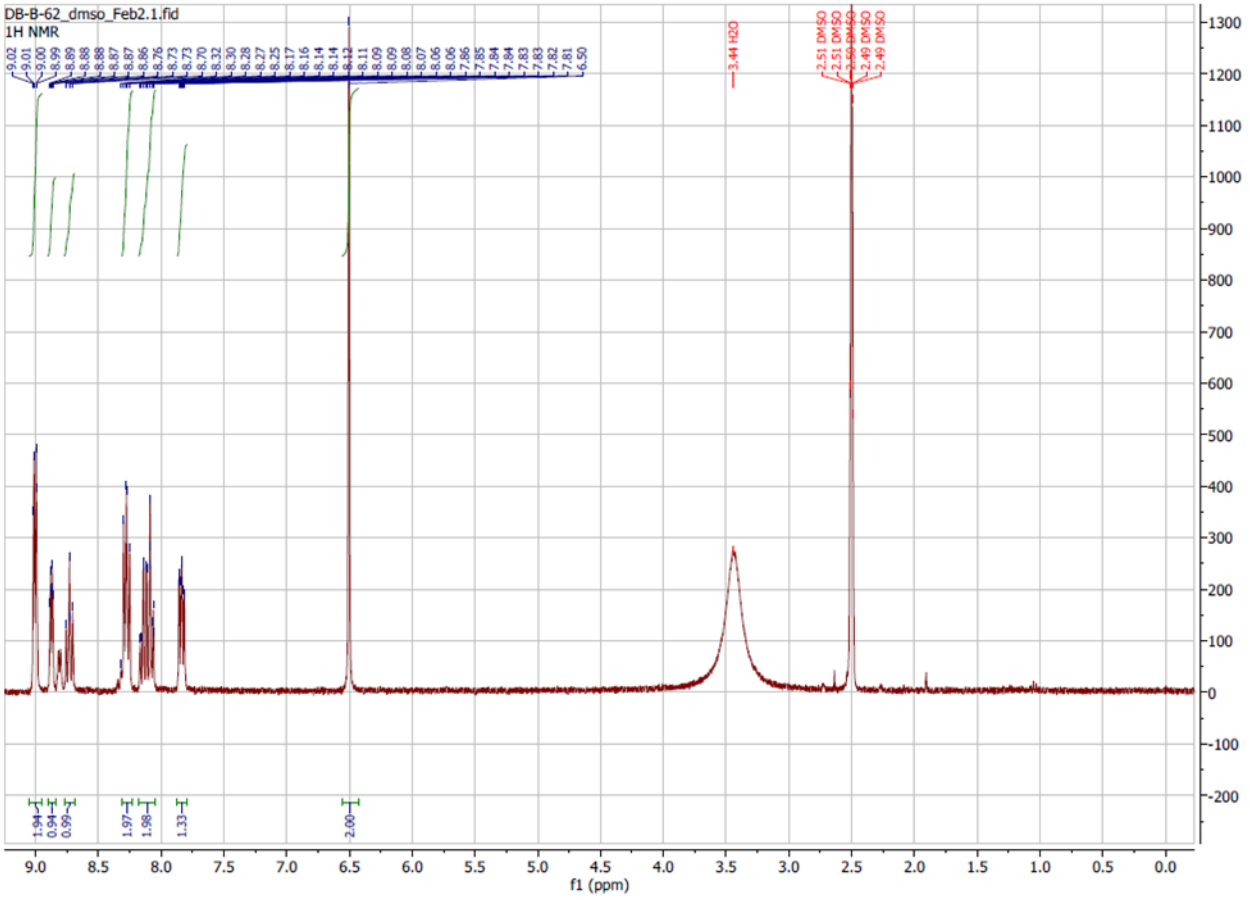

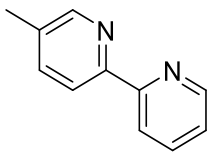

5-methyl-2,2'-bipyridine

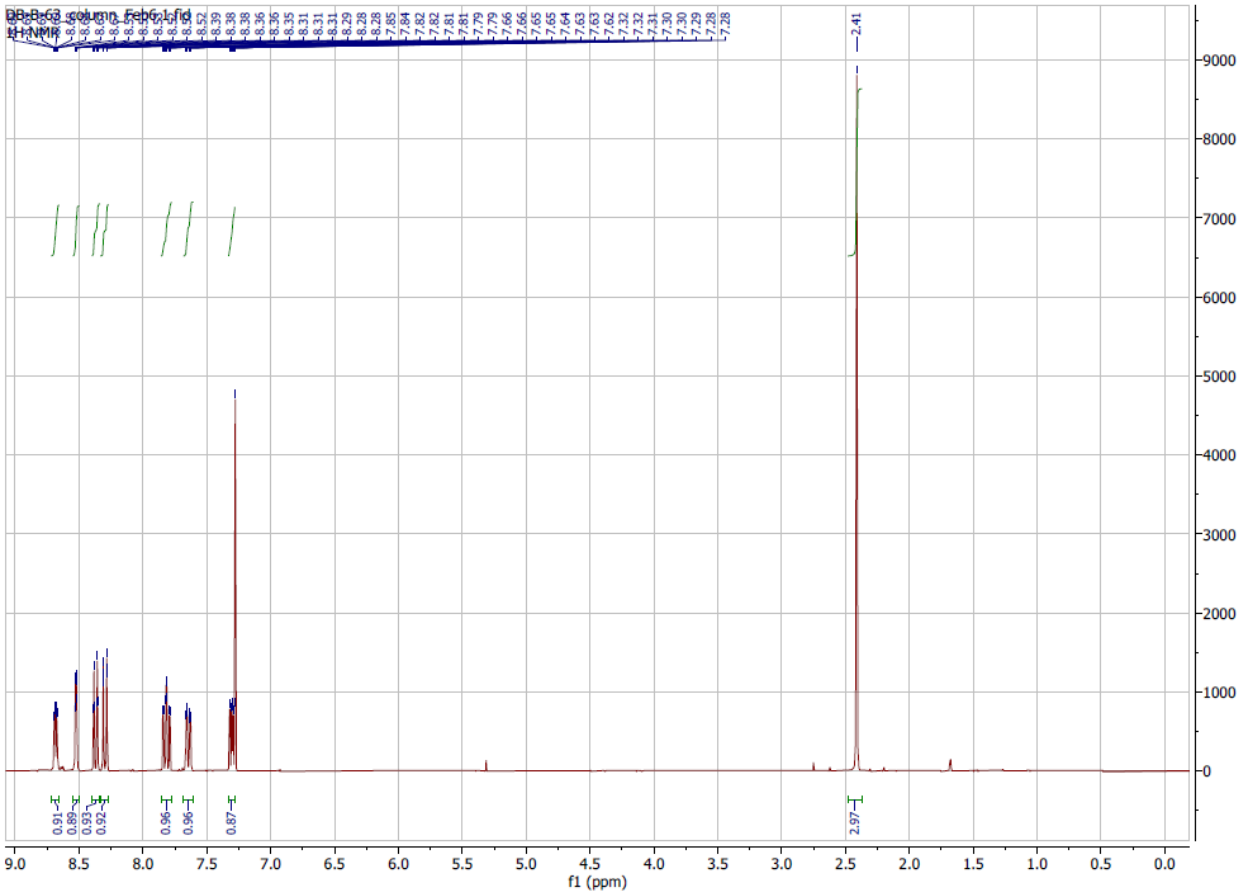

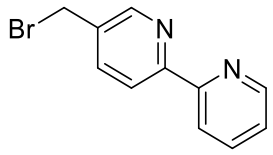

5-bromomethyl-2,2′-bipyridine

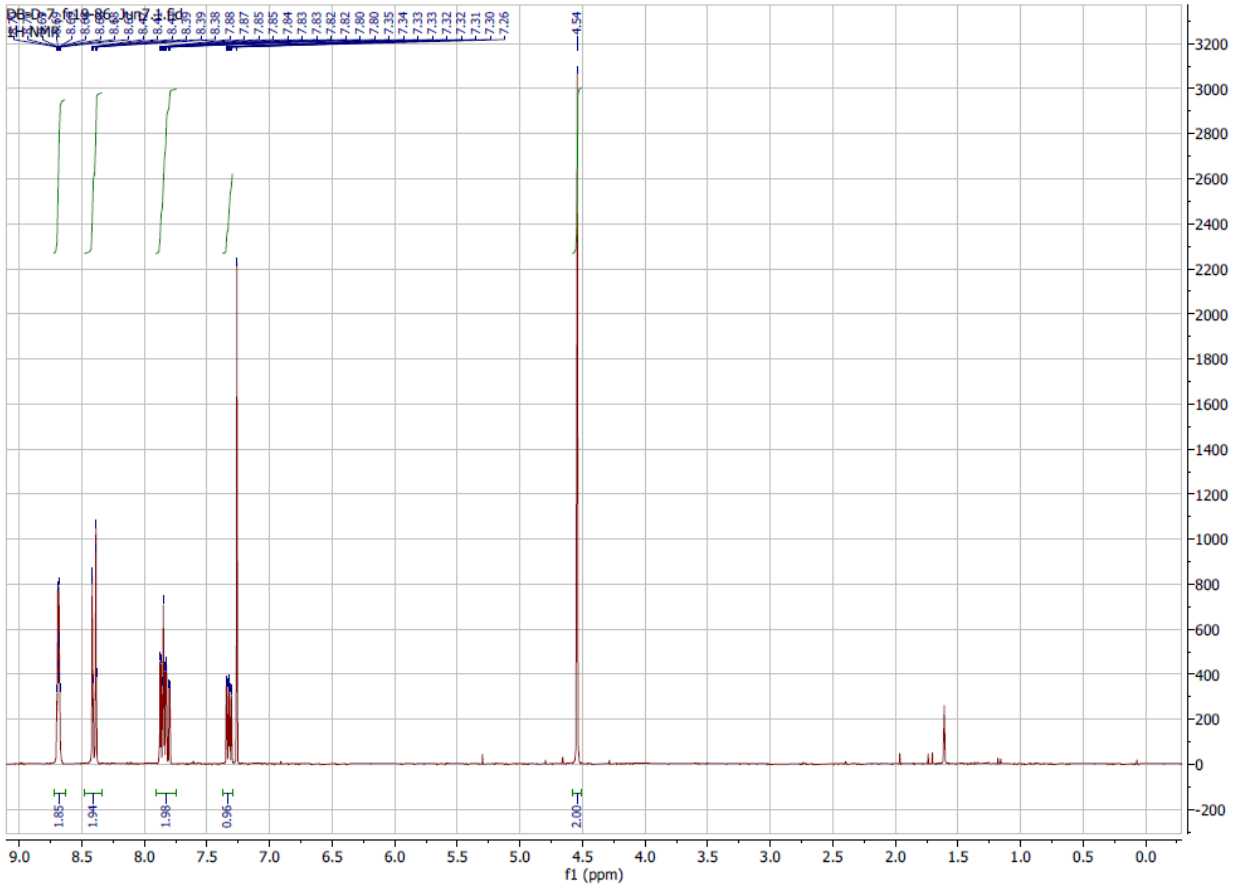

3-(2,2'-bipyridin-5-yl)-L-Alanine

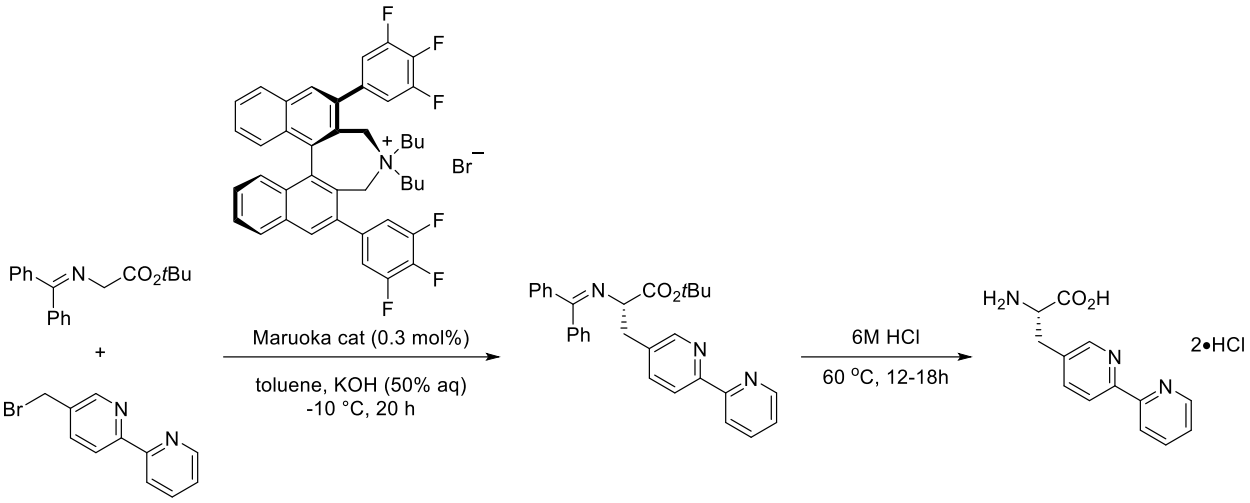

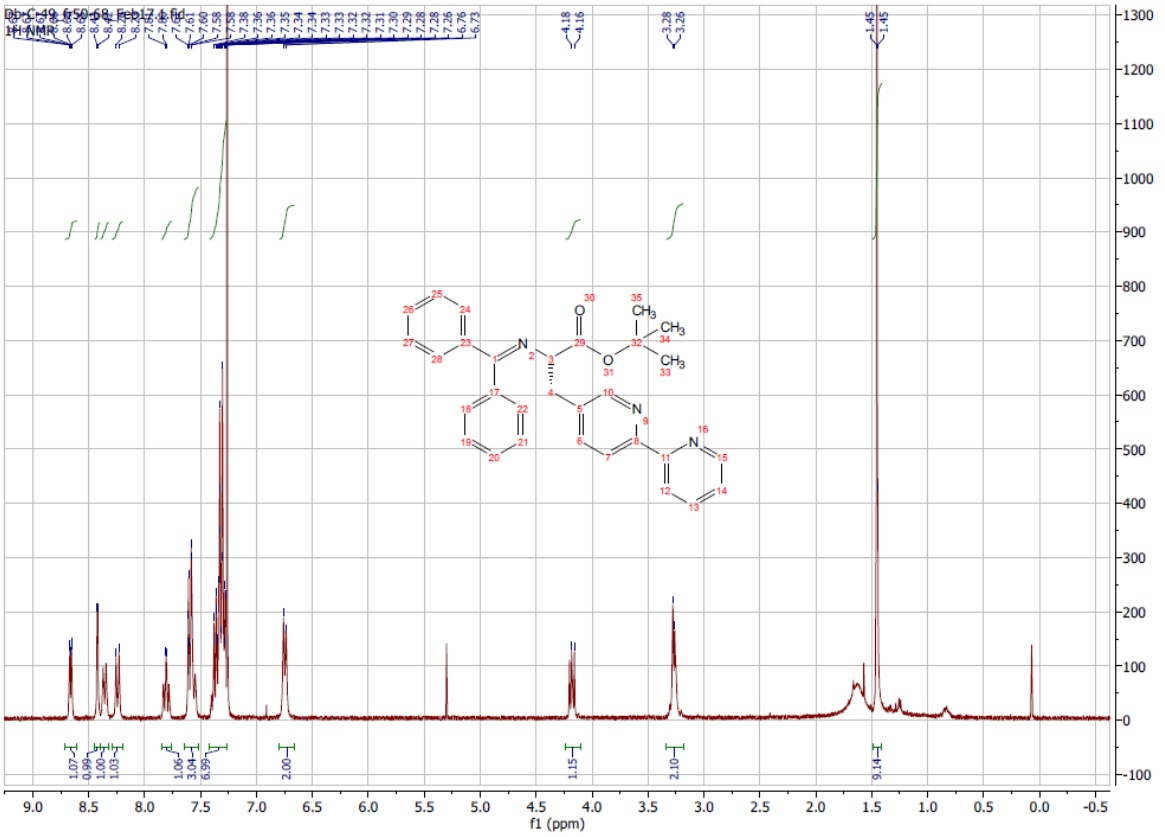

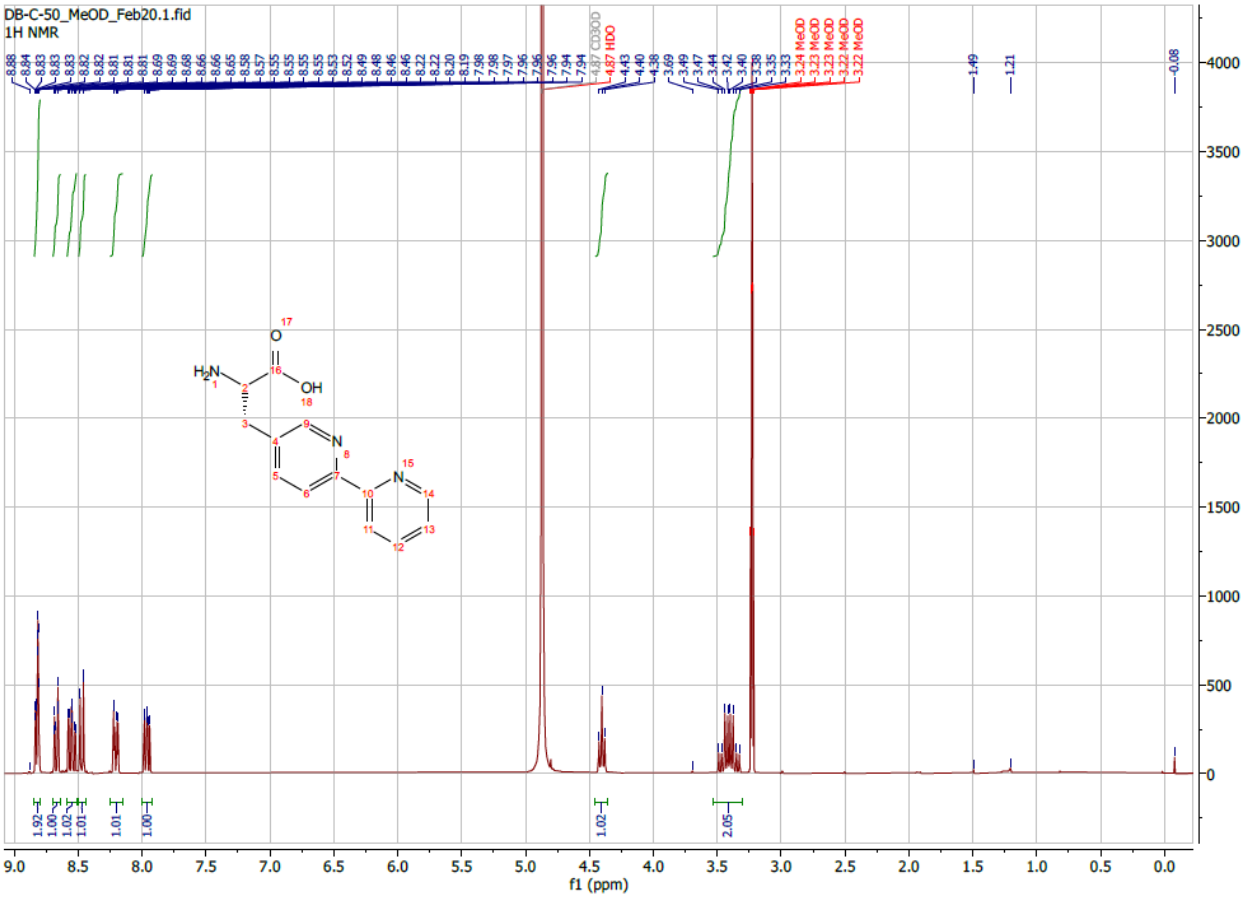
DB-C-50_MeOD_Feb20.1.fid
1H NMR
f1 (ppm)